ISBN 978-82-326-4438-4 (printed version)
ISBN 978-82-326-4439-1 (electronic version)
ISSN 1503-8181

Seongpil Cho

Doctoral Thesis

Doctoral theses at NTNU, 2020:40

Seongpil Cho

Model-based Fault Detection and Diagnosis of a Blade Pitch System in Floating Wind Turbines

NTNU
Norwegian University of
Science and Technology
Faculty of Engineering
Department of MarineTechnology

NTNU
Norwegian University of
Science and Technology

Doctoral theses at NTNU, 2020:40

NTNU

NTNU
Norwegian University of
Science and Technology

Seongpil Cho

Model-based Fault Detection and Diagnosis of a Blade Pitch System in Floating Wind Turbines

Thesis for the degree of Philosophiae Doctor

Trondheim, January 2020

Norwegian University of Science and Technology
Faculty of Engineering
Department of MarineTechnology

NTNU
Norwegian University of
Science and Technology

NTNU
Norwegian University of Science and Technology

Thesis for the degree of Philosophiae Doctor

Faculty of Engineering
Department of MarineTechnology

ISBN 978-82-326-4438-4 (printed version)
ISBN 978-82-326-4439-1 (electronic version)
ISSN 1503-8181

Doctoral theses at NTNU, 2020:40

Printed by Skipnes Kommunikasjon as

“Cogito, ergo sum”

René Descartes (1596 – 1650)

Abstract

Offshore wind turbines operate in ocean environments with irregular waves and turbulent winds and experience technical faults during their service life. Faults and failures in their actuators, sensors, and system components could lead to system interruptions. These faults change the system characteristics, the efficiency of power production, and the operational safety. Therefore, fault detection, diagnosis and accommodation techniques are required to ensure the reliability and lower the repair costs of floating wind turbines. Among wind turbine components, the blade pitch system is one of the most critical components due to its effect on the operational safety and the dynamics of wind turbines. In addition, this subsystem has the highest failure rate.

This thesis presents model-based fault detection, fault diagnosis, and fault-tolerant control schemes for blade pitch systems in a spar-type floating wind turbine. Early-stage fault detection and diagnosis should be conducted to prevent escalation of faults and failures. To detect faults of blade pitch systems, a discrete-time Kalman filter is designed to estimate the states of the blade pitch angle of the system. Residuals are generated by a Kalman filter and a threshold based on H_∞ optimization, and a linear matrix inequality (LMI) is used for residual evaluation. The fault diagnosis algorithm is based on inference methods under specific fault conditions. Another fault diagnosis scheme uses an artificial neural network and is capable of determining the fault type, location, magnitude and time. For fault detection and diagnosis, the blade pitch angle and valve spool position are measured. Fault diagnosis algorithms can be used for both condition monitoring and active fault-tolerant control purposes. The fault-tolerant controller based on a reconfiguration block with a virtual sensor and a shutdown mode controls the floating wind turbine to avoid unexpected external loads.

Numerical simulations are based on detailed numerical models for the blade pitch actuators coupled to the global analysis model and models of various faults. The proposed methods are demonstrated in case studies simulated using Simo-Riflex, which is an aero-hydro-servo-elastic simulation tool with stochastic wind and wave conditions that considers different types of faults, such as biases and fixed outputs in pitch sensors, excessive friction and wrong voltage, or slit-lock or short circuits of valves in pitch actuators. These faults contribute to imbalance rotation in the rotor, which results in different effects on the turbine structure and the platform motion. The proposed method for combining the global and hydraulic actuator models is demonstrated in case studies under stochastic wind and wave conditions and different types of faults in pitch sensors and actuators. The simulation results show that the proposed methods can effectively detect and diagnose faults at an early stage with reasonable accuracy. Additionally, the effectiveness of the fault-tolerant control systems for different load cases for single and multiple fault conditions is verified by numerical simulations.

Preface

This thesis is submitted to the Norwegian University of Science and Technology (NTNU) for partial fulfilment of the requirements for the degree of doctor of philosophy.

This doctoral work has been performed at the Department of Marine Technology and the Centre for Autonomous Marine Operations and Systems (AMOS), NTNU, Trondheim, supervised by Professor Torgeir Moan (Main supervisor) and Professor Zhen Gao (Co-supervisor). This project was funded by the Research Council of Norway (RCN) through the "MIT-NTNU-Statoil Energy project".

The thesis addresses model-based fault detection, diagnosis, and fault tolerant control of wind turbines based on the simplified and detailed hydraulic blade pitch actuator of floating wind turbines.

The thesis consists of a summary report and four research papers, written during the period August 2014 to September 2019. Three research papers have been published in and the other one paper has been submitted to international peer-reviewed scientific journals.

Seongpil Cho

23. September. 2019
Daejeon, South Korea

Acknowledgements

I would like to first express my gratitude toward my supervisor Prof. Torgeir Moan for his supervision, inspiration, support, valuable discussions and suggestions. During the past five years of research at NTNU, he helped to guide me in the right direction with his instructive comments. He has spent much time with me discussing recent research issues with his insight. He encouraged me to face and handle new problems and to become an independent researcher. Second, I would also like to thank my co-supervisor Prof. Zhen Gao for his instruction and encouragement during my Ph.D. He always provided insightful discussions regarding this research. He sets a good example by his dedication to research and he has been good at capturing new information and research trends. I also would like to thank Dr. Bjørn Skaare, who was my co-supervisor for his valuable comments and guidance for the control problem in the regular or annual meeting for the MIT-NTNU-Statoil Energy project.

I am very grateful to Associate Prof. Erin E. Bachynski for her support regarding the use of the computer code Simo-Riflex and for early conversations regarding wind turbine and spar-type floater modeling. The pleasant collaboration with her was very influential in the development of the studied concepts. I also would like to thank Associate Prof. Amir R. Nejad for enlightening me with his knowledge of hydraulics. Thanks to Dr. Minjoo Choi for fruitful discussions and for sharing his expertise on optimization and machine learning with me.

I am also grateful for my Korean friends: Kevin Koosup, Donghoe, Woongsik, Daesung, Kiyeon, and Sangwoo at Tyholt and all the Korean students at NTNU. I have also greatly benefited from my friendship and cooperation with many other Ph.D. candidates and post-doctoral fellows at NTNU. I would like to thank all the people and employees at the Department of Marine Technology who provided a comfortable and friendly working atmosphere which helped me significantly to improve my work efficiency. Particular thanks to Prof. Phill-Seung Lee, who helped me to gain ground as an independent researcher at the beginning of my research career and gave me inspiration, insightful instruction and discussion at KAIST. I would also like to acknowledge the financial support from Equinor (formerly Statoil) through the MIT-NTNU-Statoil Energy project.

Finally, I would like to give my special thanks to my parents and sisters in Korea. Their encouragement and love have been the main support that kept me going over the years and allowed me to finish this journey.

Seongpil Cho

23. September. 2019
Daejeon, South Korea

List of appended papers

This thesis contributes to the development of fault detection, fault diagnosis, and fault-tolerant control of a hydraulic blade pitch system for floating wind turbines. This thesis consists of an introductory part and four journal papers (three published and one submitted).

The following four papers are reported in Appendix A:

Paper 1

Model-based fault detection of blade pitch system in floating wind turbines

Seongpil Cho, Zhen Gao and Torgeir Moan

Published in Journal of Physics: Conference Series 2016; 753, 092012.

Paper 2

Model-based fault detection, fault isolation and fault-tolerant control of a blade pitch system in floating wind turbines

Seongpil Cho, Zhen Gao and Torgeir Moan

Published in Renewable Energy 2018; 120, 306-321.

Paper 3

Numerical modeling of the hydraulic blade pitch actuator in a spar-type floating wind turbine considering fault conditions and their effects on global dynamic responses

Seongpil Cho, Erin E. Bachynski, Amir R. Nejad, Zhen Gao and Torgeir Moan

Published in Wind Energy 2019; Early View Publication, 1-21.

Paper 4

Fault detection and diagnosis of a blade pitch system of a spar-type floating wind turbine based on a hybrid approach with a Kalman filter and artificial neural network

Seongpil Cho, Minjoo Choi, Zhen Gao and Torgeir Moan

Submitted to Wind Energy.

Declaration of authorship

All four papers that serve as the core content of this thesis are co-authored. In all of these papers, I am the first author and am responsible for developing the ideas, establishing the numerical models, algorithms, and codes, performing the analysis, presenting the results and discussions, writing, and responding to the comments and questions from reviewers and other readers. Professor Torgeir Moan is my main supervisor and Professor Zhen Gao is my co-supervisor. They are co-authors of all four papers. They have contributed to the support, discussions and constructive comments to increase the scientific quality of the publications. Associate Professor Erin E. Bachynski is the second author of Paper 3 and contributed spar-type wind turbine modeling and a global dynamic analysis using Simo-Riflex. Associate Professor Amir R. Nejad is the third authors of Paper 3. He contributed to the hydraulic actuator modeling. They have also contributed to discussions of the numerical results and comments on the paper. In addition, Dr. Minjoo Choi is the second author of Paper 4 and he contributed to 1) providing an optimization solution for an artificial neural network in Paper 4; 2) discussions and comments on the methodology of the ANN parts in the paper.

Contents

List of Figures

List of Tables

Abbreviations

AI	artificial intelligence
ANN	artificial neural network
BEM	blade element momentum
FDD	fault detection and diagnosis
FTC	fault-tolerant control
FWT	floating wind turbine
HAWT	horizontal-axis wind turbine
HPU	hydraulic power unit
IEC	International Electrotechnical Commission
JONSWAP	Joint North Sea wave project
KF	Kalman filter
GDW	generalized dynamic wake
LC	load case
LMI	linear matrix inequality
LVDT	linear variable displacement transducer
ML	machine learning
NREL	National Renewable Energy Laboratory
NTM	normal turbulence model
NWP	normal wind profile model
OC3	offshore code comparison collaboration
PAS	stuck in pitch actuator
PI	proportional integral
PSB	bias value in pitch sensor
PSF	fixed value in pitch sensor
TF	time of fault occurrence
TFD	time of fault detection
TFI	time of fault isolation
TFTC	time of fault-tolerant control
TLP	tension leg platform
VAWT	vertical axis wind turbine
VCS	short-circuit in the valve
VEF	excessive friction in the valve
VLS	slit-lock in the valve
VWV	wrong applied voltage in the valve

1. Introduction

1.1. Trend of the offshore wind industry

The wind energy industry has experienced rapid growth because of environmental issues and the demand for sustainable solutions. Wind turbines placed offshore are attractive because of the higher wind speeds and more consistent wind patterns compared to those on land. Moreover, offshore wind turbines cause less environmental damage and annoyances to people due to noise and visual effects than turbines on land. Offshore wind technology has experienced rapid development in recent years, with an annual cumulative global installed capacity of 23 GW at the end of 2018 [1]. European countries are leading the offshore wind energy market with a total installed offshore wind capacity of 18.5 GW [3], as shown in Figure 1.1. This wind capacity corresponds to 4,543 grid-connected wind turbines across 11 countries in Europe. Four hundred-nine new offshore wind turbines in 2018 were installed and grid-connected in Europe with 2.65 GW of new capacity lower than that in 2017 by 15.8% which was a record year, but the cumulative total capacity is nevertheless constantly increasing. Among cumulative installations, the UK has the largest amount of offshore wind capacity with 44% of all installations in Europe. Germany is second with 34%, followed by Denmark (7%), Belgium (6.4%) and the Netherlands (6%). The UK and Germany have 1.31 GW and 0.97 GW, respectively.

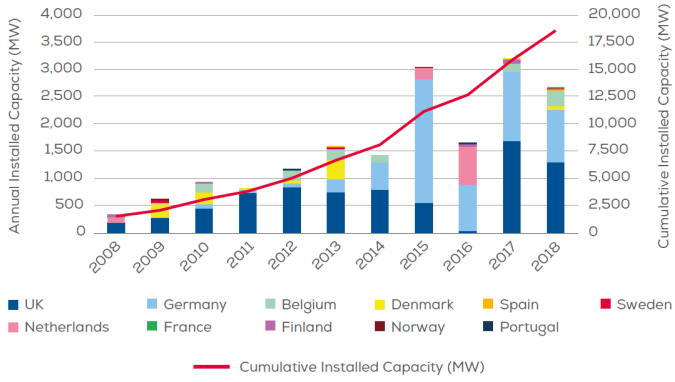

Figure 1.1: Annual offshore wind installations by country and cumulative capacity (MW) 2008 - 2018 [3].

Currently, offshore wind farms are moving further into deeper water off the shore to better capture wind energy resources. The average size of the offshore wind turbines in 2018 was 6.8 MW [3], which is 15% larger than in 2017, as shown in Figure 1.2. Since 2014, the average rated capacity of newly installed wind turbines has grown at an annual rate of 16%. In terms of the distance from the shore, Hornsea One in the UK and EnBW Hohe See in Germany are located farthest from the shore at 103 km away. Deutsche Bucht, also in Germany, follows at 93 km from the shore.

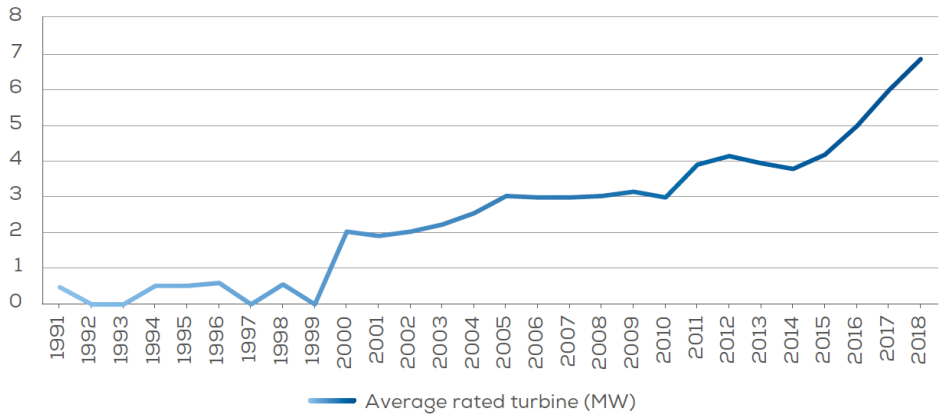

Figure 1.2: Yearly average of newly installed offshore wind turbine rated capacity (MW) [3].

Figure 1.3 describes the average water depth and the distance to shore for online, under construction and consented offshore wind farms, and the size of the bubble indicates the overall capacity of the site [2, 3]. In deeper waters (water depth greater than 50 m), floating wind turbines are more cost-effective and economical in terms of power production than bottom-fixed wind turbines [4]. Hywind Demo [5], installed in Karmøy in Norway, has shown to function well in all wind and wave conditions in the North Sea after 8 years of testing a full-scale prototype, which began in 2009. Hywind Scotland pilot park [6], the first floating offshore wind farm in the world, was installed in a water depth ranging from 90 to 120 m at a distance of 25 km from the shore, where work was conducted in 2017. In 2018, the 2MW Kincardine pilot [7] with a 77 m average water depth, was constructed for the test of the Kincardine project in Scotland, which has a 50 MW wind farm capacity with 5 turbines. France saw the grid connection of two floating offshore wind turbines: the Floatgen project [8] (2 MW) off the coast of Brittany, and the Eolink 1/10 project [9], which connected a prototype turbine of approximately 200 kW in Brittany. Therefore, it is clear that the average water depth and distance to the shore will increase as floating wind farms are developed in European countries.

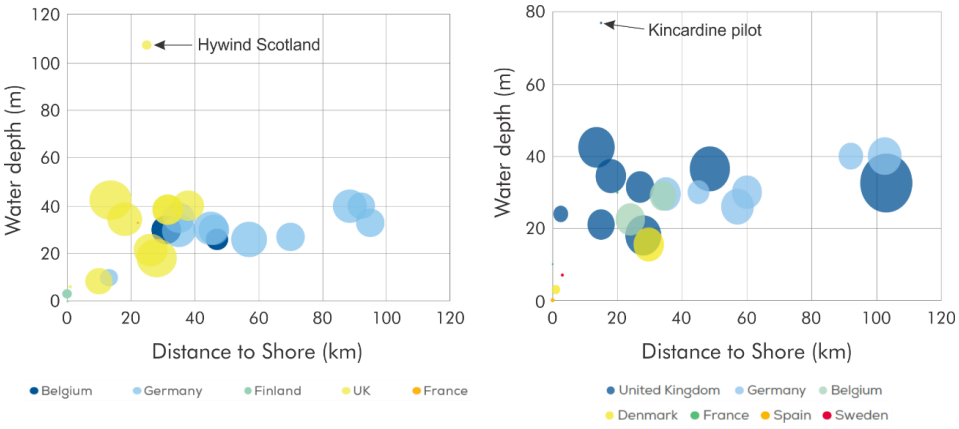

(a) (b)

Figure 1.3: Average water depth and distance to the shore for offshore wind farms under construction during (a) 2017 and (b) 2018 [2, 3].

1.2. Floating wind turbines

1.2.1. Types and components of wind turbines

Wind turbines are designed to convert energy from the wind into mechanical energy. Wind turbines are composed of a rotor that rotates due to propulsion by lift or drag forces from the wind force. Depending on the rotor axis, the wind turbines are classified into vertical-axis wind turbines (VAWT) and horizontal-axis wind turbines (HAWT). Figure 1.4 shows the two different types schematically.

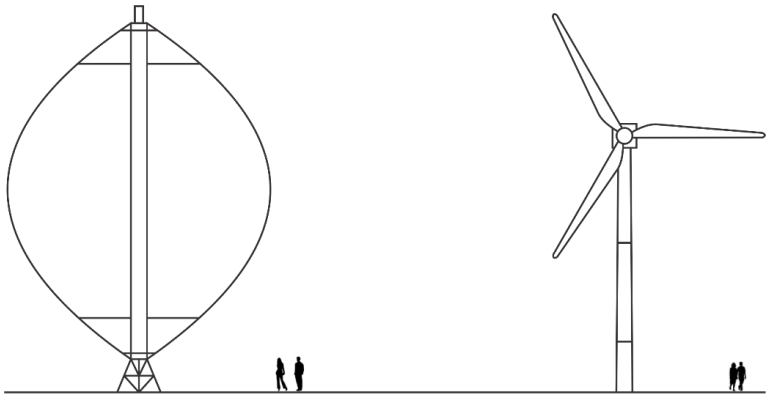

(a) (b)

Figure 1.4: (a) Vertical- and (b) Horizontal-axis wind turbines [10, 11].

The VAWT has a vertical shaft with a generator located at ground level. Vanes are mounted on the vertical shaft, which extract the wind energy. The main advantage of VAWTs is their ability to capture the wind energy from any wind direction. The most desired attributes include a silent operation, enabling urban installations and making them less visually intrusive. However, most VAWTs have difficulty being mounted high on a tower to capture higher speeds or less turbulent winds found at greater elevations above ground. Furthermore, they must utilize lower speed winds found near ground level with a consequent reduction in power output [12] since the rotor extracts less wind energy.

The HAWT has a horizontal shaft and rotor positioned on the top of the tower, which creates a more efficient system as more wind energy is produced. The HAWT has become the standard configuration for the modern large wind turbine because it has a higher efficiency than the VAWT, as shown in Figure 1.5. Currently, most commercial wind turbines connected to the grid have horizontal-axis two-bladed or three-bladed rotors. Therefore, only HAWTs are treated in this thesis.

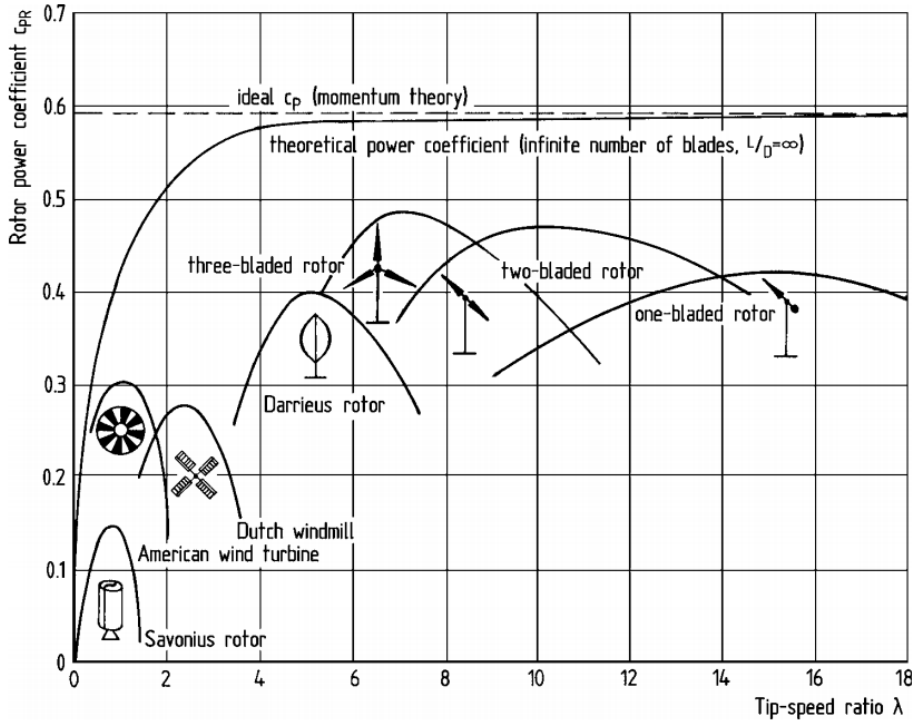

Figure 1.5: Power coefficients of wind rotors of different designs [12, 13].

The HAWT typically has a rotor with 3 blades that capture energy from the wind. This rotor is mounted at the end of a shaft that is connected to a generator through a gearbox in a nacelle. When the shaft rotates the generator, the wind turbine produces electricity.

Figure 1.6 illustrates the components involved in a three bladed HAWT [14]. Here are brief descriptions of the wind turbine components:

• Rotor: Together with the blades and hub. The hub connects to the low-speed shaft.

• Blades: Extracts wind energy and converts it into rotational energy to the low-speed shaft.

• Pitch System: Controls the rotor speed, blade pitch angle, and generator torque. This system is used to maximize the efficiency in low winds and reduce the aerodynamic loads in high winds to protect the wind turbine from structural damage.

• Brake: To slow down and stop the rotor at the cut-out wind speed or in emergency conditions.

• Low-speed shaft: Connects the rotor to the gearbox.

• Gearbox: Connects and transfers the rotational energy from the low-speed shaft into high-speed shaft.

• High-speed shaft: Driven by the gearbox. Drives the generator.

• Generator: Converts the rotational energy from the high speed shaft into electricity.

• Controller: Controls the pitch angle to generate the maximum power output and yaw system to position the wind turbine into the wind direction and develop the generator torque to the wind turbine in the operational wind speed region.

• Anemometer: Measures the wind speed and sends the data.

• Wind Vane: Measures the wind direction to control the yaw system.

• Nacelle: Located on the top of the tower and contains the drive-train assembly, shafts, gearbox, generator, converter and brake.

• Yaw system: Includes a yaw drive and motor. This system controls the nacelle and the rotor position perpendicular to the wind direction.

• Tower: Supports the nacelle and the rotor at an appropriate height. A taller tower enables a wind turbine to capture more wind energy since the wind speed increases depending on the height.

The tower is supported by bottom-fixed or floating structures, depending on the water depth. The focus in this thesis is on the pitch control of the blades in HAWTs on floating support structures. The pitch control system and procedures are described in detail in Chapter 2.

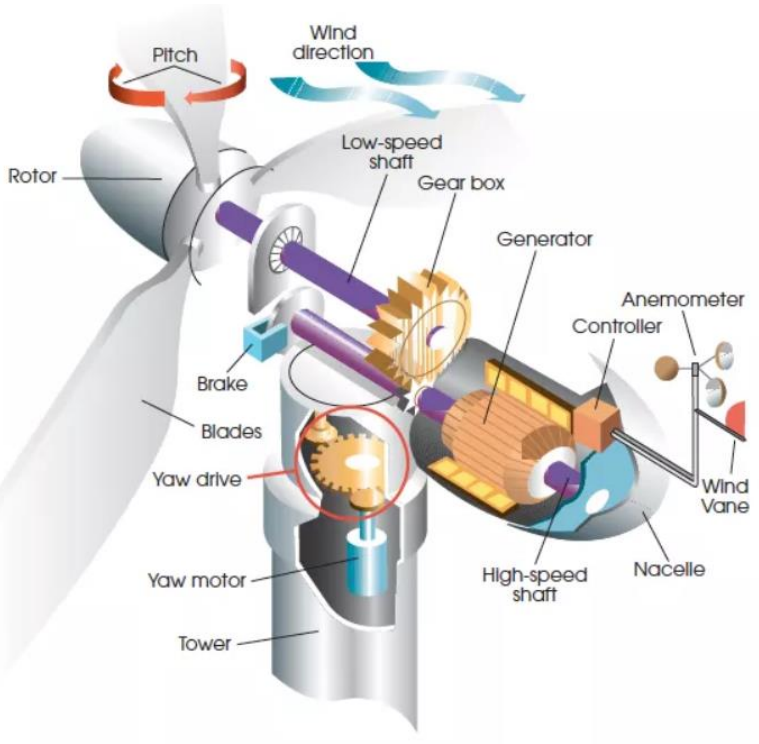

Figure 1.6: Main components of a typical modern high-power wind turbine [14].

1.2.2. Floater concepts

Several offshore wind turbines were installed and grid-connected in shallow water on bottom-fixed substructures such as a monopile, tripot, and jacket [4]. To access better and larger wind resources, wind turbine support platforms for intermediate water depth (45 - 150 m) and deep water (> 150 m) are also being considered. At water depths beyond 50 - 70m, gravity-based and monopile foundations are not economically feasible [15].

Floating structures have many merits including greater flexibility in terms of construction procedures and a resistance capability against hydrodynamic loads. The floating structures provide the required buoyancy to support the weight of the wind turbines and sufficient stability under the action of mean environmental loads. Therefore, different floating platforms are categorized with a strategy of providing static stability. There are three primary types of floating structures for offshore wind turbines: the spar, the tension-leg platform, and the semi-submersible. Figure 1.7 illustrates the current types of offshore wind turbines including three types of floating wind turbines for deep water areas where the water depth is greater than 50 m [16].

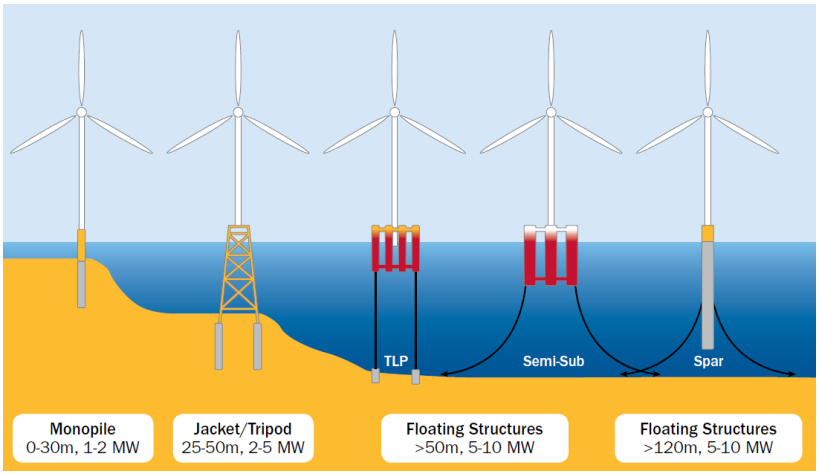

Figure 1.7: Offshore wind foundations [16].

• Spar Buoy: A very large cylindrical buoy stabilizes the wind turbine using ballast weights with catenary mooring cables hanging from the midpoint of each anchor cable to provide additional tension. In this case, the center of gravity is much lower in the water than the center of buoyancy, which creates a righting moment and a high inertial resistance to roll, pitch and usually enough draft to limit heave motion. The Hywind demo concept [5] and the Hywind Scotland pilot projects [6] consist of this slender, ballast-stabilized cylinder structure.

• Tension Leg Platform (TLP): A TLP is usually ballasted and moored by three or four pairs of vertical mooring lines in tension. Tensioned mooring lines are anchored on the seabed to add buoyancy and stability. This anchoring maintains stability through tension in the mooring lines and reserved buoyancy, which is important for preventing the mooring from going slack under extreme conditions. The TLP is the most stable platform and thus has the least impact on the dynamics and power absorption of the wind turbine. Pelastar [17] and Floating Haliade [18] are based on a tension stabilized concept integrating proven TLP technology.

• Semi-submersible: Combining the main principles of the spar and TLP designs, a semi-submerged structure obtains buoyancy from ballasted cylindrical pontoons to reach the necessary stability. A semi-submersible structure creates a large restoring moment in the roll and pitch with a water-plan area. The catenary mooring line prevents the floater from drifting from wave loads and increases the resistance to overturning. A Vestas's 2 MW wind turbine mounted on a Wind-Float [19] was installed in the Portuguese coast and has been tested. In 2018, the Kincardine pilot [7] with a 2 MW capacity was installed in Scotland.

Although there are many benefits with floating structures, there are a number of challenges such as electrical infrastructure design, operation and maintenance procedures.

1.3. Fault statistics and maintenance strategies in wind turbines

1.3.1. Fault statistics

Wind turbines are exposed to a variety of wind load conditions and there is a high possibility of unpredicted faults and failures occurring, which could lead to system interruptions and cause huge economic losses. Specifically, offshore wind turbines operate in stochastic ocean environments, such as turbulent winds, irregular waves, component erosion due to the sea water and significant disturbances.

The wind turbines experience various failure modes in mechanical and electrical components. The EU Reliawind project provides wind turbine reliability profiles from an analysis of the long-term operational data and fault records from 350 onshore wind turbines [20]. Figure 1.8 shows the relative contributions of subsystems and assemblies to the failure frequency and downtime. In a recent research article for statistics of offshore wind turbines, Carroll et al. [21] showed the results of an analysis determining the failure rates for the repair of modern offshore wind turbines and their sub-assemblies for offshore multi-megawatt turbines. The full dataset consists of over 1768 turbine years of operational data based on 350 offshore wind turbines. According to these studies, the blade pitch systems have the highest failure rates among the components and account for 24% [20] and 13.3% [21] of the total failures of wind turbines, respectively. These results confirm that pitch systems are the largest contributors to the total turbine failure rate.

The blade pitch system has an important role for pitch-regulated wind turbines, and the relevant faults change the aerodynamic torque, power, and response of the tower and the support structures. Faults in the blade pitch sensors and actuators influence the control feedback and result in imbalanced loads on the rotor, shaft, and main bearings.

The faults of the blade pitch system can be categorized into the pitch sensor and actuator faults. The pitch sensor faults occur by dust on an encoder disc, miss-adjustment of the blade pitch bearing, beyond the acceptable range of temperature and humidity or improper calibration. The incorrect pitch of a blade resulting from sensor faults causes asymmetrical forces on the blades and leads to unbalanced rotation in the rotor.

In the case of the pitch actuator faults, the high failure rate that is related to oil, valve and sludge issues accounts for a large portion (37.3%) of the total failure rate for hydraulic pitch systems as shown in Carroll et. al. [21]. Essentially, faults in the pitch actuator are mainly categorized as either mechanical or electrical faults. After these faults occur, the actuator cannot provide an adequate control of the blade pitch angle. In addition, high air content or hydraulic leakage faults in the pitch actuator can change the system's characteristics [23]. These faults affect the blade pitch angle and response delay. These faults can also affect the dynamic response of wind turbines and floaters in transient and steady-state condition. The incorrect pitching of a blade due to blade pitch faults causes

asymmetric forces on the blades, introducing an unbalanced rotation that significantly increases structural loads on the rotor and induces yaw motions of the floaters and tower base torsional bending moments. In the worst cases, it is associated with actuator seizure, which leads to inoperable conditions. Consequently, wind turbine failure rates and downtime should be reduced to ensure reliability. A method to avoid catastrophic long-term damage to the wind turbines is needed to allow for fast fault accommodation.

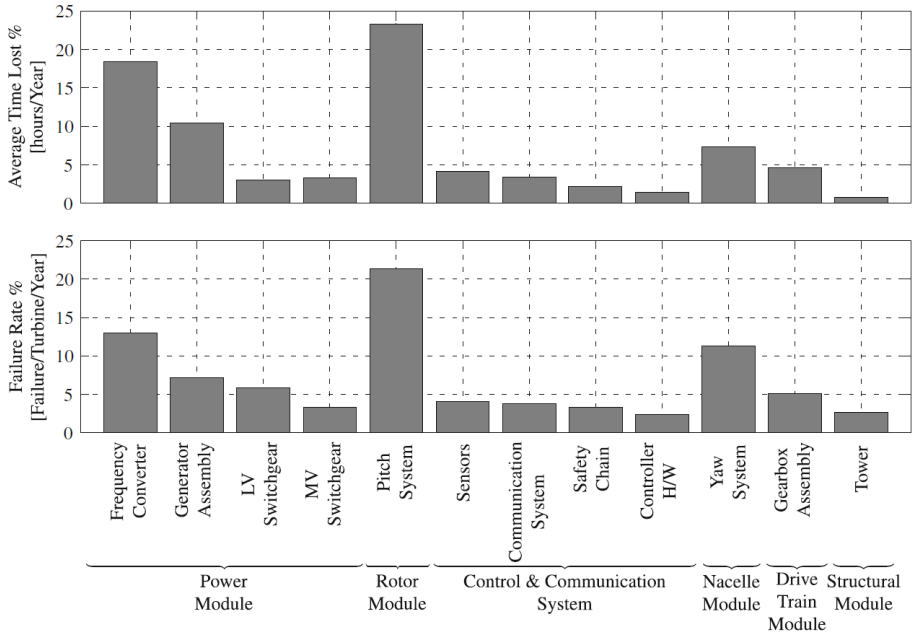

Figure 1.8: Normalized average time lost and failure rate of subsystems and assemblies for wind turbines. Values less than 2% are excluded. [20][22].

1.3.2. Maintenance strategies

Maintenance and optimal operations of offshore wind turbines have become critical issues. The ocean environment makes the maintenance of wind turbines much more complicated, raising the capital and operation costs to an undesired level because of the difficult and limited access. The reliability of an offshore wind turbine is even more important because maintenance costs account for 25-30% of the lifecycle cost of energy for offshore wind farms [24-26].

To achieve a further reduction in the cost of wind energy and ensure safety, it is essential to have proper maintenance strategies for maintaining the adequate safety level regarding fatigue, corrosion, wear, crack growth, and other degradation phenomena in the wind turbine components. An inspection and maintenance approach contributes to the safety with respect to a structural damage tolerance. Normally, the conventional maintenance strategies are corrective maintenance or a predetermined maintenance in fixed time intervals. With the corrective maintenance strategy, there is a high possibility that wind turbines that have undergone long downtimes, have a risk of damage or catastrophic failure because maintenance cannot be scheduled. Predetermined maintenance has the advantages of being schedulable allowing an efficient management than a corrective maintenance. However, the maintenance cost will be increased with regular component changes, human inspection and extra costs. Figure 1.9 illustrates the influence of the different maintenance strategies on the condition.

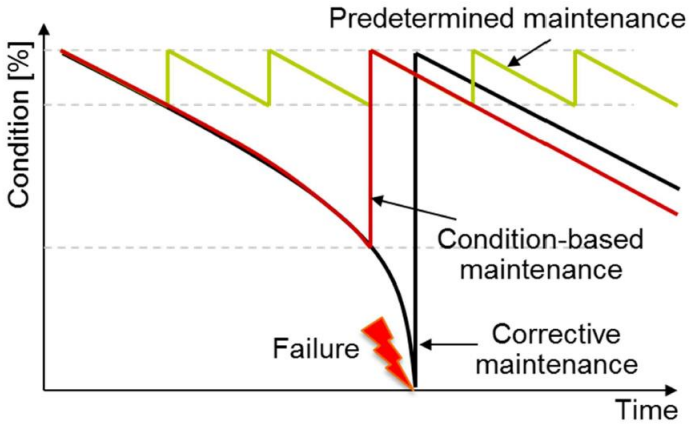

Figure 1.9: Influence of the maintenance strategy on asset condition [27].

In contrast with predetermined preventive maintenance, condition-based maintenance has a high potential to utilize the technical life of components. Condition-based maintenance is based on the information collected via measurements from condition monitoring. A number of sensors are installed on a wind turbine, e.g., anemometers, rotor speed sensors, pitch angle sensors, and vibration sensors for collecting data. The condition monitoring

with installed sensors can provide the operator with valuable information on the status of operational conditions.

Condition monitoring can identify a change in the dynamic responses of the wind turbine that represent deviations from the normal operational behavior and indicate a developing fault. In practice, 99% of equipment failures are preceded by certain indications and conditions that a failure is going to occur [24, 25].

To prevent equipment failures, fault detection and diagnosis in components at a very early stage should be conducted to give the operator opportunities to take remedial actions such as fault-tolerant control or shutdown. They are related to damage tolerant operational control before its consequences of the dangerous state of the wind turbine realized, such as tower or blade collapse. By taking appropriate steps from faults, severe damage of the monitored component and damage propagation to other components can be avoided.

However, condition monitoring still relies on an operator for information from observation and inspection, as well as determination of faults. When a fault alarm occurs, the operator takes some time to analyze the observation results. In this case, an automatic fault diagnosis function can be helpful for determining the fault types in a short amount of time, which provides enough time for a fast step to be taken, such as other operations, maintenance or repair after fault occurrence in the systems, and reduces costs as a result of possibly improved maintenance procedures [26, 27]. Therefore, condition monitoring and fault diagnosis schemes avoid unnecessary maintenance in wind turbines and provide diagnostic details for the maintenance staff by remote diagnosis, which leads to reduced repair or maintenance costs and minimizes the turbine downtime and the related revenue loss.

1.4. Fault detection and diagnosis

Fault detection and diagnosis (FDD) is a topic that has become a growing demand on operational reliability, safety and product quality. The general idea is to detect a fault occurrence in a system based on measured system data and to identify the characteristics of the fault type and its location in the system. Isermann and Ballé [28] provide definitions for important functions of such a scheme.

- Fault detection: determination of faults present in a system and the time of detection.
- Fault diagnosis: determination of the kind, size, location and time of a fault; follows fault detection.

Isermann [29] and Blanke et al. [30] provided overviews of fault detection and diagnosis techniques in practical aspects.

1.4.1. Fault detection

Fault detection methods are based on the model-based methods, and signal-based methods. These are distinguished from how the data are processed in the process of fault detection. The basic principle is to determine the relationship among the data, model, signal, and knowledge with various fault detection methods.

1.4.1.1. Model-based methods

A model-based method uses the system's input and measurement signals, which is based on the mathematical or knowledge models. Figure 1.10 shows the basic structure of model-based fault detection. Based on the input and measurement from output signals from the actual system, this method with appropriate models (healthy and faulty models) generates the residual formed as the difference between the measured data and estimated values. The residual can then be used as a fault indicator. The residual is close to zero when the system is under normal conditions. If a fault or unusual behavior occurs in the system, the residual begins to deviate from zero. The process of residual evaluation enables reliable decision-making with proper decision logic to present fault detection.

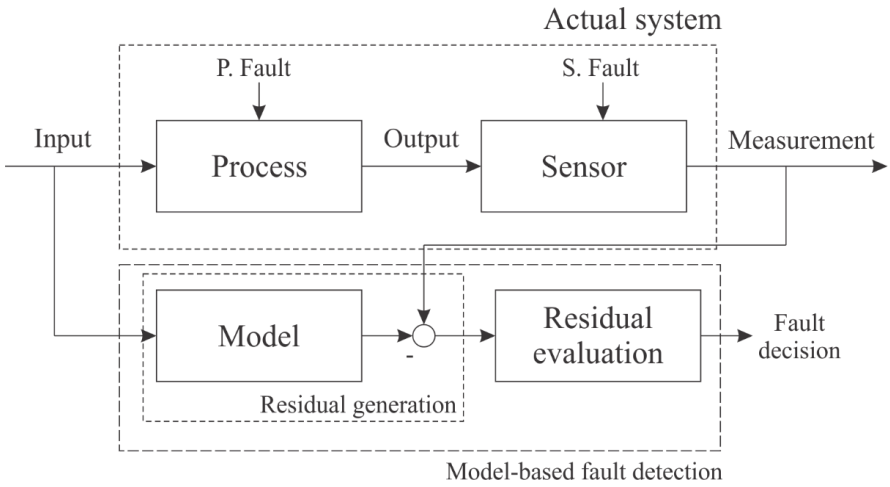

Figure 1.10: General scheme of model-based fault detection [31].

There are three types of model-based methods: 1) state and output estimators, also known as observers [31 - 35], 2) parity equations [36 - 38], and 3) identification and parameter estimation [39 - 41]. When the process parameters are all unknown, they can be determined by the parameter estimation in a model. If the process parameters are known, state estimation and parity equation methods can then be applied, which generate residuals with fixed parametric models for 1), fixed parametric or nonparametric models for 2), and adaptive nonparametric or parametric models for 3).

1.4.1.2. Signal-based methods

A signal-based fault detection method is based on the analyses of the features from the measured output signals. Suitable features from the measurements represent whether the operating conditions are under normal or fault conditions. These features can be determined by statistical methods, such as the mean, standard deviation, skewness, kurtosis, crest factor, or the power spectrum in the time and frequency domains. Figure 1.11 shows the basic scheme of the signal-based fault detection.

Signal-based methods are effective for irregular vibration detection in the mechanical components [29, 42 - 46]. The power spectrum from irregular vibration, which may correspond to particular instabilities, can be compared to find deviations from reference frequencies. In addition, other sensor signals such as the position, force, electrical current, and pressure contain oscillations with various frequencies under fault conditions compared to the normal process dynamics.

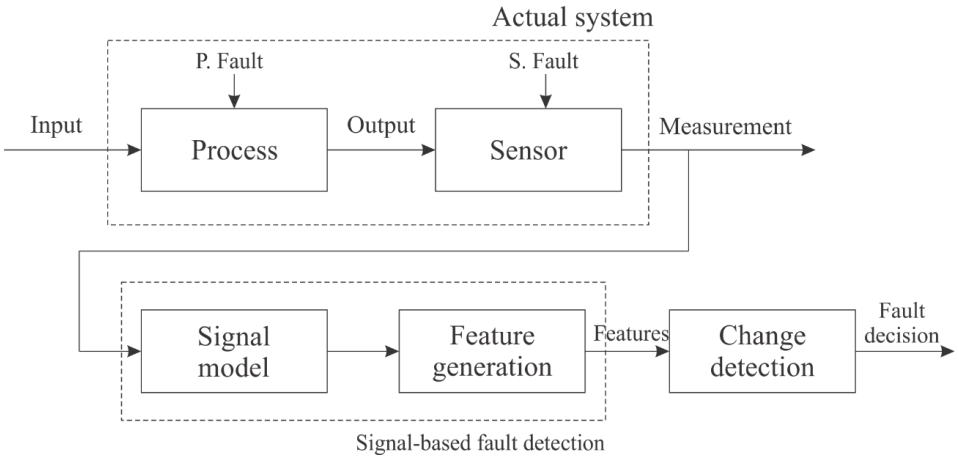

Figure 1.11: Scheme for the fault detection with signal models [29].

1.4.2. Fault diagnosis

In the condition monitoring of wind farms, there are various databases with an amount of collected and measured data from each sensor. The fault diagnosis methods need an exact function to determine the fault type with such details as the fault magnitude, location, and time of detection. In the diagnosis procedure with data acquisition and interpretation, the diagnosis system analyses and recognizes the fault patterns. Two types of algorithms can be distinguished: classification and inference methods. Classification methods can be applied for fault diagnosis in cases where the information of the fault-symptom causalities is not available. Otherwise, inference methods are applicable. Both approaches will be discussed in detail in the study.

1.4.2.1. Inference methods

If the relations between the faults and symptoms are at least partially known, then causal relations can be used: fault → events → symptoms. Inference methods are based on linguistic rules, which can be formulated in IF (condition) - THEN (conclusion) rules [47 - 49]. These methods allow conclusion to be drawn from the observed symptoms of the faults. If the condition with several symptoms is satisfied with causal relations, the fault type can be determined. When several symptoms indicate a fault, the facts are associated with AND and OR connectives, leading to Boolean rules in the form e.g. IF < S1 AND S2 > THEN < E1 >, IF < E1 AND E3 > THEN < F1 > as described in Figure 1.12.

Symptoms can be observed by heuristic methods from the operator in the form of measurements by inspection. These empirical methods can usually be represented in the form of qualitative measures. Therefore, mostly structured knowledge has to be included, which is known from inspection of the process faulty behavior.

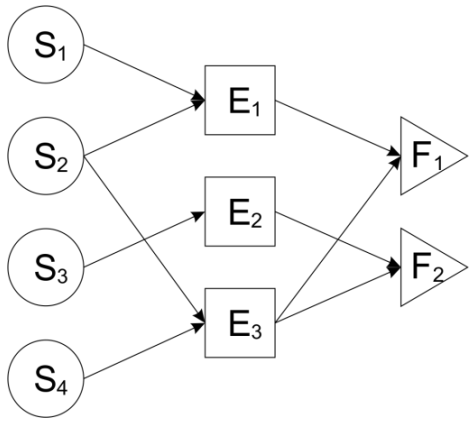

Figure 1.12: Inference methods for fault diagnosis [29].

1.4.2.2. Classification method

If the relations between features and faults are unknown, then classification methods can be used. Classification methods perform pattern recognition using data with a set of input patterns that consider their statistical variation. The classification algorithms are able to classify the data into different categories by a particular pattern. In this procedure, it is important to design a feature extractor that transforms the raw data into a suitable feature vector from the classification algorithm. Pattern recognition systems are in many cases trained by supervised learning from labeled training data. However, when the data are unlabeled, unsupervised learning can be used to discover the previously unknown patterns.

Classification methods can be divided by geometrical probabilistic classification [50 - 52], machine learning [53 - 58], and fuzzy clustering methods [59 - 62]. In recent years, machine learning (ML) has led to huge leaps for artificial intelligence (AI) and internet of things (IoT), which requires massive amounts of data collected by sensors to continue being online. Machine learning allows for a machine to be fed with raw data and to automatically discover the representations needed for classification or regression. Machine learning algorithms build a mathematical model of training data to make predictions or decisions without being explicitly programmed to perform the task. Machine learning algorithms have been applied to the applications of computer vision, speech recognition, language translation, and email filtering, where it is infeasible to develop an algorithm of specific instructions for performing the task. Machine learning algorithms can also be used for fault diagnosis in mechanical components. Figure 1.13 shows the general scheme of machine learning.

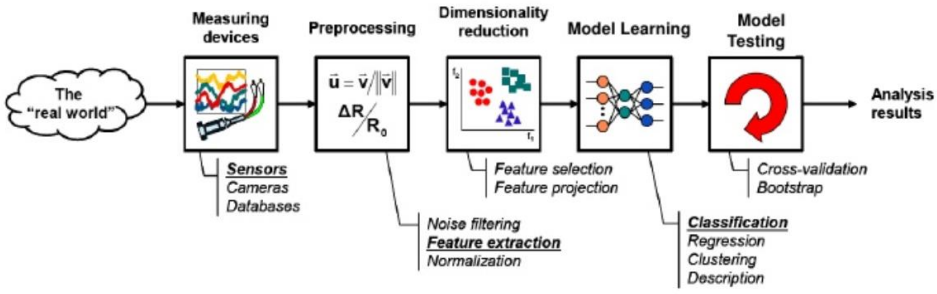

Figure 1.13: General scheme of machine learning [63].

1.5. Fault tolerant control

If the system domain experiences faults or are no longer available, then the nominal controller cannot provide the correct control to the system under unexpected faults. To maintain the operational condition in the system, it is necessary to use a different set of input and output signals. Then, a fault-tolerant control (FTC) is needed to manage the faulty system before maintenance is conducted. The fault-tolerant control is used for preventing component failures after the consequences of faults in the system.

Fault-tolerant control (FTC) methods can be divided into two categories: passive and active FTC methods [30]. In passive FTC systems [64, 65], the controllers are fixed control systems that are predetermined to be robust against faults and uncertainties throughout the entire system. Passive FTC methods are optimized while satisfying a specific fault scenario, which implies that it has limited fault-tolerant capabilities for various faults.

Active FTC methods [66 - 70] can compensate for tolerable faults by interacting with any nominal controllers to cancel the fault effects on the system. The active FTC consists of reconfiguration blocks that are linked to the nominal controller under fault conditions.

Active fault-tolerant control systems need FDD schemes due to fault information and they need to send reconfiguration signals to the nominal controller as shown in Figure 1.14. The main concept underlying this FTC scheme is to reconstruct the system output to replace the faulty measurement. Because faulty measurement cannot be used with the existing controller, a configuration block must be found that generates a suitable signal from a faulty measurement. This reconfiguration system applies a minimal change to the control loop. The existing controller then remains in the system of the control loop.

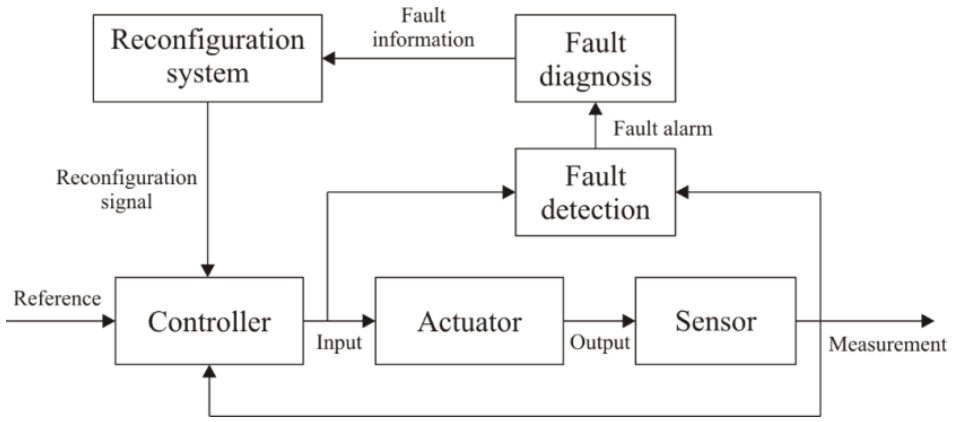

Figure 1.14: Active fault-tolerant control system based on fault detection and diagnosis.

1.6. Research objectives and contributions

1.6.1. Research objective, questions and methods

The main objective of this PhD work is to develop model-based FDD and FTC schemes that can detect, diagnose and accommodate faults in the blade pitch system of a wind turbine at an early stage. The main research questions (RQs) are how we can build a mathematical model of a blade pitch system, apply fault detection and fault diagnosis, and include fault-tolerant control schemes.

RQ1: How to build a blade pitch actuator model and link it to the global model of a floating wind turbine?

RQ2: How to apply control to the blade pitch actuator to achieve the demanded pitch angle?

RQ3: What type of faults will typically occur in this blade pitch system, and what is the influence of the turbine structure?

RQ4: What methods are used to develop FDD and FTC algorithms?

RQ5: How to verify the effectiveness of the proposed FDD and FTC schemes?

To answer these research questions (RQ), the author primarily distinguished three different research subjects: i) modeling and control, ii) fault detection, diagnosis, and fault-tolerant control, and iii) validation with numerical simulations. As the research continued, the RQs gave the results related to the appropriate methods, and Figure 1.15 shows the overall relations among the research questions, methods, and contributions. Figure 1.16 shows the scopes of the appended papers that are interconnected in this thesis, which shows how all paper are related.

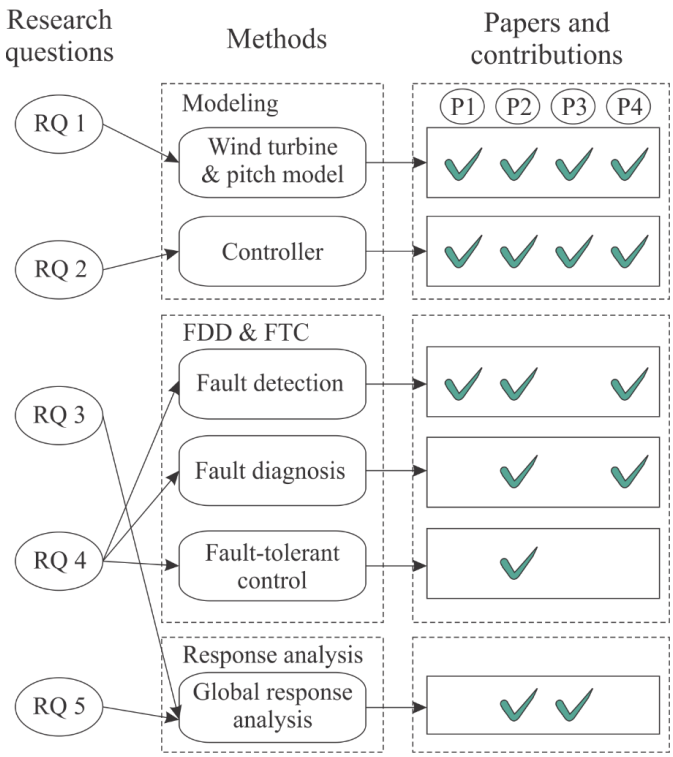

Figure 1.15: The relationship among the research questions (RQs), methods, and contributions.

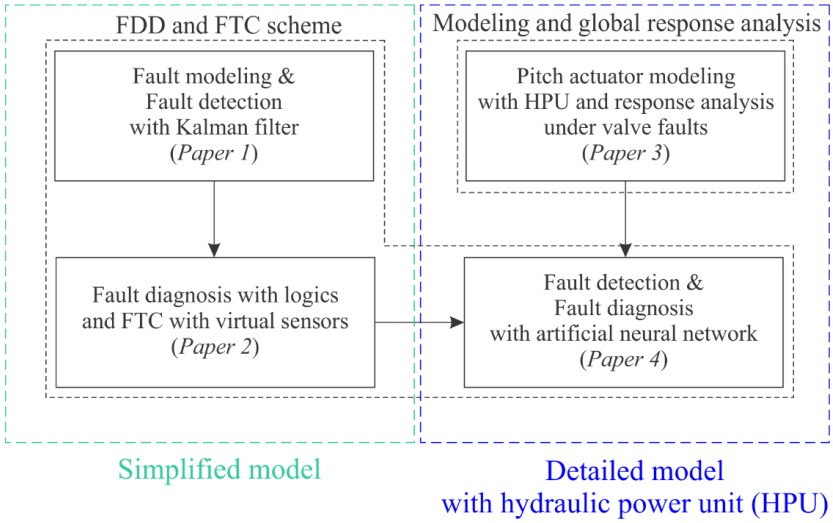

Figure 1.16: The scope of the thesis and the interconnection among appended papers.

1.6.2. Summary of the papers

Paper 1: Model-based fault detection of blade pitch system in floating wind turbines

• Status: Published in Journal of Physics: Conference Series 2016; 753, 092012.

• Authors: Seongpil Cho, Zhen Gao and Torgeir Moan

• Summary: Maintenance and repair of offshore wind turbines are challenging because of their difficult access. Specifically, faults occur unexpectedly in the components of wind turbines, such as the blades, drivetrain or generator. Faults in wind turbines can directly influence the operational safety, dynamics and power production efficiency of wind turbines. An early-stage fault detection technique should be conducted regarding maintenance and repair to prevent a catastrophic failure of wind turbines with active fault accommodation.

This paper presents a model-based fault detection scheme for a blade pitch system of floating wind turbines. To detect the faults of the blade pitch actuators and sensors, a Kalman filter is designed to estimate the states of the system. Residuals are generated by a Kalman filter and a threshold using H_∞ optimization, and linear matrix inequality (LMI) is used for the residual evaluation. The proposed method is demonstrated by case studies with bias (PSB) and fixed output (PSF) in pitch sensors and stuck (PAS) in pitch actuators. The simulation results show that the proposed method detects different realistic fault scenarios of wind turbines under the stochastic external winds and wave conditions.

Paper 2: Model-based fault detection, fault isolation, and fault-tolerant control of a blade pitch system in floating wind turbines

• Status: Published in Renewable Energy 2018; 120, 306-321.

• Authors: Seongpil Cho, Zhen Gao and Torgeir Moan

• Summary: After a successful fault detection, the main challenge is fault diagnosis. In this diagnosis procedure, the determination of the fault characteristics should be conducted, and a fault diagnosis system should analyze the pattern of faults for the decision making. Then, a fault-tolerant control (FTC) is needed to manage the faulty system before maintenance is conducted.

This paper presents model-based fault detection, fault diagnosis, and fault-tolerant control schemes focused on blade pitch systems in floating wind turbines. Faults in blade pitch systems should be detected at an early stage to prevent inoperable conditions in the wind turbine. To detect faults of the blade pitch systems, a Kalman filter is designed to estimate the blade pitch angle of the system and determine the fault time.

The fault diagnosis algorithm is based on inference methods and is capable of determining the fault type, location, and magnitude. The fault-tolerant controller with virtual sensors and a shutdown mode controls the floating wind turbine to avoid unexpected external loads. The proposed methods are demonstrated in case studies with stochastic wind and wave conditions that consider different types of faults, such as PSB, PSF, and PAS. The simulation results show that the proposed methods can detect and diagnose multiple faults effectively at an early stage. Additionally, the effectiveness of the fault-tolerant control systems for different load cases for single and multiple fault conditions is verified by numerical simulations.

Paper 3: Numerical modeling of the hydraulic blade pitch actuator in a spar-type floating wind turbine considering fault conditions and their effects on global dynamic responses

• Status: Published in Wind Energy 2019; Early View Publication, 1-21.

• Authors: Seongpil Cho, Erin E. Bachynski, Amir R. Nejad, Zhen Gao and Torgeir Moan.

• Summary: A previous blade pitch system has been modeled in Papers 1 and 2 based on the simplified model. However, this model cannot represent the exact faults in the actuator component. This paper presents the dynamic modeling and response analysis of the hydraulic pitch actuator in a floating spar-type wind turbine under valve fault conditions. A spar-type floating wind turbine concept is modeled and simulated using an aero-hydro-servo-elastic simulation tool (Simo-Riflex). A numerical model of the hydraulic blade pitch actuator with/without valve faults is developed and linked to Simo-Riflex to study the effects of faults on the global responses of the spar wind turbine, as a function of the fault magnitude and environmental conditions.

The hydraulic pitch actuator system has a high failure rate, due to oil and valve faults such as excessive friction, slit-lock on spool, wrong applied voltage, and short-circuit of the solenoid. The consequence of valve faults in a pitch actuator is that the blade cannot be pitched to the desire angle, such as a response delay, stuck, or runaway. These faults lead to an increased rotor imbalance, which has different effects on the turbine structure and the platform motion. The proposed methods are demonstrated in case studies with stochastic wind and wave conditions and different types of valve faults in pitch actuators.

Paper4: Fault detection and diagnosis of a blade pitch system of a spar-type floating wind turbine based on a hybrid approach with a Kalman filter and artificial neural network

• Status: Submitted to Wind Energy

• Authors: Seongpil Cho, Minjoo Choi, Zhen Gao and Torgeir Moan

• Summary: This paper proposes a fault detection and diagnosis method to automatically identify different fault conditions of a blade pitch system in a floating wind turbine. For fault detection, a Kalman filter is employed to estimate the blade pitch angle and the valve spool position of the system. The fault diagnosis scheme is based on an artificial neural network that is capable of determining the fault type. The proposed methods are demonstrated in case studies with stochastic wind and wave conditions that consider different types of faults, such as biases and fixed outputs in pitch sensors and excessive friction, slit-lock, wrong applied voltage, and short-circuit in actuators. The validation of the ANN model is conducted with the training model in order to prove the model's performance. The test results show that the proposed fault diagnosis methods can diagnose faults effectively with a good performance.

1.7. Thesis Structure

This thesis consists of 5 chapters and 4 appended papers, given in appendix A.

Chapter 2: Modeling of a spar floating wind turbine and a blade pitch actuator

Chapter 2 gives the basic knowledge on a blade pitch system and a baseline control system of a spar floating wind turbine under stochastic environmental loads. The mathematical model of a stochastic wind field and irregular sea waves are explained. The basis of the aero-hydro-servo-elastic model used in Simo-Riflex is explained afterwards. This chapter ends with the controller model used in this thesis.

This chapter also addresses the numerical modeling of a hydraulic pitch actuator with a simplified model and detailed model with hydraulic power units. The remainder of the chapter presents the summary of the work performed in Paper 3.

Chapter 3: Fault detection, diagnosis and fault-tolerant control of a blade pitch system using a simplified model

Chapter 3 presents the fault detection, diagnosis and fault-tolerant control scheme on a blade pitch actuator using a simplified model and appropriate fault models. The remainder of the chapter includes the simulation results based on the performance of the FDD and FTC schemes under fault conditions. Papers 1 and 2 are partly presented in this chapter.

Chapter 4: Fault detection and diagnosis of a blade pitch system using a detailed model with hydraulic power units

Chapter 4 describes a fault detection and diagnosis method to automatically identify different fault conditions of a blade pitch system with hydraulic power units in a floating wind turbine. An overview on the simulation results based on the accuracy and performance of fault diagnosis in the wind turbine is given afterwards. The overview on the fault detection and diagnosis scheme is explained, as well as how to apply this scheme to other fields. Paper 4 presents the full story of this chapter.

Chapter 5: Concluding remarks and recommendations for future work

Chapter 5 presents a summary of the works, main contribution and conclusions in this thesis. The chapter is closed with recommendations for future work.

2. Modeling of a spar floating wind turbine and a blade pitch actuator

2.1. Spar type floating wind turbine concept

A spar-type floating wind turbine is modeled as a rotor, nacelle, tower, floater, and mooring lines. The model in this thesis is based on the NREL 5 MW offshore wind turbine model [71], supported by a spar buoy floater (OC3-Hywind) [72] and three catenary mooring lines as shown in Figure 2.1. The NREL 5 MW wind turbine is a conventional three bladed upwind turbine designed by the National Renewable Energy Laboratory (NREL). This model has been used as a standard reference for baseline offshore wind turbine specifications.

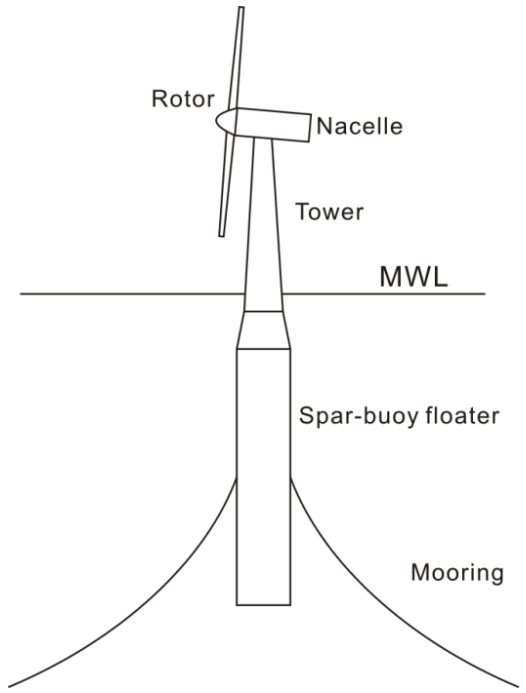

Figure 2.1: Schematic view of the floating wind turbines.

The OC3-Hywind spar-buoy platform was developed in the Offshore Code Comparison Collaboration (OC3) project. The OC3-Hywind platform features a deeply drafted, slender spar-buoy moored by three catenary mooring lines. The specifications of the NREL 5 MW reference wind turbine are provided in Table 2.1. Additionally, properties for the OC3-Hywind floater and mooring system are listed in Table 2.2 and Table 2.3, respectively.

Table 2.1: Properties of the NREL 5 MW wind turbine [71].

Rated Power (MW)	5
Rotor orientation, Configuration	Upwind, 3 blades, horizontal axis
Rotor diameter (m)	126
Hub height from the mean water level (m)	90
Cut-in, rated, cut-out wind speed (m/s)	3, 11.4, 25
Cut-in, rated rotor speed (°/s)	41.4, 72.6
Max pitch rate (°/s)	8
Gearbox ratio	97

Table 2.2: Properties of the OC3-Hywind floater [72].

Draft (m)	120
Diameter above taper (m)	6.5
Diameter below taper (m)	9.4
Center of mass (m)	(0, 0, -89.9115)
Mass, including ballast (kg)	7.466×10^6
Mass moment of inertia, I_{xx} and I_{yy} (kg·m^2)	4.229×10^9
Mass moment of inertia, I_{zz} (kg·m^2)	1.642×10^8

Table 2.3: Mooring system properties [72].

Angle between adjacent lines (deg)	120
Depth to anchors below SWL (Water depth) (m)	320
Depth to fairleads below SWL (m)	70
Mooring line diameter (m)	0.09
Equivalent mooring mass density (kg/m)	77.7066
Equivalent mooring weight in water (N/m)	698.094
Equivalent mooring extensional stiffness (N)	3.842×10^8
Additional yaw spring stiffness (Nm/rad)	9.834×10^7

2.2. Blade pitch actuator

The blade pitch systems in modern wind turbines are driven by electrical or hydraulic pitch actuators [73] as shown in Figure 2.2. An electrical pitch system adjusts the blade pitch angle using gears with an electric motor and it is able to precisely control the position. The main challenges related to electrical pitch systems are gear wear, high backlash, and low robustness against external disturbances.

On the other hand, a hydraulic pitch actuator controls the blade pitch angle by moving a hydraulic cylinder driven by a hydraulic power unit and gears are unnecessary. Hydraulic systems with a high level of stiffness and appropriate damping [74] are suitable in the case of high aerodynamic loads in large wind turbines (5 – 10 MW). In addition, hydraulic pitch actuators have a low component sensitivity to the environment with the working temperature spanning from -25°C to +55°C, which is suitable for offshore environmental conditions. The oil in the system reduces the structural vibrations and power peaks/loads, and increases the overall reliability of the turbine [75]. In this thesis, the hydraulic pitch actuator is only considered because of these reasons. The hydraulic pitch actuator can be in 2 different ways: a simplified pitch actuator and a blade pitch actuator with a hydraulic power unit.

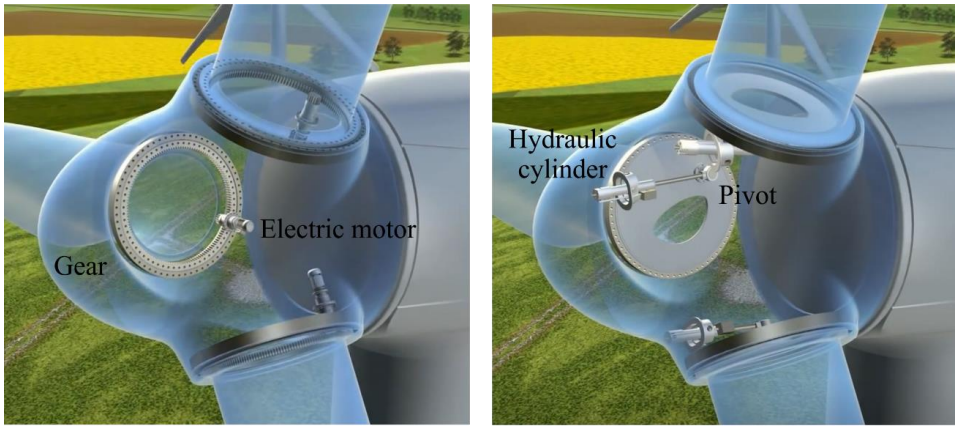

Figure 2.2: Electrical (a) and hydraulic (b) pitch actuator placed in a hub [76].

2.2.1. Simplified blade pitch actuator model

A commonly used three-blade wind turbine consists of three identical independent pitch actuators. A pitch actuator can be modeled as a 2nd order differential equation for a simplified global analysis. The blade pitch system is described as the following equation:

$$\ddot{\beta}_i + 2\zeta_{bp}\omega_{bp}\dot{\beta}_i + \omega_{bp}^2\beta_i = \omega_{bp}^2\beta_{C,i},\ i = 1,\ 2,\ \text{and}\ 3\ \text{(the blade number)}, \tag{2.1}$$

where ζ_{bp} is the damping ratio, ω_{bp} is the natural frequency of the blade pitch actuator, and $(\dot{})$ represents time derivatives. Additionally, β_i is the i^{th} blade pitch angle, and $\beta_{C,i}$ is the blade pitch angle command. The parameters are $\omega_{bp} = 11.11$ rad/s and $\zeta_{bp} = 0.6$ [23].

2.2.2. Blade pitch actuator model with a hydraulic power unit

The hydraulic pitch actuator can be driven by a hydraulic power unit. The blade pitch actuator as simplified model, was described in Eq. (2.1). Actuator faults in a simplified model can only represent changed dynamics in the change of the natural frequency and damping ratio changes such as pump wear, hydraulic leakage, or high air content [23]. However, this simplified model has limitations when applying various actuator faults in the hydraulic blade pitch actuator. Therefore, it is essential to model the hydraulic power unit to apply various actuator faults.

The hydraulic power unit consists of a hydraulic pump, an accumulator, a set of directional control valves, and a hydraulic cylinder. The blade pitch angle is controlled by a hydraulic cylinder placed in the hub of the turbine. The oil flow to and from the cylinders is controlled by a number of control valves. The energy to drive the hydraulic cylinders is supplied by a power unit placed in the nacelle, and the energy is transferred to the cylinder as oil flow.

The valve controller gives a command voltage signal to control the valve spool position based on PI control. The schematic diagram of a hydraulic actuator, as shown in Figure 2.3(a), consists of a constant pressure pump, an accumulator, a reservoir, a hydraulic cylinder, and a directional control valve. Figures 2.3(b) and 2.3(c) depict the hydraulic actuator, including the cylinder and the hydraulic power unit with a pressure pump, an accumulator, a reservoir, and valves.

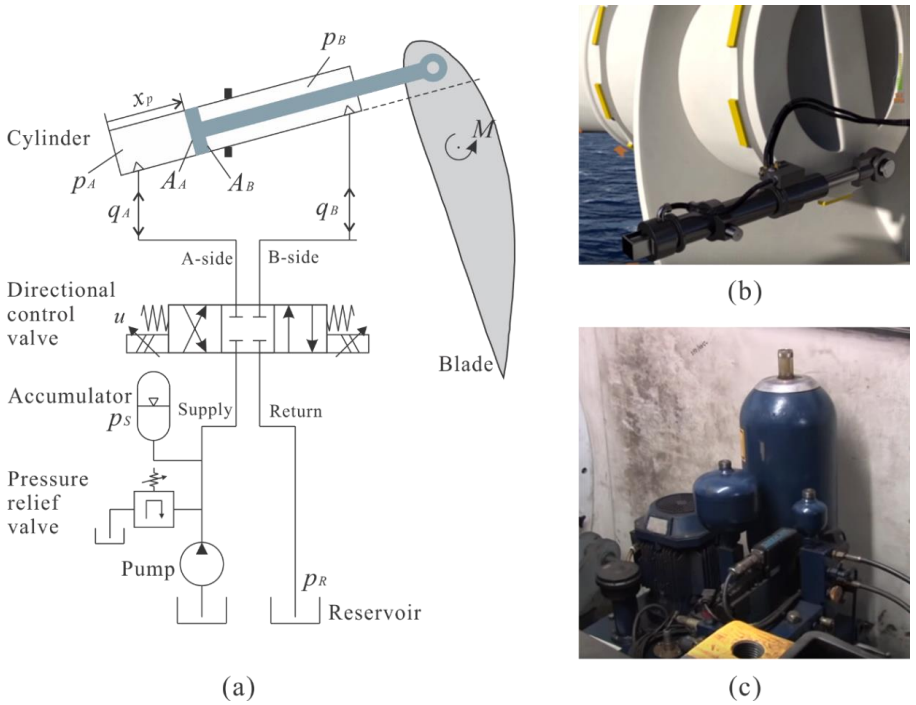

Figure 2.3: The hydraulic pitch system: (a) schematic diagram, (b) hydraulic actuator [77], and (c) hydraulic power unit [78].

2.2.2.1. Directional control valve model

The directional control valve controls the valve spool position to open and close the valves by using an electromagnetic field via the solenoid coil to move an internal steel armature assembly. Current through the coil in the solenoid generates a magnetic field across the air gap. The magnetic field produces a force between the opposing stator and the armature. The armature makes the valve spool move to the left and right sides. Figure 2.4 shows the schematic of a 4/3 directional control valve with a solenoid.

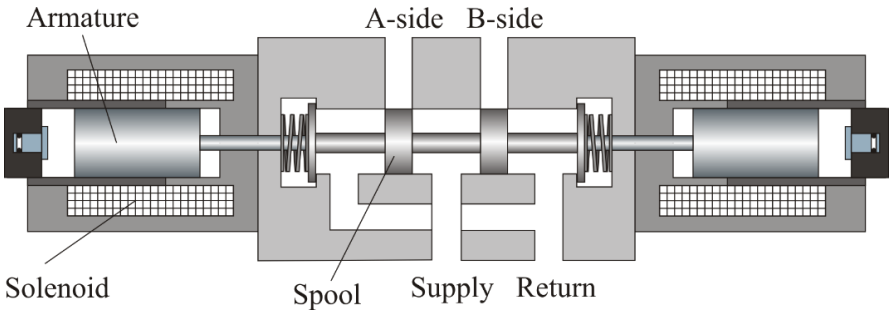

Figure 2.4: 4/3 directional control valve with a solenoid.

To control the blade pitch angle, the valve controller adjusts the hydraulic flow into the cylinder. The valve model is simplified through a second order system [79]. The valve system is then explained by the following equation:

$$\ddot{x}_{vs,i} + 2\zeta_{vs}\omega_{vs}\dot{x}_{vs,i} + \omega_{vs}^2 x_{vs,i} = \omega_{vs}^2 k_u u_{vs,i}, \; i = 1, 2, \text{ and } 3 \text{ (the blade number)}, \tag{2.2}$$

where x_{vs} is the valve spool position, u_{vs} is the control input voltage, ω_{vs} is the valve natural frequency and ζ_{vs} is the valve damping ratio of the valve system. k_u is the voltage gain and $(\dot{})$ represents the time derivatives. It is assumed that the valve spool is symmetric and zero-overlap design. k_u simplified the valve model to being only directly controlled by u_{vs}.

The hydraulic flow rate at A and B can be determined based on the spool position. The continuity equation of the hydraulic flow rate at A and B depends on the sign of the spool position,

for $x_{vs} > 0$,

$$\begin{aligned} q_A &= -k_q x_{vs}\sqrt{p_A - p_R}, \\ q_B &= k_q x_{vs}\sqrt{p_S - p_B}, \end{aligned} \tag{2.3a}$$

and for $x_{vs} < 0$,

$$\begin{aligned} q_A &= -k_q x_{vs}\sqrt{p_S - p_A}, \\ q_B &= k_q x_{vs}\sqrt{p_B - p_R}, \end{aligned} \tag{2.3b}$$

where q_A and q_B are the hydraulic flow rates to the cylinder chamber A and B sides, k_q is the valve flow coefficient, and p_S and p_R are the supply pressure and the return pressure, respectively. Table 2.4 describes properties for the directional control valve from Rexroth's valve model (RE 29093, Size 16) [80]. The supply pressure p_S is controlled to 250 bar. The k_q values can be estimated from [81, 82] with the nominal pressure drop (Δp_N) and nominal flow rate (q_N) from Rexroth's valve model [80].

Table 2.4: Properties of the directional control valve [80].

Valve natural frequency, ω_{vs} (rad/s)	141
Valve damping ratio, ζ_{vs}	0.74
Minimum, maximum valve position, $x_{vs,min}$, $x_{vs,max}$ (m)	-0.02, 0.02
Minimum, maximum input voltage, $u_{vs,min}$, $u_{vs,max}$ (V)	-10, 10
Valve voltage gain, k_u (m/V)	0.002
Valve flow gain, k_q ($\mathrm{m}^2/\mathrm{s}/\sqrt{\mathrm{bar}}$)	0.0233

2.2.2.2. Blade pitch dynamics

As illustrated in Figure 2.3, a cylinder model in the actuator is a single-rod and double-acting cylinder that consists of a piston. The cylinder produces the force from the hydraulic pressure acting on the piston from the oil flow. The pressure dynamics based on the flow mechanism into two chambers (A and B sides) in the cylinder are written by

$$\dot{p}_A = \frac{E_{eff}}{V_A(x_p)}(q_A - A_A\dot{x}_p), \tag{2.4a}$$

$$\dot{p}_B = \frac{E_{eff}}{V_B(x_p)}(q_B + A_B\dot{x}_p), \tag{2.4b}$$

where V_A and V_B are the total control volume of chambers A and B, respectively, depending on the piston position x_p. A_A and A_B are the areas of the piston on the A and B sides, respectively. E_{eff} is the effective bulk modulus of the hydraulic fluid, which is assumed to be incompressible.

By calculating the hydraulic pressures on sides A and B of the cylinder, the piston force F can be obtained:

$$F = P_A A_A - P_B A_B. \tag{2.5}$$

The blade pitch angle can be controlled by a pitch moment from the piston force F. Figure 2.5 shows the geometry of the hydraulic pitch actuator. The geometry has a relationship between the piston position x_p and the pitch angle β, described as

$$x_p(\beta_p) = \sqrt{L_p^2 + r_p^2 - 2L_p r_p \cos(\alpha_0 - \beta)} - l_p/2, \tag{2.6}$$

where r_p is the torque arm, l_p is the rod length, L_p is the length between the pivot and the rotational center, and α_0 is the initial angle between the pin-to-center axis and the torque arm when $x_p = 0$. From the geometry of this actuator, the blade pitch moment $M_{T,p}$ can be described by

$$M_{T,bp} = F r_p g(\beta), \tag{2.7}$$

where $g(\beta_p)$ is a force factor represented by $g(\beta) = \frac{1}{r_p}\frac{dx_p}{d\beta}$.

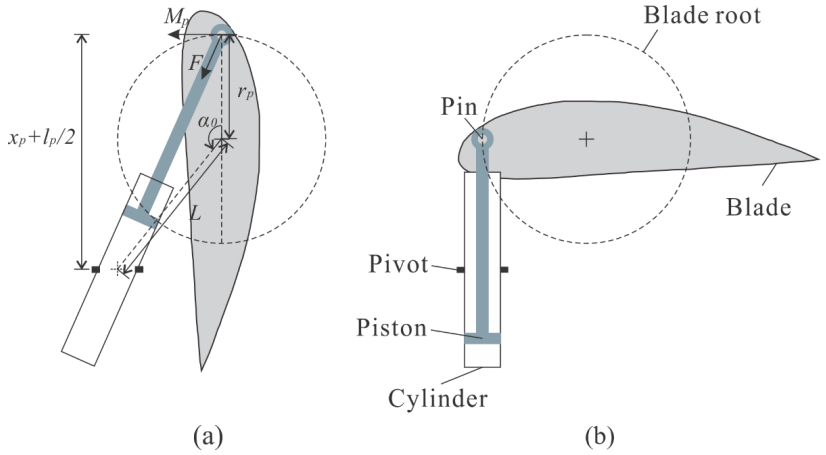

Figure 2.5: Geometry of the blade pitch actuator: (a) β = 0 ° and (b) β = 90 °.

The blade pitch angle dynamics are described by

$$J_{bp}\ddot{\beta} + B_{bp}\dot{\beta} = M_{T,bp} + M_A, \tag{2.8}$$

where J_{bp} is the blade inertia, B_{bp} is the viscous damping coefficient of the blade pitch, and M_A is the aerodynamic pitching moment.

Table 2.5 shows the pitch actuator geometries and parameters.

Table 2.5: Pitch actuator geometries and parameters [83].

Piston rod length, l_p (m)	2
Torque arm, r_p (m)	1
Pin-to-center axis length, L_p (m)	1.7
Initial angle, α_0 (rad)	2.5128
Blade pitch inertia, J_{bp} (kg·m^2)	28600
Blade pitch viscous damping coefficient, B_{bp} (N·s/rad)	8.545×10^5
Effective bulk modulus, E_{eff} (bar)	18000

2.2.2.3. Valve spool position control

The geometrical relationship, as described in Eq. (2.6), is the relationship between β and x_p. x_p is controlled by the valve spool position x_{vs} corresponding to the desired position [84]. The valve spool position is controlled according to the control input voltage in the directional control valve.

The control input u_{vs} can be calculated by a PI controller from the piston position error $e(t)$, that is,

$$u_{vs}(t) = k_p\left(e(t) + \frac{1}{T_i}\int_0^t e(\tau)d\tau \right), e(t) = (x_p(\beta) - x_p(\beta_C)), \tag{2.9}$$

where k_p is the proportional gain, T_i is the integral time, and the position error $e(t)$ is given as a function of the blade pitch angle β and the blade pitch command β_C from the baseline controller. Paper 3 describes how to calculate k_p and T_i with Routh's methods, and the Ziegler-Nichols method, as described in [85].

2.3. Fully coupled numerical model

The dynamic responses of the wind turbine model have been simulated with Simo-Riflex-Aerodyn (SRA) [86, 87, 88], which is an aero-hydro-servo-elastic code for fully coupled nonlinear time-domain numerical simulations of offshore wind turbines. Hydrodynamic forces and moments on the rigid hull, according to first order potential flow theory and Morison-type viscous drag, have been accounted for in Simo [86]. The flexible elements for the tower, shaft, mooring system and blades are modeled in Riflex [87] with the finite element solver. Aerodyn [88] calculates the aerodynamic forces and moments on the blades based on the blade element momentum (BEM) method or the generalized dynamic wake (GDW) including tower shadow, dynamic stall, and skewed inflow correction. The models for structural dynamics, hydrodynamics, aerodynamics, and mooring line dynamics are simultaneously considered with an external code that consists of 1) a baseline control system for a torque and pitch controller and 2) a model of the blade pitch system under various operational conditions. Figure 2.6 (a) shows the data transmission of Simo-Riflex-Aerodyn (SRA) and the controller algorithm.

For the modeling of a blade pitch actuator with the hydraulic power unit described in Section 2.2, the fully coupled model needs to be modified because other physical values are transferred: the blade pitch moment. To conduct data transmission between Riflex and the Java code, Simo-Riflex (SR) ver. 4.15 developed by SINTEF Ocean has been used for numerical simulation. In SR ver. 4.15, Riflex takes the role of calculating the aerodynamic forces and moments on the blades based on the BEM on behalf of the Aerodyn. Figure 2.6 (b) shows the data transmission of the SR and controller algorithm. The simulation was first conducted by SRA in Papers 1 and 2. Eventually, SR was used for simulations in Papers 3 and 4. In addition, SR can be used also for the previous studies in Papers 1 and 2.

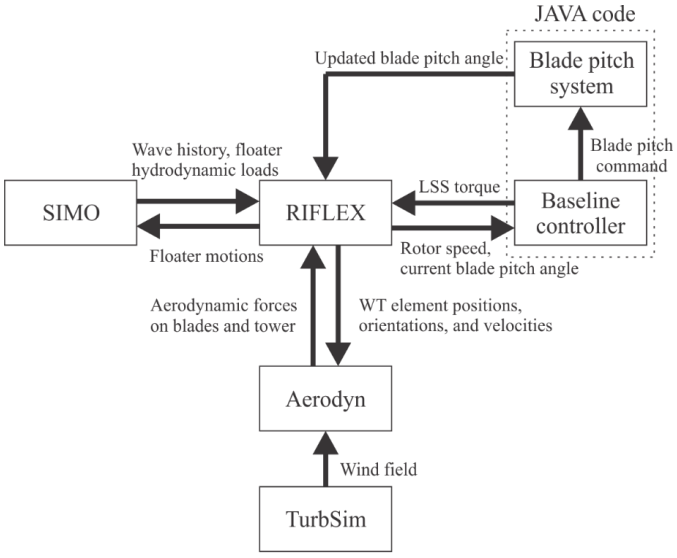

(a) Simo-Riflex-Aerodyn (SRA)

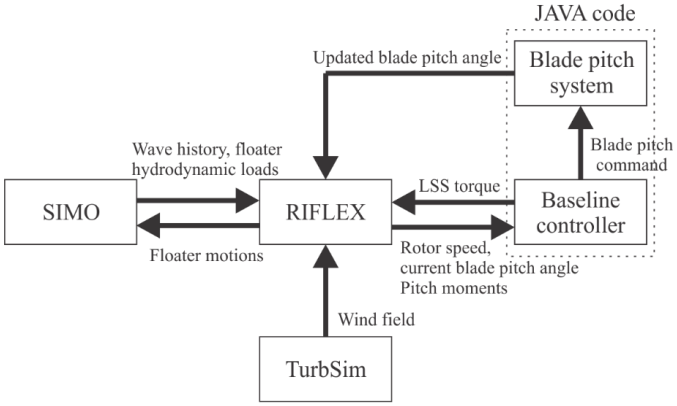

(b) Simo-Riflex (SR)

Figure 2.6: Data transmission between the fully coupled model and controller: (a) SRA and (b) SR.

2.4. Wind turbine control strategies under normal and fault conditions

Wind turbines are normally designed to maximize the generated power and ensure continued reliability during operation. The region from the cut-in wind speed to the cut-out wind speed is divided into below-rated (Region II) and above-rate regions (Region III) of the wind speed, as illustrated in Figure 2.7. A baseline control system can be used to optimize the power productivity of a wind turbine in operational regions (Region II and III).

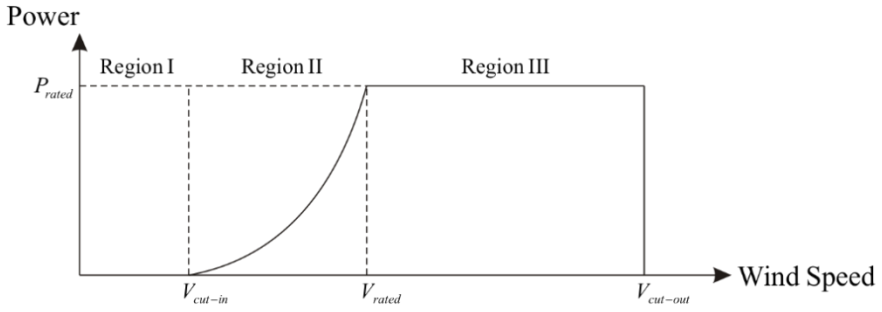

Figure 2.7: Ideal power curve as a function of the mean wind speed at the nacelle height on the wind speed characteristics.

The baseline control system has a blade pitch and generator torque controller. In Region II, the maximum power is captured by adjusting the generator torque maintaining an optimal tip speed of the blades [71]. Within this region, the blade pitch controller is not active. In Region III, the blade pitch controller is activated to adjust the blade pitch angle to keep the aerodynamic loads within a rated power output at a constant rotor speed. A blade pitch command is computed based on the gain-scheduled proportional-integral (PI) controller as the function of the generator torque error based on a constant-torque strategy [89] in floating wind turbines.

Figure 2.8 shows a block diagram of the baseline control system that represents how the system makes the blade pitch system interact with other systems by measuring the generator speed and pitch angle. The parameters can be described, where Ω_r is the rotor speed, Ω_g is the generator speed, $\Omega_{g,m}$ is the measured generator speed, $\Omega_{g,rated}$ is the rated generator speed, Q_g is the generator torque, Q_a is the aerodynamic torque, β_m is the measured blade pitch angle, and V_{wind} is the wind speed.

Since this baseline controller includes the pitch actuator and sensor models, the controller and model need to be validated by the control performance. Figure. 2.9 shows the comparison of the control performance with different blade pitch models: 1) NREL blade pitch model (BPNREL), 2) simplified blade pitch actuator, and 3) blade pitch actuator

with the hydraulic power unit. The BPNREL model assumes that the demanded pitch angle can be obtained with a certain pitch rate and no pitch actuator dynamics are considered. In this figure, the performances are almost identical for the three methods.

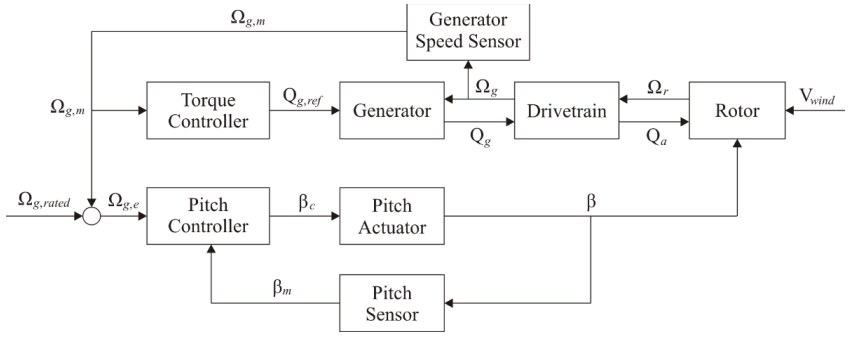

Figure 2.8: A block diagram of the baseline control.

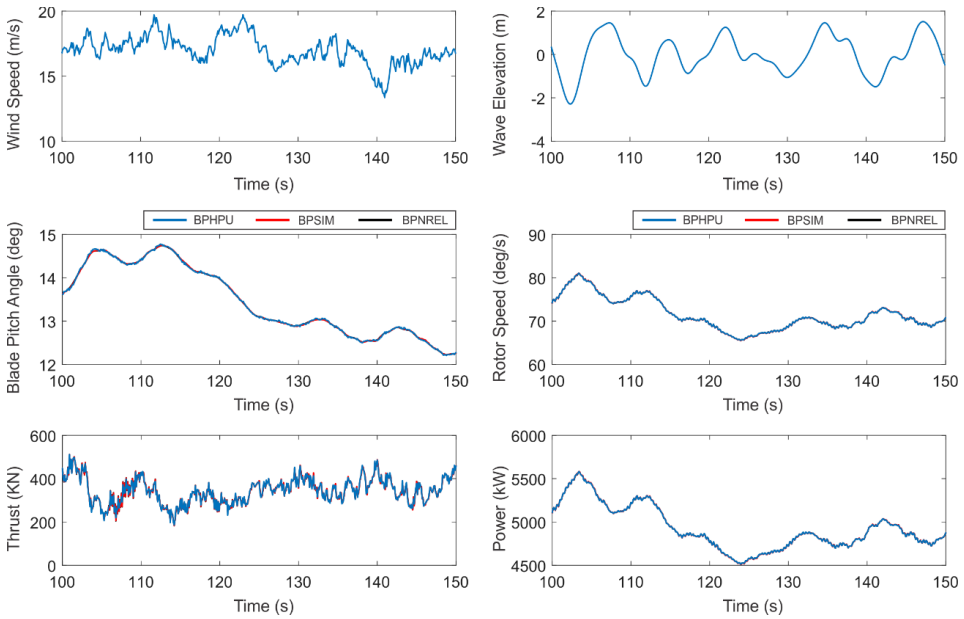

Figure 2.9: Comparison of the control performance with different control methods: 1) NREL blade pitch model (BPNREL), 2) simplified blade pitch actuator (BPSIM), and 3) blade pitch actuator with the hydraulic power unit (BPHPU).

Figure 2.10 shows the control procedure for a wind turbine with the FDD and FTC schemes. The baseline controller regulates the blade pitch and generator torque control for the power production in operational conditions. The sensors in the condition monitoring system measure the blade pitch angle, tower acceleration, rotor speed, wind

speed, and other physical values for wind turbines. By using an FDD algorithm, the system can detect and diagnose faults at an early stage. After successful FDD, the fault-tolerant controller selects a remedial action based on the protection strategy. If the fault is tolerable, it can be accommodated by a reconfiguration system. If the situation is intolerable and the wind turbine is not in a safe state, then the wind turbine goes to shutdown mode.

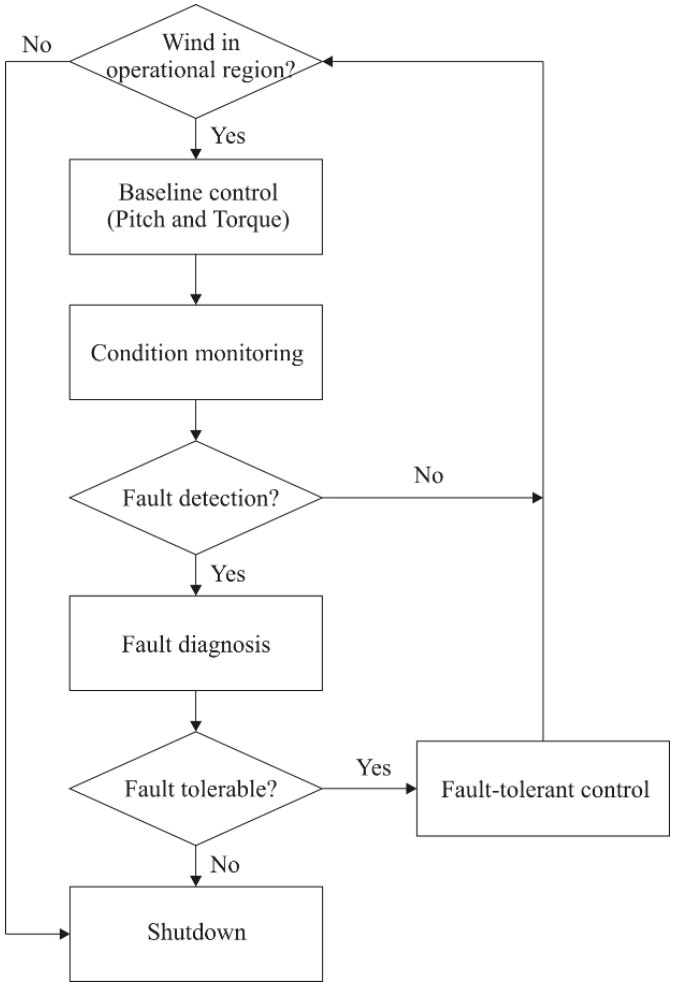

Figure 2.10: Control procedure for a wind turbine with FDD and FTC.

2.5. Environmental conditions

The floating wind turbine operates under variable wind conditions, such as a stochastic wind model that presents realistic wind and wave loads. The wind model is based on the IEC 61400-3 design code [91]. The turbulent wind field U_w (x, y, z, t) is commonly modeled by a mean wind and a fluctuating component as described by

$$U_w(t) = U_m + U_f(t), \tag{2.10}$$

where U_m is the mean wind speed represented as the normal wind profile model (NWP) and U_f is the fluctuating wind for the normal turbulence model (NTM). The turbulent wind U_w is modeled using Turbsim [92] according to the Kaimal turbulence model including the turbulence intensity with IEC Class C. The turbulence intensity is a function of the wind speed at the hub height. The wind model was based on IEC 61400-3 [91]. In the vertical plane, 32 × 32 points were used over an area of 160 × 160m, with a time step of 0.05 seconds for the wind field generation. The wind shear model was according to the power law with exponent 0.14.

Offshore wind farms have been primarily installed in European offshore sites, mostly in the North Sea (62%), the Irish Sea (15%), the Baltic Sea (14%), and the Atlantic Ocean (9%) [3]. The North Sea registered the largest amount of grid connections (1,651 MW), representing 62% of the installations. For irregular waves in the North Sea, the Joint North Sea Wave Project (JONSWAP) wave spectrum was used. The peak period (T_p) and significant wave height (H_s) were decided based on their correlation with wind speed for the Statfjord site in the North Sea [93]. Wind and wave directions are aligned.

The wind condition is generally correlated with wave conditions. To examine the lifetime loads on the wind turbine, a joint wind and wave distribution is required. Therefore, the joint wind-wave distribution for the Northern North Sea [94] was used to choose the relevant environmental conditions for numerical simulation. Load cases with different wind and wave conditions were provided by simulating the dynamic responses of the floating wind turbine, as given in Table 2.6, which provides four categories of the load cases.

Table 2.6: Load cases based on winds and waves.

Load case	U_w (m/s)	Turbulence model	H_s (m)	T_p (s)
1	11.2	IEC Class C	3.2	10.0
2	14		3.62	10.30
3	17		4.2	10.50
4	20		4.8	10.80

3. Fault detection, diagnosis and fault-tolerant control of a blade pitch system using a simplified model

3.1. State space model of the simplified blade pitch system

A simplified blade pitch actuator has been modeled as a 2nd order differential equation described in Eq. (2.1). This differential equation can be transformed into a state space representation. State space representations provide a convenient way to model and analyze systems with multiple inputs and outputs. The state space representation of the simplified blade pitch actuator is described by

$$\begin{aligned}\dot{\mathbf{x}}_{bp}(t) &= \mathbf{A}_{bp}\mathbf{x}_{bp}(t) + \mathbf{B}_{bp}\mathbf{u}_{bp}(t) + \mathbf{w}_{bp}(t),\\ \mathbf{y}_{bp}(t) &= \mathbf{C}_{bp}\mathbf{x}_{bp}(t) + \mathbf{v}_{bp}(t),\end{aligned} \tag{3.1 a}$$

or

$$\dot{\mathbf{x}}_{bp}(t) = \begin{bmatrix}\dot{\boldsymbol{\beta}}_i(t)\\ \ddot{\boldsymbol{\beta}}_i(t)\end{bmatrix} = \begin{bmatrix}\mathbf{0}_{3\times3} & \mathbf{I}_{3\times3}\\ -\omega_{bp}^2\,\mathbf{I}_{3\times3} & -2\omega_{bp}\zeta_{bp}\,\mathbf{I}_{3\times3}\end{bmatrix}\begin{bmatrix}\boldsymbol{\beta}_i(t)\\ \dot{\boldsymbol{\beta}}_i(t)\end{bmatrix} + \begin{bmatrix}\mathbf{0}_{3\times3}\\ \omega_{bp}^2\,\mathbf{I}_{3\times3}\end{bmatrix}\mathbf{u}_{bp}(t) + \begin{bmatrix}\mathbf{w}_{\beta,i}(t)\\ \mathbf{w}_{\dot{\beta},i}(t)\end{bmatrix},$$

$$\mathbf{y}_{bp}(t) = \begin{bmatrix}\mathbf{I}_{3\times3} & \mathbf{0}_{3\times3}\end{bmatrix}\begin{bmatrix}\boldsymbol{\beta}_i(t)\\ \dot{\boldsymbol{\beta}}_i(t)\end{bmatrix} + \mathbf{v}_{bp,i}(t),$$

$$i = 1,\ 2 \text{ and } 3, \tag{3.1 b}$$

where $\mathbf{x}_{bp}(t)$, $\mathbf{u}_{bp}(t)$, and $\mathbf{y}_{bp}(t)$ are the state vector, input vector, and measurement vector by the blade pitch angle, respectively, and $\mathbf{A}_{bp}$, $\mathbf{B}_{bp}$, and $\mathbf{C}_{bp}$ are system matrices representing the state transition, input, and measurement matrices, respectively. In Eq. (3.1), the input vector $\mathbf{u}_{bp}(t)$ consists of a set of the blade pitch command $\beta_C(t)$. Uncertain disturbances are given, including the process noise vector $\mathbf{w}_{bp}(t)$ and the measurement noise vector $\mathbf{v}_{bp}(t)$. The process and measurement noises in a state-space model of the blade pitch system are assumed to be zero-mean Gaussian white noises. Observability, controllability, and stability for this blade pitch system are checked according to the observability matrix, controllability matrix, pole and Nyquist diagram from Chen [95].

3.2. Fault description and modeling

A fault occurring in the blade pitch system affects the control system and the dynamic responses of a wind turbine. The incorrect blade pitch leads to unbalanced rotation in the rotor due to asymmetrical forces on the blades. Therefore, a fault occurring in the sensors and actuators can affect the system characteristics, or lead to inoperable conditions, which result in hydraulic leakage, valve blockage or pump blockage [23]. In this case, the blade pitch system cannot properly perform the role of an aerodynamic brake while large wind loads are acting on the rotor.

The blade pitch system faults are categorized by the pitch sensor and actuator fault. In this thesis, three types of faults can be considered: a bias value (PSB), a fixed output (PSF), and a stuck actuator (PAS) in the blade pitch system, as shown in Papers 1 and 2. PSB is an offset value that is added to the measurement from the sensor. PSF retains the last measurement after fault occurrence. The PSB and PSF are main faults of the blade pitch sensor. PAS is mainly caused by a valve blockage, which is mainly due to clogging the valve or short-circuit in the hydraulic blade pitch actuator. Table 3.1 describes the updated fault equations of the blade pitch system. Parameters can be described, where $\beta_{PSB}(k)$ is the pitch bias angle, $\beta_{PSF}(k)$ is the fixed pitch angle after the fault, and β_{PAS} is the pitch angle for the stuck actuator.

Table 3.1: Fault equations.

Status	Fault value
Fault-free sensor	$\beta_m(k) = \beta(k) + v(k)$
Biased output (PSB)	$\beta_m(k) = \beta(k) + \beta_{PSB}(k) + v(k)$
Fixed output (PSF)	$\beta_m(k) = \beta_{PSF}(k)$
Stuck (PAS)	$\beta(k+1) = \beta_{PAS},\ \dot{\beta}(k+1) = 0$

Faults of the blade pitch sensor and actuator typically result in structural loading on the turbine structure because of rotor imbalance. These faults also affect the stability of the floater or the support structure.

3.3. Fault detection, fault diagnosis and fault-tolerant control methods

3.3.1. Fault detection

Model-based fault detection approaches detect faults based on the system model and estimator. Figure 3.1 shows the basic structure of the model-based fault detection with a Kalman filter. Based on the input command $u(k)$ and measured output $y_m(k)$, the states and measurements are estimated by a Kalman filter. By comparing the residual and threshold, normal or fault conditions are identified.

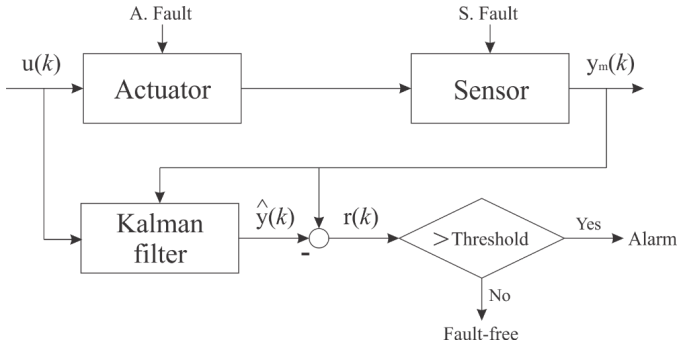

Figure 3.1: Scheme of an observer-based fault detection in the blade pitch system.

3.3.1.1. Observer design based on the discrete-time state-space model

The state-space model of the blade pitch system in the discrete time domain with disturbance and faults in the pitch actuator and sensor are transferred from the proposed system (3.1) and applied with the Euler discretization approach,

$$\begin{aligned}\mathbf{x}_{bp}(k+1) &= \mathbf{\Phi}_{bp}\mathbf{x}_{bp}(k) + \mathbf{\Psi}_{bp}\mathbf{u}_{bp}(k) + \mathbf{\Gamma}_{bp,f}\mathbf{f}_{bp,A}(k) + \mathbf{\Gamma}_{bp,d}\,\mathbf{w}_{bp}(k),\\ \mathbf{y}_{bp}(k) &= \mathbf{H}_{bp}\mathbf{x}_{bp}(k) + \mathbf{\Xi}_{bp,f}\mathbf{f}_{bp,S}(k) + \mathbf{\Xi}_{bp,d}\,\mathbf{v}_{bp}(k),\end{aligned} \tag{3.2}$$

where $\mathbf{\Phi}_{bp} = \mathbf{I}_{bp} + \mathbf{A}_{bp}T$, $\mathbf{\Psi}_{bp} = \mathbf{B}_{bp}T$ and $\mathbf{H}_{bp} = \mathbf{C}_{bp}$ (sampling time T). Here, $\mathbf{\Phi}$, $\mathbf{\Psi}$, $\mathbf{H}$, $\mathbf{\Gamma}_d$, $\mathbf{\Gamma}_f$, $\mathbf{\Xi}_d$, and $\mathbf{\Xi}_f$ are known matrices in a discretized system. In addition, $\mathbf{f}_A(k)$ and $\mathbf{f}_S(k)$ are the actuator and sensor fault vectors.

The Kalman filter for the healthy case is designed as follows,

$$\begin{aligned}\hat{\mathbf{x}}_{bp}(k+1) &= \mathbf{\Phi}_{bp}\hat{\mathbf{x}}_{bp}(k) + \mathbf{\Psi}_{bp}\mathbf{u}_{bp}(k) + \mathbf{K}_{bp}(\mathbf{y}_{bp}(k) - \mathbf{H}_{bp}\hat{\mathbf{x}}_{bp}(k)),\\ \hat{\mathbf{y}}_{bp}(k) &= \mathbf{H}_{bp}\hat{\mathbf{x}}_{bp}(k),\end{aligned} \tag{3.3}$$

where $\hat{\mathbf{x}}_{bp}(k)$, $\hat{\mathbf{y}}_{bp}(k)$, and $\mathbf{K}_{bp}$ are the estimated state vector, estimated output vector, and Kalman gain matrix in the blade pitch system, respectively.

3.3.1.2. Fault modeling

The state-space model for the blade pitch system (3.2) is updated when faults occur in the system. Table 3.2 describes the fault vectors in the actuator and values in the sensor. If a fault occurs in the pitch system, the fault value is applied in the pitch system equation in this algorithm.

Table 3.2: Mathematical model of faults applied in numerical simulations.

Type	Fault value
Biased output (PSB)	$\mathbf{f}_A(k) = 0$, $f_S(k) = \beta_{PSB}$
Fixed output (PSF)	$\mathbf{f}_A(k) = 0$, $f_S(k) = -\beta(k) + \beta_{PSF} - v_{bp}(k)$
Stuck (PAS)	$\mathbf{f}_A(k) = \begin{bmatrix} -\beta(k) - T\dot{\beta}(k) + \beta_{PAS} - w_{bp,1}(k) \\ (\omega_{bp}^2\ \beta(k) + 2\zeta_{bp}\ \omega_{bp}\ \dot{\beta}(k) - \omega_{bp}^2\ \beta_C(k))T - w_{bp,2}(k) \end{bmatrix}$, $f_S(k) = \beta_{PAS}$

3.3.1.3. Residual generation and evaluation

A residual $r(k)$ is described as follows:

$$r(k) = y_m(k) - \hat{y}(k). \tag{3.4}$$

A residual energy $J(k)$ is defined by the L_2 norm [31] as follows:

$$J(k) = \left\| r(k) \right\|_{2,\Delta k} = \left(\sum_{i=k-\Delta k}^{k} r^T(\kappa) r(\kappa) d\kappa \right)^{1/2}. \tag{3.5}$$

The residual determines the fault status by applying fault detection logic with the threshold J_{th},

$$\begin{aligned} &J(k) < J_{th}, \ \text{fault} - \text{free}, \\ &J(k) > J_{th}, \ \text{fault}. \end{aligned} \tag{3.6}$$

If the residual energy exceeds this threshold, the fault can be detected. Otherwise, the fault-free state is indicated. The threshold design procedure using H_∞ optimization and linear matrix inequality (LMI) was described in Paper 1 with more details on the derivation.

3.3.2. Fault diagnosis using the inference method

Fault diagnosis makes a decision after a detection alarm occurs. An inference method-based fault diagnosis algorithm [29] is used in this chapter.

Figure 3.2 shows a fault diagnosis algorithm using the measurements of the blade pitch and nacelle yaw angle. Initially, the trend of the pitch measurement $\beta_{i,k}$ must be determined. If the faulty sensor continuously outputs $\beta_{i,k+1}$ - $\beta_{i,k}$ = 0, then the diagnosis algorithm makes a decision for the fault: either PSF or PAS. Then, by comparing the standard deviation of the nacelle yaw angle in the normal $\sigma_{Yaw,n}$ and fault conditions $\sigma_{Yaw,f}$, the two faults can be differentiated. If the fault estimation errors are bounded in a certain range δ, then the algorithm decides the fault as a PSB.

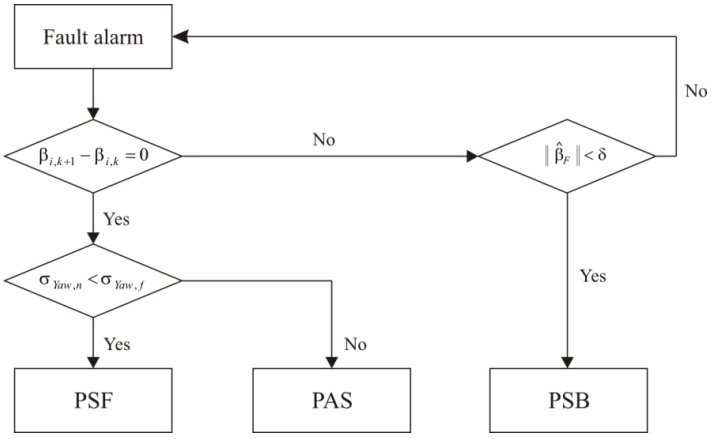

Figure 3.2: Algorithm for fault diagnosis with a single pitch sensor.

3.3.3. Fault tolerant control with virtual sensors

If the sensors and actuators are no longer available due to a fault occurrence, then the controller cannot control the system in an appropriate action. In this chapter, a fault-tolerant control (FTC) scheme is suggested, which includes a reconfiguration block and a nominal PI controller to minimize the unexpected fault effects. The FTC scheme reconstructs the system output y_c to replace the faulty measurement y_f. Because the nominal PI controller cannot use the faulty measurement y_f, a configuration block need to generate a suitable signal y_c from y_f and u_f. Figure 3.3 shows the block diagram of the control reconfiguration for the sensor and actuator faults.

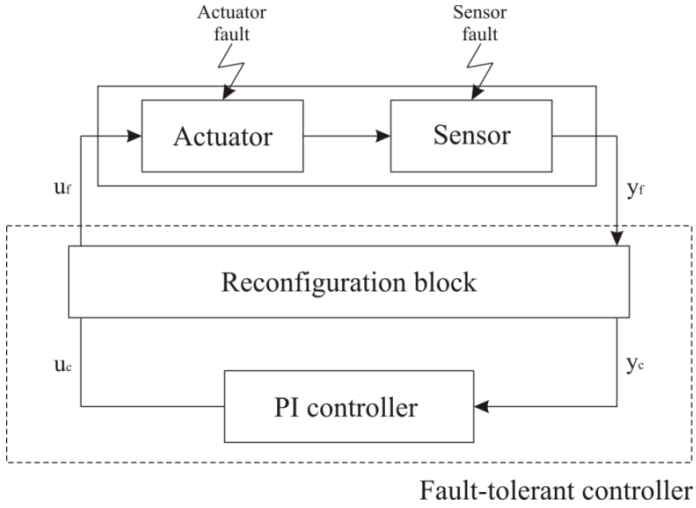

Figure 3.3: Control reconfiguration for the sensor and actuator faults.

In this chapter, virtual sensors [30] are used to calculate the state vectors by replacing the measurements from the faulty system. The virtual sensor is defined as follows:

$$\begin{aligned}
&\hat{\mathbf{x}}_{bp,\mathrm{v}}(k+1) = \boldsymbol{\Phi}_{bp}\hat{\mathbf{x}}_{bp,\mathrm{v}}(k) + \boldsymbol{\Psi}_{bp}\mathbf{u}_{bp,c}(k) + \mathbf{K}_{bp,\mathrm{v}}(\mathbf{y}_{bp,f}(k) - \mathbf{H}_{bp,f}\hat{\mathbf{x}}_{bp}(k)),\\
&\mathbf{y}_{bp,c}(k) = \mathbf{H}_{bp,\mathrm{v}}\hat{\mathbf{x}}_{bp,\mathrm{v}}(k) + \mathbf{P}\,\mathbf{y}_{bp,f}(k),\\
&\mathbf{u}_{bp,f}(k) = \mathbf{u}_{bp,c}(k),
\end{aligned} \tag{3.7}$$

where $\mathbf{H}_{\mathrm{v}} = \mathbf{H}$. If the fault detection scheme detects any faults in the pitch sensor of the i^{th} blade, the value in $\mathbf{H}_{\mathrm{v}}$ allocated by the faulty sensor is replaced by 0 in $\mathbf{H}_f$ which means that this sensor is no longer available. $\mathbf{P}$ is a design parameter, and for $\mathbf{P} = \mathbf{0}$ only observed values are used, and $(_{\mathrm{v}})$ represents values in the virtual sensors.

Figure 3.4 shows the reconfiguration procedure with the virtual sensor. The matrix $\mathbf{H}_{bp,f}$ reflects the sensor faults. The virtual sensor estimates the state $\hat{\mathbf{x}}_{bp,f}$ of the faulty system and replaces the faulty system output. This system output $\mathbf{y}_{bp,\mathrm{c}}$ is corrected by using the other available sensor values. If this virtual sensor works well, then the virtual sensor state $\mathbf{x}_{\mathrm{v}}$ is equivalent to the state of the nominal system $\mathbf{x}_{bp}$. Hence, the controller reacts like the same system as before.

Actuator faults are critical to the safety of wind turbines when the pitch actuator is under inoperable conditions regardless of the controller command in Esbensen and Sloth. [23]. Then, the blade cannot be pitched anymore at the aerodynamic load from the wind loads. Therefore, pitch actuator faults require a safe and rapid shutdown of the wind turbine as a standard from Jonkman et al. [71].

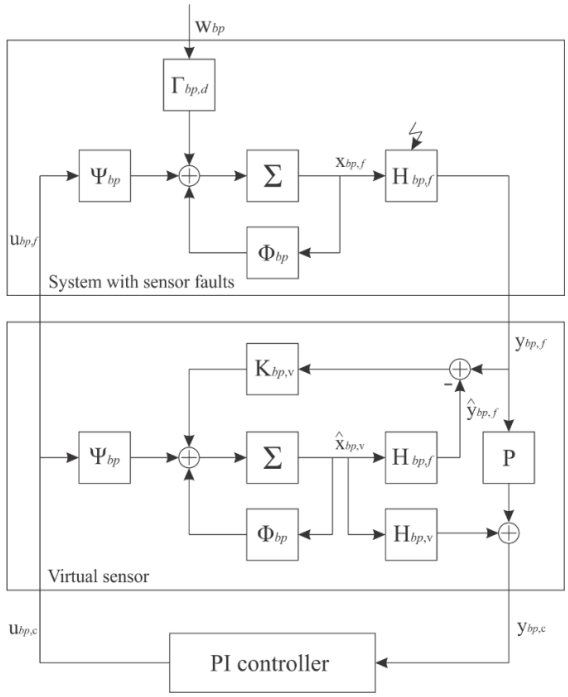

Figure 3.4: Reconfiguration with a virtual sensor after sensor fault.

3.4. Simulation results and discussion

Faults of the blade pitch system affect the dynamic behaviors of the wind turbine. In this section, the simulation results are presented to investigate the dynamic responses and performance of the proposed FDD and FTC schemes. Simulations of the wind turbine are conducted under PSB, PSF, and PAS on a single blade and multiple blades. In this simulation, the load cases described in Table 2.5 were used to study the dynamic response of the floating wind turbine.

The fault detection algorithm can effectively detect faults in actuators and sensors by the residual energy and threshold. When a fault alarm is set to 1, it means that a fault is detected. The residual energy is normalized to adjust the scale factor. The normalized residual energy J_N is described as follows:

$$J_N(k) = J(k) / J_{th}. \tag{3.8}$$

Figure 3.5 shows the simulation results for the blade pitch angle, the normalized residual energy, a fault detection alarm and fault diagnosis under LC4. In Figure 3.5 (a), a PSB occurs after 250 s, which corresponds to a -3° offset value on blade 3. The normalized

residual is greater than the threshold, and then the observer detects the PSB fault immediately. In Figure 3.5 (a), the diagnosis algorithm analyses the PSB fault after successful detection.

In the PSF and PAS faults, the pitch angle measurement shows a constant value that represents the same values comparing the last measurement value before the faults. The pitch angle oscillates irregularly at a large amplitude and the pitch angle difference between the fault-free blades (blades 1, 2) and faulty blade (blade 3) is given as the unbalanced rotation. The PSF and PAS simulation results show the same pattern in Figures 3.5 (b) and (c).

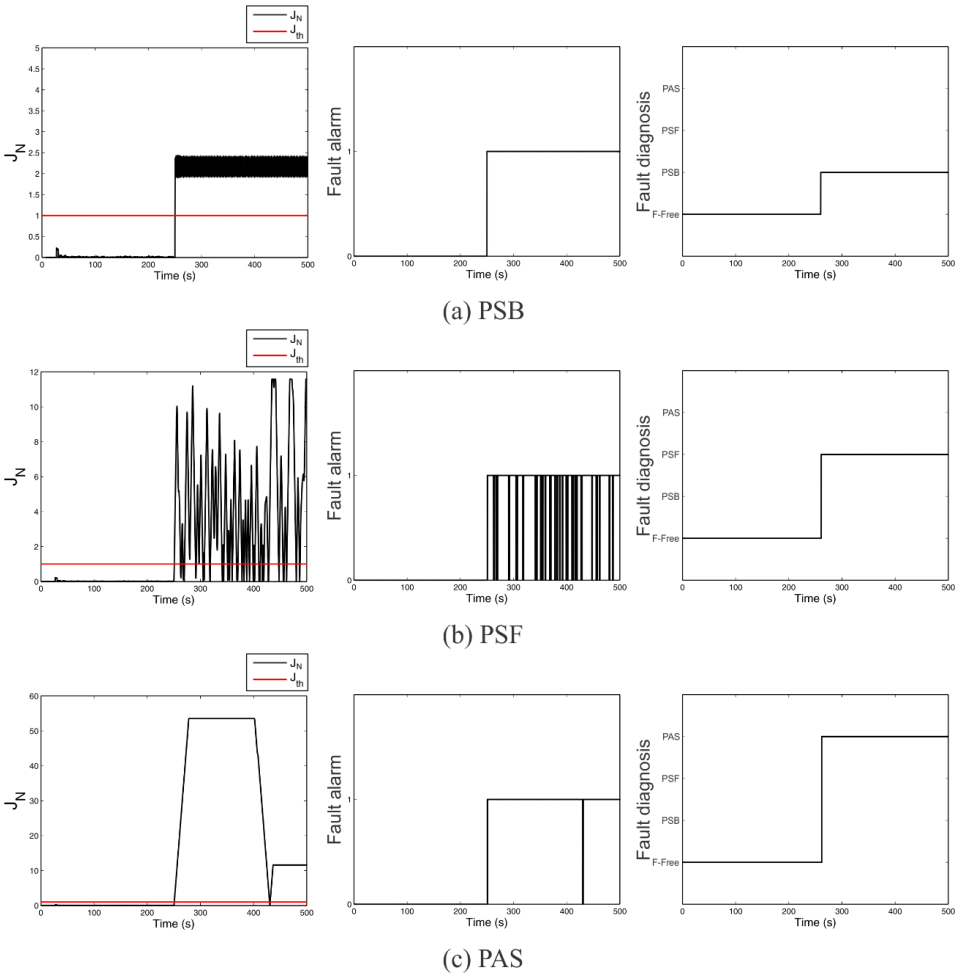

Figure 3.5: Simulation results of the (a) PSB, (b) PSF and (c) PAS cases corresponding to the blade pitch angle under LC4: normalized residual energy (J_N), fault detection alarm, and fault diagnosis.

Paper1 and 2 presented the results and performance of this fault detection algorithm within a reasonable time after a fault is generated. Therefore, this method can guarantee fault detection at an early stage in the blade pitch system.

A series of simulations are conducted to evaluate the FDD and FTC schemes against different fault scenarios and load cases. Each simulation has a 1-h duration to reduce the stochastic uncertainty for each load case. Paper 2 shows the effects of the fault cases on the normalized mean and standard deviation of the surge, roll, pitch, and yaw motions of a floating wind turbine. The results show that faults influence a significant amount of platform yaw motions compared with other motions such as the surge, roll and pitch motions, because the incident variations in an aerodynamic thrust caused by an unbalanced rotation on the rotor directly affect the instability of the platform motion, especially the yaw motion. Additionally, Paper 2 shows that the torsional moment is more affected by faults than the fore-aft and side-to-side bending moments. In fault accommodation, the mean and standard deviation results demonstrate that the proposed FTC schemes with signal correction for sensor faults have a good performance. The platform motions with FTC schemes in the PSB and PSF faults have nearly equivalent values as the fault-free case.

Figure 3.6 shows the platform roll and yaw motions in the PSB and PSF cases for LC4 to check the effectiveness of the FTC for sensor faults. After 250 s, the FDD algorithm can precisely diagnose the faults and the FTC scheme conducts a signal correction for faulty sensors, which means that the FTC successfully eliminates the unbalanced rotation in the rotor during the PSB and PSF faults. The FTC with signal correction brings the wind turbine back to normal operational conditions. However, instability still occurs in the wind turbine when a nominal controller (PI controller) is used during the PSB and PSF faults.

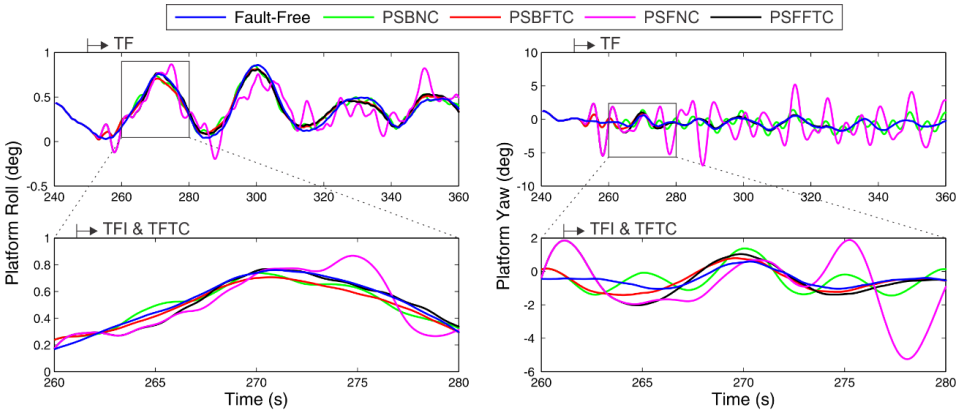

(a) Roll (b) Yaw

Figure 3.6: Comparison of the platform pitch and yaw motions under PSB and PSF fault conditions with nominal PI and fault-tolerant controllers under LC4.

In addition, the effect of faults on the tower with the proposed FTC schemes should be presented. The FTC schemes using a virtual sensor demonstrate better performance than the nominal PI controller. Figure 3.7 shows the torsional moment and side-to-side bending moment on the tower base in the PSB and PSF cases to validate the FTC scheme from 230 to 330s. These results show that the FTC scheme successfully eliminates the unbalance rotation in the rotor during the PSB and PSF faults.

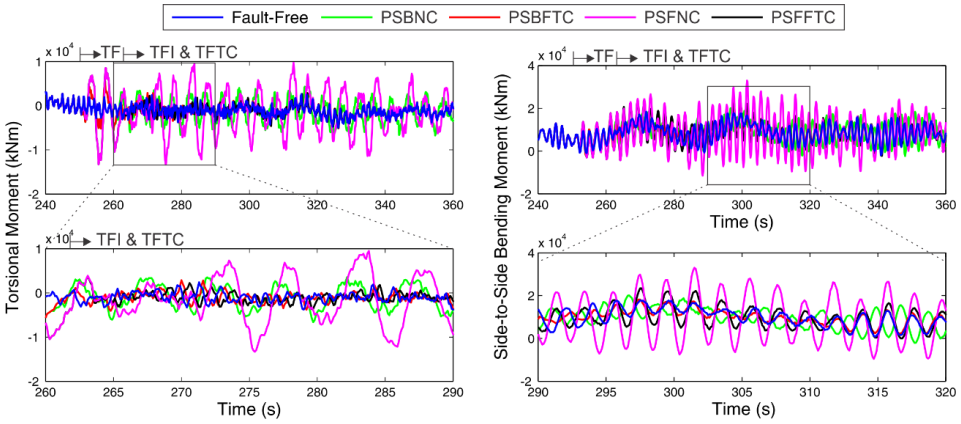

(a) Tower base torsional moment

(b) Tower base side-to-side bending moment

Figure 3.7: Comparison of the torsional and side-to-side bending moments on the tower base under PSB and PSF fault conditions with nominal PI and fault-tolerant controllers under LC4.

4. Fault detection and diagnosis of a blade pitch system using a detailed model with hydraulic power units

4.1. Modeling and fault description

4.1.1. Blade pitch and valve systems

The hydraulic pitch actuator with the hydraulic power unit was modeled as described in Section 2.2.2 from Paper 3. To estimate the blade pitch angles and valve positions, models inserted in the Kalman filter are built as 2nd order differential equations of motion. Consider the blade pitch system that describes a blade pitch command from the pitch controller and the pitch angle measurement in Eq. (2.1).

As the blade pitch angle command from the pitch controller varies, the voltage value for the controlling spool position eventually adjusts the hydraulic flow into the cylinder for the cylinder described in Section 2.2.2. The valve spool position x_{vs} described in Eq. (2.2) is calculated from the voltage u_{vs} defined by a second order system.

To measure the blade pitch angle, incremental rotary encoders installed on the blade roots can be used. Linear variable displacement transducers (LVDTs) are used to measure the position of the valve spool. Figure 4.1 shows the schematic diagram of the blade pitch system with the sensor distribution. The measurements must be accurate and reliable, because the turbine monitoring and control are using sensor data during wind turbine operations. The state space representation of the valve systems is described by

$$\begin{aligned}\dot{\mathbf{x}}_{vs}(t) &= \mathbf{A}_{vs}\mathbf{x}_{vs}(t) + \mathbf{B}_{vs}\mathbf{u}_{vs}(t) + \mathbf{w}_{vs}(t),\\ \mathbf{y}_{vs}(t) &= \mathbf{C}_{vs}\mathbf{x}_{vs}(t) + \mathbf{v}_{vs}(t),\end{aligned} \tag{4.1a}$$

or

$$\dot{\mathbf{x}}_{vs}(t) = \begin{bmatrix}\dot{\mathbf{x}}_{vs,i}(t)\\ \ddot{\mathbf{x}}_{vs,i}(t)\end{bmatrix} = \begin{bmatrix}\mathbf{0}_{3\times3} & \mathbf{I}_{3\times3}\\ -\omega_{vs}^2\,\mathbf{I}_{3\times3} & -2\omega_{vs}\zeta_{vs}\,\mathbf{I}_{3\times3}\end{bmatrix}\begin{bmatrix}\mathbf{x}_{vs,i}(t)\\ \dot{\mathbf{x}}_{vs,i}(t)\end{bmatrix} + \begin{bmatrix}\mathbf{0}_{3\times3}\\ \omega_{vs}^2\,\mathbf{I}_{3\times3}\end{bmatrix}\mathbf{u}_{vs,i}(t) + \begin{bmatrix}\mathbf{w}_{x_{vs,i}}(t)\\ \mathbf{w}_{\dot{x}_{vs,i}}(t)\end{bmatrix},$$

$$\mathbf{y}_{vs}(t) = \begin{bmatrix}\mathbf{I}_{3\times3} & \mathbf{0}_{3\times3}\end{bmatrix}\begin{bmatrix}\mathbf{x}_{vs,i}(t)\\ \dot{\mathbf{x}}_{vs,i}(t)\end{bmatrix} + \mathbf{v}_{vs,i}(t),$$

$$i = 1,\ 2 \text{ and } 3, \tag{4.1b}$$

where $\mathbf{x}_{vs}(t)$, $\mathbf{u}_{vs}(t)$, and $\mathbf{y}_{vs}(t)$ are the state vector, input vector, and measurement vector by the valve spool position, respectively, and $\mathbf{A}_{vs}$, $\mathbf{B}_{vs}$ and $\mathbf{C}_{vs}$ are system matrices representing the state transition, input and measurement matrices, respectively. Uncertain disturbances are given, including the process noise vector $\mathbf{w}_{vs}(t)$ and the measurement noise vector $\mathbf{v}_{vs}(t)$. Process and measurement noises in the state-space model of the blade pitch system, described by Eq. (4.1), are assumed to be zero-mean Gaussian white noises.

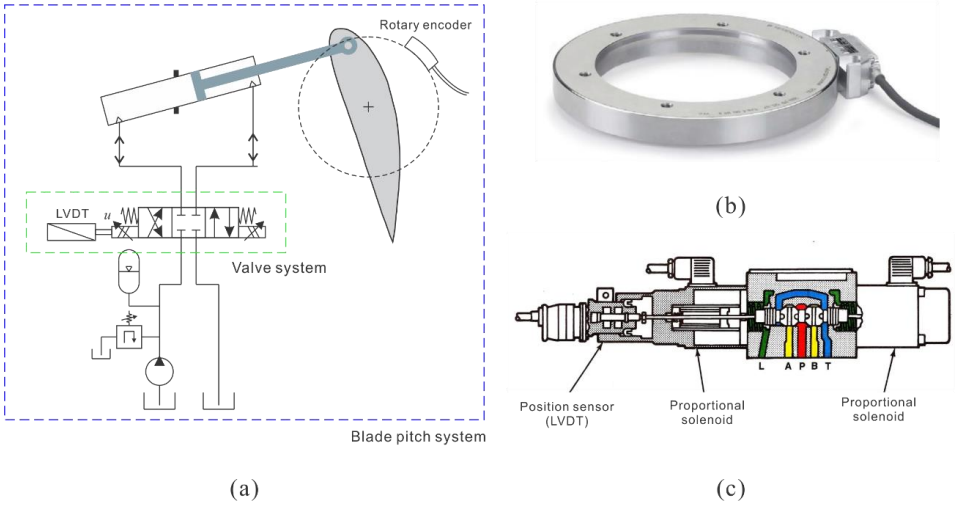

Figure 4.1: Position sensors distributions for measurement of the blade pitch angle and valve spool position: (a) Schematic diagram, (b) incremental rotary encoder [98], and (c) valve system with a spool position feedback transducer [99].

4.1.2. Fault description and scenarios

In the case of hydraulic actuator faults, Carroll et. al. [21] showed that the high failure rate related to oil, valve and sludge issues accounts for a large portion (37.3%) of the total failure rate for hydraulic pitch systems. Specifically, a valve fault can change the system characteristics [100].

Especially, faults in the directional control valves are mainly categorized by mechanical and electrical faults. Mechanical faults are related to oil contamination and sludge build-up on the surface of a spool that disturb the spool movement by increasing friction in the valve. This fault is called excessive friction in valves (VEF). This sludge narrows the clearance and more particles enter into the clearance space. In the worst case, the sludge buildup and the particles become hardened and cause high static friction. If the excessive friction is larger than the maximum force from the solenoid, it will seize the valve spool. This phenomenon is commonly referred to as 'slit-lock' (VSL).

Electrical faults are related to residual current through the solenoid due to the damage or dirt armature. When the solenoid coil reaches the magnetic saturation level, the coil is overheated due to high inrush currents. In extreme cases, the core of the solenoid is subjected to damages or the coil inductance is permanently changed. Then, it applies a wrong voltage and the current cannot move through the circuit via the applied voltage. The wrong applied voltage (VWV) resulting from a changed coil impedance can be described by changing the value of the valve voltage gain k_u. Furthermore, if solenoids cannot properly dissipate the heat generated by their residual current or go through a high inrush current due to faults, then the solenoid is damaged and burnt-out which means that the insulation around the coil windings will burn, and the coil will short out. As the solenoid short-circuit occurs (VCS), the applied voltage has been changed as zero.

After these faults occur, the valve cannot provide an adequate amount of flow in the cylinder from the control input. These faults influence the results of the pressure, piston force, blade pitch angle and response delay. These faults can also affect the global dynamic response of the wind turbines in transient and steady-state conditions. The incorrect pitching of a blade due to faults causes asymmetric forces on the blades, introducing an unbalanced rotation that significantly increases the structural loads on the rotor. In the worst cases, it is associated with valve seizure that leads to inoperable conditions.

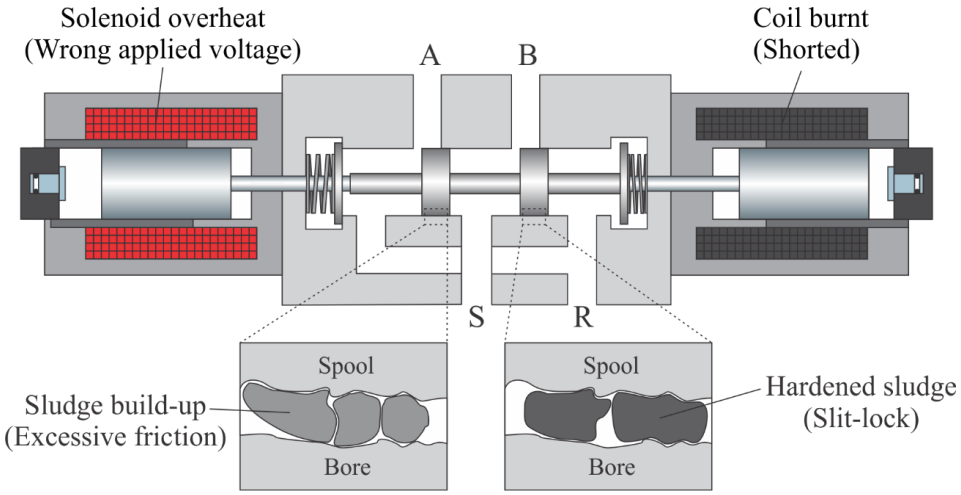

Figure 4.2: Illustration of the mechanical and electrical valve faults.

Paper 3 describes the updated fault values in the valve model and the consequences in each fault. In this chapter, six fault types are considered in the pitch sensor and actuator of the blade pitch system. Table 4.1 describes the fault types.

Table 4.1: Fault description.

Fault number	Fault name	Fault occurrence location
1	Bias value (PSB)	Pitch sensor
2	Fixed output (PSF)	
3	Excessive friction (VEF)	Directional control valve
4	Slit lock on spool (VSL)	
5	Wrong applied voltage (VWV)	
6	Short-circuit (VCS)	

4.2. Fault detection and diagnosis

Fault detection and diagnosis methods are described in this section. Figure 4.3 shows the basic structure of the FDD schemes in the general system. Based on the input command $u(k)$ and the measured output $y(k)$, states and outputs are estimated by the Kalman filters. By comparing measured and estimated values, changes of a state are identified by residuals compared to a threshold. If the fault detection decision making algorithm determines that the state has a fault condition, an artificial neural network model diagnoses the fault type with the arrayed ANN inputs using feature extraction from faults. Paper 4 describes the configuration of the input of the ANN model.

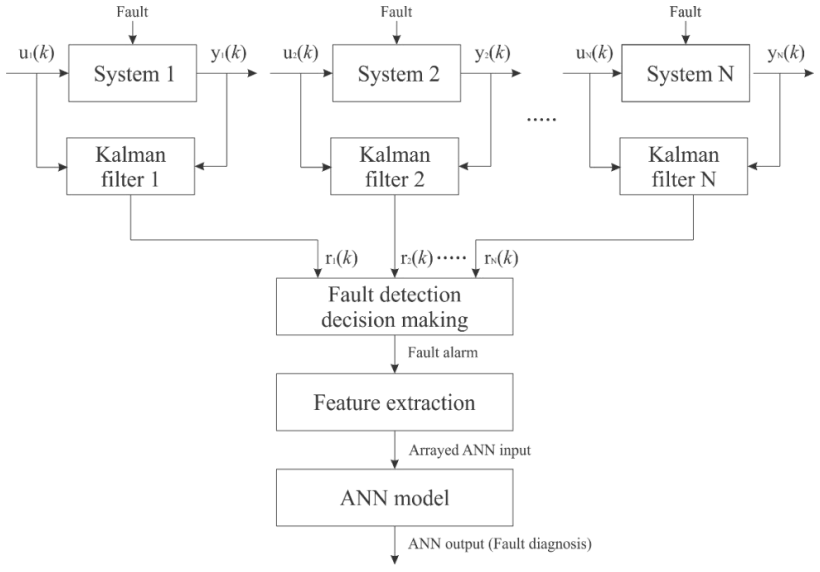

Figure 4.3: Overall procedure for the FDD Scheme in general systems.

4.2.1. Fault detection with a Kalman filter

A Kalman filter as a model-based method, which is often used in fault detection, satellite navigation device, computer vision, or computer games [101], is used. Using the input command $u(k)$ and measured output $y(k)$, the Kalman filter estimates the states and outputs.

The discrete-time state-space model of the blade pitch system with disturbance and faults in the pitch actuator and sensor can be transferred from the proposed system (4.1) where the Euler discretization approach is applied:

$$\begin{aligned} \mathbf{x}_{vs}(k+1) &= \mathbf{\Phi}_{vs}\mathbf{x}_{vs}(k) + \mathbf{\Psi}_{vs}\mathbf{u}_{vs}(k) + \mathbf{\Gamma}_{f\,vs}\mathbf{f}_{Avs}(k) + \mathbf{\Gamma}_{d\,vs}\,\mathbf{w}_{vs}(k), \\ \mathbf{y}_{vs}(k) &= \mathbf{H}_{vs}\mathbf{x}_{vs}(k) + \mathbf{\Xi}_{f\,vs}\mathbf{f}_{Svs}(k) + \mathbf{\Xi}_{d\,vs}\,\mathbf{v}_{vs}(k), \end{aligned} \tag{4.2}$$

where $\mathbf{\Phi}_{vs} = \mathbf{I}_{vs} + \mathbf{A}_{vs}T$, $\mathbf{\Psi}_{vs} = \mathbf{B}_{vs}T$, and $\mathbf{H}_{vs} = \mathbf{C}_{vs}$. Here, $\mathbf{\Phi}$, $\mathbf{\Psi}$, $\mathbf{H}$, $\mathbf{\Gamma}_d$, $\mathbf{\Gamma}_f$, $\mathbf{\Xi}_d$, and $\mathbf{\Xi}_f$ are known constant matrices in the discretized system. In addition, T is the sampling time and $\mathbf{f}_A(k)$ and $\mathbf{f}_S(k)$ are the actuator and sensor fault vectors described in Cho et al. [97], respectively.

An observer for the healthy case based on the Kalman filter method is designed as follows:

$$\begin{aligned} \hat{\mathbf{x}}_{vs}(k+1) &= \mathbf{\Phi}_{vs}\hat{\mathbf{x}}_{vs}(k) + \mathbf{\Psi}_{vs}\mathbf{u}_{vs}(k) + \mathbf{K}_{vs}(\mathbf{y}_{vs}(k) - \mathbf{H}_{vs}\hat{\mathbf{x}}_{vs}(k)), \\ \hat{\mathbf{y}}_{vs}(k) &= \mathbf{H}_{vs}\hat{\mathbf{x}}_{vs}(k), \end{aligned} \tag{4.3}$$

where $\hat{\mathbf{x}}_{vs}(k)$, $\hat{\mathbf{y}}_{vs}(k)$, and $\mathbf{K}_{vs}$ are the estimated state vector, estimated output vector, and the Kalman gain matrix, respectively. In terms of the residual generation and evaluation procedure, Section 3.2 describes this procedure.

4.2.2. Fault diagnosis with the ANN method

4.2.2.1. Training, validation, and test procedure using ANN

An artificial neural network is employed in the fault diagnosis procedure in this section. An ANN is a framework of machine learning algorithms that automatically identifies the system's characteristics from the training data. In ANN implementations, artificial neurons receive input signals and process them with hidden layers that are computed by some nonlinear function for calculating the output results. Figure 4.4 illustrates a simple illustration of an ANN.

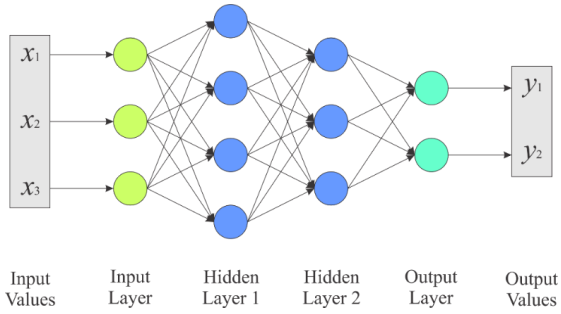

Figure 4.4: A simple illustration of an artificial neural network (ANN).

In this thesis, an artificial neural network determines the fault among the six fault types, which are described in Table 4.1. In the process of fault diagnosis using an ANN, the training, validation, and test procedure are essential for building the fault diagnosis model. The ANN algorithm makes the predictive model with training and validation data. Then, the final performance evaluation to evaluate the accuracy of the model is conducted with the labelled test data for the predictive model. While training a model, the label is separated before training begins. Upon completion of training, the data that were removed are used to test the performance of the learned model. Figure 4.5 shows the flowchart of the training, validation, and test procedure. The details of the training, validation, and test procedure are described in Paper 4.

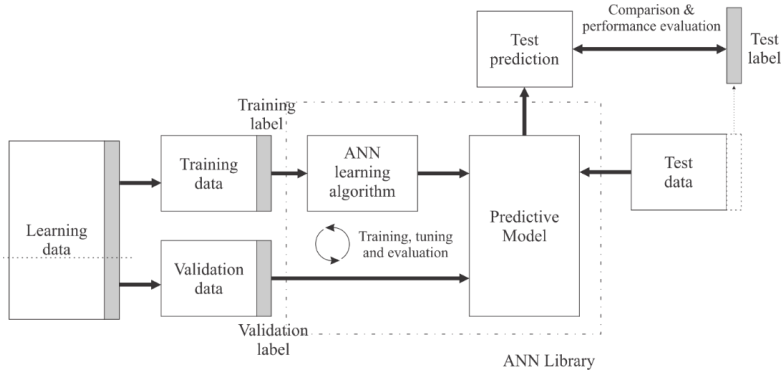

Figure 4.5: Flowchart of the general training, validation and test procedure.

4.2.2.2. Fault diagnosis results

Essentially, the fault diagnosis model was trained, validated, and tested with an ANN library based on TensorFlow [102] coded by Python. Then, the FDD scheme in Java code imports the optimized predictive model exported from the ANN library. Via the predictive model imported in Java code, the fault diagnosis can be conducted in combination with Simo-Riflex with the same structure after successful fault detection. Figure 4.6 shows the data transmission between the ANN library and the FDD scheme in Java for the optimized predictive model.

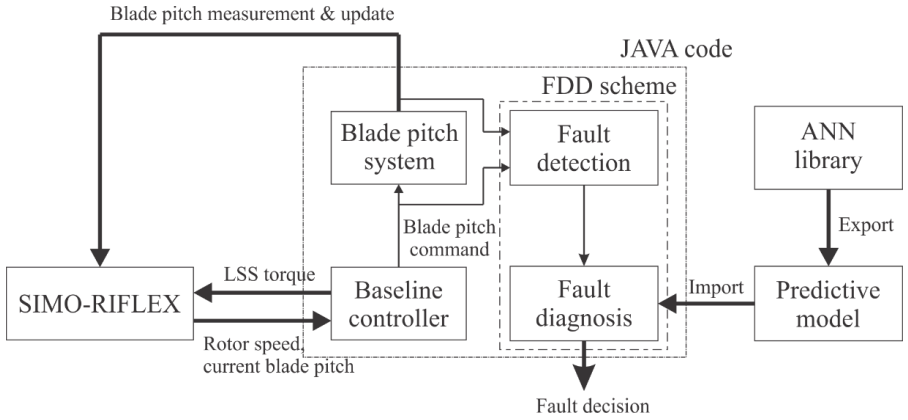

Figure 4.6: Data transmission among the SR, JAVA code and neural network model.

For a fault diagnosis, 50 simulations in each fault type simulated from the Simo-Riflex simulator have been performed with a new wind profile generated by Turbsim [92] and different fault occurrence times. Note that the fault diagnosis algorithm can be activated after the fault detection signal occurs. Figure 4.7 shows the fault detection and diagnosis in real-time. In Figure 4.7 (a), Fault 1 (PSB), corresponding to a -3° sensor bias on blade 3, occurs after 150 s (time of fault, TF). Concurrently, the fault detection algorithm detects the fault at 153 s (time of fault detection, TFD). In the fault detection signal, zero indicates the fault-free condition and 1 indicates the fault condition. Then the fault diagnosis scheme classifies the fault 1 at 170 s (time of fault diagnosis, TFDG). Fault 3 (VEF) and Fault 5 (VWV) are detected and diagnosed in the same pattern in Figures 4.7 (b) and (c), respectively.

Table 4.2 presents the fault diagnosis results obtained by the ANN scheme on a different set of examples under different fault conditions. In each fault type, the ANN is tested with the range of rated wind speed (11.2 – 24 m/s) correlated with the wave conditions. The results describes that the ANN based fault diagnosis has a good performance, with an overall accuracy of approximately 97.33 %.

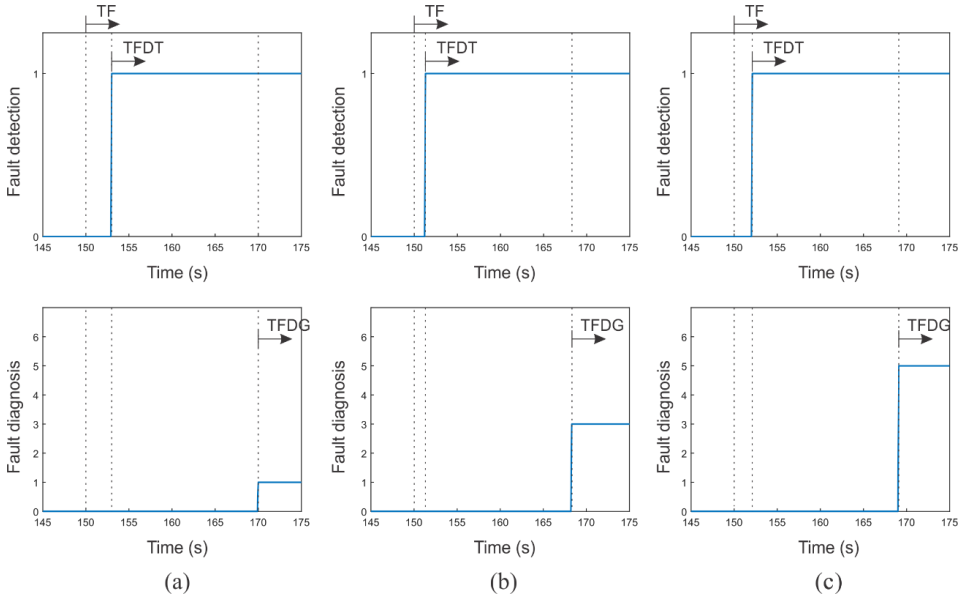

Figure 4.7: Fault detection and diagnosis in the faulty blade (blade 3) in real time: (a) fault 1 (PSB), (b) fault 3 (VEF), and (c) fault 5 (VWV).

Even if the ANN scheme shows a high accuracy, the scheme incorrectly diagnoses the faults with 2.67 % which is critical for the system. If the scheme makes a fault decision with not much difference to the score in the vector in the ANN's output layer after the Softmax function procedure, the scheme automatically performs two more diagnoses. Then the diagnosis scheme makes a final decision with the results of the triple fault diagnosis tests. Paper 4 describes the fault diagnosis correction in an incorrect decision procedure. Based on these results, it should be noted that the proposed ANN-based fault diagnosis method presented here is capable of properly diagnosing faults in the operation of the monitored component.

Table 4.2: Fault diagnosis results.

	Fault 1	Fault 2	Fault 3	Fault 4	Fault 5	Fault 6
No. simulations	50	50	50	50	50	50
No. failures	0	3	0	1	1	3
No. successes	50	47	50	49	49	47
Accuracy (%)	100	94	100	98	98	94
Overall accuracy (%)	97.33					

5. Concluding remarks and recommendations for future work

5.1. Concluding remarks

This thesis describes the model-based fault detection, fault diagnosis (FDD), and fault-tolerant control (FTC) schemes in the blade pitch system of a floating wind turbine. The wind turbine model is based on a NREL 5 MW wind turbine model mounted on an OC3-Hywind floater with three catenary mooring lines. The blade pitch system is considered to be either a simplified model with 2nd-order differential equations or an advanced model with a detailed hydraulic power unit. Numerical simulations under various environmental conditions with the correlated winds and waves are conducted using Simo-Riflex Ver. 4.15. FDD and FTC techniques are applied to the blade pitch system to detect and diagnose of unexpected faults at an early stage to prevent catastrophic failures.

The key results of the blade pitch system modeling, baseline controller, fault detection, fault diagnosis, and fault-tolerant control are summarized in Sections 5.1.1 – 5.1.6. The original contributions are summarized in Section 5.2. Some of the limitations of the present work and recommendations for future work are presented in Section 5.3.

5.1.1. Blade pitch system and baseline controller

A blade pitch system was modeled using two different types: a simplified pitch actuator and a hydraulic pitch actuator with a hydraulic power unit. To avoid a complex problem, the blade pitch actuator was modeled using 2nd order differential equations to simplify the model for global analysis. However, this model has a limitation in applying various types of faults. To capture the dynamics of the exact model of the blade pitch actuator and the various actuator faults, the hydraulic power unit should be modeled. The hydraulic power unit, with the hydraulic pump, accumulator, a set of directional control valves, and a hydraulic cylinder, was modeled to drive the hydraulic pitch actuator and to apply various faults in real applications.

The baseline controller was achieved by determining the reference rotor speed to maintain a constant torque above the rated wind speed. The blade pitch angle was controlled by directional control valves that regulate the flows to the two cylinder sides.

5.1.2. Fault modeling

Up to 25% of the hydraulic system's failures are caused by oil contamination with poor filtration. In this thesis, six types of faults in the pitch sensors and pitch actuators were considered. These faults include the bias value (PSB), fixed value (PSF) in pitch sensors, excessive friction (VEF), slit lock (VSL) on the spool, wrong applied voltage (VWV) and short-circuit (VCS) in the directional control valves. These faults result in sludge buildup on the surface of the spool and bore, which increases the possibility of excessive friction (VEF) and slit lock (VSL) on spool. An additional current through the solenoid overheats it and changes its coil impedance through the solenoid, which is subject to damage and causes wrong applied voltage (VWV) and short-circuit(VCS).

5.1.3. Fault detection

Here, a fault detection method is suggested based on a Kalman filter with a focus on the blade pitch actuator and sensor faults. In fault detection, a Kalman filter is used for residual generation and a threshold is used to detect the fault conditions. H_∞ norm and a linear matrix inequality (LMI) technique are used to set a threshold for the residual evaluation to detect faults in the blade pitch actuators and sensors. The proposed method is shown to detect all faults in a case study with 6 fault types in pitch sensors and pitch actuators at the early stage.

5.1.4. Fault diagnosis

In fault diagnosis, a single blade pitch angle and a nacelle yaw angle measurement are employed to diagnose the faults in the blade pitch system via the inference method. Based on fault diagnosis logic, the fault diagnosis decision can be made by comparing the measured values of the blade pitch and the nacelle yaw motion.

In an artificial neural network model, pre-trained ANN models are used for fault diagnosis after successful fault detection. In the diagnosis procedure, the training, validation, and ANN model tests uses numerical simulation results that were generated by Simo-Riflex combined with Java code. The accuracy in the validation procedure is approximately 98%. Additionally, the diagnostic performance, experimentally verified with the test procedure, shows a 96 % accuracy in each fault type and different environmental (wind and waves) conditions.

5.1.5. Fault-tolerant control

Two fault-tolerant control schemes are suggested for reconfigurations using a virtual sensor for sensor faults and a shutdown for actuator faults. The FTC controller accommodates PSB and PSF faults by correcting the system output $\mathbf{y}_c$ with the virtual sensor. These FTC schemes can accommodate single and multiple sensor faults. If the

FTC controller works well, then the system recognizes the nominal system and reacts in the same way as before. However, faults in the pitch actuator that are intolerable require another wind turbine FTC method. Once the actuator faults are diagnosed, an emergency shutdown of the wind turbine should be conducted to prevent other failures.

5.1.6. Response analysis

The difference in the pitch angles of the three blades is the main cause of rotor imbalance, which affects the yaw motion and tower base torsional bending moment. Additionally, rotor imbalance causes a blade root bending moment in the flap-wise direction that influences the aerodynamic thrust, platform pitch motion, and tower base fore-aft bending moment.

PSB, VEF, and VWV had minor effects on the floating wind turbine responses compared with the other faults. The PSF, VCS and VSL faults lead to an increased aerodynamic thrust due to the difference in the blade pitch angle between the fault-free and faulty blades. The VSL^{-} fault is the most severe fault in terms of the platform yaw motion and the tower base bending moment. The fault-induced frequency incurring from the VSL^{-} fault is the 1P frequency of the wind turbine. If the fault continues, the damage in the wind turbine structure will be amplified.

5.2. Original contributions

This thesis includes original contributions to the development of the modeling, controller, FDD and FTC schemes for the blade pitch system of a spar-type floating wind turbine.

• *Blade pitch system modeling*

The modeling of a hydraulic pitch system is implemented and added to Java. In the first stage, the simplified pitch actuator is modeled to apply faults and conduct a global analysis. Then, a detailed hydraulic pitch actuator with a hydraulic power unit, including a pump, valves, and hydraulic cylinders, is developed to apply detailed fault conditions in the valve.

• *Wind turbine control system*

The blade pitch and generator torque controllers are implemented in Java, coupled with the Riflex, and tested to achieve satisfactory performance of blade pitching. In the blade pitch actuator model with the hydraulic power unit, the additional PI controller for the valve control is modeled.

• *Fault modeling in the pitch sensors and the pitch actuators*

Faults in blade pitch sensors and pitch actuators are considered and modeled in Java. In the blade pitch actuator, the mechanical and electrical faults in the valves are considered.

• *Fault detection scheme*

The fault detection scheme is designed using a Kalman filter to present an estimation and fault detection strategies for different types of faults that might occur in the blade pitch system. To set a threshold, H_∞ norm and linear matrix inequality (LMI) theories are used.

• *Fault diagnosis scheme*

Fault diagnosis schemes are designed using 2 different methods. The inference method with appropriate logics for fault diagnosis is developed in Java. The ANN-based fault diagnosis is developed in Python using the TensorFlow library. These two schemes are tested to achieve a satisfactory performance with a high overall accuracy for fault diagnosis.

• *Fault-tolerant controller*

A fault-tolerant controller using a virtual sensor is designed to achieve a satisfactory performance when all the control components function normally again after a fault occurs. This controller is added to Java.

• *Response analysis*

Simulations using Simo-Riflex are conducted to check the wind turbine performances and the dynamic responses, e.g., the blade root bending moments, platform motions, and tower base bending moments of floating wind turbines, under blade pitch fault conditions considering different ocean environmental load cases.

5.3. Recommendations for future work

The method established in this thesis refers to the FDD and FTC schemes for the blade pitch system of wind turbines on spar support structures. This model can be extended to other applications.

• *ANN-based FDD scheme for other wind turbine components*

- The FDD method can be applied to all wind turbine components to ensure damage tolerant operational control. The proposed FDD schemes based on the ANN methods can be applicable to other components, such as the drivetrain, generator, or yaw system in the wind turbine. In addition, the FDD scheme can be modified to diagnose multiple faults in the blade pitch system or other components. Further studies could also consider the application of the proposed methods by using data obtained from measurements during field operations of wind turbines.

• *Wind estimation*

- Depending on the site where wind turbines are installed, strong wind loads, such as gusts or turbulent winds, acting on the rotor or blades can affect the lifetime of the wind turbine. Therefore, accurate wind estimation is essential for the reliable operation of the wind turbine for the characterization and prediction of wind resources as well as for the integration of wind power into the energy systems. Wind estimation can be conducted based on the measurement of the rotor rotational speed, the blade pitch angle, the generator torque and the power production with the following methods: a Kalman filter and an artificial neural network.

• *Model predictive control* (*MPC*)

As the size of the wind turbines increases, the blades and the tower become increasingly flexible. Control of the flexible parts in the wind turbines in the stochastic wind fields is very challenging. To enhance the robustness in the controller and the load alleviation strategies in the wind turbines, model predictive control can be applied to achieve better balancing of the tuning parameter and to predict its controlled outputs. An online optimization procedure based on a pre-defined cost function can be used to calculate the optimal control sequence.

• *Fault prognosis*

Condition and health monitoring is one of the main maintenance methodologies for wind energy industries. A fault in the mechanical components of wind turbines usually escalates as a smooth and crescent degradation of behavior and performance. If a suitable fault prognosis method with condition monitoring is used, operators can predict these incipient, or gradually developed faults. Afterwards, they can take action before causing major problems, premature breakdown or damage to other components. Additionally, it can estimate the remaining lifetime of the component.

References

[1] Global Wind Reports 2018. (2019). Global Wind Energy Council.

[2] Offshore Wind in Europe: Key Trends and Statistics 2017. (2018). The European Wind Energy Association, 2018.

[3] Offshore Wind in Europe: Key Trends and Statistics 2018. (2019). The European Wind Energy Association, 2019.

[4] Twidell, J., & Gaudiosi, G. (Eds.). (2009). Offshore wind power (Vol. 425). Multi-Science Publishing Company.

[5] Hywind demo. (2019, Dec. 26). Retrieved from https://www.equinor.com/en/what-we-do/hywind-where-the-wind-takes-us.html

[6] Hywind Scotland. (2019, Dec. 26). Retrieved from https://www.equinor.com/en/what-we-do/hywind-where-the-wind-takes-us.html#floating-wind

[7] Kincardine Offshore Wind farm Project. (2019, Dec. 26). Retrieved from http://pilot-renewables.com/

[8] Floatgen. (2019, Dec. 26). Retrieved from https://floatgen.eu/en

[9] Eolink. (2019, Dec. 26). Retrieved from http://www.eolink.fr/

[10] Gipe, P. (2004). Wind power: Renewable energy for home, farm, and business. White River Junction, VT: Chelsea Green Pub.

[11] Bianchi, F. D., De Battista, H., & Mantz, R. J. (2006). Wind turbine control systems: principles, modelling and gain scheduling design. Springer Science & Business Media.

[12] Wilson, R., & Lissaman, P. B. S. (1974). Applied aerodynamics of wind power machines, Oregon State University.

[13] Hau, E. (2013). Wind turbines: fundamentals, technologies, application, economics. Springer Science & Business Media.

[14] Lynn, P. A. (2011). Onshore and offshore wind energy: an introduction. John Wiley & Sons.

[15] Musial, W., Butterfield, S., & Ram, B. (2006). Energy from offshore wind (No. NREL/CP-500-39450). National Renewable Energy Laboratory (NREL).

[16] Arapogianni, A., et al. (2013). Deep Water; The next step for offshore wind energy. European Wind Energy Association (EWEA).

[17] Pelastar. (2019, Dec. 26). Retrieved from https://pelastar.com/

[18] Haliade. (2019, Dec. 26). Retrieved from https://www.alstom.com/press-releases-news/2013/9/alstoms-6mw-haliade-offshore-wind-turbine-loaded-at-ostend

[19] Wind float. (2019, Dec. 26). Retrieved from http://www.principlepowerinc.com/

[20] Wilkinson, M., & Hendriks, B. (2010). Reliability-focused research on optimizing Wind Energy system design, operation and maintenance: Tools, proof of concepts, guidelines & methodologies for a new generation. Collaborative Project: Large Scale Integrated Project, FP7-ENERGY-2007-1-RTD.

[21] Carroll, J., McDonald, A., & McMillan, D. (2016). Failure rate, repair time and unscheduled O&M cost analysis of offshore wind turbines. Wind Energy, 19(6), 1107-1119.

[22] Chaaban R, Ginsberg D, Fritzen CP. (2014) Structural load analysis of floating wind turbines under blade pitch system faults. In Wind Turbine Control and Monitoring (pp. 301-334). Springer.

[23] Esbensen, T., and Sloth, C. (2009). Fault diagnosis and fault-tolerant control of wind turbines. Master's thesis, Aalborg University, Aalborg, Denmark.

[24] Tavner, P. (2012). Offshore wind turbines: reliability, availability and maintenance. The Institution of Engineering and Technology.

[25] Dinwoodie, I., McMillan, D., Revie, M., Lazakis, I., & Dalgic, Y. (2013). Development of a combined operational and strategic decision support model for offshore wind. Energy Procedia, 35, 157-166.

[26] Buck, B. H., & Langan, R. (2017). Aquaculture Perspective of Multi-Use Sites in the Open Ocean: The Untapped Potential for Marine Resources in the Anthropocene. SpringerOpen.

[27] Coronado, D., & Fischer, K. (2015). Condition monitoring of wind turbines: state of the art, user experience and recommendations. Fraunhofer Institute for Wind Energy and Energy System Technology IWES Northwest, Bremerhaven, Germany.

[28] Isermann, R., & Ballé, P. (1997). Trends in the application of model-based fault detection and diagnosis of technical processes. Control engineering practice, 5(5), 709-719.

[29] Isermann, R. (2006). Fault-diagnosis systems: an introduction from fault detection to fault tolerance. Springer Science & Business Media.

[30] Blanke, M., Kinnaert, M., Lunze, J., Staroswiecki, M., & Schröder, J. (2006). Diagnosis and fault-tolerant control (Vol. 2). Berlin: springer.

[31] Ding, S. X. (2008). Model-based fault diagnosis techniques: design schemes, algorithms, and tools. Springer Science & Business Media.

[32] Chen, W., Ding, S. X., Haghani, A., Naik, A., Khan, A. Q., & Yin, S. (2011). Observer-based FDI schemes for wind turbine benchmark. IFAC Proceedings Volumes, 44(1), 7073-7078.

[33] Wei, X., Verhaegen, M., & van Engelen, T. (2010). Sensor fault detection and isolation for wind turbines based on subspace identification and Kalman filter techniques. International Journal of Adaptive Control and Signal Processing, 24(8), 687-707.

[34] Commault, C., Dion, J. M., Sename, O., & Motyeian, R. (2002). Observer-based fault detection and isolation for structured systems. IEEE Transactions on Automatic Control, 47(12), 2074-2079.

[35] Frank, P. M., & Ding, X. (1994). Frequency domain approach to optimally robust residual generation and evaluation for model-based fault diagnosis. Automatica, 30(5), 789-804.

[36] Frank, P. M. (1990). Fault diagnosis in dynamic systems using analytical and knowledge-based redundancy: A survey and some new results. automatica, 26(3), 459-474.

[37] Ballé, P. (1999). Fuzzy-model-based parity equations for fault isolation. Control Engineering Practice, 7(2), 261-270.

[38] Gertler, J. (1995, June). Diagnosing parametric faults: from parameter estimation to parity relations. In Proceedings of 1995 American Control Conference-ACC'95 (Vol. 3, pp. 1615-1620). IEEE.

[39] Bellali, B., Hazzab, A., Bousserhane, I. K., & Lefebvre, D. (2012). Parameter estimation for fault diagnosis in nonlinear systems by ANFIS. Procedia Engineering, 29, 2016-2021.

[40] Cimpoesu, E. M., Ciubotaru, B. D., & Stefanoiu, D. (2013, May). Fault detection and diagnosis using parameter estimation with recursive least squares. In 2013 19th International Conference on Control Systems and Computer Science (pp. 18-23). IEEE.

[41] Duyar, A., Eldem, V., Merrill, W., & Guo, T. H. (1994). Fault detection and diagnosis in propulsion systems-A fault parameter estimation approach. Journal of Guidance, Control, and Dynamics, 17(1), 104-108.

[42] Nejad, A. R., Odgaard, P. F., Gao, Z., & Moan, T. (2014). A prognostic method for fault detection in wind turbine drivetrains. Engineering Failure Analysis, 42, 324-336.

[43] Chakkor, S., Baghouri, M., & Hajraoui, A. (2014). Performance analysis of faults detection in wind turbine generator based on high-resolution frequency estimation methods. International Journal of Advanced Computer Science and Applications, 5(4), 139-148.

[44] Watson, S. J., Xiang, B. J., Yang, W., Tavner, P. J., & Crabtree, C. J. (2010). Condition monitoring of the power output of wind turbine generators using wavelets. IEEE Transactions on Energy Conversion, 25(3), 715-721.

[45] Pozo, F., & Vidal, Y. (2016). Wind turbine fault detection through principal component analysis and statistical hypothesis testing. Energies, 9(1), 3.

[46] Feng, Z., & Liang, M. (2014). Fault diagnosis of wind turbine planetary gearbox under nonstationary conditions via adaptive optimal kernel time–frequency analysis. Renewable Energy, 66, 468-477.

[47] Chang-hao, Y., Chang-an, Z., & Xiao-jian, H. (2008, December). Inference method for fault diagnosis of complex systems based on Bayesian network. In 2008 Second International Symposium on Intelligent Information Technology Application (Vol. 3, pp. 131-136). IEEE.

[48] Clever, S., Muenchhof, M., & Mueller, D. (2009). A Fault Diagnosis Toolbox Applying Classification and Inference Method. IFAC Proceedings Volumes, 42(8), 486-491.

[49] Song, X. D., Shao, W., Qiu, Z. Z., & Chen, Y. X. (2013). Study on Fuzzy Inference Method for Fault Diagnosis Expert System. In Advanced Materials Research (Vol. 658, pp. 639-642). Trans Tech Publications.

[50] Kincses, T. Z., Antal, A., Nitsche, M. A., Bártfai, O., & Paulus, W. (2004). Facilitation of probabilistic classification learning by transcranial direct current stimulation of the prefrontal cortex in the human. Neuropsychologia, 42(1), 113-117.

[51] Tatsuoka, K. K. (1985). A probabilistic model for diagnosing misconceptions by the pattern classification approach. Journal of Educational Statistics, 10(1), 55-73.

[52] Kéri, S., Szlobodnyik, C., Benedek, G., Janka, Z., & Gádoros, J. (2002). Probabilistic classification learning in Tourette syndrome. Neuropsychologia, 40(8), 1356-1362.

[53] Santos, P., Villa, L., Reñones, A., Bustillo, A., & Maudes, J. (2015). An SVM-based solution for fault detection in wind turbines. Sensors, 15(3), 5627-5648.

[54] Zeng, J., Lu, D., Zhao, Y., Zhang, Z., Qiao, W., & Gong, X. (2013, June). Wind turbine fault detection and isolation using support vector machine and a residual-based method. In 2013 American Control Conference (pp. 3661-3666). IEEE.

[55] Malik, H., & Mishra, S. (2015). Application of probabilistic neural network in fault diagnosis of wind turbine using FAST, TurbSim and Simulink. Procedia Computer Science, 58, 186-193.

[56] Wang, L., Zuo, S., Song, Y. D., & Zhou, Z. (2014). Variable torque control of offshore wind turbine on spar floating platform using advanced RBF neural network. In Abstract and Applied Analysis (Vol. 2014). Hindawi.

[57] Li, S., Wunsch, D. C., O'Hair, E. A., & Giesselmann, M. G. (2001). Using neural networks to estimate wind turbine power generation. IEEE Transactions on energy conversion, 16(3), 276-282.

[58] Bach-Andersen, M., Rømer-Odgaard, B., & Winther, O. (2018). Deep learning for automated drivetrain fault detection. Wind Energy, 21(1), 29-41.

[59] Simani, S., Farsoni, S., & Castaldi, P. (2015). Fault diagnosis of a wind turbine benchmark via identified fuzzy models. IEEE Transactions on Industrial Electronics, 62(6), 3775-3782.

[60] Simani, S., Farsoni, S., & Castaldi, P. (2015). Wind turbine simulator fault diagnosis via fuzzy modelling and identification techniques. Sustainable Energy, Grids and Networks, 1, 45-52.

[61] Almeida, R. J., & Sousa, J. M. C. (2006). Comparison of fuzzy clustering algorithms for classification. In 2006 International Symposium on Evolving Fuzzy Systems (pp. 112-117). IEEE.

[62] Gosain, A., & Dahiya, S. (2016). Performance analysis of various fuzzy clustering algorithms: a review. Procedia Computer Science, 79, 100-111.

[63] L Rokach, Introduction to machine learning. (2019, Dec. 26). Retrieved from https://www.slideshare.net/liorrokach/introduction-to-machine-learning-13809045

[64] Sloth, C., Esbensen, T., & Stoustrup, J. (2010, June). Active and passive fault-tolerant LPV control of wind turbines. In Proceedings of the 2010 American Control Conference (pp. 4640-4646). IEEE.

[65] Kamal, E., Aitouche, A., Ghorbani, R., & Bayart, M. (2012). Robust fuzzy fault-tolerant control of wind energy conversion systems subject to sensor faults. IEEE Transactions on Sustainable Energy, 3(2), 231-241.

[66] Shi, F., & Patton, R. (2015). An active fault tolerant control approach to an offshore wind turbine model. Renewable Energy, 75, 788-798.

[67] Seron, M. M., De Doná, J. A., & Richter, J. H. (2013). Integrated sensor and actuator fault-tolerant control. International Journal of Control, 86(4), 689-708.

[68] Fan, L. L., & Song, Y. D. (2012). Neuro-adaptive model-reference fault-tolerant control with application to wind turbines. IET Control Theory & Applications, 6(4), 475-486.

[69] Vidal, Y., Tutivén, C., Rodellar, J., & Acho, L. (2015). Fault diagnosis and fault-tolerant control of wind turbines via a discrete time controller with a disturbance compensator. Energies, 8(5), 4300-4316.

[70] Sloth, C., Esbensen, T., & Stoustrup, J. (2011). Robust and fault-tolerant linear parameter-varying control of wind turbines. Mechatronics, 21(4), 645-659.

[71] Jonkman, J., Butterfield, S., Musial, W., & Scott, G. (2009). Definition of a 5-MW reference wind turbine for offshore system development (No. NREL/TP-500-38060). National Renewable Energy Lab.(NREL), Golden, CO (United States).

[72] Jonkman, J. (2010). Definition of the Floating System for Phase IV of OC3 (No. NREL/TP-500-47535). National Renewable Energy Lab.(NREL), Golden, CO (United States).

[73] Chiang, M. H. (2011) A novel pitch control system for a wind turbine driven by a variable-speed pump-controlled hydraulic servo system Mechatronics, 21, 753-761

[74] Lu B, Li Y, Wu X and Yang Z (2009) A review of recent advances in wind turbine condition monitoring and fault diagnosis Proceedings of the 2005 IEEE International Conference on Robotics and Automation ICRA 2005 pp 2290-2295

[75] Fritz Schur Energy. Pros and cons of hydraulic pitch systems, (2019, Dec. 26). Retrieved from https://www.fsenergy.com/technology/hydraulic-vs-electric-pitch/

[76] Liebherr, Liebherr-Components for Wind Turbines [Youtube Video]. (2019, Dec. 26). Retrieved from https://www.youtube.com/watch?v=DeIuvwZwYP8&t=80s

[77] DSTI - Dynamic Sealing Technologies, Inc., How Do Rotary Unions Work in Wind Turbines? [Youtube Video]. (2019, Dec. 26). Retrieved from https://www.youtube.com/watch?v=QvisCF0jWs0

[78] William Lyons, Wind Turbine Tour [Youtube Video]. (2019, Dec. 26). Retrieved from https://www.youtube.com/watch?v=8wK1qmRv_l8

[79] Karpenko, M., & Sepehri, N. (2005). Fault-tolerant control of a servohydraulic positioning system with crossport leakage. IEEE Transactions on Control Systems Technology, 13(1), 155-161.

[80] Directional control valves, pilot-operated, with electrical position feedback and integrated electronics (OBS): RE29093 (2016), Rexroth. 1-20.

[81] Albers, P. (2010). Motion control in offshore and dredging. Springer Science & Business Media.

[82] Šulc, B., & Jan, J. A. (2002). Non linear modelling and control of hydraulic actuators. Acta Polytechnica, 42(3).

[83] Hydraulic Cylinders: 380 bar Series-Production Range, Liebherr.

[84] Merritt, H., Merritt, H. E., & Merritt, H. E. (1967). Hydraulic control systems. John Wiley & Sons.

[85] Dutton, K., Thompson, S., & Barraclough, B. (1997). The art of control engineering. Harlow: Addison Wesley.

[86] SINTEF Ocean. (2018). SIMO 4.15.0 User Guide.

[87] SINTEF Ocean. (2018). RIFLEX 4.15.0 User Guide.

[88] Moriarty, P. J., & Hansen, A. C. (2005). AeroDyn theory manual (No. NREL/TP-500-36881). National Renewable Energy Lab., Golden, CO (US).

[89] Larsen, T.J. and Hanson, T.D. (2007). A method to avoid negative damped low-frequency tower vibration for a floating, pitch controlled wind turbine. Journal of Physics: Conference Series (Vol. 75, p. 012073).

[90] International Electrotechnical Commission. (2005). IEC 61400-1: Wind turbines part 1: Design requirements. International Electrotechnical Commission.

[91] International Electrotechnical Commission. (2009). IEC 61400-3 Wind Turbines Part3: Design Requirements for Offshore Wind Turbines. International Electrotechnical Commission: Geneva, Switzerland.

[92] Jonkman, B. J., & Buhl Jr, M. L. (2006). TurbSim user's guide (No. NREL/TP-500-39797). National Renewable Energy Lab.(NREL), Golden, CO (United States).

[93] Hasselmann, K., Barnett, T. P., Bouws, E., Carlson, H., Cartwright, D. E., Enke, K., ... & Meerburg, A. (1973). Measurements of wind-wave growth and swell decay during the Joint North Sea Wave Project (JONSWAP). Ergänzungsheft 8-12.

[94] Johannessen, K., Meling, T. S., & Hayer, S. (2001, January). Joint distribution for wind and waves in the northern North Sea. In The Eleventh International Offshore and Polar Engineering Conference. International Society of Offshore and Polar Engineers.

[95] Chen, C. T. (1998). Linear system theory and design. Oxford University Press, Inc.

[96] Cho, S., Gao, Z., & Moan, T. (2016). Model-based fault detection of blade pitch system in floating wind turbines. Journal of Physics: Conference Series (Vol. 753, No. 9, p. 092012)

[97] Cho, S., Gao, Z., & Moan, T. (2018). Model-based fault detection, fault isolation and fault-tolerant control of a blade pitch system in floating wind turbines. Renewable energy, 120, 306-321.

[98] HEIDENHAIN GMBH, Incremental angle encoder / bearingless / high-accuracy / steel scale [Image]. (2019, Dec. 26). Retrieved from https://www.directindustry.com/prod/dr-johannes-heidenhain-gmbh/product-155-1239189.html

[99] Mariners Repository, Hydraulics 3 - Flow control [Image]. (2019, Dec. 26). Retrieved from http://marinersrepository.blogspot.com/p/hydraulics-3-volume-control.html

[100] Watton, J. (2007). Modelling, monitoring and diagnostic techniques for fluid power systems. Springer Science & Business Media.

[101] Faragher, R. (2012). Understanding the basis of the Kalman filter via a simple and intuitive derivation. IEEE Signal processing magazine, 29(5), 128-132.

[102] Tensorflow tutorial. (2019, Dec. 26). Retrieved from https://www.tensorflow.org/tutorials

[103] Cho S, Bachynski E, Rasekhi Nejad A, Gao Z, Moan T. (2019). Numerical modeling of hydraulic blade pitch actuator in a spar-type floating wind turbine considering fault conditions and their effects on global dynamic responses. Wind Energy, Early View Publication, 1-21.

Appendix A: Selected papers

A1. Paper 1

Model-based fault detection of blade pitch system in floating wind turbines

Seongpil Cho, Zhen Gao and Torgeir Moan

Published in Journal of Physics: Conference Series 2016; 753, 092012.

Model-based fault detection of blade pitch system in floating wind turbines

S Cho[1, 2], Z Gao[1, 2] and T Moan[1, 2]

[1] Department of Marine Technology, Norwegian University of Science and Technology (NTNU), Trondheim, Norway.
[2] Centre for Autonomous Marine Operations and Systems (AMOS), Norwegian University of Science and Technology (NTNU), Trondheim, Norway.

Corresponding author's e-mail address: seongpil.cho@ntnu.no

Abstract. This paper presents a model-based scheme for fault detection of a blade pitch system in floating wind turbines. A blade pitch system is one of the most critical components due to its effect on the operational safety and the dynamics of wind turbines. Faults in this system should be detected at the early stage to prevent failures. To detect faults of blade pitch actuators and sensors, an appropriate observer should be designed to estimate the states of the system. Residuals are generated by a Kalman filter and a threshold based on H_∞ optimization, and linear matrix inequality (LMI) is used for residual evaluation. The proposed method is demonstrated in a case study that bias and fixed output in pitch sensors and stuck in pitch actuators. The simulation results show that the proposed method detects different realistic fault scenarios of wind turbines under the stochastic external winds.

1. Introduction

Maintenance and repair of offshore wind turbines are challenging because of the difficult access. Especially, faults occur unexpectedly in components of wind turbines such as blades, drivetrain or generator. Faults in wind turbines can directly influence the operational safety, dynamics and power production efficiency of wind turbines. An early-stage fault diagnosis technique should be conducted regarding maintenance and repair to prevent loss of energy production and economic values of wind turbines with active fault accommodation. Therefore, there is a growing demand for fault-tolerant control which can be achieved an efficient fault diagnosis and accommodation.

The blade pitch system is crucial to adjust the blade pitch angle for controlling rotor speed, aerodynamic force, torque, and power. The main faults of the blade pitch system occur in its blade pitch sensor and actuator. These faults influence control feedback and result in imbalance loads on the rotor, shaft, and the main bearings. The detection of faults allows for fast accommodation to avoid catastrophic long term damages in the wind turbines.

A model-based fault detection method comprises residual generation and evaluation based on a threshold method [1][2]. The residual signal must be close to zero in a normal condition. In a model-based approach, the faults are detected typically by a residual signal, the value of which must be greater than zero in a fault condition. The threshold based on the H_∞ norm that represents a maximum effect of the disturbance was employed by Zhang et al. [2]. Also, linear matrix inequality (LMI) was used to determine the optimal H_∞ norm and to design a robust fault detection observer [2].

Sensor fault detection and isolation in the blade pitch system, generator shaft and converter were simulated by Odgaard et al. [3]. Chen et al. [4] applied observer-based FDI schemes to the model presented by [3]. The simulations in those studies were performed in frequency domain analyses that have limitations on fast detection of the pitch sensor and actuator faults. Wang et al. [5] used a time-domain approach that ensured fast fault detection for floating wind turbines.

This paper deals with a fault detection method in blade pitch sensors and actuators of a wind turbine model by using Kalman filter. The case study is based on the NREL 5MW wind turbine model [6] supported by the spar buoy floater (OC3 Hywind) [7]. The dynamic behavior of the wind turbine model is simulated by using Simo-Riflex-Aerodyn (SRA) [8] and external control code for a PI pitch and torque controller. A subroutine is added to SRA to account for pitch actuator and sensor. The observer based on Kalman filter estimates the states of the system based on a mathematical model, sensor measurements, and input commands. Faults generated in blade pitch sensors and actuators can be detected by this observer based on residual generation and evaluation method by using a threshold. Faults in the blade pitch system are given in the input file of SRA to test the feasibility of the fault detection. Fault magnitude, type and occurrence time are decided in advance. The optimal threshold is computed by H_∞ norm and the LMI approach.

This paper is organized as follows: Section 2 describes the blade pitch system consisted of the baseline controller, pitch actuator, and pitch sensor. In Section 3 fault detection schemes of the blade pitch system are introduced with Kalman filter, H_∞ norm and the LMI approach for threshold design. In Section 4, simulation results for the fault detection technique are presented by a residual method and fault decision by a fault detection criterion. The conclusions are presented in Section 5.

2. Blade pitch system

Wind turbines should be designed to maximize generated power and ensure continued reliability during operation. The operational region from the cut-in wind speed to the cut-out wind speed is divided into below-rated (Region II) and above-rated regions (Region III) of wind speed as illustrated in Figure 1. In order to optimize the productivity of a wind turbine in Region II and III, its power output must be maximized from the cut-in wind speed ($V_{cut\text{-}in}$, 3m/s) to the rated wind (V_{rated}, 11.4m/s) in Region II and constant until the cut-out wind speed ($V_{cut\text{-}out}$, 25m/s) in Region III achieved by adjusting the blade pitch angle and controlling generator torque with blade pitch and torque controller. A blade pitch system mainly comprises a PI controller, pitch actuator and pitch sensor.

2.1. Baseline Control system

The baseline control system includes two separate controllers for regulating blade pitch angles and generator torque, respectively. In Region II, the control strategy is to capture the maximum power by maintaining optimal tip speed ratio [6]. The generator torque is inversely proportional to the filtered generator speed. Within this region, the blade pitch controller is not active and maximum power is achieved by adjusting the generator torque.

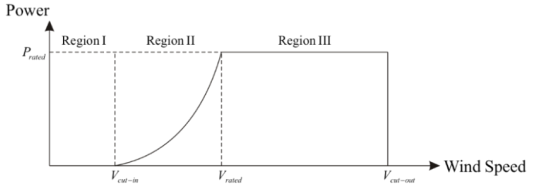

Figure 1. Ideal power curve as a function of the wind speed

In Region III, a constant torque variable pitch controller is used for floating wind turbines regarding stability issue [9] by modified gains of the controller. A blade pitch reference $\beta_{ref}(t)$ is computed based on gain-scheduled proportional-integral (PI) controller as the function of the generator torque error $e(t)$ based on a constant-torque strategy [10] in floating wind turbines.

$$\beta_{ref}(t) = K_P(\beta)e(t) + K_I(\beta)\int_0^{t_1} e(t)dt\,,\ e(t) = f(\tau_{g,ref} - \tau\,(t)) \tag{1}$$

The blade pitch control system of the wind turbine regulates the blade pitch angle and the generator speed. The values of control gains are described as follows

$$K_P(\beta) = GK(\beta)K_{P,0},\ K_I(\beta) = GK(\beta)K_{I,0},\ GK(\beta) = 1/(1+\beta/K_K) \tag{2}$$

where $K_P(\beta)$ is the proportional gain, $K_I(\beta)$ is the integration gain, $GK(\beta)$ is the gain correction factor, K_K is the pitch angle where the gain function is equal to 0.5 for the NREL 5MW wind turbine [6].

Using the properties for the recommended response characteristics, the resulting gains are $K_{P,0}$ = 0.0188268s, $K_{I,0}$ = 0.00806863, and K_K = 0.11 [6]. The pitch rate limit is set from -8 to 8°/s based on General Electric (GE)'s long-blade test program. Also, the pitch range is also set from 0° to 90°. Figure 2 shows a block diagram of the baseline control system that can represent how the system interacts the blade pitch system with other systems by measuring the generator speed and pitch angle. The parameters can be described in Figure 2 that Ω_r is the rotor speed, Ω_g is the generator speed, $\Omega_{g,m}$ is the measured generator speed, $\Omega_{g,rated}$ is the rated generator speed, τ_g is the generator torque, τ_a is the aerodynamic torque, and β_m is the measured blade pitch angle, and V_w is the wind speed.

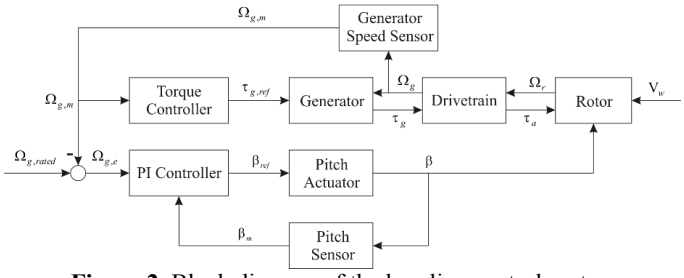

Figure 2. Block diagram of the baseline control system

2.2. Pitch actuator

Regulating each blade pitch angle individually, a 2nd-order pitch actuator is modeled to the 5 MW turbine model. Consider the blade pitch system that describes a blade pitch reference from the PI controller and the pitch angle measurement

$$\ddot{\beta}_i + 2\zeta\omega_n\dot{\beta}_i + \omega_n^2\beta_i = \omega_n^2\beta_{ref}\ ,\ i = 1,\ 2 \text{ and } 3 \tag{3}$$

where ω_n is the natural frequency and ζ is the damping ratio of the actuator. The parameters are ω_n = 11.11 rad/s and ζ = 0.6 [1].

Eq. (3) can also be represented as state space form including varying parameters as

$$\dot{\mathbf{x}}(t) = \mathbf{A}\mathbf{x}(t) + \mathbf{B}u(t) + \mathbf{w}(t)$$

or

$$\begin{bmatrix}\dot{\beta}_i(t)\\ \ddot{\beta}_i(t)\end{bmatrix} = \begin{bmatrix}0 & 1\\ -\omega_n^2 & -2\zeta\omega_n\end{bmatrix}\begin{bmatrix}\beta_i(t)\\ \dot{\beta}_i(t)\end{bmatrix} + \begin{bmatrix}0\\ \omega_n^2\end{bmatrix}\beta_{ref,i}(t) + \begin{bmatrix}w_{i,1}\\ w_{i,2}\end{bmatrix},\ i = 1,\ 2 \text{ and } 3 \tag{4}$$

where $\mathbf{x}(t)$ and $u(t)$ are the state vector and input command by the individual blade pitch angle in the blade 1,2 and 3, respectively. **A** and **B** are system matrices: the state transition matrix and input matrix.

The actuator model in Eq. (4) describes the dynamic behavior between a pitch reference from the controller and the measurement of a pitch angle.

2.3. Pitch sensor

Since the turbine monitoring and control are based on sensor data during wind turbine operation, it is important that the acquired data should be accurate and reliable. A discretized control system including measurement noise is used in this paper. Measurement noise modeled as zero-mean

Gaussian distribution to the deterministic values according to the standard deviation is added to the pitch sensor model. Measurement equation for the sensor in the blade 1, 2 and 3, respectively is represented by a state space form as

$$y(t) = \mathbf{C}\mathbf{x}(t) + v(t)$$

or

$$\beta_{i,mes}(t) = \begin{bmatrix} 1 & 0 \end{bmatrix} \begin{bmatrix} \beta_i(t) \\ \dot{\beta}_i(t) \end{bmatrix} + v_{i,\beta}(t), \; i = 1, 2 \text{ and } 3 \tag{5}$$

where $y(t)$ is the pitch angle measurement in the blade 1, 2 and 3 and $\mathbf{C}$ is the measurement matrix.

3. Fault detection methods

Basic methods for establishing and evaluating residual are described in this section. Figure 3 shows the basic structure of model-based fault detection. Based on the input command $u(k)$ and measured output $y(k)$, states and measurements are estimated by an observer. By comparing measured and estimated values, changes of a state are identified by a threshold.

3.1. Observer design based on discrete-time space model in the blade pitch system

The continuous system (4) and (5) should be discretized for suitable numerical computing and employing observer. The discrete-time state space model of the blade pitch system with disturbance and faults in the pitch actuator and sensor can be transferred from the proposed system (4) and (5) that Euler discretization approach is applied.

$$\begin{aligned} \mathbf{x}(k+1) &= \mathbf{\Phi}\mathbf{x}(k) + \mathbf{\Psi}\mathbf{u}(k) + \mathbf{\Gamma}_f \mathbf{f}_A(k) + \mathbf{\Gamma}_d \mathbf{w}(k) \\ y(k) &= \mathbf{H}\mathbf{x}(k) + \mathbf{\Xi}_f f_S(k) + \mathbf{\Xi}_d v(k) \end{aligned} \tag{6}$$

where $\mathbf{\Phi} = \mathbf{I} + \mathbf{A}T$ and $\mathbf{\Psi} = \mathbf{\Gamma}_f = \mathbf{B}T$. Here, $\mathbf{\Phi}$, $\mathbf{\Psi}$, $\mathbf{H}$, $\mathbf{\Gamma}_d$, $\mathbf{\Gamma}_f$, $\mathbf{\Xi}_d$ and $\mathbf{\Xi}_f$ are known constant matrices in a discretized system. T is sampling time. The sensor noise is given as the uncertain disturbance including the process noise vector $\mathbf{w}(k)$ and measurement noise $v(k)$. Regarding faults, $\mathbf{f}_A(k)$ and $f_S(k)$ are the actuator fault vector and sensor fault value, respectively.

The observer with fault-free case based on Kalman filter is designed as follows,

$$\begin{aligned} \hat{\mathbf{x}}(k+1) &= \mathbf{\Phi}\hat{\mathbf{x}}(k) + \mathbf{\Psi}\mathbf{u}(k) + \mathbf{K}(y(k) - \mathbf{H}\hat{\mathbf{x}}(k)) \\ \hat{y}(k) &= \mathbf{H}\hat{\mathbf{x}}(k) \end{aligned} \tag{7}$$

where $\hat{\mathbf{x}}(k)$, $\hat{y}(k)$ and $\mathbf{K}$ are the estimated state vector, estimated output and Kalman gain matrix.

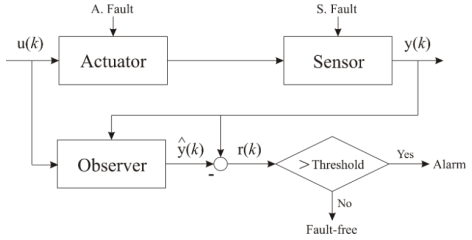

Figure 3. Scheme of observer-based fault diagnosis in the blade pitch system

3.2. Fault modelling

A pitch actuator is internally controlled by a pitch controller connected to a pitch sensor. A fault occurring in pitch system can influence the closed-loop control system and the dynamics of a wind turbine. Faults of the blade pitch system are mainly categorized by the pitch sensor and actuator fault.

The pitch sensor fault occurs by dust on encoder disc, miss-adjustment of the blade pitch bearing, beyond acceptable range of temperature and humidity or improper calibration. These causes can result in the unbalanced rotation of the rotor from the sensor bias and fixed outputs from last measurements.

The fault-free sensor is modeled as

$$\beta_{mes}(k) = \beta(k) + v(k) \tag{8}$$

Bias (PSB) can be represented by a constant offset value that is added to the measurement from the sensor

$$\beta_{mes}(k) = \beta(k) + \beta_{bias}(k) + v(k) \tag{9}$$

where $\beta_{bias}(k)$ is the pitch bias angle.

Fixed output (PSF) of sensor is that keeps the last measurement after the fault occurrence described as

$$\beta_{mes}(k) = \beta_{fixed}(k) \tag{10}$$

where $\beta_{fixed}(k)$ is the pitch after the fault.

The stuck actuator (PAS) is mainly due to valve blockage in a hydraulic pitch actuator system. Once one of the valves is blocked, the piston cannot move in pitch actuator and the ability to pitch the blade. This stuck actuator is described as

$$\beta(k+1) = \beta_{SA},\ \dot{\beta}(k+1) = 0 \tag{11}$$

where β_{SA} is the pitch angle for the stuck actuator.

These faults for the blade pitch sensor and actuator frequently appear and result in structural loading of the turbine due to rotor imbalance and affect the stability of the floating platform.

Modeling the faults in the system, the state space model for the blade pitch system (6) should be updated. Table 1 describes the fault vectors in the actuator and values in the sensor. If a fault occurs in the pitch system, the fault value is applied in the pitch system equation in this algorithm.

Table 1. Mathematical model of faults applied in numerical simulations

Location	Type	Fault value
Sensor	Biased output (PSB)	$\mathbf{f}_A(k) = 0,\ f_S(k) = \beta_{Bias}$
	Fixed output (PSF)	$\mathbf{f}_A(k) = 0,\ f_S(k) = -\beta(k) + \beta_{fixed} - v(k)$
Actuator	Stuck (PAS)	$\mathbf{f}_A(k) = \begin{bmatrix} -\beta(k) - T\dot{\beta}(k) + \beta_{AS} - w_1(k) \\ (\omega_n^2\beta(k) + 2\zeta\omega_n\dot{\beta}(k) - \omega_n^2\beta_{ref}(k))T - w_2(k) \end{bmatrix},\ f_S(k) = \beta_{Bias}$

3.3. Residual generation and evaluation

A residual $r(k)$ is difference between the measured and estimated values described as

$$r(k) = y(k) - \hat{y}(k) \tag{12}$$

A residual energy $J(k)$ is defined by L_2 norm which is described by root-mean-square (RMS) of residual as

$$J(k) = \|r(k)\|_2 = \left(\int_{k_1}^{k_2} r^T(k) r(k) dk \right)^{1/2} \tag{13}$$

Since the residual energy in fault cases includes fault information, the generated residual energy should be evaluated by fault detection logic. The residual determines the fault status by applying fault detection logic with threshold J_{th} in Eq. (14).

$$\begin{aligned} &J(k) < J_{th},\ \text{fault} - \text{free} \\ &J(k) > J_{th},\ \text{fault} \end{aligned} \tag{14}$$

The threshold is generated with the uncertainty that is bounded. Hence, while the residual energy is less than this threshold, the fault-free state can be indicated. Otherwise, the fault can be detected.

3.4. Threshold design

Since residual energy defined by RMS of the residual is used for fault detection, H_2 norm could be used for threshold design. H_2 norm gives a characterization of the RMS-value of the system response to uncertain inputs. However, H_∞ norm is more fundamental norm for systems and provides a measure of a worst-case system gain. H_∞ optimization is a robust method considered various uncertainties, especially disturbance. It also measures the maximum effect of the disturbances on the residual. H_∞ optimization problems are frequency-domain oriented as described in (15)

$$H_\infty = \left\| \mathbf{G}_{rd}(z) \right\|_\infty = \sup_\omega \left(\mathbf{G}_{rd}(j\omega) \right) \tag{15}$$

where $\mathbf{G}_{rd}(z)$ is disturbance transfer function.

As described in (16), residual energy $J(k)$ is consisted of $r_d(k)$ and $r_f(k)$.

$$J(k) = \left\| r_d(k) + r_f(k) \right\|_2 \tag{16}$$

where $r_d(k)$ and $r_f(k)$ are residuals in disturbance and fault, respectively.

If the system is a fault-free state, $r_f(k)$ should be zero. Then the residual energy is expressed as

$$J(k) = \left\| r_d(k) \right\|_2 \le \left\| \mathbf{G}_{rd}(z) \right\|_\infty \left\| v \right\|_2 \le \gamma_{\min} \delta_d \tag{17}$$

where the residual energy is bounded by $\left\| \mathbf{G}_{rd} \right\|_\infty \left\| v \right\|_2$. $\gamma_{\min}$ is determined in Appendix A with more details for the derivation of the threshold.

Therefore, the threshold is set as

$$J_{th} = \gamma_{\min} \delta_d \,. \tag{18}$$

4. Simulation results and discussion

In this section, a series of simulation results are presented where one blade has faults in the pitch sensor and actuator. The results prove the performance of the fault detection technique under different fault scenarios with the baseline controller. Simulations for the wind turbine subjected to a stochastic wind speed are conducted under three different fault conditions: bias (PSB), fixed output (PSF) in sensors, and a stuck actuator (PAS). For these three cases, blade 3 is subjected to a fault at 200s.

4.1. Wind modelling

Wind turbines operate under variable wind conditions such as a stochastic wind model presenting realistic winds. Turbsim [11] which is the turbulent wind simulator is used to generate realistic turbulent wind model and to test the turbine controllers in a more realistic scenario in this study. The wind model is based on the IEC 61400-3 design code. The stochastic wind data have the following characteristics in Table 2. As shown in Figure 4 that the range of the stochastic wind (12 – 24.2 m/s) covers the Region III, as its values range from 11.4 m/s up to the maximum of 25 m/s.

Table 2. Turbulent wind characteristics

Turbulence model	Kaimal's model
IEC wind type	NTM
Wind profile type	Power law profile
Grid size	160 × 160
Reference height	90m
Mean wind speed	17 m/s
Surface roughness length	0.0003 m

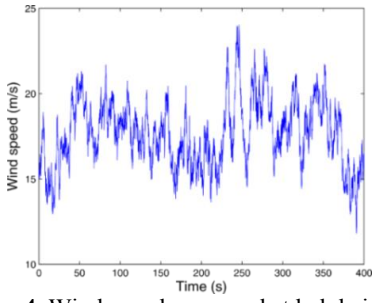

Figure 4. Wind speed measured at hub height

4.2. Effects of sensor and actuator faults

This section studies effects of faults in pitch sensors and actuators. Figure 5 shows simulation results in comparison with the pitch angle reference and measurement from a faulted blade. Each simulation has a duration of 400s where the first 200s shows the fault-free operation of the wind turbine. After 200s, sensor measurement difference caused by pitch sensor and actuator faults starts to occur. In PSB, an offset value (-3°) takes place between the reference and measurement corresponding to pitch bias. In the case of a PSF and a PAS, the pitch angle measurement shows a constant value that is the same amount of last measurement value before faults. The blade is seized that cannot respond to the change in the wind speed in the PAS case. However, a blade still operates as the pitch reference command in the PSF case that results in oscillating pitch angle. The difference between reference and measurement values makes the pitch angle oscillate irregularly with a large amplitude. Also, it makes pitch angle difference between a fault-free (blade 1, 2) and faulty (blade 3) blade.

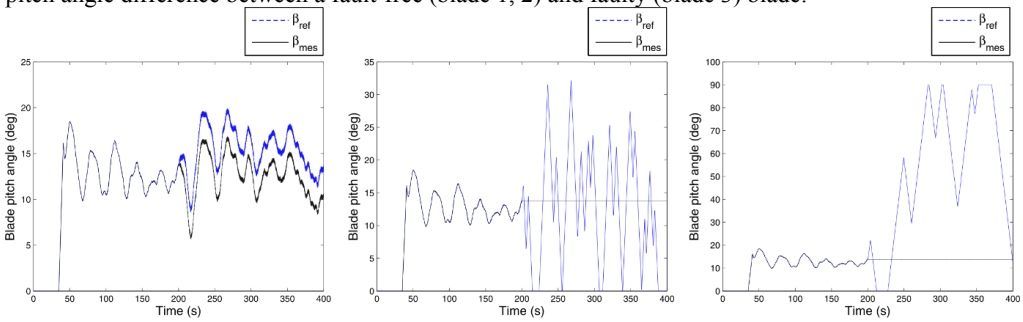

Figure 5. Comparison between pitch reference and measurement in the faulty blade (Blade 3) pitch corresponding (a) Sensor bias, (b) Fixed output in sensor and (c) Stuck actuator

Figure 6 shows a pitch angle difference between a fault-free (blade 1) and faulty (blade 3) blade corresponding to a PSB, PSF, and PAS. The incorrect pitching of a blade due to sensor measurement difference causes asymmetry forces on blades affecting the rotor introducing an unbalanced rotation. It means that a fault occurred in sensors and actuators can affect rotor dynamics and platform motions of wind turbines.

Figure 7 shows the changes of rotor speed, aerodynamic thrust, and platform yaw motion in a wind turbine due to PSB, PSF, and PAS after 200s. Incident variations in an aerodynamic thrust due to an unstable rotor speed directly affect instability of platform motions, especially a yaw motion. A PSF fault has a largest effect on dynamic behaviors compared with PSB and PAS because the magnitude of changes in aerodynamic thrust and platform yaw motion is highly increased. It concludes that structural loads are dangerously increased on the rotor, drivetrain or tower of the wind turbine.

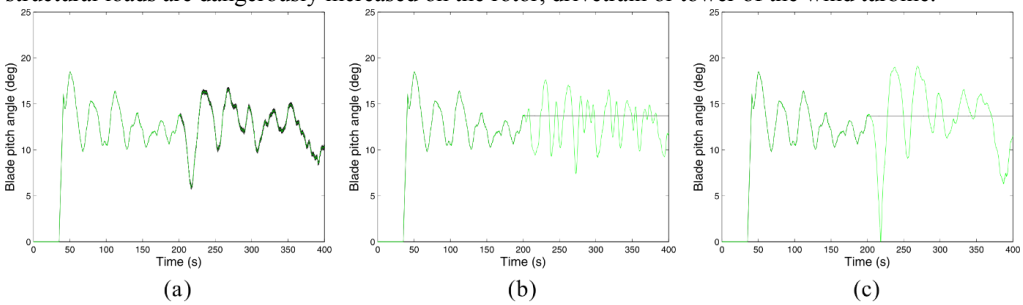

Figure 6. Measured pitch angles using sensors in fault-free (blade 1, green) and faulted (blade 3, black) blade pitch system under different fault cases corresponding (a) PSB, (b) PSF and (c) PAS

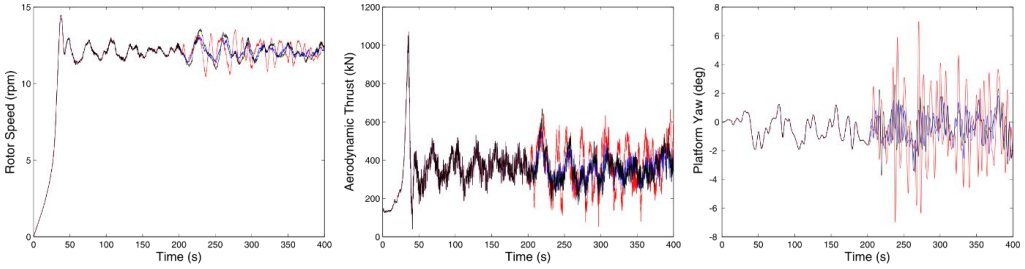

(a) (b) (c)

Figure 7. Effect of faults on (a) rotor speed, (b) aerodynamic thrust and (c) platform yaw motion under different fault cases corresponding PSB (blue), PSF (red) and PAS (black)

4.3. Fault detection results

Fault detection for the blade pitch system takes into account the faults that influence dynamics of the wind turbine. Faults in actuators and sensors can be detected effectively by the residual energy and the threshold. When the residual energy is greater than the threshold, a fault alarm is set to 1 which means that a fault is detected. The residual energy should be normalized to adjust scale factor from data. The normalized residual energy J_N is described as

$$J_N(t) = J(t)/J_{th} \tag{19}$$

Figure 8 shows simulation results in connection with the blade pitch angle, normalized residual energy, and fault alarm. In Figure 8 (a), a blade pitch sensor bias value gradually occurs during 10s after 200s in the wind turbine corresponding to a sensor bias of -3° on blade 3. At the same time, the normalized residual exceeds the threshold, and then the observer detects the blade pitch bias fault immediately by setting to fault alarm in Figure 8 (b) and (c), respectively.

Simulation results on PSF and PAS show the same pattern as well in Figures 9 and 10, respectively. These are illustrated that it is possible to detect a pitch offset on a blade 3 based on the fault detection algorithm.

For reliability of this fault detection algorithm, 15 simulations runs are conducted for mean wind speeds from 11 to 25 m/s as an increment of 1m/s. As listed in Table 3, average fault detection time in sensor and actuator faults is within 4 seconds after fault generated. It means that this method can guarantee the fault detection at the early stage in the blade pitch system.

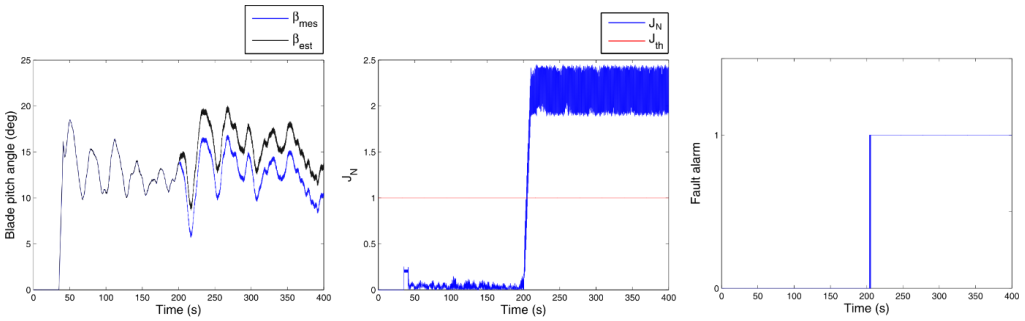

(a) (b) (c)

Figure 8. Simulation results of the PSB case corresponding the blade pitch angle: (a) pitch angle measurement (blue) and estimation (black), (b) normalized residual energy and (c) fault alarm

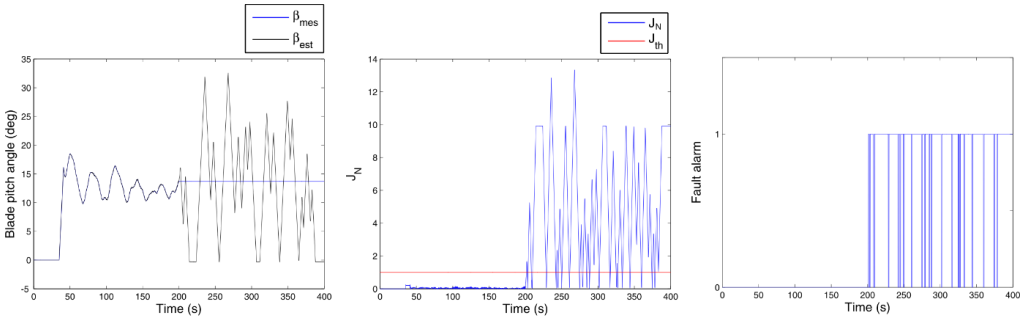

(a) (b) (c)

Figure 9. Simulation results of the PSF case corresponding the blade pitch angle: (a) pitch angle measurement (blue) and estimation (black), (b) normalized residual energy and (c) fault alarm

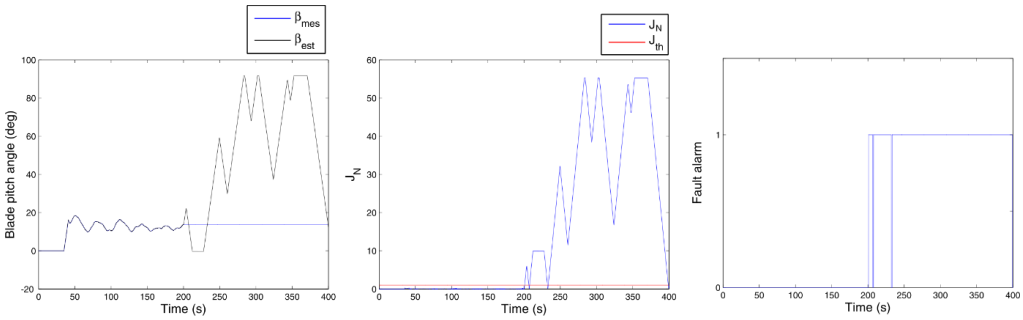

(a) (b) (c)

Figure 10. Simulation results of the PAS case corresponding the blade pitch angle: (a) pitch angle measurement (blue) and estimation (black), (b) normalized residual energy and (c) fault alarm

Table 3. Detection time of each fault after fault occurrence

Location	Type	Average detection time
Sensor	Biased output	3.7s
	Fixed output	1.3s
Actuator	Stuck	1.1s

5. Conclusion

Faults in the floating wind turbine should be detected at the early stage to prevent catastrophic failures. The fault detection method is suggested based on an observer designed by Kalman filter focus on the blade pitch actuator and sensor faults. In a model-based approach, it is typical that a fault is detected by residual signal and threshold. A Kalman filter is used for residual generation, and H_∞ norm and an LMI technique are used to set a threshold for residual evaluation for detecting faults in blade pitch actuators and sensors. The proposed method is shown to detect all three faults in a case study that bias and fixed output in pitch sensors and stuck in pitch actuators at the early stage. In the future, an algorithm to decide more accurate by the fault status to isolate described faults in the blade pitch system will be addressed. It can be used in the fault-tolerant control to avoid propagating damages in the floating wind turbine.

Appendix A. Threshold design

A1. Residual generator in frequency domain

Remember that for the state space form (4); the residual generator can be realized as a composition of Kalman filter (7). It transforms by setting $\mathbf{e}(k) = \mathbf{x}(k) - \hat{\mathbf{x}}(k)$, the residual system equations can be re-written as

$$\begin{aligned} \mathbf{e}(k+1) &= \overline{\mathbf{\Phi}}\mathbf{e}(k) + \overline{\mathbf{\Gamma}}_d \mathbf{w}(k) + \overline{\mathbf{\Gamma}}_f \mathbf{f}_A(k) \\ r(k) &= \mathbf{H}\mathbf{e}(k) + \mathbf{\Xi}_d v(k) + \mathbf{\Xi}_f f_S(k) \end{aligned} \tag{20}$$

Where $\overline{\mathbf{\Phi}} = \mathbf{\Phi} - \mathbf{K}\mathbf{H}$, $\overline{\mathbf{\Gamma}}_d = \mathbf{\Gamma}_d - \mathbf{K}\mathbf{\Xi}_d$ and $\overline{\mathbf{\Gamma}}_f = \mathbf{\Gamma}_f - \mathbf{K}\mathbf{\Xi}_f$.

Residual generator also can be defined in frequency domain as

$$r(z) = r_d(z) + r_f(z) = \mathbf{G}_{rd}(z)v(z) + \mathbf{G}_{rf}(z)f(z) \tag{21}$$

where $\mathbf{G}_{rd}(z) = \mathbf{H}(z\mathbf{I} - \overline{\mathbf{\Phi}})^{-1}\mathbf{\Gamma}_d + \mathbf{\Xi}_d$ and $\mathbf{G}_{rf}(z) = \mathbf{H}(z\mathbf{I} - \overline{\mathbf{\Phi}})^{-1}\mathbf{\Gamma}_f + \mathbf{\Xi}_f$. $\mathbf{G}_{rd}(z)$ is the disturbance transfer function, and $\mathbf{G}_{rf}(z)$ is the fault transfer function.

A2. Linear matrix inequality (LMI) in a discrete-time system

Consider a system (6) and observer (7). For a given constant $\gamma > 0$, system (6) is asymptotically stable and satisfies

$$\left\| G_d(z) \right\|_\infty \le \gamma \tag{22}$$

There exists a matrix K and a symmetric matrix $P > 0$ such that

$$\begin{bmatrix} \overline{\mathbf{\Phi}}^T \mathbf{P} \overline{\mathbf{\Phi}} - \mathbf{P} + \mathbf{H}^T\mathbf{H} & \overline{\mathbf{\Phi}}^T \mathbf{P} \overline{\mathbf{\Gamma}}_d + \mathbf{H}^T \mathbf{\Xi}_d \\ \mathbf{\Xi}_d^T \mathbf{H} & \mathbf{\Xi}_d^T \mathbf{\Xi}_d + \overline{\mathbf{\Gamma}}_d^T \mathbf{P} \overline{\mathbf{\Gamma}}_d - \gamma^2 \mathbf{I} \end{bmatrix} < 0 \tag{23}$$

where γ is a design parameter named as the performance bound.

References

[1] Esbensen T and Sloth C 2009 *Fault diagnosis and fault-tolerant control of wind turbines* (Master's thesis: Aalborg University) p 167

[2] Zhang Y, Wu L, Li J and Chen X 2012 LMI approach to mixed H_-/H_∞ fault detection observer design *Transactions of Tianjin University* **18** pp 343-349

[3] Odgaard P F, Stousturp J and Kinnaert M 2009 Fault-tolerant Control of Wind Turbines - a benchmark model, *Proceedings of the 7th IFAC Symposium on Fault Detection, Supervision and Safety of Technical Processes* (Barcelona: Spain) pp 155 - 160

[4] Chen W, Ding S X, Haghani A, Naik A, Khan A Q and Yin S 2011 Observer-based FDI Schemes for Wind Turbine Benchmark *Proceedings of the 18th IFAC World Congress* (Milano: Italy) pp 7073 – 7078

[5] Wang L, Wu L, Guan Y and Wang G 2015 Online Sensor Fault Detection Based on an Improved Strong Tracking Filter *Sensors* **15** pp 4578-4591

[6] Jonkman J, Butterfield S, Musial W and Scott G 2009 Definition of a 5-MW reference wind turbine for offshore system development *Technical Report NREL/TP-500-38060* (USA) p 63

[7] Jonkman J 2010 Definition of the floating system for Phase IV of OC3 *Technical Report NREL/TP-500-47535* (USA) p 31

[8] Bachinski E 2014 Simo-Riflex-Aerodyn manual *MARINTEK Technical Report* (Norway) p 51

[9] Larsen TJ and Hanson TD 2007 A method to avoid negative damped low-frequency tower vibration for a floating, pitch controlled wind turbine *Journal of Physics Conference Series* **75** pp 12-73

[10] Etemaddar M, Blanke M, Gao Z and Moan T 2016 Response analysis and comparison of a spar-type floating offshore wind turbine and an onshore wind turbine under blade pitch controller faults *Wind energy* **19** pp 35-50

[11] Jonkman J and Kilcher L 2012 TurbSim User's Guide *Technical Report NREL* (USA) p76

A2. Paper 2

Model-based fault detection, fault isolation and fault-tolerant control of a blade pitch system in floating wind turbines

Seongpil Cho, Zhen Gao and Torgeir Moan

Published in Renewable Energy 2018; 120, 306-321.

Renewable Energy 120 (2018) 306–321

Contents lists available at ScienceDirect

Renewable Energy

journal homepage: www.elsevier.com/locate/renene

Model-based fault detection, fault isolation and fault-tolerant control of a blade pitch system in floating wind turbines

Seongpil Cho [a, b, *], Zhen Gao [a, b], Torgeir Moan [a, b]

[a] Department of Marine Technology, Norwegian University of Science and Technology (NTNU), Trondheim, Norway
[b] Centre for Autonomous Marine Operations and Systems (AMOS), Norwegian University of Science and Technology (NTNU), Trondheim, Norway

ARTICLE INFO

Article history:
Available online 29 December 2017

Keywords:
Floating wind turbine
Fault detection and isolation
Fault-tolerant control
Kalman filter
Virtual sensor

ABSTRACT

This paper presents model-based fault detection, fault isolation, and fault-tolerant control schemes focused on blade pitch systems in floating wind turbines. Fault detection, isolation, and accommodation techniques are required to achieve high power capture efficiency and structural reliability in floating wind turbines. Faults in blade pitch systems should be detected at an early stage to prevent catastrophic failures. To detect faults of the blade pitch systems, a Kalman filter is designed to estimate the blade pitch angle of the system. The fault isolation algorithm is based on inference methods and capable of determining the fault type, location, magnitude and time. The fault-tolerant controller based on a reconfiguration block with a virtual sensor and shutdown mode controls the floating wind turbine to avoid unexpected external loads. The proposed methods are demonstrated in case studies with stochastic wind and wave conditions that considering different types of faults, such as biases and fixed outputs in pitch sensors and stuck pitch actuators. The simulation results show that the proposed methods can detect and isolate multiple faults effectively at an early stage. Additionally, the effectiveness of the fault-tolerant control systems for different load cases for single and multiple fault conditions is verified by numerical simulations.

1. Introduction

The wind energy industry has experienced rapid growth because of environmental issues and the demand for sustainable solutions. Offshore wind technology in particular has experienced rapid development in recent years, with an annual cumulative global installed capacity of 12.105 GW by the end of 2015 [1]. Historically, most wind turbines were installed in shallow water on bottom-fixed substructures. Currently, offshore wind farms are moving further into deeper water at an average distance of 43.3 km [2] from the shore to capture the high wind energy density. In deeper water, floating wind turbines are more cost effective than bottom-fixed wind turbines. Development projects for floating wind turbines are emerging, including the Hywind 2 project in Scotland and the WindFloat Atlantic and Pacific project in the USA.

Floating wind turbines operate in stochastic ocean environments, such as turbulent winds, irregular waves, and significant disturbances, and they might experience unexpected failures that could lead to system interruptions and cause huge economic losses. Therefore, maintenance and optimal operations of floating wind turbines become critical issues because of limited access. The reliability of an offshore wind turbine is even more important because maintenance costs account for 30% of the overall cost of energy [3]. Faults in wind turbines occur in the sensors, actuators, and system components, and faults with the potential to propagate to turbine failures change the system behavior, the operational safety, and the power production efficiency of the wind turbines. Consequently, wind turbine failure rates should be reduced to ensure reliability and decrease downtime.

A nominal controller may be inefficient and unstable under fault conditions. To supervise potential faults in sensors, actuators or other components, different control techniques are needed. These methods are called fault detection and isolation (FDI) and fault-tolerant control (FTC) techniques. The FDI technique can provide the operator with valuable information on the type, location, and magnitude of the fault. The FTC is a dynamic system that can compensate for sensor and actuator faults by interacting with any pre-existing nominal controllers to cancel the fault effects on the

* Corresponding author. Department of Marine Technology, Norwegian University of Science and Technology (NTNU), Trondheim, Norway.
E-mail address: seongpil.cho@ntnu.no (S. Cho).

https://doi.org/10.1016/j.renene.2017.12.102
0960-1481/

Abbreviations

FDI	fault detection and isolation
FTC	fault-tolerant control
FWT	floating wind turbine
LMI	linear matrix inequality
MF#	number (#) of multiple faults
NC	nominal PI control
NREL	National Renewable Energy Laboratory
NTM	normal turbulence model
NWP	normal wind profile model
PAS	stuck in pitch actuator
PSB	bias value in pitch sensor
PSF	fixed value in pitch sensor
TF	time of fault occurrence
TFD	time of fault detection
TFI	time of fault isolation
TFTC	time of fault-tolerant control

system. The FTC consists of reconfiguration blocks that are linked to the nominal controller in fault conditions. The FDI and FTC techniques use real-time sensor data to clearly detect, isolate and accommodate the wind turbine faults to improve their reliability and reduce the cost of repairs.

The FDI and FTC of wind turbines have been subjected to intensive research. FDI techniques are based on model-based methods and signal-processing methods. For the model-based methods, the system model could be mathematical or knowledge-based. Faults are detected based on residual generation by state variables or parameter estimations. Chen et al. [4] and Wei et al. [5] proposed model-based FDI schemes using a diagnostic observer for the pitch system and drive train faults to the benchmark model. A diagnostic technique for imbalance fault identification based on a probabilistic neural network was presented by Malik et al. [6]. For signal-processing-based fault detection, mathematical or statistical operations are performed on the measurements. Fault detection and isolation schemes applying data-driven design methods to avoid difficult modeling were used by Dong et al. [7]. Santos et al. [8] presented a multi-sensory system combined with a data-mining solution for fault diagnosis and classification using support vector machines in wind turbines. Ghane et al. [9] and Feng et al. [10] demonstrated statistical change detection for a gearbox model of a wind turbine using frequency analysis.

Fault-tolerant control methods can be divided into two categories: passive and active FTC methods [11]. In passive FTC systems, the controllers are fixed control systems predetermined to be robust against faults and uncertainties throughout the entire system. Passive FTC methods are optimized while satisfying a specific fault scenario, which implies that it has limited fault-tolerant capabilities for various faults. Additionally, this approach does not need FDI schemes and controller reconfiguration. Active FTC methods react to system component failures by reconfiguring control references so that acceptable performance and stability of the system can be maintained. An active FTC relies on an FDI scheme, which should feed real-time information to accommodate the faults by reconfiguring control references in the system. Shi and Patton [12] proposed an active fault-tolerant control approach based on an extended state observer to an offshore wind turbine model. By using a bank of virtual sensors and actuators, Seron et al. [13] suggested a FTC scheme that manages sensor and actuator faults. Fan et al. [14] proposed an FTC scheme that is a combination of model reference adaptive control with neural network compensation. Vidal et al. [15] presented a disturbance compensator for controllers to estimate actuator faults and design fault-tolerant controllers.

Fault occurrence rates and their effects are an important factor in the design of wind turbines. Carroll et al. [16] showed the results of an analysis determining the failure rates for the repair of modern offshore wind turbines and their sub-assemblies. According to this study, the blade pitch systems have the highest failure rates among the components and account for 13.3% of the total failures of wind turbines. The blade pitch system is critical for pitch-regulated variable-speed wind turbines, and the relevant faults change the aerodynamic load and power output immediately and thus affect the response of the tower and support structures. The main faults of the blade pitch system occur in the blade pitch sensors and actuators. These faults influence the control feedback and result in imbalanced loads on the rotor, shaft, and main bearings. The detection of faults allows for fast accommodation to avoid catastrophic long-term damage to the wind turbines. The effect of pitch system faults on turbine performance and platform motion in wind turbine components has been studied in recent years for specific fault scenarios [17–19].

This paper focuses on model-based FDI and FTC methods in the blade pitch sensors and actuators of a floating wind turbine model. Faults generated in blade pitch sensors and actuators can be detected by a Kalman filter based on residual generation and an appropriate evaluation method. The simple cases of faults, such as bias (PSB) and fixed values in pitch sensors (PSF) and stuck in pitch actuators (PAS), are predetermined by the fault magnitude, type and occurrence time to verify the feasibility of the FDI method. The FTC for the fault scenarios considered in this paper provides a complete solution for immediately accommodating faults. The objectives of this work are as follows:

- Present detection and isolation strategies for different types of faults that might occur in the blade pitch system;
- Design an active fault-tolerant controller to achieve satisfactory performance when all control components are back to functioning normally after a fault occurs; and
- Verify the effectiveness of the proposed FDI and FTC schemes under blade pitch system faults by comparing the structural load, response, and safety of floating wind turbines and considering different wind and wave conditions.

This paper is organized as follows. Section 2 describes the floating wind turbine model, baseline controller, blade pitch system and faults. Section 3 introduces the fault detection, fault isolation, and fault-tolerant control schemes for the blade pitch system. Section 4 describes environmental load cases, such as waves and aerodynamic loads, acting on the floating wind turbine. Section 5 presents the simulation results for the fault detection and isolation technique according to a residual method and fault decision and accommodation according to a fault detection criterion. Section 6 provides the conclusions.

2. Methodology

2.1. Floating wind turbine concept

A floating wind turbine is modeled as a rotor, nacelle, tower, floater, and mooring system. The model in this paper is based on the variable-speed pitch-regulated NREL 5 MW offshore wind turbine model [20] supported by the spar buoy floater (OC3-Hywind) [21] and three catenary mooring lines as shown in Fig. 1. The specifications of the NREL 5 MW reference wind turbine are provided in Table 1. Additionally, properties for the OC3-Hywind floater are listed in Table 2.

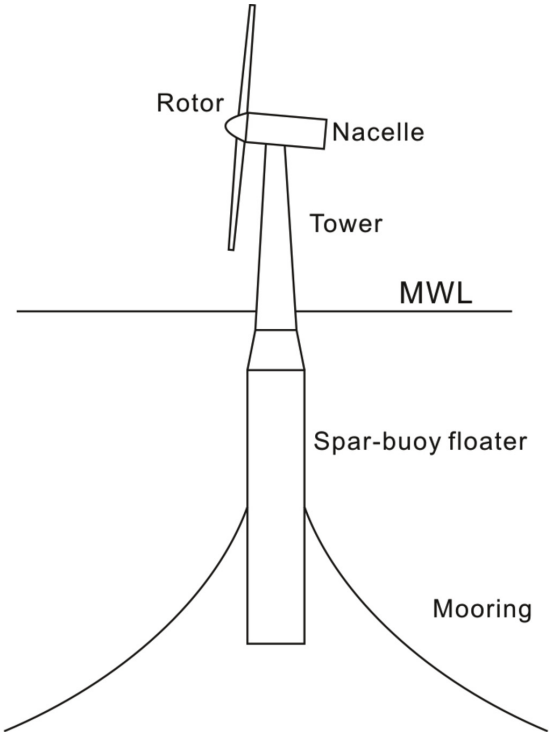

Fig. 1. Schematic view of the floating wind turbines.

2.2. Fully coupled numerical model

The dynamic behavior of the floating wind turbine model is simulated with the Simo-Riflex-Aerodyn software (SRA) [22], which is an aero-hydro-servo-elastic code for fully coupled nonlinear time-domain numerical simulations of offshore wind turbines while simultaneously considering the aerodynamics, hydrodynamics, structural dynamics and mooring line dynamics with an control code for a proportional-integral (PI) pitch and a torque controller under various operational conditions. Models coded by JAVA are added to the SRA to account for the pitch actuator and sensor. Fault data in the blade pitch system are provided in the input file of the SRA to test the feasibility of the fault detection.

2.3. Baseline controller

The baseline control system includes two separate controllers for regulating blade pitch angles and generator torque. The operational region is divided into below-rated and above-rated regions of wind speed. Below the rated wind speed within low wind speeds, the control strategy is to capture the maximum power by adjusting the generator torque and maintaining the optimal tip speed of the blades [20]. Within this region, the blade pitch controller is not active and maximum power is achieved by adjusting the generator torque and then the rotation speed.

Table 1
Properties for the NREL 5 MW wind turbine [20].

Rated Power (MW)	5
Rotor orientation, Configuration	Upwind, 3 blades, horizontal axis
Rotor diameter (m)	126
Hub height from the mean water level (m)	90
Cut-in, rated, cut-out wind speed (m/s)	3, 11.4, 25
Cut-in, rated rotor speed (rpm)	6.9, 12.1
Max pitch rate (°/s)	8
Gearbox ratio	97

Table 2
Properties for the OC3-Hywind floater [21].

Water depth (m)	320
Draft (m)	120
Diameter above taper (m)	6.5
Diameter below taper (m)	9.4
Center of mass (m)	(0, 0, −89.9115)
Mass, including ballast (kg)	7.466×10^6
Mass moment of inertia, I_{xx} and I_{yy} (kg·m^2)	4.229×10^9
Mass moment of inertia, I_{zz} (kg·m^2)	1.642×10^8

Above the rated wind speed, the blade pitch system controls the blade pitch angle to keep aerodynamic loads within specified limits by producing a rated power output at a constant rotor speed. A constant-torque variable pitch controller is used for floating wind turbines to improve the dynamic response of the system and reduce the motion of the floater response to stability issues [23] by modifying the gains of the controller [21]. A blade pitch reference is calculated based on the gain-scheduled PI controller as a function of the generator torque error based on a constant-torque strategy [21] for floating wind turbines.

2.4. Blade pitch system

A commonly used blade pitch system consists of three identical independent pitch actuators and sensors with PI controllers. Regulating each blade pitch angle individually, a 2nd-order pitch actuator is modeled for the 5 MW wind turbine. Consider the blade pitch system that describes a blade pitch reference from the PI controller and the pitch angle measurement:

$$\ddot{\beta}_i + 2\zeta\omega_n\dot{\beta}_i + \omega_n^2\beta_i = \omega_n^2\beta_C, \quad \mathrm{i} = 1, 2 \text{ and } 3(\text{the blade number}) \tag{1}$$

where ζ is the damping ratio, ω_n is the natural frequency of the actuator, and $\dot{()}$ represents the time derivatives. The parameters are $\omega_n = 11.11$ rad/s and $\zeta = 0.6$ [24]. Additionally, β_i is the ith blade pitch angle, and β_C is the blade pitch command.

The recorded measurements must be accurate and reliable because the turbine monitoring and control are based on sensor data during wind turbine operations. A discretized control system that includes process and measurement noises are used in this paper. Process and measurement noises in a state-space model of the blade pitch system described by Eq. (2) are zero-mean Gaussian white noises.

$$\begin{aligned} \dot{\mathbf{x}}(t) &= \mathbf{A}\mathbf{x}(t) + \mathbf{B}\mathbf{u}(t) + \mathbf{w}(t) \\ \mathbf{y}(t) &= \mathbf{C}\mathbf{x}(t) + \mathbf{v}(t) \end{aligned} \tag{2a}$$

or

$$\begin{aligned} \dot{\mathbf{x}}(t) = \begin{bmatrix} \dot{\boldsymbol{\beta}}_i(t) \\ \ddot{\boldsymbol{\beta}}_i(t) \end{bmatrix} &= \begin{bmatrix} \mathbf{0}_{3\times3} & \mathbf{I}_{3\times3} \\ -\omega_n^2\mathbf{I}_{3\times3} & -2\omega_n\zeta\mathbf{I}_{3\times3} \end{bmatrix} \begin{bmatrix} \boldsymbol{\beta}_i(t) \\ \dot{\boldsymbol{\beta}}_i(t) \end{bmatrix} \\ &\quad + \begin{bmatrix} \mathbf{0}_{3\times3} \\ \omega_n^2\mathbf{I}_{3\times3} \end{bmatrix} \boldsymbol{\beta}_{C,i}(t) + \begin{bmatrix} \mathbf{w}_{\beta,i}(t) \\ \mathbf{w}_{\dot{\beta},i}(t) \end{bmatrix}, \quad \mathrm{i} \\ &= 1, 2 \text{ and } 3\mathbf{y}(t) = [\mathbf{I}_{3\times3} \quad \mathbf{0}_{3\times3}] \begin{bmatrix} \boldsymbol{\beta}_i(t) \\ \dot{\boldsymbol{\beta}}_i(t) \end{bmatrix} + \mathbf{v}_i(t) \end{aligned} \tag{2b}$$

where $\mathbf{x}(t)$, $\mathbf{u}(t)$ and $\mathbf{y}(t)$ are the state vector, input vector and measurement vector by the blade pitch angle, respectively; and $\mathbf{A}$, $\mathbf{B}$

and **C** are system matrices representing the state transition, input and measurement matrices, respectively. Uncertain disturbances are given, including the process noise vector $\mathbf{w}(t)$ and measurement noise vector $\mathbf{v}(t)$. This blade pitch system is observable, controllable and stable according to the observability matrix, controllability matrix, pole and Nyquist diagram from Chen [25].

2.5. Fault description

According to the wind turbine reliability analyses [16], the most common faults occur in the blade pitch system. A fault occurring in the blade pitch system can influence the closed-loop control system and the dynamics of a wind turbine. The incorrect pitch of a blade resulting from faults causes asymmetrical forces on the blades and lead to unbalanced rotation in the rotor. Therefore, a fault occurring in the sensors and actuators can affect the system characteristics or lead to inoperable conditions that have resulted in hydraulic leakage, valve blockage or pump blockage [24]. There is a high possibility that a blade pitch system under multiple fault conditions in blades cannot perform a role of an aerodynamic brake properly while large wind loads are acting on the rotor.

Faults of the blade pitch system are mainly categorized by the pitch sensor and actuator fault. To model the faults, the pitch actuator and sensor equations are updated. In this paper, three types of faults in the pitch sensor and actuator of the blade system can be considered: bias value (PSB), fixed output (PSF) in the pitch sensor and stuck actuator (PAS) as shown in Cho et al. [26]. PSB can be represented by a constant offset value that is added to the measurement from the sensor. PSF of the sensor retains the last measurement after fault occurrence. PAS is mainly caused by valve blockage which is mainly due to debris that could clog the valve in the flow in the hydraulic pitch actuator and represents one of the hazards announced by the fault analysis with a level of occurrence and severity by Esbensen and Sloth [24].

Faults to the blade pitch sensor and actuator frequently occur and result in the structural loading of the turbine because of rotor imbalance, and they affect the stability of the floating platform. Other faults, such as hydraulic leakage and high air content in oil, can occur only by changing the natural frequency and damping ratio in the actuator. Therefore, these uncritical topics are not evaluated in this paper.

3. Fault detection, fault isolation and fault-tolerant control methods

Fig. 2 shows the control procedure for a pitch-regulated wind turbine. The baseline controller regulates the wind turbine power production through blade pitch and generator torque control under normal operational conditions. The condition monitoring system with sensors measures the blade pitch angle, tower acceleration, and rotor speed. By using a fault detection and isolation algorithm, the system can detect, isolate, and accommodate faults at an early stage. Upon fault detection, the fault-tolerant controller selects a remedial action based on the protection strategy. If the fault is tolerable, then it can be accommodated by a signal correction in the case of sensor faults. If the situation is intolerable and the wind turbine is not in a safe state, then the controller brings the turbine to a shutdown mode.

3.1. Fault detection

In fault detection, faults in a system and their detection time are determined. Model-based approaches detect faults by comparing the generated residual from the measured pitch angle and threshold. The basic methods for establishing and evaluating the residual are described in this section. Currently, observer methods are the main model-based approaches for detecting faults. In this paper, a Kalman filter, which is a classical method used in fault detection and other fields, is used. Fig. 3 shows the basic structure of model-based fault detection. Based on the input command $u(k)$ and measured output $y(k)$, the states and measurements are estimated by an observer. By comparing the measured and estimated values, changes of a state are identified by a threshold.

3.1.1. Observer design based on the discrete-time space model

The discrete system is more suitable for numerical computing and employing an observer than the continuous system. The discrete-time state-space model of the blade pitch system with disturbance and faults in the pitch actuator and sensor can be transferred from the proposed system (2) where the Euler discretization approach is applied.

$$\begin{aligned}\mathbf{x}(k+1) &= \mathbf{\Phi}\mathbf{x}(k) + \mathbf{\Psi}\mathbf{u}(k) + \mathbf{\Gamma}_f\mathbf{f}_A(k) + \mathbf{\Gamma}_d\mathbf{w}(k)\\ \mathbf{y}(k) &= \mathbf{H}\mathbf{x}(k) + \mathbf{\Xi}_f\mathbf{f}_S(k) + \mathbf{\Xi}_d\mathbf{v}(k)\end{aligned} \tag{3}$$

where $\mathbf{\Phi} = \mathbf{I} + \mathbf{A}T$, $\mathbf{\Psi} = \mathbf{B}T$ and $\mathbf{H} = \mathbf{C}$. Here, $\mathbf{\Phi}$, $\mathbf{\Psi}$, $\mathbf{H}$, $\mathbf{\Gamma}_d$, $\mathbf{\Gamma}_f$, $\mathbf{\Xi}_d$, and $\mathbf{\Xi}_f$ are known constant matrices in a discretized system. In addition, T is sampling time and $\mathbf{f}_A(k)$ and $\mathbf{f}_S(k)$ are the actuator and sensor fault vectors described in Cho et al. [26], respectively.

The observer with a healthy case based on the Kalman filter method is designed as follows:

$$\begin{aligned}\hat{\mathbf{x}}(k+1) &= \mathbf{\Phi}\hat{\mathbf{x}}(k) + \mathbf{\Psi}\mathbf{u}(k) + \mathbf{K}\Big(\mathbf{y}(k) - \mathbf{H}\hat{\mathbf{x}}(k)\Big)\\ \hat{\mathbf{y}}(k) &= \mathbf{H}\hat{\mathbf{x}}(k)\end{aligned} \tag{4}$$

where $\hat{\mathbf{x}}(k), \hat{\mathbf{y}}(k)$ and $\mathbf{K}$ are the estimated state vector, estimated output vector, and Kalman gain matrix, respectively.

3.1.2. Residual generation and evaluation

A residual $r(k)$ is the difference between the measured and estimated values described as follows:

$$r(k) = y(k) - \hat{y}(k) \tag{5}$$

A residual energy $J(k)$ is defined by the L_2 norm [27], which is described by the root-mean-square (RMS) of the residual as follows:

$$J(k) = \|r(k)\|_{2,k} = \left(\sum_{i=1}^{n} r_i^T(k) r_i(k)\right)^{1/2} \tag{6}$$

Because the residual energy in fault cases includes fault information, the generated residual energy should be evaluated by fault detection logic. The residual determines the fault status by applying fault detection logic with threshold J_{th}.

$$\begin{aligned}&J(k) < J_{th}, \text{fault} - \text{free}\\ &J(k) > J_{th}, \text{fault}\end{aligned} \tag{7}$$

The threshold is generated with bounded uncertainty. Hence, when the residual energy is less than this threshold, the fault-free state is indicated. Otherwise, the fault can be detected. The threshold design procedure using H_∞ optimization and linear matrix inequality (LMI) was described in Cho et al. [26] with more details for the derivation.

If the system is a fault-free state, the residual energy is expressed as

$$J(k) = \| r_d(k) \|_2 \le \| \mathbf{G}_{rd}(z) \|_\infty \| v \|_2 \le \gamma_{\min}\delta_d \tag{8}$$

where $r_d(k)$ is a disturbance residual, $\mathbf{G}_{rd}(z)$ is a disturbance transfer function, $\gamma_{\min}$ is a minimum design parameter for a

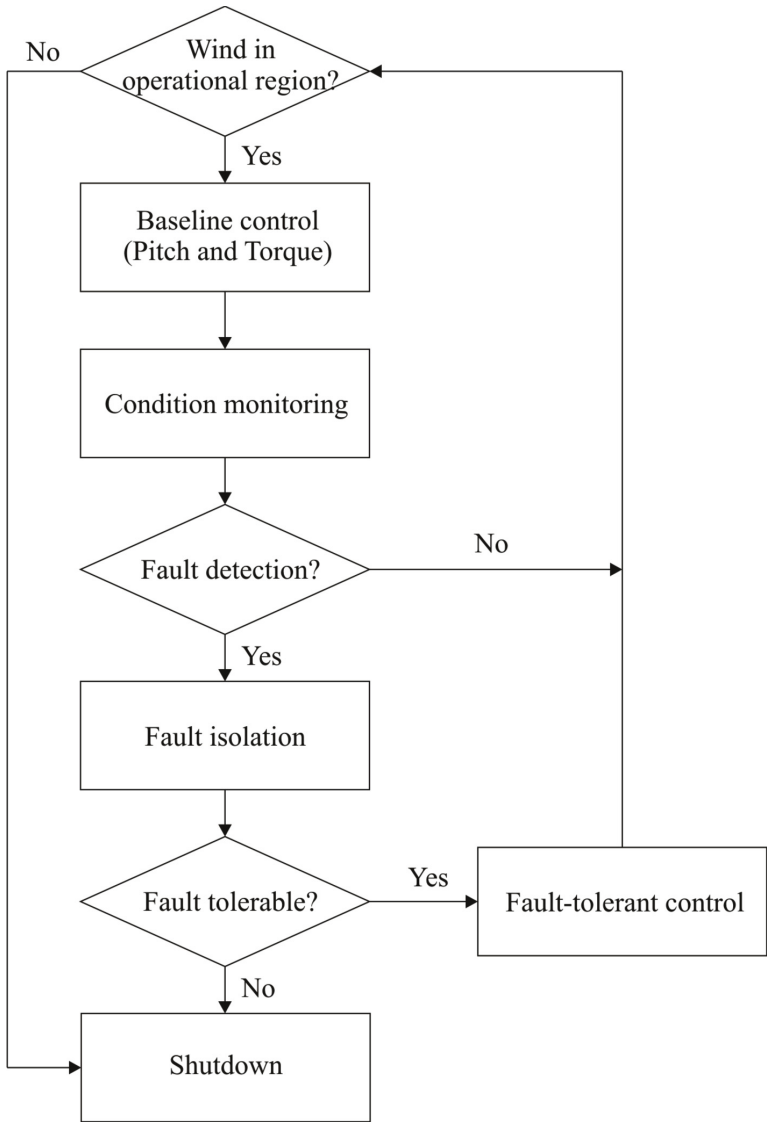

Fig. 2. Control procedure for a wind turbine with FDI and FTC.

performance bound and δ_d is a measurement noise boundary. $\mathbf{G}_{rd}(z)$ is defined in frequency domain and $\gamma_{\min}$ is calculated according to LMI in a discrete-time system described in Cho et al. [26]. In addition, δ_d is defined by sensor resolution.

Therefore, the threshold is set as follows:

$$J_{th} = \gamma_{\min}\delta_d. \tag{9}$$

3.2. Fault isolation

After a successful fault detection, the main challenge is fault isolation. Fault isolation means determining the type, location, and magnitude of a fault following detection. The fault isolation decision can be made after the residual generator has generated a detection alarm that indicates the occurrence of a fault as presented in Fig. 3. This paper suggests a fault isolation algorithm based on a Kalman filter using inference methods [4,28].

Most wind turbines have a single pitch sensor in each blade. As shown in Fig. 4 (a), PSF faults cannot be easily distinguished from PAS faults solely by measurements of the pitch angle. However, the nacelle yaw motions are completely different between the two faults illustrated in Fig. 4 (b). The reason why nacelle yaw motions are different under PSF and PAS faults depends on whether the pitch actuators are still working or not. The blade is seized in the PAS case and cannot respond to the pitch command (control value). However, the blade can still pitch in the PSF case, but the pitch

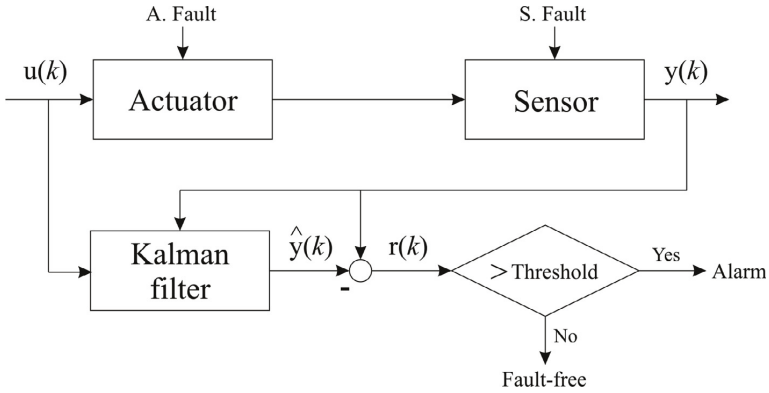

Fig. 3. Scheme of observer-based fault detection in the blade pitch system.

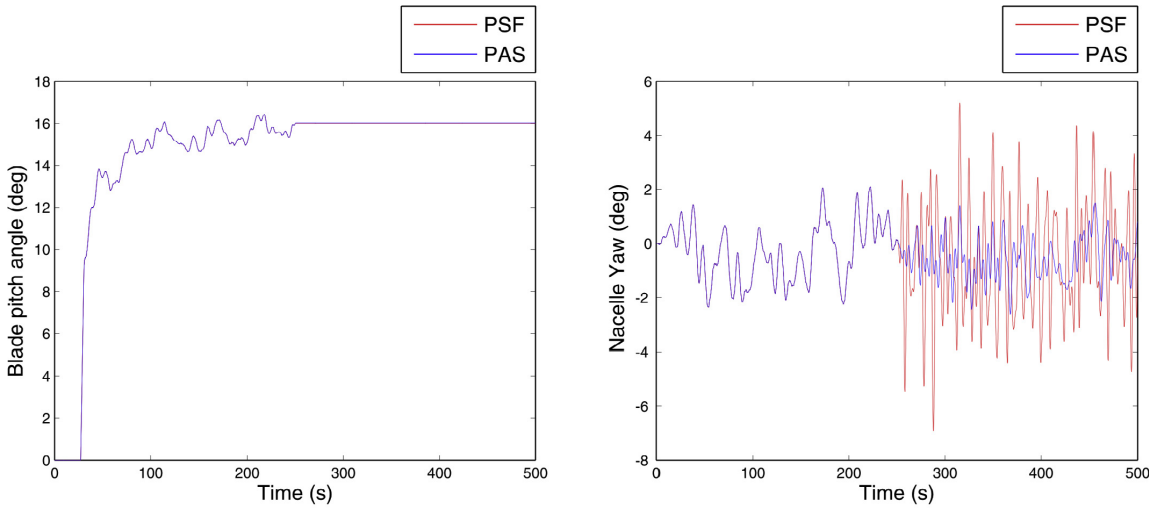

Fig. 4. Comparison of the effects of PSF and PAS faults on the blade pitch angle and nacelle yaw.

sensor gives a fixed value and the pitch command is affected by faults, which results in an oscillating irregular pitch angle with a large amplitude than PAS. This leads to a larger yaw motion under PSF, as shown in Fig. 4. The pitch command from the pitch controller can be influenced by the difference between reference and measurement values that makes a pitch angle oscillate and consequently a wind turbine unstable that results in the unbalanced rotor. Alternatively, fault isolation can be conducted using measurements of nacelle yaw motions.

Fig. 5 shows an algorithm for fault isolation using the single blade pitch angle and nacelle yaw angle measurements. Initially, the trend of the pitch measurement $\beta_{i,k}$ must be determined. If the faulty sensor keeps outputting $\beta_{i,k+1}-\beta_{i,k}=0$, then the algorithm decides that the fault is PSF or PAS. Then, by comparing the standard deviation of the nacelle yaw angle in normal $\sigma_{Yaw,n}$ and fault conditions $\sigma_{Yaw,f}$, the two faults can be differentiated. Once $\sigma_{Yaw,f}$ is greater than $\sigma_{Yaw,n}$, then the algorithm makes a decision of PSF in the pitch system. Otherwise, the algorithm indicates that there is PAS in the pitch system. To identify PSB, the estimation error should be determined, which can be performed by the residual of the pitch angle from the residual generator. If the fault estimation errors are bounded in a certain range δ, then the algorithm makes a decision that the fault is a PSB.

In the verification procedure, 300 simulations of each fault case were conducted with a duration of 300 s to evaluate the algorithm of fault isolation. The location, magnitude and time of the faults were randomly generated. Once a fault alarm occurred, this algorithm isolated 99% of these faults after 11.5 s. Then, the algorithm makes a fault isolation decision regarding the faults generated from Fig. 6. PSF and PAS can be distinguished by the standard deviation values of the nacelle yaw angle σ_{Yaw}.

3.3. Fault-tolerant control

If the sensors and actuators experience faults or are no longer available, then the controller cannot provide the correct control

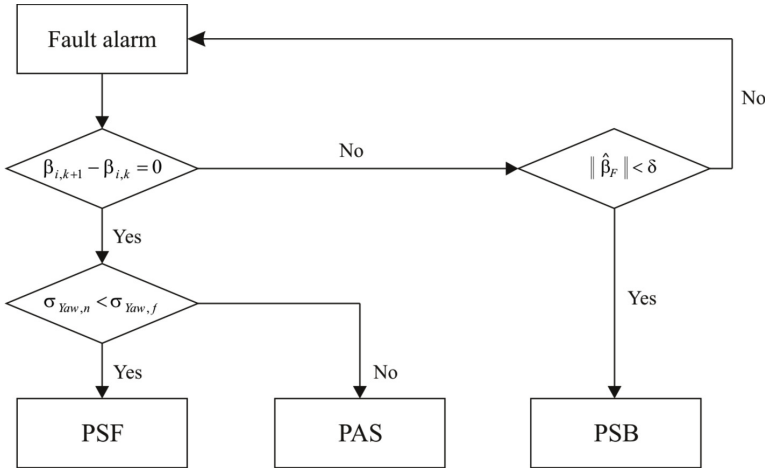

Fig. 5. Algorithm of fault isolation with a single pitch sensor.

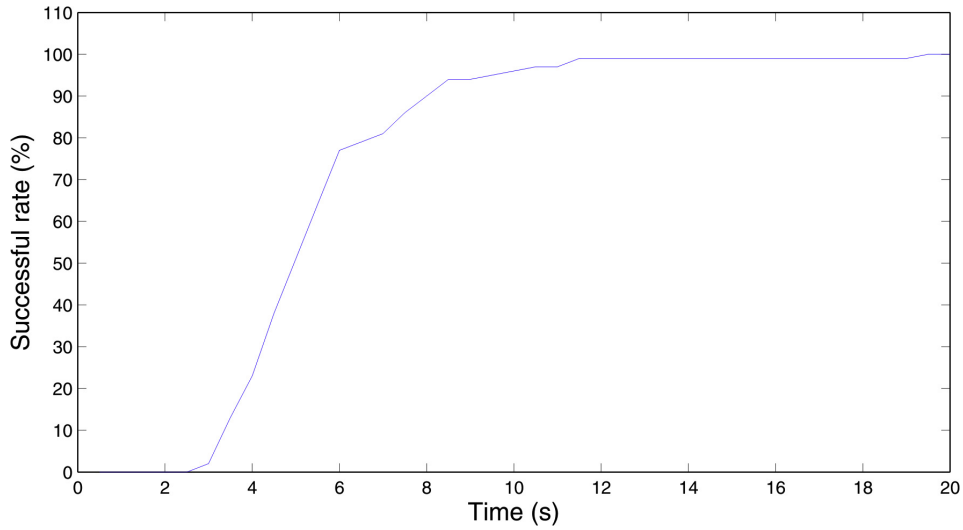

Fig. 6. Successful rates of fault isolation at each number of steps.

actions for the system. To minimize the potential risks of unexpected faults, new control techniques are needed to manage the faulty system before maintenance is conducted. In this paper, a fault-tolerant control (FTC) scheme is suggested that includes a reconfiguration block and a nominal PI controller after successful fault isolation. The main concept underlying this FTC scheme is to reconstruct the system output y_c to replace the faulty measurement y_f. Because faulty measurement y_f cannot be used with the existing controller, a configuration block must be found that generates a suitable signal y_c from y_f and u_f. Fig. 7 shows the block diagram of the control reconfiguration scheme for sensor and actuator faults.

In the scheme, virtual sensors [11] are used to represent the main part of the reconfiguration block for the FTC to conduct signal corrections. The virtual sensor can be used to calculate state vectors by replacing the measurements from the faulty system. The virtual sensor is defined by the state-space model as follows:

$$\begin{aligned} \hat{\mathbf{x}}_V(k+1) &= \mathbf{\Phi}\hat{\mathbf{x}}_V(k) + \mathbf{\Psi}\mathbf{u}_c(k) + \mathbf{K}_V\left(\mathbf{y}_f(k) - \mathbf{H}_f\hat{\mathbf{x}}(k)\right) \\ \mathbf{y}_c(k) &= \mathbf{H}_V\hat{\mathbf{x}}_V(k) + \mathbf{P}\mathbf{y}_f(k) \\ \mathbf{u}_f(k) &= \mathbf{u}_c(k) \end{aligned} \tag{10}$$

where $\mathbf{P}$ is a design parameter, and for $\mathbf{P} = \mathbf{0}$, only observed values are used; and $(_v)$ represents values in the virtual sensors. The matrix of $\mathbf{H}_v$ is set as equal to measurement matrix $\mathbf{H}$ in Eq. (3). If the fault detection scheme detects any faults in the pitch sensor of the ith blade, the value in $\mathbf{H}_v$ allocated by the faulted sensor has been replaced by 0 in $\mathbf{H}_f$ which means that this sensor is no longer available anymore.

Fig. 8 shows the reconfiguration with the virtual sensor after faults. The sensor faults are reflected by the matrix $\mathbf{H}_f$. The virtual

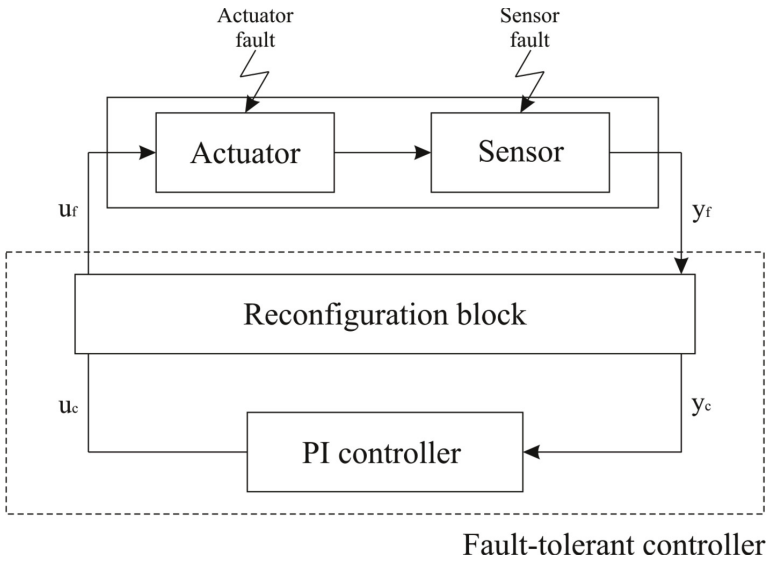

Fig. 7. Control reconfiguration for sensor and actuator faults.

sensor estimates the state of the faulty system $\hat{\mathbf{x}}_f$ and replaces the faulty system output. This system output $\mathbf{y}_c$ is improved by using the available sensor values and observing only the difference between the nominal and the faulty output. If this virtual sensor works well, then the state of the virtual sensor $\mathbf{x}_v$ is equivalent to the state of the nominal system $\mathbf{x}$. Hence, the controller recognizes the same system and reacts in the same way as before.

Actuator faults are critical to the safety of wind turbines when leaving the pitch actuator inoperable regardless of the controller command as shown in Esbensen et al. [24]. Then, the blade cannot be pitched effectively at the large aerodynamic torque above the nominal value. Therefore, pitch actuator faults require a rapid shutdown of the wind turbine as a standard from Jonkman et al. [20]. Once PAS faults are isolated, a safe and fast shutdown of the turbine could be reconfigured to continue power production in response to other faults.

4. Load cases

Floating wind turbines are exposed to a variety of loads in their lifetime. Critical environmental conditions, such as waves, wind gusts, turbulence, and sudden wind direction shifts, are another source of transient loading. For floating wind turbines, appropriate wave conditions must be combined with the wind conditions.

The floating wind turbine operates under variable wind conditions, such as a stochastic wind model that present realistic wind and wave loads. The wind model is based on the IEC 61400-3 design code [31]. A turbulent wind field U_w (x, y, z, t) is commonly modelled by a mean wind and a fluctuating component as described by

$$U_w(t) = U_m + U_f(t) \tag{11}$$

where U_m is the mean wind speed represented as the normal wind profile model (NWP) and U_f is the fluctuating wind for the normal turbulence model (NTM). The turbulent wind U_w is modeled using Turbsim [29] to generate realistic turbulent wind fields according to the Kaimal turbulence model including the turbulence intensity with IEC Class C. The turbulence intensity is a function of the wind speed at the hub height [30,31]. The wave condition is modeled by the JONSWAP wave spectrum. The significant wave height (H_s) and peak period (T_p) are set based on their correlation with wind speed for the Statfjord site in the northern North Sea.

The load cases used to study the dynamic response of the floating wind turbine are given in Table 3. Four independent simulations for turbulent wind and irregular waves were conducted by representing the mean value and standard deviation of the dynamic response for 1-h ensembles.

5. Simulation results and discussion

In this section, a series of simulation results are presented to investigate the performance of the proposed FDI and FTC schemes. Simulations of the wind turbine subjected to a stochastic wind speed are conducted under three different fault conditions: PSB, PSF, and PAS on a single blade and multiple blades.

5.1. Fault detection, fault isolation, and fault-tolerant control with a single fault

5.1.1. Fault detection and isolation results

Faults in the blade pitch system influence the structural dynamics of the wind turbine. Faults in actuators and sensors can be detected effectively by the residual energy and the threshold. When the residual energy exceeds the threshold, a fault alarm is set to 1, which means that a fault is detected. The residual energy should be normalized to adjust the scale factor from the data. The normalized residual energy J_N is described as follows:

$$J_N(k) = J(k)/J_{th} \tag{12}$$

Fig. 9 shows simulation results in connection with the blade pitch angle, normalized residual energy, a fault detection alarm and fault isolation under LC4. In Fig. 9 (a), a PSB occurs abruptly after 250 s in the wind turbine corresponding to a sensor bias of −3° on

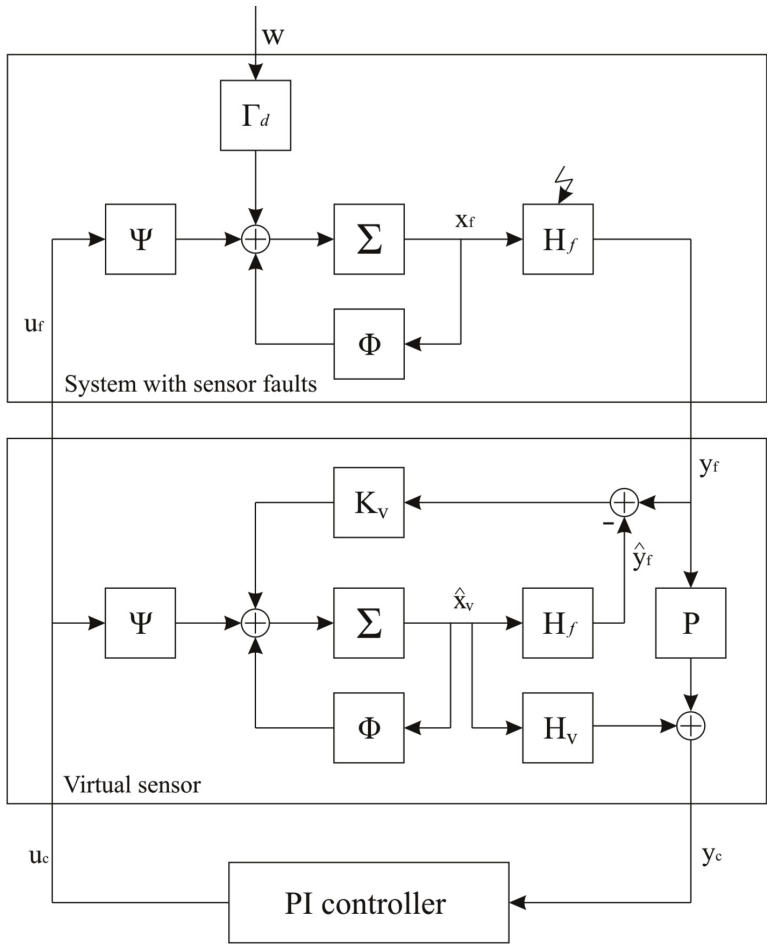

Fig. 8. Reconfiguration with a virtual sensor after sensor faults.

blade 3. Concurrently, an offset value (-3°) occurs between the reference and measurement corresponding to pitch bias. The normalized residual exceeds the threshold, and then the observer detects the blade pitch bias fault immediately by setting to the fault alarm in Fig. 9 (b). As shown in Fig. 9 (c), the PSB fault can be isolated by the fault isolation algorithm after successful detection.

In the case of PSF and PAS, the pitch angle measurement shows a constant value that is the same as the last measurement value before the faults. The difference between the reference and measurement values makes the pitch angle oscillate irregularly at a large amplitude and the pitch angle difference between fault-free (blades 1, 2) and faulty blade (blade 3) occur as unbalanced rotation. The PSF and PAS simulation results show the same pattern in Figs. 10 and 11, respectively, which indicate that faults on blade 3 can be detected based on the fault detection and isolation algorithm.

Cho et al. [26] studied a series of simulations for the reliability of this fault detection algorithm that can detect sensor and actuator faults within a reasonable time after a fault is generated. Therefore, this method can guarantee fault detection at an early stage in the blade pitch system.

Table 3
Wind and wave conditions.

Load case	U_w (m/s)	Turbulent model	H_s (m)	T_p (s)
1	11.2	IEC Class C	3.2	10.0
2	14		3.62	10.30
3	17		4.2	10.50
4	20		4.8	10.80

5.1.2. Structural response of the floating wind turbine under fault conditions

In this section, numerical results for the fault effects in pitch sensors and actuators are presented. The main objective of the FDI and FTC systems is to avoid unexpected mechanical loads and maximize energy capture. The simulations are conducted to evaluate the proposed FDI and FTC schemes against different fault scenarios. Each simulation has a 1-h duration to reduce the stochastic uncertainty for each load case.

Ocean environmental loads, such as wave and wind loads, excite the structural dynamics of the floating wind turbine. The responses are normalized to adjust the scale factor according to the

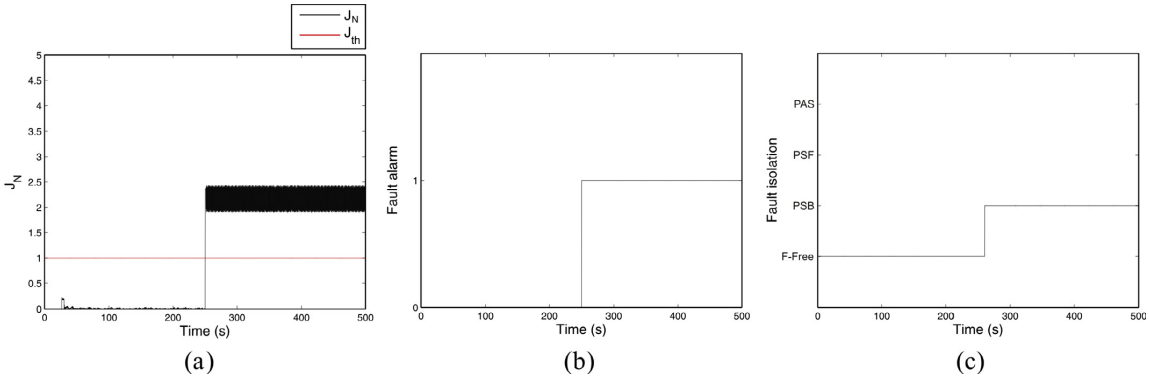

Fig. 9. Simulation results of the PSB case corresponding to the blade pitch angle under LC4: (a)normalized residual energy, (b) fault detection alarm, and (c) fault isolation.

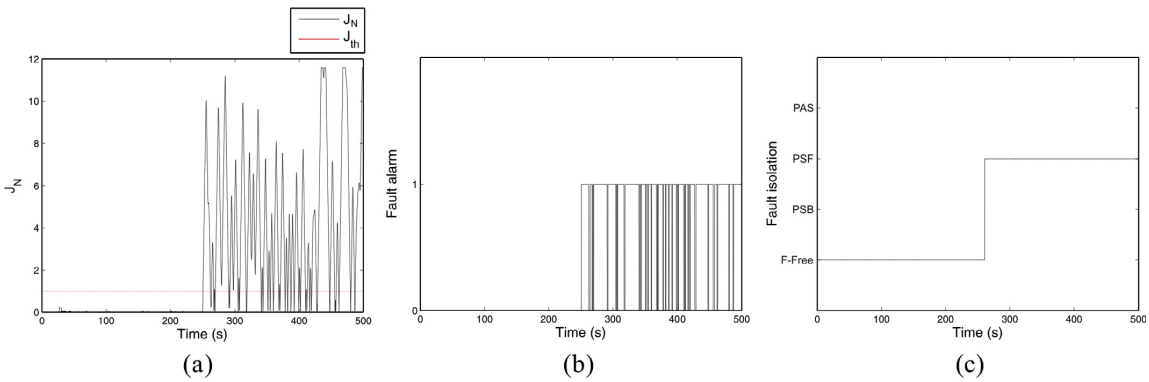

Fig. 10. Simulation results of the PSF case corresponding to the blade pitch angle under LC4: (a) normalized residual energy, (b) fault detection alarm, and (c) fault isolation.

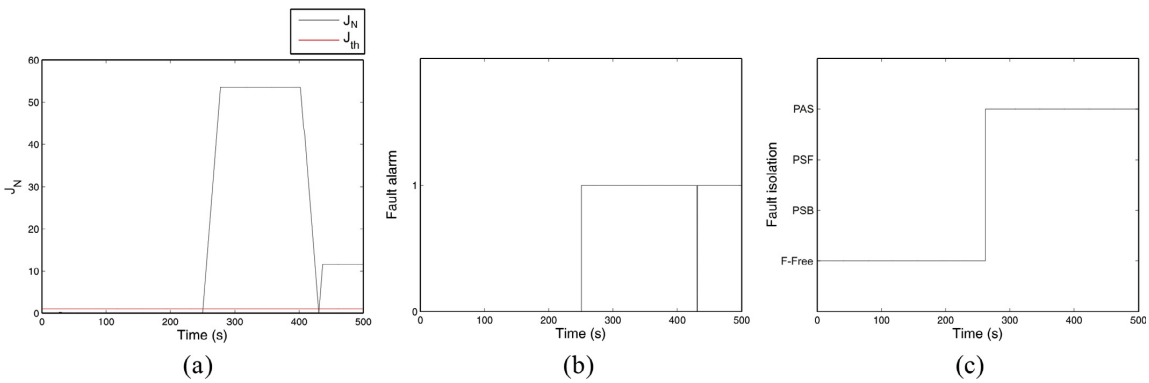

Fig. 11. Simulation results of the PAS case corresponding to the blade pitch angle under LC4: (a) normalized residual energy, (b) fault detection alarm, and (c) fault isolation.

corresponding values from the fault-free case as described

$$RV_{norm} = \frac{RV_i}{RV_{f-free}} \quad i = 1, 2, 3, 4, 5, 6 \tag{13}$$

where RV_{norm} is the response value normalized by the means and standard deviations of the fault-free case $RV_{f\text{-}free}$, and RV_i is the ith response value (1: NC under PSB, 2: FTC under PSB, 3: NC under PSF, 4: FTC under PSF, 5: NC under PAS, and 6: shutdown under PAS).

In particular, the mean and standard deviation (STD) values are calculated for the structural dynamics. Fig. 12 shows the effects of a series of fault cases on the normalized mean and STD of the surge, roll, pitch, and yaw motions of a floating wind turbine. The results show that faults affect a significant amount of platform yaw motions compared with the surge, roll and pitch motions because the incident variations in an aerodynamic thrust caused by an unbalanced rotor speed directly affect the instability of platform motion, especially the yaw motion as described by Cho et al. [26].

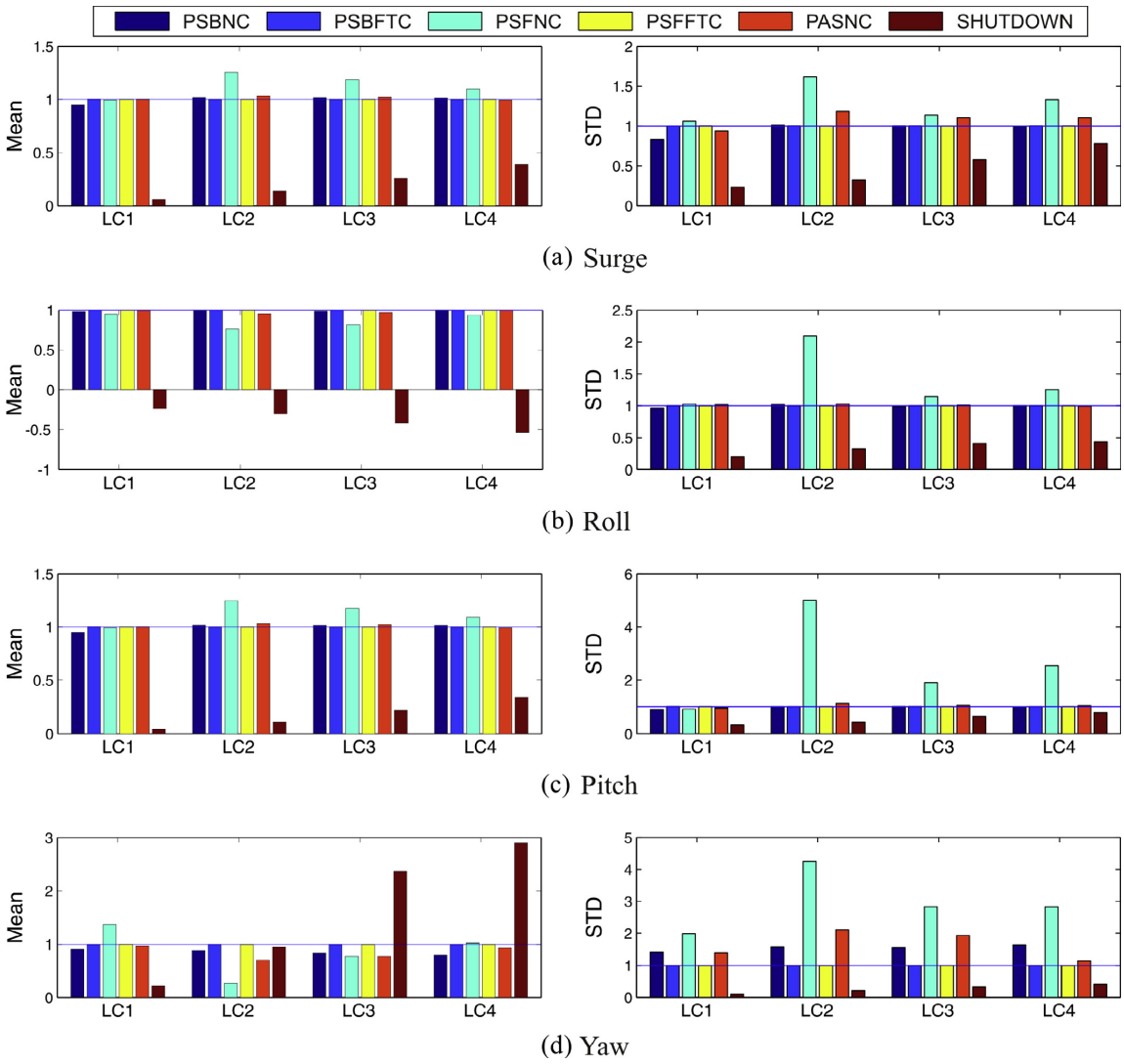

Fig. 12. Mean values and standard deviations (STDs) of the platform surge, roll, pitch, and yaw motions for the floating wind turbine under PSB, PSF and PAS fault conditions with nominal PI and fault-tolerant controllers (blue line: fault-free; dark blue bar: nominal PI controller with PSB; blue bar: FTC controller with PSB; cyan bar: nominal PI controller with PSF; yellow bar: FTC controller with PSF; orange bar: nominal PI controller with PAS; and brown bar: shutdown). (For interpretation of the references to colour in this figure legend, the reader is referred to the web version of this article.)

In the case of PAS, the actuator fault cannot tolerate the reconfiguration block. In cases of platform yaw motion of the FTC in a pitch actuator fault, the fault accommodation is a shutdown to stop wind turbine operations. In this procedure, the standard deviation should be reduced significantly. However, the mean value has been changed because of the unbalanced pitch arrangement even if a wind turbine has undergone shutdown states. As shown in Fig. 13, the yaw motion with shutdown presents a positive stable condition. However, the rotor has undergone an unbalanced state because the faulted blade has been seized and the other blades are feathered. Although the results of the nominal and fault-tolerant controllers are similar, changing the dimensionless value generates more considerable differences as described in Table 4. The motions and structural loads of wind turbines can decay to zero by the emergency shutdown. Jiang et al. [18] showed that the dynamic response of wind turbines from the beginning of the shutdown can be unstable but ultimately decay over time.

The PSF fault has a greater effect on dynamic behavior than the PSB and PAS faults. In fault accommodation, the mean and STD results demonstrate that the proposed FTC schemes with signal correction for sensor faults have good performance. The platform motions with FTC schemes in PSB and PSF faults have nearly equivalent values as the fault-free case, which are close to 1. The

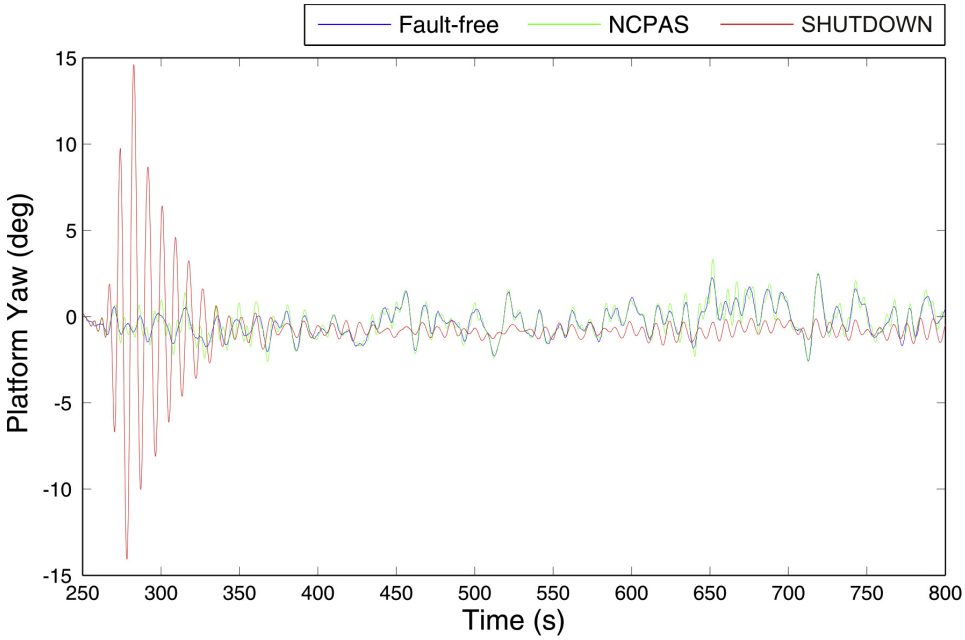

Fig. 13. Platform yaw motion after PAS fault (blue line: fault-free; green line: nominal controller with PAS; and red line: shutdown with PAS). (For interpretation of the references to colour in this figure legend, the reader is referred to the web version of this article.)

Table 4
Mean and dimensionless values of platform yaw under LC4.

	Yaw (Mean)	Yaw (Dimensionless)
Fault-free	−0.1458	1
NC in PAS fault	−0.1303	0.8937
Shutdown in PAS fault	−0.8083	5.55439

signal correction brings the floating wind turbine back to normal operational conditions, which means that the FTC scheme with FDI is apparently able to accommodate the fault effects on the pitch system.

Fig. 14 shows the platform roll and yaw motions in sensor fault cases for LC4 to check the effectiveness of the FTC for sensor faults. After 250 s, the FDI and FTC algorithms can detect and isolate the faults precisely and conduct signal correction as fault accommodation for faulty sensors, which means that the fault accommodation successfully eliminates unbalanced rotation in the rotor during the PSB and PSF faults. However, unbalanced rotation still occurs in the rotor when a nominal PI controller is used during the faults and leads to instability in the floating wind turbine.

Additionally, the effect of faults on the tower during fault accommodation with the proposed FTC schemes should be presented. Fig. 15 shows a comparison of the normalized mean and STD for the tower torsional, fore-aft, and side-to-side bending moments. The bending moments are calculated by the local coordinate system for each component. The results show that the torsional moment is more affected by faults than the fore-aft and side-to-side bending moments. The torsional moment under fault conditions is significant because of the unbalanced aerodynamic loads on the rotor. The PSF fault has a much greater effect on the vibration (STD) than the two other fault cases because of the large oscillation. In fault accommodation, the mean and STD results of the FTC schemes using signal correction from the redundancy sensor demonstrates better performance than the nominal PI controller as shown in Fig. 15. The bending moments present nearly equivalent values for both the fault-free case and FTC schemes. In the case of PAS, the bending moments decay to zero with the shutdown.

Fig. 16 illustrates the torsional moment and side-to-side bending moment on the tower base in sensor fault cases for LC4 to validate the pitch FTC scheme from 230 to 330 s. After 250 s the FDI and FTC algorithms can detect and isolate the fault precisely and conduct successful signal correction to eliminate the unbalanced rotation during the PSB and PSF faults. The bending moments when a nominal PI controller without the FTC is used increase in the two PSB and PSF cases because of the rotor imbalance and the growth in the aerodynamic thrust force.

5.2. Fault detection, fault isolation, and fault-tolerant control with multiple faults

In this section, the performance of the FDI and FTC schemes is demonstrated for cases with multiple fault scenarios. Simulations for the floating wind turbine subjected to various load cases are conducted considering simultaneous PSB and PSF faults in multiple blades. Faults in actuators and sensors can be detected effectively by the residual energy and the threshold.

Fig. 17 shows simulation results in connection with the normalized residual energy, fault alarm, and fault isolation. A PSB corresponding to a sensor bias of -3° abruptly occurs on blade 3 after 100 s, and then a PSF occurs on blade 2 after 200 s. Concurrently, the normalized residual is greater than the threshold, and then the observer detects the PSB and PSF faults immediately by

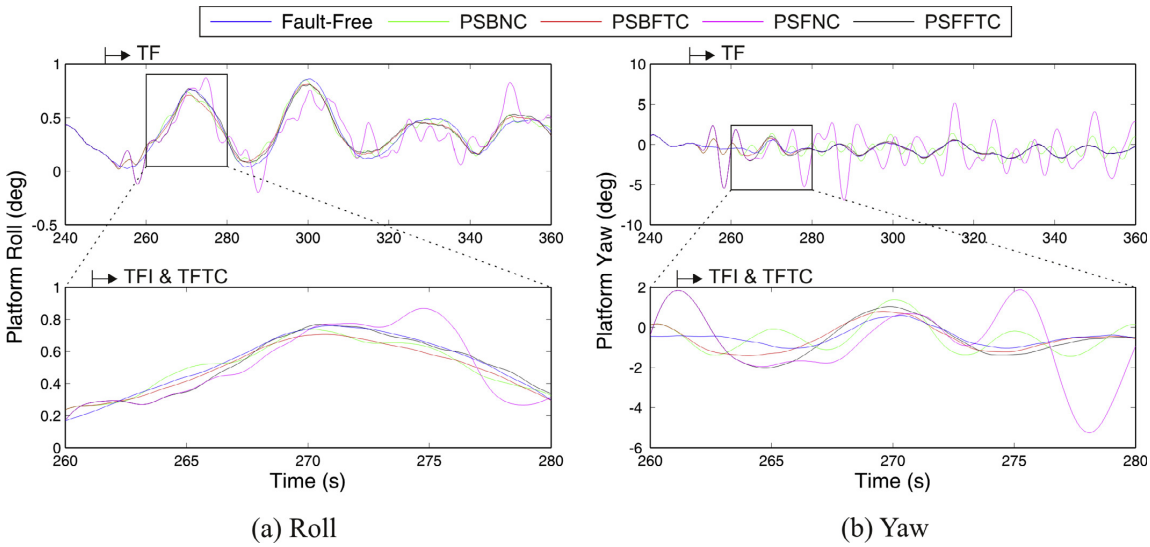

Fig. 14. Comparison of the platform pitch and yaw motions under PSB and PSF fault conditions with nominal PI and fault-tolerant controllers under LC4.

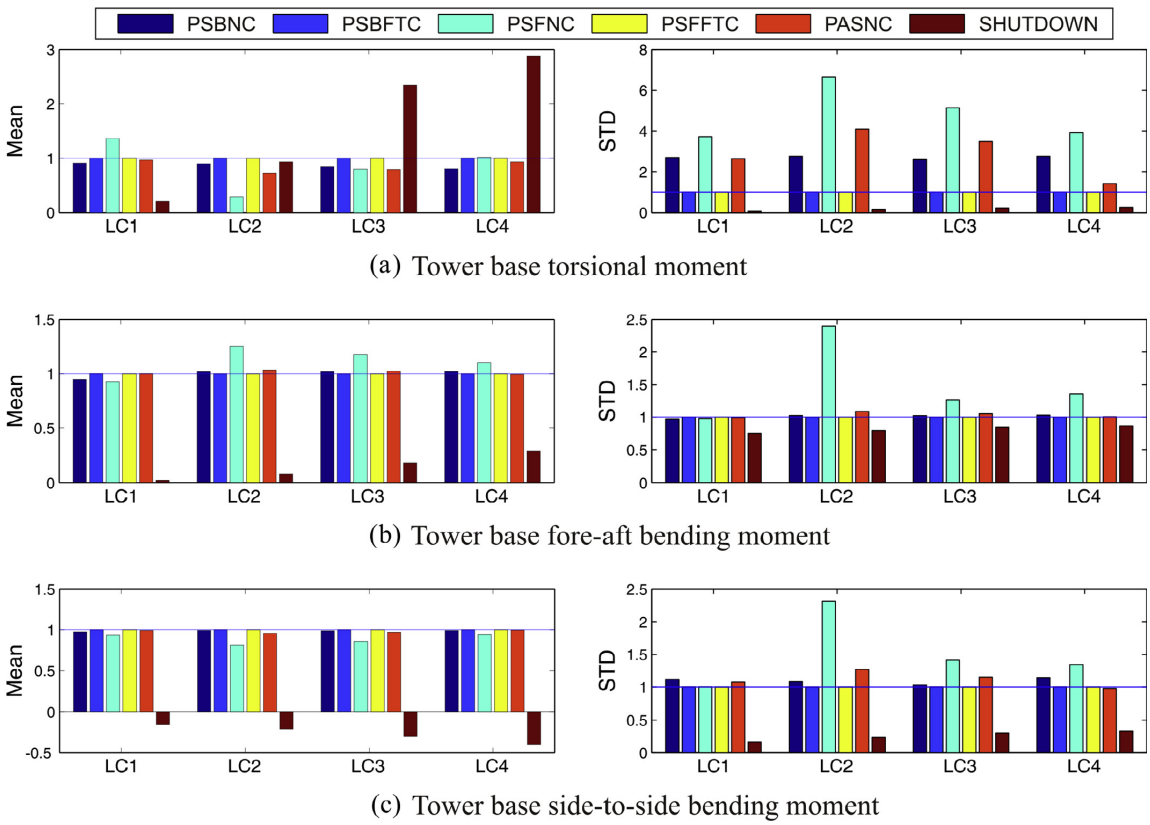

Fig. 15. Mean values and standard deviations (STDs) of the torsional, fore-aft and side-to-side bending moments for the floating wind turbine under PSB, PSF and PAS fault conditions with nominal PI and FTC controllers (blue line: fault-free; dark blue bar: nominal PI controller with PSB; blue bar: FTC controller with PSB; cyan bar: nominal PI controller with PSF; yellow bar: FTC controller with PSF; orange bar: nominal PI controller with PAS; and brown bar: shutdown). (For interpretation of the references to colour in this figure legend, the reader is referred to the web version of this article.)

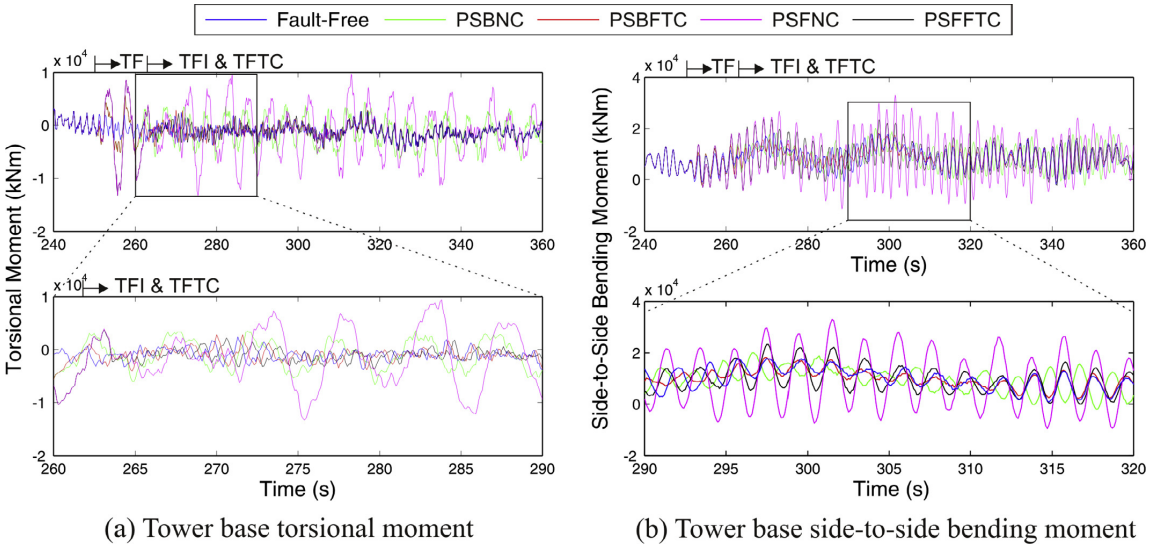

Fig. 16. Comparison of the torsional and side-to-side bending moments under PSB and PSF fault conditions with nominal PI and fault-tolerant controllers under LC4.

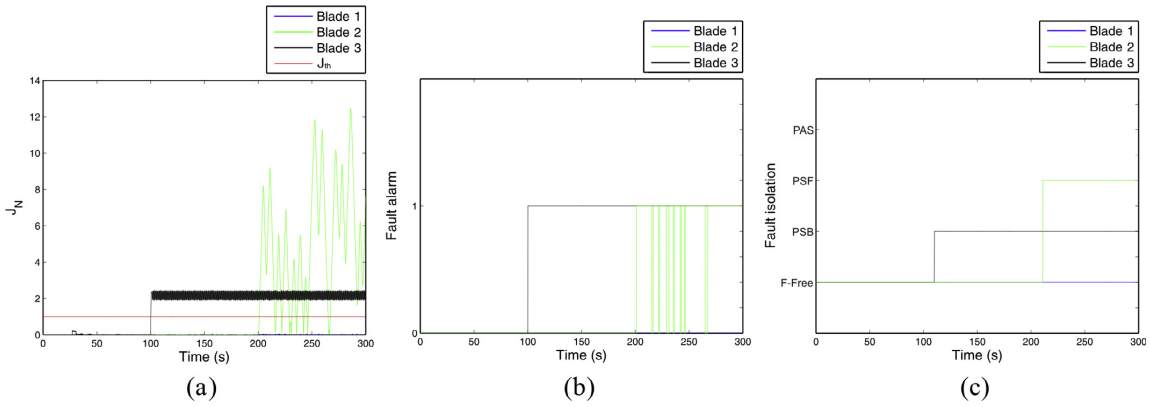

Fig. 17. Simulation results of the PSB and PSF cases corresponding to the blade pitch angle: (a) normalized residual energy, (b) fault detection alarm and (c) fault isolation under LC4.

setting to fault alarm as shown in Fig. 17 (a) and (b), respectively. Based on the fault isolation algorithm described in Section 3.2, the faults are isolated as shown in Fig. 17(c). These results indicate that the presented method can guarantee the FDI at an early stage in the blade pitch system.

Figs. 18 and 19 show the platform yaw motion and torsional moment in the tower base for LC4 in PSB and PSF faults at 100 s and 200 s, respectively. The FDI algorithm can detect and isolate faults precisely within 11.5 s. After a successful FDI, the FTC controller with virtual sensors conducts signal correction after 111.5 s. The results indicate that yaw motion with the FTC controller converges to fault-free yaw motion when the FDI is complete. In PSB faults without the FTC controller and only a nominal PI controller, the imbalanced loads act on the rotor representing the unstable values of platform yaw.

Moreover, the occurrence of a PSF fault in blade 2 after 200 s decreases of the stability of the wind turbine. More precisely, the FTC scheme with the FDI demonstrates a highly effective fault accommodation. After the FDI, the FTC controller is well activated in 211.5 s and control is gradually restored as evidenced by the convergence of the platform yaw in the FTC (red line) case with the line of the fault-free case. However, without the FTC, two faults are observed in the rotor in blades 2 and 3; therefore, the platform yaw with a nominal PI controller is magnified over time to a greater degree than that observed with fault-free yaw motion. The torsional moment in the tower base in Fig. 19 presents similar behavior in Fig. 18. Those figures represent the effectiveness of the FTC, which means that the system can return to a normal state.

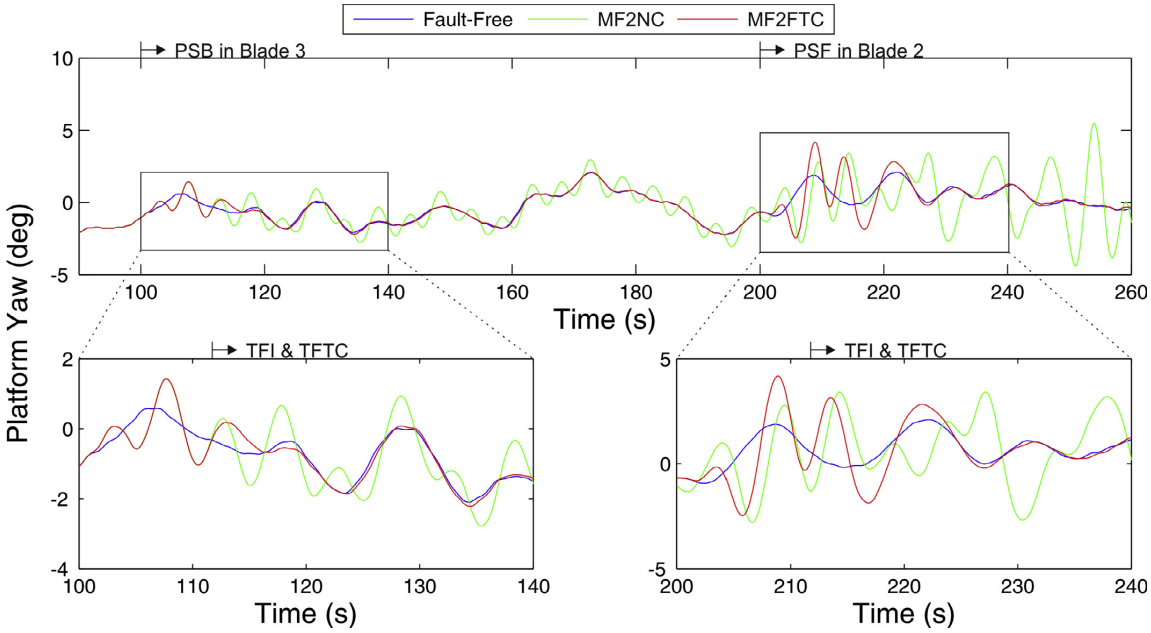

Fig. 18. Comparison of the platform yaw motion under PSB and PSF fault conditions with nominal PI and fault-tolerant controllers under LC4.

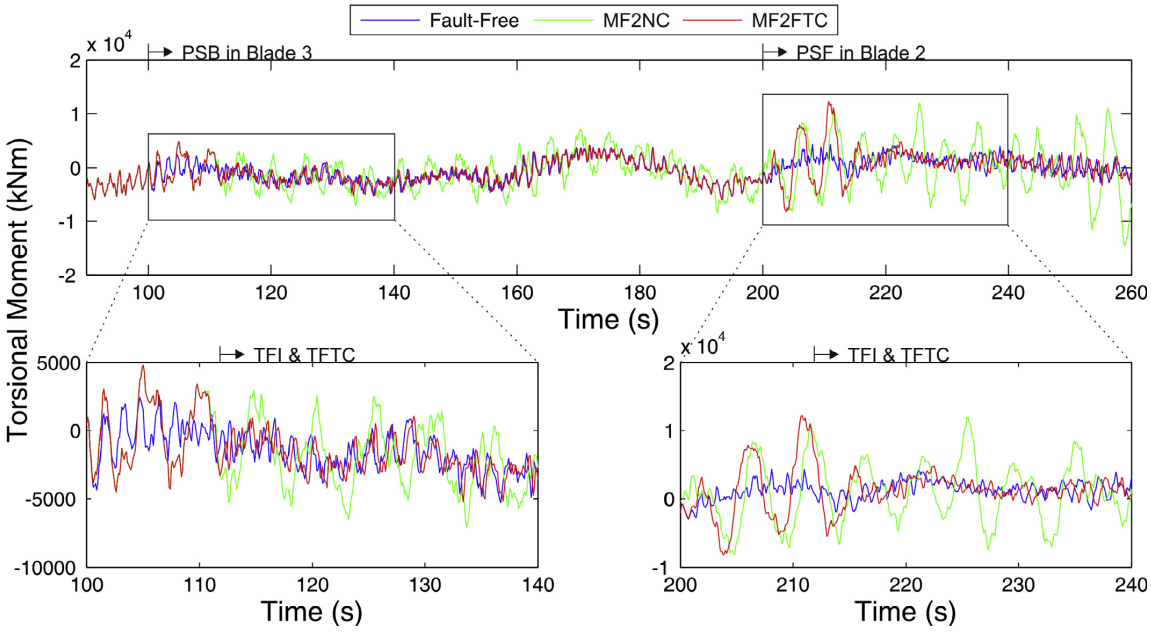

Fig. 19. Comparison of the tower base torsional moment under PSB and PSF fault conditions with nominal PI and fault-tolerant controllers under LC4.

6. Conclusions

Fault detection and isolation techniques should be applied to floating wind turbines for the detection and isolation of unexpected faults at an early stage to prevent catastrophic failures. Here, a fault detection method is suggested based on a Kalman filter with focus on blade pitch actuator and sensor faults. In fault detection, a Kalman filter is used for residual generation and a threshold is used for detecting fault conditions in the blade pitch actuators and sensors. In fault isolation, a single blade pitch angle and nacelle yaw angle measurement are employed to isolate faults in the blade pitch system by the inference method. Based on fault isolation logic, the

fault isolation decision can be made by comparing the measurement values of the blade pitch and nacelle yaw motion.

Two fault-tolerant control schemes are suggested for reconfigurations using a virtual sensor for sensor faults and shutdown for actuator faults. The FTC controller accommodates the PSB and PSF faults by correcting the system output $\mathbf{y}_c$ with the virtual sensor. These FTC schemes can accommodate single and multiple sensor faults. If the FTC controller works well, then the system recognizes the nominal system and reacts in the same way as before. However, faults in the pitch actuator that are intolerable require another wind turbine FTC method. Once the PAS faults are isolated, an emergency shutdown of the wind turbine should be conducted to prevent other failures.

The results of the numerical simulations clearly indicate the effectiveness of the proposed FDI and FTC schemes for load cases with faults. The proposed FDI method can effectively detect and isolate all three faults (PSB, PSF, and PAS) at an early stage. With the proposed FTC strategy, the system response in simulations with single and multiple faults is close to the response of wind turbines in the fault-free condition, which means that the FTC scheme can identify and correct faults within a reasonable time. Finally, the proposed FDI and FTC schemes can be easily applied in practice.

Acknowledgments

This work was supported by the MIT-NTNU-Statoil Wind Turbine Program (Project No. 40136503) funded by Statoil. The authors gratefully acknowledge the supports of Statoil and the Research Council of Norway through the Centre for Autonomous Marine Operations and Systems (AMOS) at NTNU for the present study.

References

[1] Global Wind Statistics 2015, Global Wind Energy Council, 2016.
[2] The European Offshore Wind Industry – Key Trends and Statistics 2015, The European Wind Energy Association, 2016.
[3] I. Dinwoodie, D. McMillan, M. Revie, I. Lazakis, Y. Dalgic, Development of a combined operational and strategic decision support model for offshore wind, Energy Procedia 35 (2013) 157–166.
[4] W. Chen, S.X. Ding, A. Haghani, A. Naik, A.Q. Khan, S. Yin, Observer-based FDI schemes for wind turbine benchmark, in: Proceedings of the 18th IFAC World Congress (Milano: Italy), 2011, pp. 7073–7078.
[5] X. Wei, M. Verhaegen, T. Engelen van, Sensor fault detection and isolation for wind turbines based on subspace identification and Kalman filter techniques, Int. J. Adapt. Control Signal Process. 24 (8) (2010) 687–707.
[6] H. Malik, S. Mishra, Application of probabilistic neural network in fault diagnosis of wind turbine using FAST, TurbSim and Simulink, Procedia Comput. Sci. 58 (2015) 186–193.
[7] J. Dong, M. Verhaegen, Data driven fault detection and isolation of a wind turbine benchmark, IFAC Proc. Vol. 44 (1) (2011) 7086–7091.
[8] P. Santos, L. Villa, A. Reñones, A. Bustillo, J. Maudes, An SVM-based solution for fault detection in wind turbines, Sensors 15 (3) (2015) 5627–5648.
[9] M. Ghane, A.R. Nejad, M. Blanke, Z. Gao, T. Moan, Statistical fault diagnosis of wind turbine drivetrain applied to a 5MW floating wind turbine, J. Phys. Conf. (2016) 753, 052017.
[10] Z. Feng, M. Liang, Fault diagnosis of wind turbine planetary gearbox under nonstationary conditions via adaptive optimal kernel time–frequency analysis, Renew. Energy 66 (2014) 468–477.
[11] M. Blanke, M. Kinnaert, J. Lunze, M. Staroswiecki, J. Schröder, Diagnosis and Fault-tolerant Control, second ed., Springer, Berlin, 2010.
[12] F. Shi, R. Patton, An active fault tolerant control approach to an offshore wind turbine model, Renew. Energy 75 (2015) 788–798.
[13] M.M. Seron, J.A. De Doná, J.H. Richter, Integrated sensor and actuator fault-tolerant control, Int. J. Control 86 (4) (2013) 689–708.
[14] L. Fan, Y. Song, Neuro-adaptive model-reference fault-tolerant control with application to wind turbines, IET Control Theory Appl. 6 (4) (2012) 475–486.
[15] Y. Vidal, C. Tutivén, J. Rodellar, L. Acho, Fault diagnosis and fault-tolerant control of wind turbines via a discrete time controller with a disturbance compensator, Energies 8 (5) (2015) 4300–4316.
[16] J. Carroll, A. McDonald, D. McMillan, Failure rate, repair time and unscheduled O&M cost analysis of offshore wind turbines, Wind Energy 19 (2016) 1107–1119, https://doi.org/10.1002/we.1887.
[17] E.E. Bachynski, M. Etemaddar, M.I. Kvittem, C. Luan, T. Moan, Dynamic analysis of floating wind turbines during pitch actuator fault, grid loss, and shutdown, Energy Procedia 35 (2013) 210–222.
[18] Z. Jiang, M. Karimirad, T. Moan, Dynamic response analysis of wind turbines under blade pitch system fault, grid loss, and shutdown events, Wind Energy 17 (2014) 1385–1409, https://doi.org/10.1002/we.1639.
[19] M. Etemaddar, M. Blanke, Z. Gao, T. Moan, Response analysis and comparison of a spar-type floating offshore wind turbine and an onshore wind turbine under blade pitch controller faults, Wind Energy 19 (2016) 35–50, https://doi.org/10.1002/we.1819.
[20] J. Jonkman, S. Butterfield, W. Musial, G. Scott, Definition of a 5-MW Reference Wind Turbine for Offshore System Development, Technical Report NREL/TP-500-38060 USA, 2009.
[21] J. Jonkman, Definition of the Floating System for Phase IV of OC3, Technical Report NREL/TP-500-47535 USA, 2010.
[22] E. Bachinski, Simo-riflex-aerodyn Manual, MARINTEK Technical Report Norway, 2014.
[23] T.J. Larsen, T.D. Hanson, A method to avoid negative damped low-frequency tower vibration for a floating, pitch controlled wind turbine, J. Phys. Conf. (2007) 75, 012073.
[24] T. Esbensen, C. Sloth, Fault Diagnosis and Fault-tolerant Control of Wind Turbines, Master's thesis, Aalborg University, Aalborg, Denmark, 2009.
[25] C.-T. Chen, in: Linear System Theory and Design, third ed., Oxford University press, 1999.
[26] S. Cho, Z. Gao, T. Moan, Model-based fault detection of blade pitch system in floating wind turbines, J. Phys. Conf. (2016) 753, 092012.
[27] S.X. Ding, in: Model-based Fault Diagnosis Technique: design schemes, algorithms and tools, second ed., Springer, London, 2013.
[28] R. Isermann, Model-based fault-detection and diagnosis – status and applications, Annu. Rev. Control 29 (2005) 71–85.
[29] J. Jonkman, L. Kilcher, TurbSim User's Guide, Technical Report NREL USA, 2012.
[30] IEC 61400–61401: Wind Turbines – Part 1: Design Requirements, International Electrotechnical Commission, 2005.
[31] IEC 61400–61403: Wind Turbines – Part 3: Design Requirements for Offshore Wind Turbines, International Electrotechnical Commission, 2005.

A3. Paper 3

Numerical modeling of the hydraulic blade pitch actuator in a spar-type floating wind turbine considering fault conditions and their effects on global dynamic responses

Seongpil Cho, Erin E. Bachynski, Amir R. Nejad, Zhen Gao and Torgeir Moan

Published in Wind Energy 2019; Early View Publication, 1-21.

Received: 4 February 2019 | Revised: 10 July 2019 | Accepted: 30 September 2019

DOI: 10.1002/we.2438

RESEARCH ARTICLE

WILEY

Numerical modeling of the hydraulic blade pitch actuator in a spar-type floating wind turbine considering fault conditions and their effects on global dynamic responses

Seongpil Cho[1,2] | Erin E. Bachynski[1,2] | Amir R. Nejad[1] | Zhen Gao[1,2] | Torgeir Moan[1,2]

[1] Department of Marine Technology, NTNU, Trondheim, Norway

[2] Centre for Autonomous Marine Operations and Systems (AMOS), NTNU, Trondheim, Norway

Correspondence
Seongpil Cho, Department of Marine Technology, NTNU, Trondheim, Norway.
Email: seongpil.cho@ntnu.no

Funding information
Research Council of Norway; Equinor, Grant/Award Number: 40136503

Abstract

This paper deals with numerical modeling of the hydraulic blade pitch actuator and its effect on the dynamic responses of a floating spar-type wind turbine under valve fault conditions. A spar-type floating wind turbine concept is modeled and simulated using an aero-hydro-servo-elastic simulation tool (Simo-Riflex [SR]). Because the blade pitch system has the highest failure rate, a numerical model of the hydraulic blade pitch actuator with/without valve faults is developed and linked to SR to study the effects of faults on global responses of the spar-type floating wind turbine for different faults, fault magnitudes, and environmental conditions. The consequence of valve faults in the pitch actuator is that the blade cannot be pitched to the desired angle, so there may be a delay in the response due to excessive friction and the wrong voltage, or slit lock may cause runaway blade pitch. A short circuit may cause the blade to get stuck at a particular pitch angle. These faults contribute to rotor imbalance, which result in different effects on the turbine structure and the platform motions. The proposed method for combining global and hydraulic actuator models is demonstrated in case studies with stochastic wind and wave conditions and different types of valve faults.

KEYWORDS

blade pitch actuator faults, fault characteristics, floating wind turbine, global dynamic responses, hydraulic pitch actuator

Abbreviations: IEC, International Electrotechnical Commission; M#, number (#) of magnitudes; NEM, normalized expected maximum; NREL, National Renewable Energy Laboratory; NRMS, normalized root mean square; OC3, Offshore Code Comparison Collaboration; TF, time of fault occurrence; VCS, circuit shortage in the valve; VEF, excessive friction in the valve; VSL, slit lock in the valve; VWV, wrong voltage applied in the valve

The peer review history for this article is available at https://publons.com/publon/10.1002/we.2438.

1 | INTRODUCTION

Offshore wind turbines operate in ocean environments with irregular waves and turbulent winds and also experience technical faults during their service life. Faults and failures in the actuators, sensors, and system components can lead to system interruptions. They change the system characteristics, the efficiency of power production, and the operational safety. Significant economic losses are associated with operation and maintenance—up to 30% of the life cycle cost for offshore wind farms.[4,5]

Hydraulic pitching drives are still in the majority in older wind turbines as described in Hau.[6] Statistical data on downtime per failure and failure rates of wind turbine sub-systems have been employed to evaluate the wind turbine reliability.[1-3,7] Using failure statistics for wind turbines in Sweden, Ribrant and Bertling[1] showed that the failures in pitch systems accounted for 27.5% of the total component failures. According to the RELIAWIND report,[2] the pitch system has 21.3% and 23.4% contribution to the total failure rate and downtime, respectively. Carroll et al[3] analyzed the failure rates for the offshore wind turbines and their subassemblies, finding that the hydraulics and pitch systems have the highest failure rates among the system components and account for over 14% of the total failures of wind turbines. NordzeeWind[7] shows that the pitch system accounts for over 20% of the production stops.

According to the mentioned references, it is clear that blade pitch systems contribute to the failure rate and downtime of wind turbines. The blade pitch system is critical for wind turbines to maintain constant power generation in above-rated regions of wind speed while protecting the wind turbine from damage. Faults in the blade pitch sensors and actuators influence the control system and result in imbalanced loads on the rotor, main bearings, and shaft. Imbalanced aerodynamic loads on the rotor also affect the power production and the structural responses of the blades, tower, and support structure.

Detailed dynamic analyses of wind turbines under fault situations are required to identify critical conditions and understand the performance of wind turbines. Studies of the effect of pitch system faults on wind turbine performance, loads, and platform motions in wind turbine components have been conducted for specific fault scenarios. Jiang et al[8] and Chaaban et al[9] examine the structural response of floating wind turbines under various pitch mechanism faults. Bachynski et al[10] show the performance of different types of floating wind turbines under pitch actuator fault, grid loss, and shutdown, using a SR-AeroDyn tool. Etemaddar et al[11] analyzed the fault effects in the pitch system on onshore and offshore wind turbines using the extreme response analysis in short term with the HAWC2. These studies focused on the effect of the blade pitch actuator faults on global dynamic responses of the wind turbine. However, the details of the blade pitch actuator were not modeled.

The blade pitch systems of modern wind turbines are driven by electrical or hydraulic pitch actuators.[12] An electrical pitch system requires gears to adjust the pitch angle with an electric motor. It is able to control the position precisely. The main challenges related to electrical pitch systems are gear wear, high backlash, and low robustness against external disturbances. On the other hand, a hydraulic pitch actuator is controlled by a servo or directional control valve, and gears are unnecessary, thus reducing backlash and preventing wear. Hydraulic systems with a high level of stiffness and appropriate damping are suitable in the case of high aerodynamic loads. In particular, rapid load changes in the blade root due to turbulence and wind gusts are controlled and dampened and not transferred through the mechanical system.[13] In addition, hydraulic pitch actuators have low component sensitivity to environment; for example, temperature spans from −25°C to +55°C does not affect the system's performance. The oil in the system reduces structural vibrations and power peaks/loads and increases the overall reliability of the turbine.[14]

Dynamic modeling of the hydraulic actuator for the blade pitch system (valve, cylinder, pump, and reservoir) has been carried out to observe the behavior of wind turbines due to the large blade deflection[15] and fault conditions.[16,17] In these studies, the input voltage is assumed to be directly proportional to the flow rate constants, and the valve spool position is not considered. However, the response of an actual valve is delayed with respect to the input voltage. Carroll et al[3] show that oil, valve, and sludge issues account for a large portion (37.3%) of the total failure rate of hydraulic pitch systems. Therefore, valve modeling and dynamic analysis are essential when considering valve faults in the blade pitch actuator.

This paper focuses on coupled nonlinear aero-hydro-servo-elastic simulations of spar-type floating wind turbines under valve fault conditions. The main contributions of the present work are (a) the numerical modeling of the hydraulic pitch actuator including valve model and spool position controller and (b) modeling of the pitch actuator faults related to mechanical and electrical failures. The hydraulic pitch actuator model is inserted into the global simulation model to investigate how these faults affect the dynamic responses of a floating wind turbine. The objectives of this paper are as follows:

a. Model a hydraulic pitch actuator including a pump, valves, and hydraulic cylinders.
b. Design a proportional-integral (PI) valve controller to achieve satisfactory performance of blade pitching.
c. Model faults in valves.
d. Conduct numerical simulations under fault conditions in aero-hydro-servo-elastic tools coupled with the modeled blade pitch actuator.
e. Compare the wind turbine performance and dynamic responses, eg, blade root bending moments, platform motions, and tower base bending moments, in fault conditions considering different environmental load cases.

In this paper, Section 2 shows the floating wind turbine model, baseline controller, and the hydraulic blade pitch system. Section 3 includes the fault modeling and scenarios for directional control valves. Section 4 shows the simulation results for wind turbine performance, blade root bending moments, platform motions, and tower base bending moments. Section 5 provides the conclusions.

2 | CASE STUDY MODEL AND METHODOLOGY

2.1 | Floating wind turbine model and fully coupled numerical simulation

A spar-type floating turbine has been modeled as a rotor, tower, nacelle, floater, and mooring lines. The model in this paper is based on the National Renewable Energy Laboratory (NREL) 5-MW offshore wind turbine model[18] supported by a spar buoy floater (OC3-Hywind)[19] and three catenary mooring cables as shown in Figure 1. The NREL 5-MW wind turbine specifications are listed in Table 1. In addition, the OC3-Hywind floater properties are provided in Table 2.

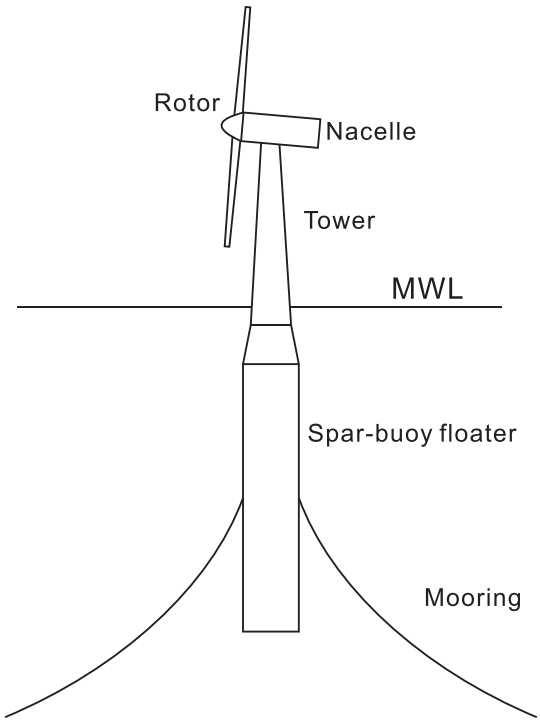

FIGURE 1 Schematic view of a spar-type floating wind turbine

TABLE 1 Properties for the National Renewable Energy Laboratory (NREL) 5-MW wind turbine[18]

Rated power, MW	5
Rotor orientation and configuration	Upwind, three blades, horizontal axis
Rotor diameter, m	126
Hub height from the mean water level, m	90
Cut-in, rated, cut-out wind speed, m/s	3, 11.4, 25
Cut-in, rated rotor speed, °/s	41.4, 72.6
Max pitch rate, °/s	8
Gearbox ratio	97

TABLE 2 Properties for the OC3-Hywind floater[19]

Water depth, m	320
Draft, m	120
Diameter above taper, m	6.5
Diameter below taper, m	9.4
Center of mass, m	(0, 0, −89.9115)
Mass, including ballast, kg	7.466×10^6
Mass moment of inertia (I_{xx} and I_{yy}), kg·m^2	4.229×10^9
Mass moment of inertia (I_{zz}), kg·m^2	1.642×10^8

The dynamic responses of the wind turbine model have been simulated with SR,[20,21] which is an aero-hydro-servo-elastic code for fully coupled nonlinear time-domain numerical simulations. Hydrodynamic forces and moments on the rigid hull, according to first-order potential flow theory and Morison-type viscous drag, have been accounted for in Simo.[20] The flexible elements for the blades, shaft, tower, and mooring system with the finite element solver are modeled in Riflex.[21] Additionally, Riflex calculates the aerodynamic forces and moments on the blades based on the blade element momentum (BEM) method including tower shadow, dynamic stall, and skewed inflow correction.[21] The models for structural dynamics, hydrodynamics, and aerodynamics are considered simultaneously with an external code that consists of (a) a baseline control system for a torque and pitch controller and (b) a model of the blade pitch system under various operational conditions. Figure 2 shows the data transmission of SR and controller algorithm.

2.2 | Baseline controller for operational wind turbines

The baseline control system consists of the blade pitch and generator torque controllers. In the below-rated wind speed region, the torque controller is active to capture the maximum power by regulating the generator torque and thus maintaining the optimal tip speed ratio.[18] In above-rated wind speed region, the blade pitch controller adjusts the blade pitch angle to reduce the aerodynamic loads while producing the rated power. For floating wind turbines, the blade pitch controller may be used to improve the system responses and reduce the floater motions.[22] In the baseline controller[18] developed by NREL, the pitch actuator is not modeled; it is assumed that the blade pitch angle can be adjusted directly the pitch command. In this paper, a hydraulic pitch actuator is modeled and interacts with the baseline controller with modified proportional and integral gain values.[19] Figure 3 shows the block diagram of the modified baseline controller, where Ω_r is the rotor speed, Ω_g is the generator speed, $\Omega_{g,m}$ is the measured generator speed, $\Omega_{g,\text{rated}}$ is the rated generator speed, Q_g is the generator torque, Q_a is the aerodynamic torque, β_m is the measured blade pitch angle, and V_{wind} is the wind speed.

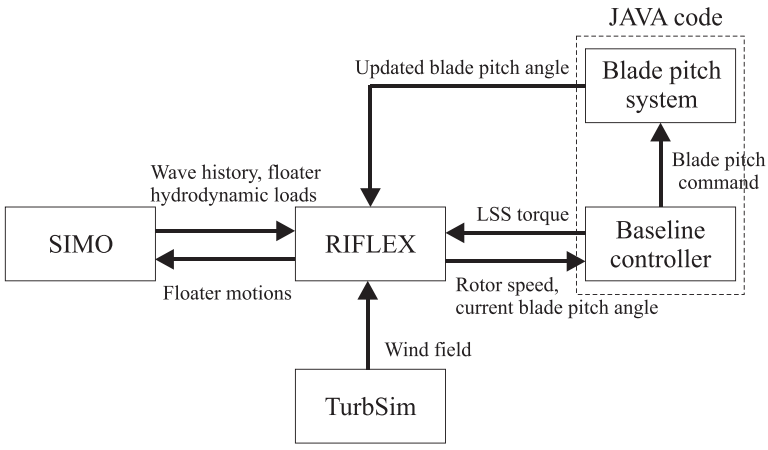

FIGURE 2 Data transmission between Simo-Riflex (SR) and controller

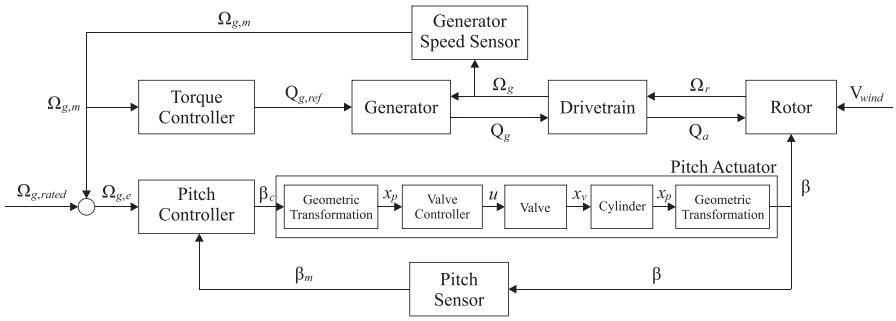

FIGURE 3 Block diagram of the baseline controller

2.3 | Hydraulic actuator system

The hydraulic pitch system includes the hydraulic pump, a set of directional control valves, a fluid tank, and a hydraulic cylinder. The blade pitch angle is controlled by a hydraulic cylinder placed in the hub of the turbine. Hydraulic pitch control is not sensitive to vibrations. The oil flow to and from the cylinders is controlled by a number of valves, in particular a control valve. The energy to drive the hydraulic cylinders is supplied by a power unit placed in the nacelle, and the energy is transferred to the hub via a rotary union.

The system controller provides a command voltage signal to control the valve spool position based on the difference between the blade pitch angle and the reference signals. The schematic diagram of a hydraulic actuator as shown in Figure 4A consists of a constant pressure pump, an accumulator, a reservoir, a hydraulic cylinder, and a directional control valve.

2.3.1 | Directional control valve model

The directional control valve uses an electromagnetic field via the solenoid coil to move an internal steel armature assembly. This assembly controls the position of the main cylinder to change the state of the main valve to open or closed. Figure 5 shows the schematic of a 4/3 directional control valve with solenoid.

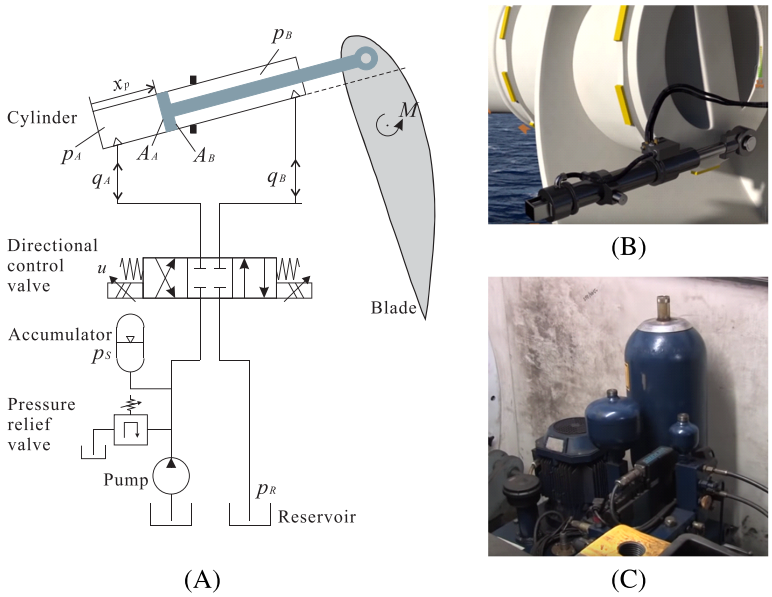

FIGURE 4 The hydraulic pitch system: (A) schematic diagram, (B) hydraulic actuator,[23] and (C) hydraulic power station[24] [Colour figure can be viewed at wileyonlinelibrary.com]

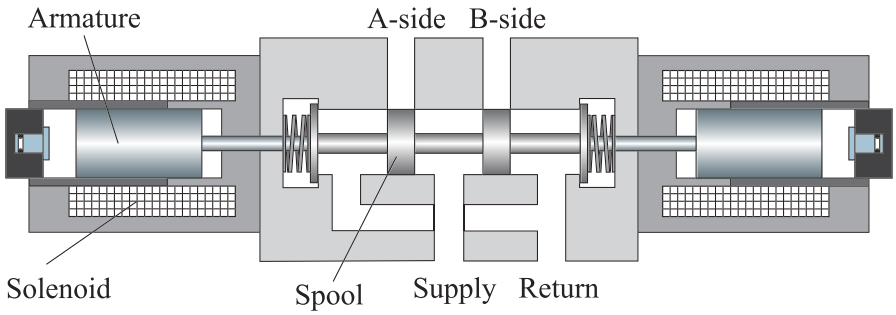

FIGURE 5 4/3 directional control valve with solenoid [Colour figure can be viewed at wileyonlinelibrary.com]

To control the blade pitch angle, the valve spool position control adjusts the hydraulic flow into the cylinder. The valve spool position x_{vs} is calculated from the control input voltage u_{vs} through a second-order system[25] given by

$$\ddot{x}_{vs} + 2\zeta_{vs}\omega_{vs}\dot{x}_{vs} + \omega_{vs}^2 x_{vs} = \omega_{vs}^2 k_u u_{vs}, \tag{1}$$

where ω_{vs} is the valve natural frequency, ζ_{vs} is the valve damping ratio, k_u is the voltage gain, respectively, and ($\dot{}$) represents the time derivatives. It is assumed that the valve spool is symmetric with zero overlap design.

As described in Figure 6, flow directions can be determined by the valve spool position. If the spool is at the right-side position ($x_{vs} > 0$) as shown in Figure 6B, hydraulic fluid flows from the pump (supply) into the cylinder chamber B side and from the cylinder chamber A side to the reservoir tank (return). On the other hand, if the spool position is set to the left-side position ($x_{vs} < 0$) in Figure 6C, then the hydraulic fluid can flow from pump to A side and B side to the reservoir tank. Hydraulic fluid cannot flow when the valve spool is at the neutral position ($x_{vs} = 0$).

The hydraulic flow rate at A and B can be determined based on the spool position. The continuity equation of hydraulic flow rate at A and B depends on the sign of the spool position:

For $x_{vs} > 0$,

$$\begin{aligned} q_A &= -k_q x_{vs}\sqrt{p_A - p_R}, \\ q_B &= k_q x_{vs}\sqrt{p_S - p_B}, \end{aligned} \tag{2a}$$

and for $x_{vs} < 0$,

$$\begin{aligned} q_A &= -k_q x_{vs}\sqrt{p_S - p_A}, \\ q_B &= k_q x_{vs}\sqrt{p_B - p_R}, \end{aligned} \tag{2b}$$

where q_A and q_B are the hydraulic flow rates to the cylinder chamber A and B sides, k_q is the valve flow coefficient, and p_S and p_R are the supply pressure and the return pressure, respectively. Table 3 describes properties for the directional control valve from Rexroth's valve model (RE 29093, size 16).[26] The supply pressure p_S is set to 250 bars controlled by the accumulator.

From Merritt,[27] the valve flow coefficient can be calculated by

$$k_q = \frac{C_d A_d}{x_{vs,\max}}\sqrt{\frac{2}{\rho_{\text{fluid}}}}, \tag{3}$$

where C_d is the discharge coefficient, A_d is the discharge area, and ρ_{fluid} is the density of fluid.

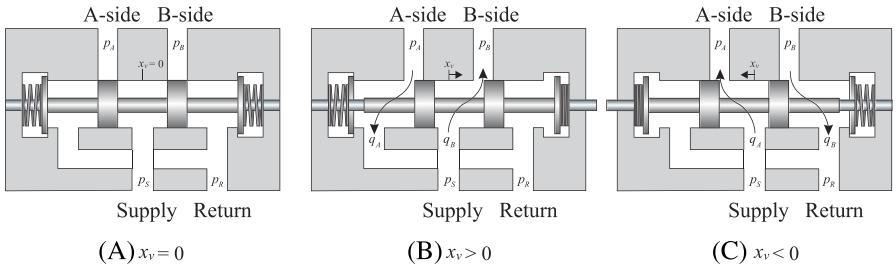

FIGURE 6 Flow mechanism of the valve with spool position [Colour figure can be viewed at wileyonlinelibrary.com]

TABLE 3 Properties for the directional control valve[26]

Valve natural frequency (ω_{vs}), rad/s	141
Valve damping ratio (ζ_{vs})	0.74
Minimum and maximum valve position ($x_{vs,min}$, $x_{vs,max}$), m	−0.02, 0.02
Minimum and maximum input voltage ($u_{vs,min}$, $u_{vs,max}$), V	−10, 10
Valve voltage gain (k_u), m/V	0.002
Valve flow gain (k_q), $m^2/s/\sqrt{bar}$	0.0233

However, it is hard to directly calculate the exact discharge coefficient C_d values from the technical data. Alternatively, k_q values can be estimated by Equation 4 from Albers[28] and Šulc and Jan[29] with the nominal pressure drop (Δp_N) and nominal flow rate (q_N) from Rexroth's valve model.[26]

$$k_q = \frac{q_N}{x_{vs,max}\sqrt{0.5\Delta p_N}} \tag{4}$$

2.3.2 | Blade pitch dynamics

Calculation of hydraulic force in a cylinder

As illustrated in Figure 4, the hydraulic actuator is modeled by a single-rod and double-acting cylinder that consists of a piston inside a cylindrical housing. The cylinder produces the force from hydraulic pressure acting on the piston. The pressure dynamics based on the flow mechanism into two chambers (A and B sides) in the cylinder are written by

$$\dot{p}_A = \frac{E_{\text{eff}}}{V_A(x_p)}(q_A - A_A\dot{x}_p), \tag{5a}$$

$$\dot{p}_B = \frac{E_{\text{eff}}}{V_B(x_p)}(q_B + A_B\dot{x}_p), \tag{5b}$$

where V_A and V_B are the total control volumes of chambers A and B depending on the piston position x_p. A_A and A_B are the areas of the piston on the A and B sides. E_{eff} is the effective bulk modulus of the hydraulic fluid that is assumed to be incompressible. Additionally, the volumes V_A and V_B are calculated by

$$\begin{aligned} V_A(x_p) &= V_{A0} + A_A x_p, \\ V_B(x_p) &= V_{B0} + A_B(l_p - x_p), \end{aligned} \tag{6}$$

where V_{A0} and V_{B0} are the initial volumes of the two-cylinder chamber.

By calculating hydraulic pressures in sides A and B of the cylinder, the piston force F can be obtained as follows:

$$F = P_A A_A - P_B A_B. \tag{7}$$

Blade pitch dynamics

The blade pitch angle can be adjusted by the hydraulic actuator controlled by a pitch moment from piston force F acting on the rigid bar. Figure 7 shows the geometry of the hydraulic pitch actuator. The geometry of the actuator is related to the piston position x_p and the pitch angle β by

$$x_p(\beta) = \sqrt{L_p^2 + r_p^2 - 2L_p r_p \cos(\alpha_0 - \beta)} - l_p/2, \tag{8}$$

where r_p is the torque arm, l_p is the rod length, L_p is the length between the pivot and rotational center, and α_0 is the initial angle between the pin-to-center axis and the torque arm when x_p = 0. From the geometry of this actuator, the blade pitch torque $M_{T,bp}$ can be described by

$$M_{T,bp} = F r_p g(\beta), \tag{9}$$

where the $g(\beta)$ is a force factor represented by $g(\beta) = \dfrac{1}{r_p}\dfrac{dx_p}{d\beta}$.

107

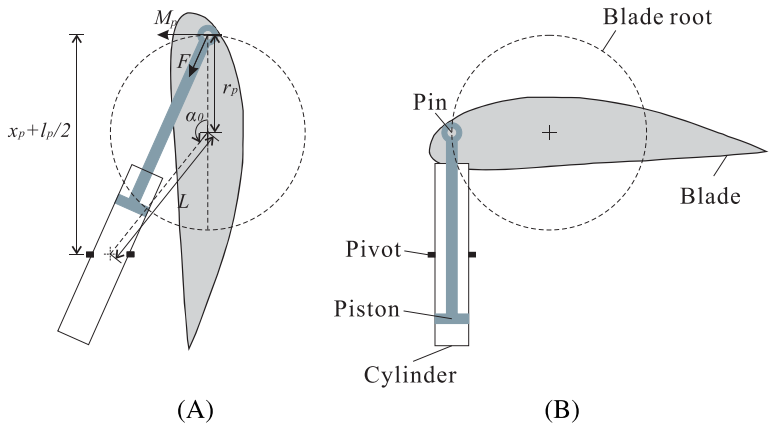

FIGURE 7 Geometry of the blade pitch actuator: (A) β = 0° and (B) β = 90° [Colour figure can be viewed at wileyonlinelibrary.com]

The pitch angle dynamics are governed by

$$J_{bp}\ddot{\beta} + B_{bp}\dot{\beta} = M_{T,bp} + M_A, \tag{10}$$

where J_{bp} is the pitch inertia, B_{bp} is the viscous damping coefficient, and M_A is the aerodynamic pitching moment.

Table 4 shows the pitch actuator geometries and parameters. However, it is hard to directly measure the viscous damping coefficient B_{bp}. Therefore, an alternative method, described in Section 2.4, was used to estimate B_{bp}.

2.4 | Valve spool position control

The blade pitch angle β can be determined by the piston position x_p in the hydraulic cylinder based on the geometrical relationship as described in Equation (8). The piston position x_p of the cylinder is controlled by the valve spool position x_{vs} corresponding to the desired position. The valve spool position is changed according to the input voltage applied to the directional control valve.

First, the control input u_v can be calculated by a PI controller from the piston position error $e(t)$ feedback to the directional control valve position as follows:

$$u_{vs}(t) = k_p\left(e(t) + \frac{1}{T_i}\int_0^t e(\tau)d\tau\right),\ e(t) = (x_p(\beta) - x_p(\beta_C)), \tag{11}$$

where k_p is the proportional gain, T_i is the integral time, and the position error $e(t)$ is given as function of the blade pitch angle β and pitch command β_C from the pitch controller in Figure 3.

In order to calculate the proportional gain k_p, the valve and pitch cylinder systems need to be transformed by transfer function in steady-state condition. The directional control valve model can be described by the transfer function $G_{vs}(s)$ obtained from Equation (1).

TABLE 4 Pitch actuator geometries and parameters[30]

Piston rod length (l_p), m	2
Torque arm (r_p), m	1
Pin-to-center axis length (L_p), m	1.7
Initial angle (α_0), rad	2.5128
Pitch inertia (J_{bp}), kg·m^2	28 600
Viscous damping coefficient (B_{bp}), N·s/rad	8.545×10^5
Effective bulk modulus (E_{eff}), bar	18 000

$$G_{vs}(s) = \frac{X_{vs}(s)}{U_{vs}(s)} = \frac{\omega_{vs}^2 k_u}{s^2 + 2\zeta_{vs}\omega_{vs}s + \omega_{vs}^2}, \tag{12}$$

where $U_{vs}(s)$ and $X_{vs}(s)$ are the transfer functions of the valve system input (voltage) and output (valve spool position). The blade pitch system in a steady-state condition can be modeled by third-order transfer function from Merritt.[27] .

$$G_{bp}(s) = \frac{B(s)}{X_{vs}(s)} = \frac{C_p\omega_p^2}{s^3 + 2\zeta_p\omega_p s^2 + \omega_p^2 s}, \tag{13}$$

$$\omega_p = g\sqrt{\frac{E_{eff}}{J_{bp}}\left(\frac{A_A^2}{V_A} + \frac{A_B^2}{V_B}\right)},\ \varsigma_p = \frac{B_{bp}}{2\sqrt{J_{bp}E_{eff}g\left(\frac{A_A^2}{V_A} + \frac{A_B^2}{V_B}\right)}} \tag{14}$$

$$C_p = \frac{\left(\frac{A_A k_q\sqrt{\Delta p_A}}{V_A} + \frac{A_B k_q\sqrt{\Delta p_B}}{V_B}\right)}{g\left(\frac{A_A^2}{V_A} + \frac{A_B^2}{V_B}\right)}, \tag{15}$$

where $X_{vs}(s)$ and $B(s)$ are the transfer functions of the blade pitch system input (valve spool position) and output (blade pitch angle), ω_p is the natural frequency of piston system, ζ_p is the damping ratio, and C_p denotes the flow rate gain. The volume V and force factor g can be changed to influence each natural frequency and damping ratio of the pitch system in steady-state condition. The minimum damping ratio for the system is 0.2 from Merritt.[27] Then, B_{bp} is calculated by Equation (14).

Total system transfer function $G_T(s)$ can be derived by

$$G_T(s) = G_{vs}(s)\,G_{bp}(s) = \frac{B(s)}{U_{vs}(s)} = \frac{\omega_{vs}^2\omega_p^2 k_u C_p}{s\left(s^2 + 2\zeta_{vs}\omega_{vs}s + \omega_{vs}^2\right)\left(s^2 + 2\zeta_p\omega_p s + \omega_p^2\right)}. \tag{16}$$

To set the critical proportional gain $k_{p,\text{crit}}$, the characteristic equation and Routh's methods were applied. Stability should be checked in every piston position in cylinder for the pitch angles from 0° to 90°. Using an empirical method and applying $k_{p,\text{crit}}$ values from 1 to 300 in the system, the critical proportional gain is found to be $k_{p,\text{crit}}$ = 139.2 V/rad in every piston position and pitch angle. The period of oscillation T_c = 0.3012 second can be calculated by applying $k_{p,\text{crit}}$ and Routh's methods as described in Dutton et al. [31] Using the Ziegler-Nichols method,[31] the proportional gain and integral time are therefore set to $k_p = 0.45k_{p,\text{crit}}$ and $T_i = T_c/1.2$ in case of PI control, respectively. The blade pitch control system is tested for the 15° step reference signal in Figure 8. The response of the blade pitch angle, valve spool position, and control input voltage shown here demonstrates the ability to follow the pitch angle reference and for controller performance.

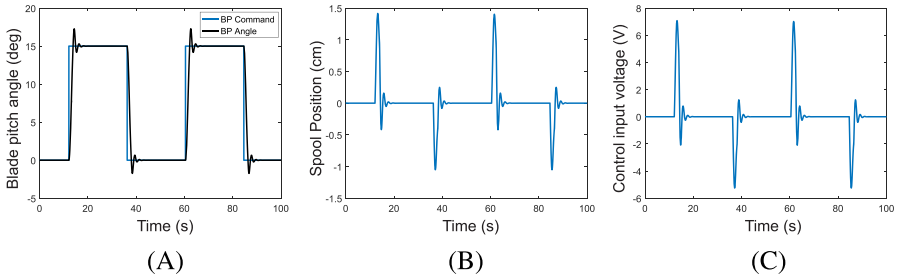

FIGURE 8 The step response of the blade pitch system with 15° step reference signal: (A) blade pitch angle, (B) valve spool position, and (C) control input voltage [Colour figure can be viewed at wileyonlinelibrary.com]

3 | FAULT MODELING AND SCENARIOS

Carroll et al[3] show that oil, valve, and sludge issues account for a large portion (37.3%) of the total failure rate for hydraulic pitch systems. Valve faults can change the system characteristics.[25]

Basically, faults in the directional control valves are mainly categorized as mechanical or electrical faults. Mechanical faults are related to oil contamination and sludge that disturb the spool movement, acting as increasing friction in the valve. Electrical faults may be related to additional and residual current through the solenoid due to damage or dirt on the armature. After these faults occur, the valve cannot provide an adequate amount of flow in the cylinder from control input. These faults influence the results of pressure, piston force, blade pitch angle, and response delay. They also could affect the global dynamic response of wind turbines in transient and steady-state conditions. The incorrect pitching of a blade due to faults causes asymmetric forces on blades, introducing an unbalanced rotation, which increases structural loads on the rotor significantly. In the worst cases, it is associated with valve seizure that leads to inoperable conditions.

In this paper, four different cases of valve faults are considered (two mechanical faults and two electrical faults): excessive friction (VEF), slit lock (VSL) on spool, wrong voltage applied (VWV), and circuit shortage (VCS), in the directional control valve. Figure 9 illustrates mechanical and electrical valve faults. These faults are selected based on information in Institute of Electrical and Electronics Engineers,[2] Cho et al,[32] and Watton.[33]

3.1 | Mechanical faults

Directional control valves operate over thousands of cycles with adequate oil and undergo mechanical and thermal stresses periodically in a normal operation state. The operational conditions mainly influence the service life of the valve. According to Carroll et al,[3] oil contamination causes up to 25% of the total failures in hydraulic systems. Oil contamination with poor filtration results in sludge buildup on the surface of spool and bore. The sludge is a mixture of rusted metal particles, sand, dust, and polish compound.

As the sludge builds up on the spool, the clearances between the spool and body decrease. This decreased clearance space leads to more force being required to move the spool as the static friction increases. This fault is called excessive friction in valves (VEF). The increasing friction is modeled as follows:

$$\ddot{x}_{vs} + 2\zeta_{vs}\omega_{vs}\dot{x}_{vs} + \omega_{vs}^2 x_{vs} = \omega_{vs}^2 k_u u_{vs} - F_F, \tag{17}$$

$$F_F = F_C \mathrm{sgn}(\dot{x}_{vs}), \tag{18}$$

where F_C is the Coulomb friction. The value of friction F_F in the normal condition is set to 0 because it is negligible in real valve spools.

This sludge narrows the clearance, allowing more particles into the clearance space. In the worst case, these mixtures with sludge buildup and particles become hardened. If the friction is larger than the maximum force from the solenoid, the valve spool will be seized. This phenomenon is commonly referred to as "slit lock." When slit lock (VSL) in valves occurs, the spool position is described by

$$x_{vs} = x_{vs,\mathrm{VSL}}, \tag{19}$$

where $x_{vs,\mathrm{VSL}}$ is the spool position after the VSL fault.

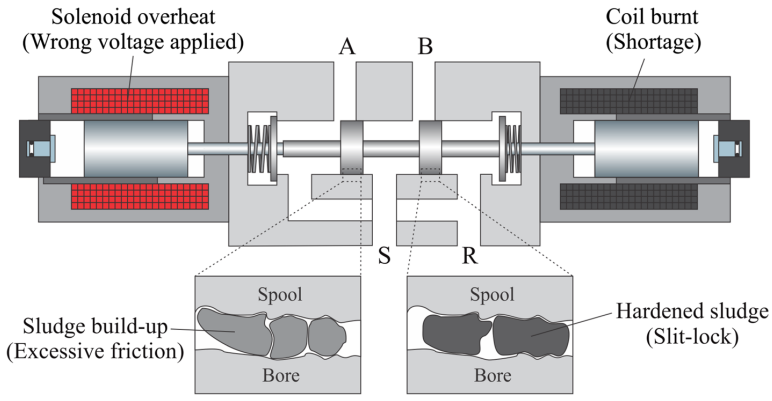

FIGURE 9 Illustration of mechanical and electrical valve faults [Colour figure can be viewed at wileyonlinelibrary.com]

3.2 | Electrical faults

When the solenoid coil reaches the magnetic saturation level, the coil is overheated caused by high inrush currents. This phenomenon changes its coil impedance and the current through the solenoid. In extreme cases, the core of the solenoid is subject to damages, or the coil inductance is permanently changed. Then, it applies the wrong voltage.

The wrong voltage applied (VWV) resulting from changed coil impedance can be described by changing the valve voltage gain k_u,

$$k_u = k_{u,\mathrm{WV}}, \tag{20}$$

where $k_{u,\mathrm{WV}}$ is changed voltage gain.

Furthermore, if solenoids cannot properly dissipate the heat generated by their residual current or go through high inrush current due to faults, then the solenoid is damaged and burnt out, which means that the insulation around the coil windings will burn and the coil will short out. When a solenoid circuit shortage occurs (VCS), the voltage applied is as follows:

$$u_{vs} = u_{\mathrm{VCS}} = 0, \tag{21}$$

where u_{VCS} is the voltage value in the VCS fault. If a VSC fault occurs in the valve system, the spool position reacts and moves to a neutral position that allows no flow due to the spring described in Figure 5. Then, the valve is closed, and the actuator gets stuck in the same position. Table 5 describes the updated fault values in the valve model and consequences in each fault.

4 | SIMULATION RESULTS AND DISCUSSION

In this section, simulation results are presented to illustrate the effect of the valve fault conditions. Numerical simulations are conducted under four different fault cases: VEF, VSL, VWV, and VCS, on a single blade.

4.1 | Environmental conditions

Four load cases with different wind and wave conditions were selected for simulating the dynamic responses of the floating wind turbine, as given in Table 6.

The turbulent wind field $U_w(x, y, z, t)$ represented by the normal wind profile and the normal turbulence model is modeled by using TurbSim[34] according to the Kaimal turbulence model. The wind model was based on the International Electrotechnical Commission (IEC) 61400-1[35] and 3[38]. In the vertical plane, 32 × 32 points were used over an area of 160 × 160 m, with time step of 0.05 second of the wind field generation. The wind shear was modeled according to the power law with exponent 0.14.

TABLE 5 Mathematical model of faults applied in numerical simulations

Type	Fault Modeling	Consequence
VEF	$\ddot{x}_{vs} + 2\zeta_{vs}\omega_{vs}\dot{x}_{vs} + \omega_{vs}^2 x_{vs} = \omega_{vs}^2 k_u u_{vs} - F_F$	Response delay
VSL	$x_{vs} = x_{vs,\mathrm{VSL}}$	Blade pitch runaway
VWV	$\ddot{x}_{vs} + 2\zeta_{vs}\omega_{vs}\dot{x}_{vs} + \omega_{vs}^2 x_{vs} = \omega_{vs}^2 k_{u,\mathrm{WV}} u_{vs}$	Response delay
VCS	$u_{vs} = u_{\mathrm{VCS}} = 0$	Actuator stuck

Abbreviations: VCS, circuit shortage in the valve; VEF, excessive friction in the valve; VSL, slit lock in the valve; VWV, wrong voltage applied in the valve.

TABLE 6 Load cases based on winds and waves

Load Case	U_w, m/s	Turbulence Model	H_s, m	T_p, s
1	11.2	IEC Class C	3.2	10.0
2	14		3.62	10.30
3	17		4.2	10.50
4	20		4.8	10.80

For irregular waves, the Joint North Sea Wave Project (JONSWAP) wave spectrum was used. The peak period (T_p) and significant wave height (H_s) were decided based on their correlation with wind speed for the Statfjord site in the North Sea.[36] Wind and wave directions are aligned. Six 1-hour simulations with different random seeds are carried out for each load case and fault condition to capture the significant stochastic variation.[8]

4.2 | Fault description

The fault studied here can degrade the control quality and accuracy. In order to identify representative and comparable fault magnitudes, we examine the squared integral error of the blade pitch e_{IEBP} during the response in each simulation:

$$e_{IEBP} = \int_{TF}^{\tau} (\beta_{actual}(t) - \beta_C(t))^2 dt. \tag{22}$$

On the basis of the load cases described in Table 6, the fault magnitude has been decided by measuring e_{IEBP}. Figure 10 shows the average e_{IEBP} values for VEF and VWV faults during 400 seconds after fault occurs. The time of fault (TF) is 100 seconds after the turbine reaches the steady-state condition.

For the response study, several different magnitudes M1, M2, and M3 are simulated to illustrate the severity of the faults. The input corresponding to M1, M2, and M3 here has been decided based on the value of e_{IEBP} = 0.006, 0.018, and 0.03 (in fault-free e_{IEBP} = 0.001 432) in VEF and VWV faults, respectively, and is given in Table 7. In case of the VSL fault, both the positive (VSL^+) and negative (VSL^-) stuck valve spool positions have been considered. There is no magnitude in the VCS fault. The fault-free cases correspond to normal operation.

Figure 11 shows the response in terms of the valve spool position and blade pitch angle under four valve faults in the blade pitch system (blade 3). Two faults, VEF and VWV, make the responses of valve position and blade pitch angle slower due to increased friction and gain change, respectively. As shown in Figure 11A, the valve spool cannot move to until the solenoid force is larger than the excessive friction due to sludge in VEF fault. If the solenoid force exceeds the friction, the valve spool moves quickly to follow the control input, and the blade pitch angle increases suddenly in Figure 11B. In this case, the direction change of the valve spool delays the response of the blade pitch system. The VWV fault delays the response due to gain change.

The valve spool position is stuck after occurrence of a VSL fault. However, the valve is still open, and hydraulic fluid flows continuously to the cylinder, making the pitch angle increase. This fault depends on the direction of the valve position. If the valve is stuck in the right position (positive, VSL^+), the blade pitch angle continuously increases to the maximum pitch angle. If it is left (negative, VSL^-), the pitch angle decreases

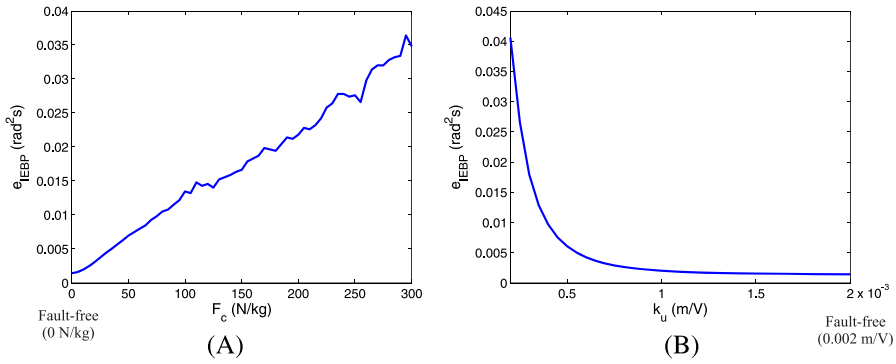

FIGURE 10 Integral error of the blade pitch depends on the fault magnitudes: (A) excessive friction in the valve (VEF) and (B) wrong voltage applied in the valve (VWV) [Colour figure can be viewed at wileyonlinelibrary.com]

TABLE 7 List of magnitudes for VEF and VWV faults

	Magnitude			
Fault Case	M1	M2	M3	Theoretical Permissible Range
VEF (F_c), N/kg	45	155	260	<400
VWV (k_u), m/V	0.0005	0.0003	0.000 23	>0

Abbreviations: VEF, excessive friction in the valve; VWV, wrong voltage applied in the valve.

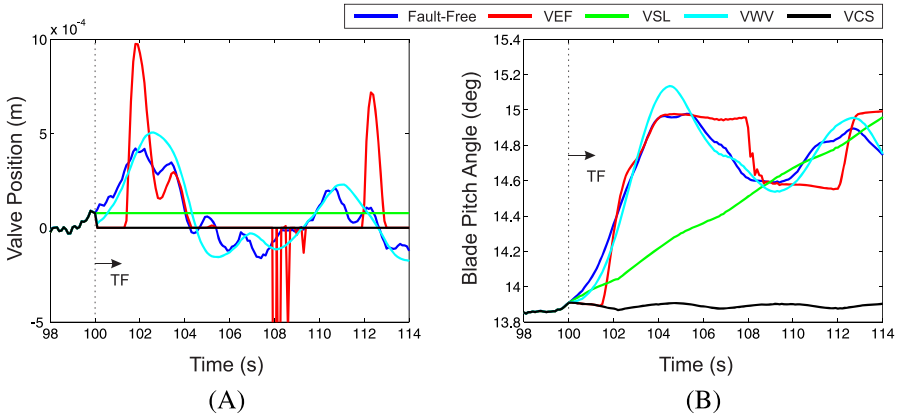

FIGURE 11 Comparison of the valve position and blade pitch angle under fault conditions under LC3: (A) valve position and (B) blade pitch angle. VCS, circuit shortage in the valve; VEF, excessive friction in the valve; VSL, slit lock in the valve; VWV, wrong voltage applied in the valve [Colour figure can be viewed at wileyonlinelibrary.com]

to the minimum pitch angle. When VCS occurs, the input voltage goes to 0 value, and the valve position returns to the neutral position due to the restoring force of the spring. Then, the valve will be closed, and the actuator gets stuck.

4.3 | Wind turbine performances and response analysis

Numerical results for the dynamic responses of the spar-type floating wind turbine under valve faults are presented. The simulations are conducted to evaluate the effect of different fault scenarios. Six realizations of each load case, each lasting for 1 hour, are carried out. The root-mean-square (RMS) values are calculated for the responses for floating wind turbine after fault occurrence (TF is 100 s). The response values are normalized by the corresponding results in the fault-free cases as

$$RV_{\text{norm}} = \frac{RV_i}{RV_{\text{f-free}}} \; i = 1,\ 2,\ 3,\ 4, \tag{23}$$

where RV_{norm} is the response value normalized by response value in the fault-free case $RV_{\text{f-free}}$ and RV_i is the ith response value (1: VEF, 2: VSL, 3: VWV, and 4: VCS).

4.3.1 | Wind turbine performance

As shown in Figure 12, the blade pitch angle has been influenced by the valve faults in VEF, VWV, and VCS in faulty blade (blade 3). However, these pitch angle differences do not affect the results of rotor speed and power very much.

Figure 13 shows the results of the rotor speed, power, and blade pitch angle under VSL fault. If the valve spool is stuck in the right-side position (VSL^+, positive x_v), hydraulic fluid can flow continuously into the B side of cylinder, and piston moves to the left side of the cylinder until the pressure relief valve starts to work. Due to the difference of blade pitch angle between blades 1 and 3, the rotor speed starts to decrease gradually, which influences power output because of the loss of the generator torque acting on the low-speed shaft described in Figure 13A. Then, the pitch controller adjusts the blade pitch angle of fault-free blades (blades 1 and 2) to 0° to maintain the rated rotor speed, which also increases the aerodynamic thrust. On the other hand, if the valve is locked in the left-side position, the hydraulic fluid can flow to the A side of cylinder. The pitch angle on the faulty blade decreases to 0° due to the piston moving to the right side. In this case, the rotor speed and power output are not influenced significantly by stuck blade 3 as shown in Figure 13B. The aerodynamic torque increases due to the stuck blade (blade 3), and the pitch controller adjusts other two blades (blades 1 and 2) to reduce the aerodynamic torque by increasing their blade pitch angles, thus maintaining the rotor speed.

Figure 14 shows the normalized RMS values of the rotational speed, aerodynamic thrust, and generator power after fault occurrence. VEF, VWV, and VCS faults have little effect on the rotor speed and power production from generator. For VSL fault when the valve spool is stuck at the right position (VSL^+), the generator cannot produce any power because the rotor has been stopped. The blade pitch angle difference (around 20° between blades 1 and 3 in case of VSL^-) causes an increase of aerodynamic thrust as the wind speed increases.

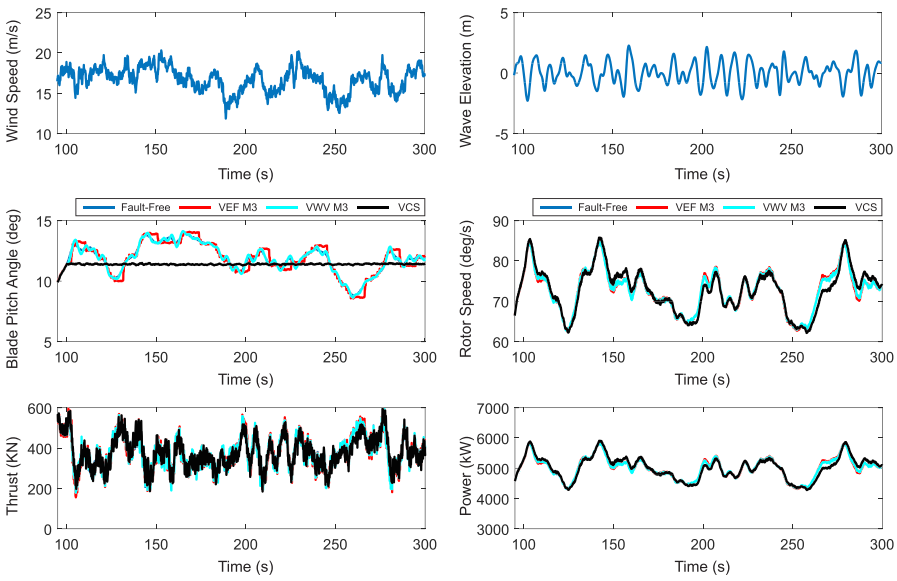

FIGURE 12 Effects of excessive friction in the valve (VEF), wrong voltage applied in the valve (VWV), and circuit shortage in the valve (VCS) faults on wind speed, wave elevation, the blade pitch angle, rotor speed, aerodynamic thrust, and power under LC3 [Colour figure can be viewed at wileyonlinelibrary.com]

4.3.2 | Blade root bending moments

Fault in a pitch actuator affects the torsional, flap-, and edge-wise bending moments in the blade roots. Figure 15 illustrates the load and blade root bending moment directions. Figure 16 shows the effects of fault cases on the RMS of the blade root bending moments, of floating wind turbine. The value in Figure 16 is the difference of RMS values of the blade root bending moment between normal blade (blade 1) and faulty blade (blade 3) along each axis, normalized as follows:

$$\frac{mean\left(RMS\left(M_{\mathrm{BR,fault\text{-}free}}\right)\right) - RMS\left(M_{\mathrm{BR,Blade3}}\right)}{mean\left(RMS\left(M_{\mathrm{BR,fault\text{-}free}}\right)\right)}, \tag{24}$$

where *mean* (*RMS* ($M_{\mathrm{BR,\ fault\text{-}free}}$)) = (*RMS* ($M_{\mathrm{BR,\ Blade1}}$) + *RMS* ($M_{\mathrm{BR,\ Blade2}}$) + *RMS* ($M_{\mathrm{BR,\ Blade3}}$))/3 and *RMS* ($M_{\mathrm{BR,\ fault\text{-}free}}$) corresponds to the fault-free condition.

Figure 16 shows that the blade root bending moments due to faults depend on the difference of the blade pitch angle between blades 1 and 3. In fault-free condition, the value of the metric in Figure 16 is nearly 0, implying no rotor imbalance.

In case of VEF faults, the variation of the blade root bending moment along the torsional direction has above 25% of the magnitude of the fault-free blade root bending moments, while the differences in the flap- and edge-wise bending moments are almost 0. VWV has little effect on the blade root bending moment along the torsional, flap-, and edge-wise directions. In VSL^{-}, as the wind speed increases, the difference in flap-wise moments between faulted and fault-free blades can be increased from one to three times. There is also imbalance in the torsion and flap-wise moments for VCS. The imbalance shown here affects the platform motions and tower base bending moments.

4.3.3 | Platform motions and tower base bending moments

The platform motions and tower bending moments are mainly related to wind and wave loads. The spar-type platform has large yaw stiffness from the mooring system. Wave loads do not influence yaw motion much because of the floater's cylindrical shape. Figures 17 and 18 show the effects of fault cases on the RMS of the platform motions and tower base bending moments of floating wind turbine. VEF and VWV faults brought slow response of blade pitch angle. VEF and VWV faults have little effect on platform motions (roll, pitch, and yaw) and tower base bending moments (torsional, fore-aft, and side-side).

The VCS fault tends to cause the actuator to get stuck and leads to aerodynamic imbalance on the rotor plane depending on the operating condition. As a consequence, the yaw and tower torsional moments increase. Yaw motion is increased by approximately 20%, and the torsional

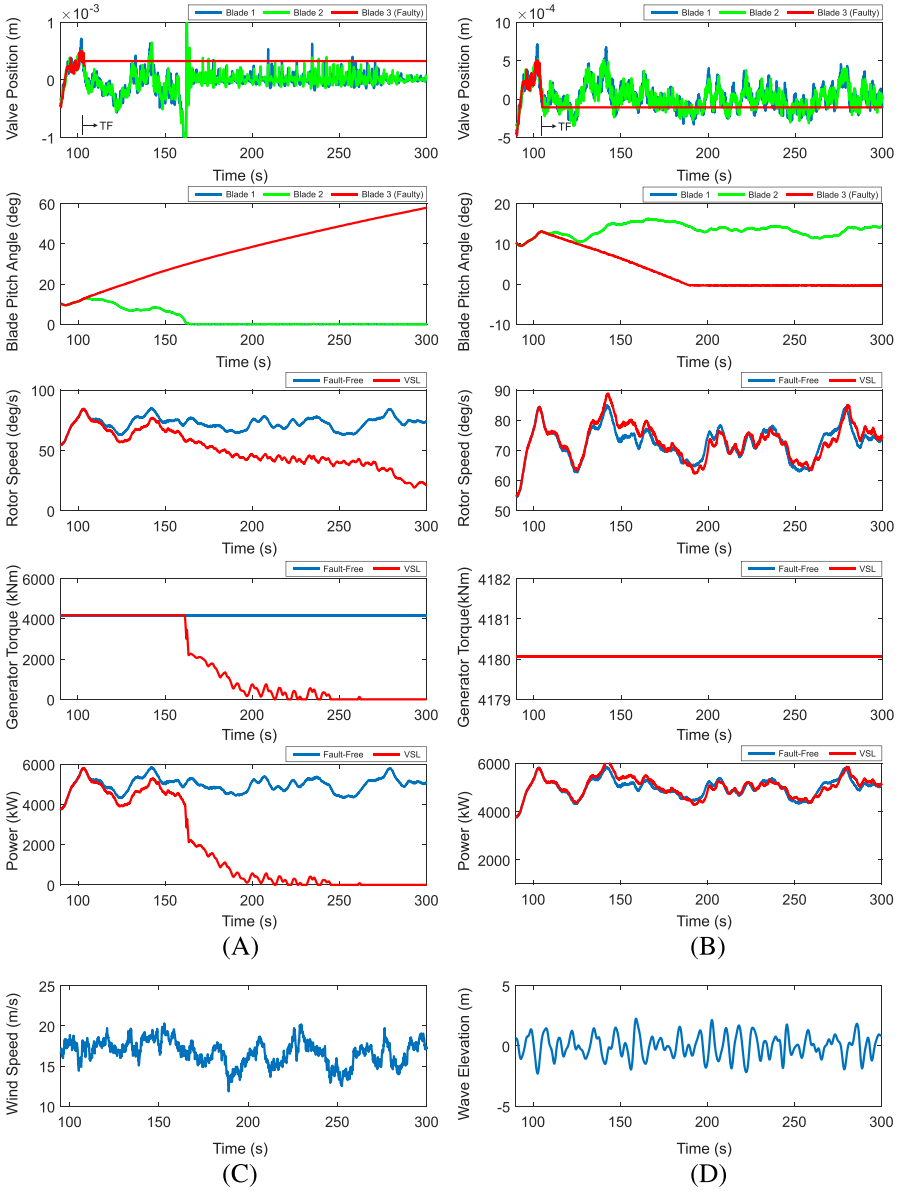

FIGURE 13 Effects of VSL fault on the valve position, blade pitch angle, rotor speed, aerodynamic torque, and power: (A) positive (VSL^{+}) and (B) negative spool position (VSL^{-}) under LC3 with (C) wind speed and (D) wave elevation [Colour figure can be viewed at wileyonlinelibrary.com]

moment can be doubled compared with fault-free conditions. This fault does not greatly affect platform motions (roll and pitch) and tower base bending moments (fore-aft and side-side).

The dynamic responses in case of VSL depend on the spool position. While continuously increasing or decreasing the blade pitch angle in VSL^{+} (positive valve position) or VSL^{-} (negative valve position) faults, increasing blade pitch angle difference causes rotor imbalance. The severe rotor imbalance under VSL fault occurs when the faulty blade is pitched to 0° based on the stuck spool position. The yaw motion is increased by approximately two times, and torsional moment is up to four times larger than the fault-free conditions under VSL^{-} faults. In addition, the increasing aerodynamic thrust as shown in Figure 14B affects platform pitch motion and tower base fore-aft bending moments in Figures 17C and 18C.

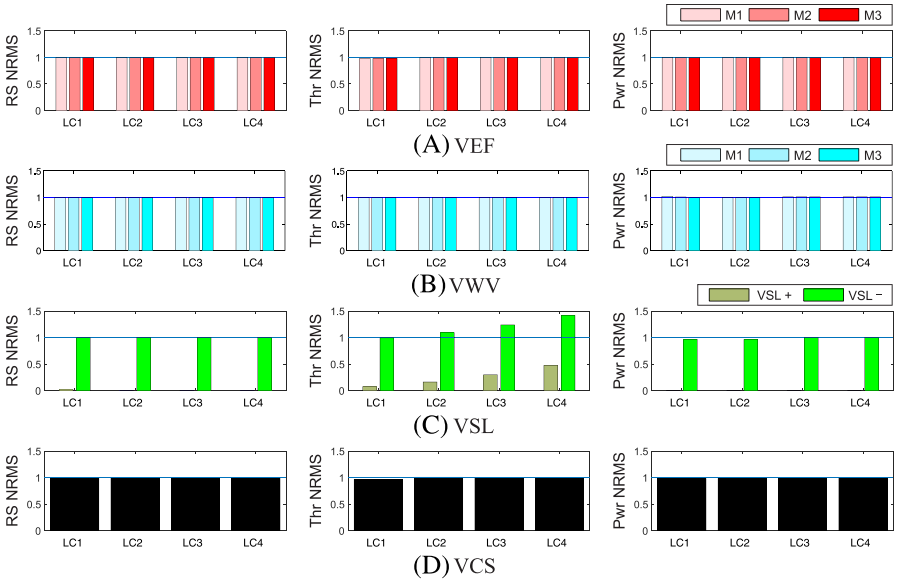

FIGURE 14 Normalized root-mean-square (NRMS) values of the rotor speed, thrust, and power production described by Equation (23) for the floating wind turbine under (A) excessive friction in the valve (VEF), (B) slit lock in the valve (VSL), (C) wrong voltage applied in the valve (VWV), and (D) circuit shortage in the valve (VCS) fault conditions with different fault magnitudes [Colour figure can be viewed at wileyonlinelibrary.com]

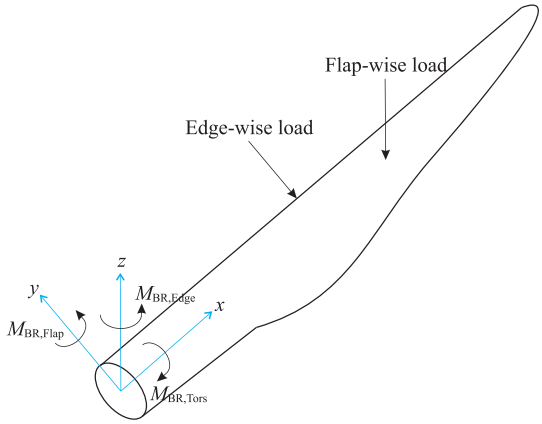

FIGURE 15 The schematic of blade for direction of loads and blade root bending moments [Colour figure can be viewed at wileyonlinelibrary.com]

If the pitch angle difference is beyond a certain limit (above 30°), one or more of the blades acts as a brake, and the rotor speed starts to decrease. With decreasing rotor speed, the wind turbine loses the generator torque acting on the low-speed shaft VSL^{+} fault. The pitch and fore-aft bending moment also decreased. When the faulty blade (blade 3) angle reaches 90°, the rotor has lost much of the aerodynamic thrust, and it affects the results of platform motions and tower base bending moments. The platform motions and tower base bending moments were not affected by the change of the blade root torsional and edge-wise bending moments.

Figure 19 shows a comparison of normalized expected maxima of platform motions and tower base bending moments in above-rated wind speed region. Response values that are platform motions and tower base bending moments are divided by the fault-free values of the expected maxima. These faults have been considered: VEF M3, VSL^{-}, VWV M3, and VSC. Similar to the RMS values shown in Figures 16 and 17, the

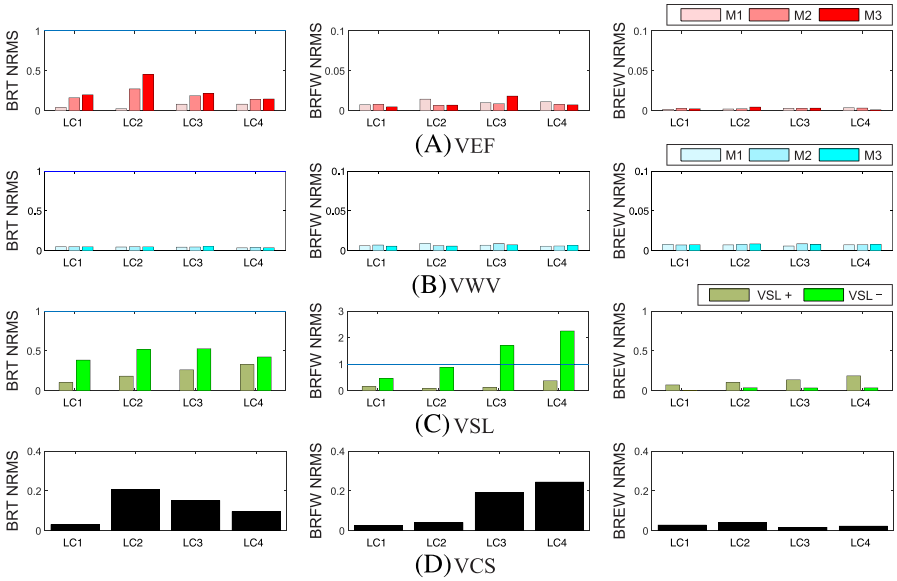

FIGURE 16 Normalized root-mean-square (NRMS) values of the blade root torsional (BRT), blade root flap-wise (BRFW), and blade root edge-wise (BREW) bending moments described by Equation (24) for the floating wind turbine under (A) excessive friction in the valve (VEF), (B) slit lock in the valve (VSL), (C) wrong voltage applied in the valve (VWV), and (D) circuit shortage in the valve (VCS) fault conditions with different fault magnitudes [Colour figure can be viewed at wileyonlinelibrary.com]

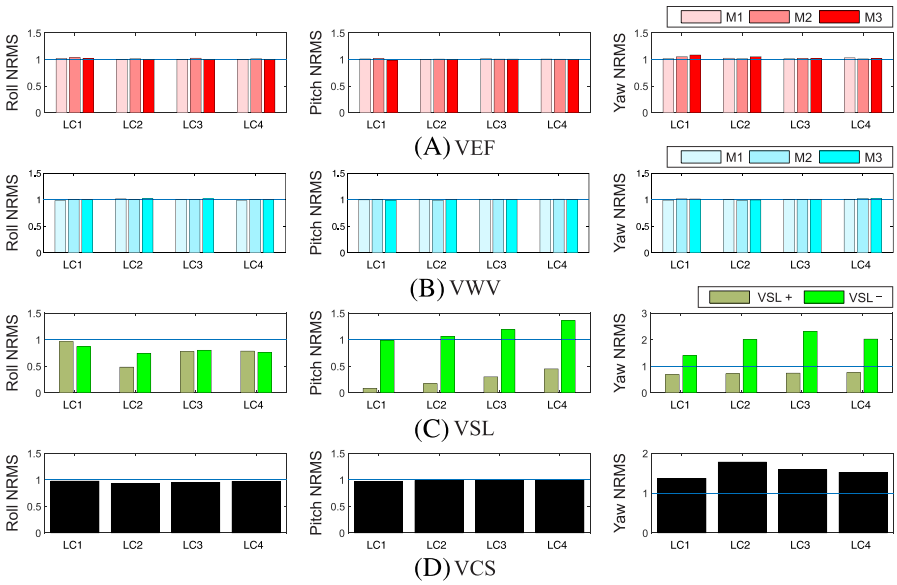

FIGURE 17 Normalized root-mean-square (NRMS) values of the platform roll, pitch, and yaw motions described by Equation (23) for the floating wind turbine under (A) excessive friction in the valve (VEF), (B) slit lock in the valve (VSL), (C) wrong voltage applied in the valve (VWV), and (D) circuit shortage in the valve (VCS) fault conditions with different fault magnitudes [Colour figure can be viewed at wileyonlinelibrary.com]

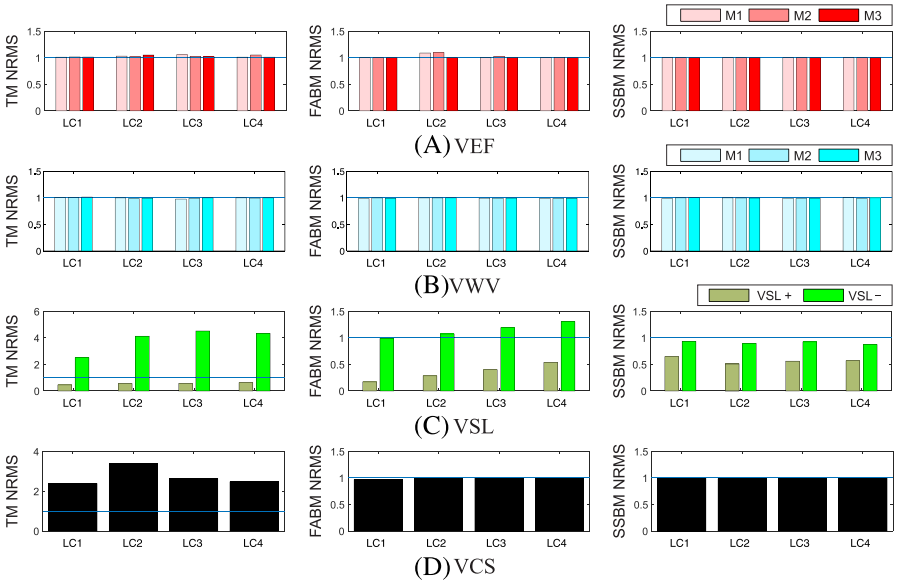

FIGURE 18 Root-mean-square (RMS) values of the torsional moment (TM), fore-aft bending moment (FABM), and side-side bending moment (SSBM) described by Equation (23) for the floating wind turbine under (A) excessive friction in the valve (VEF), (B) slit lock in the valve (VSL), (C) wrong voltage applied in the valve (VWV), and (D) circuit shortage in the valve (VCS) fault conditions with different fault magnitudes [Colour figure can be viewed at wileyonlinelibrary.com]

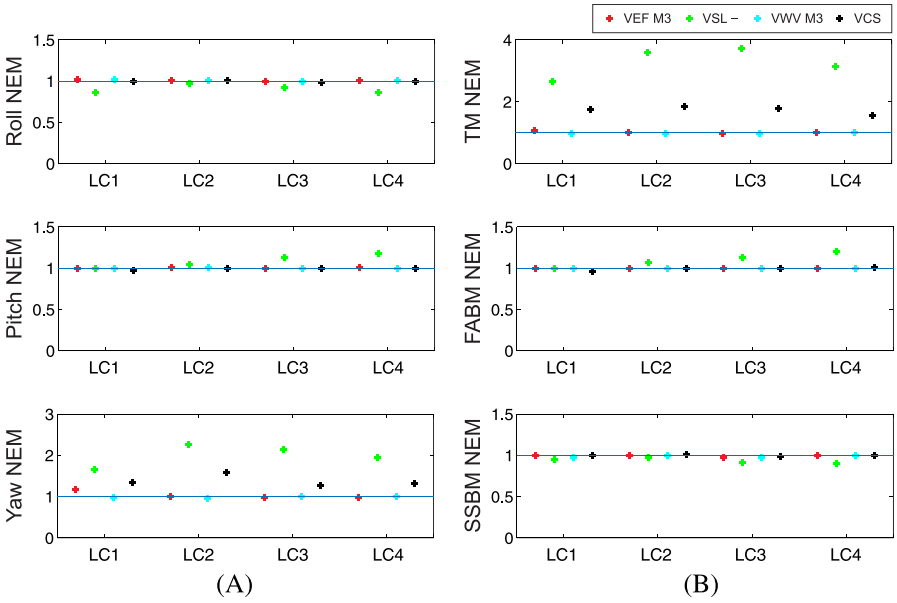

FIGURE 19 Normalized expected maximum (NEM) response values: (A) platform motions and (B) tower base bending moments [Colour figure can be viewed at wileyonlinelibrary.com]

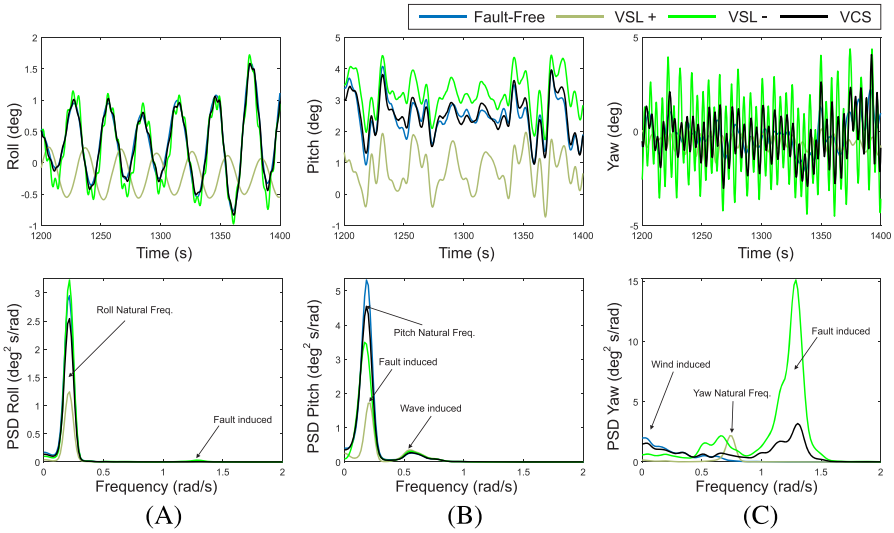

FIGURE 20 Time realization and power spectral density (PSD) of the platform (A) roll, (B) pitch, and (C) yaw motions in LC3 [Colour figure can be viewed at wileyonlinelibrary.com]

platform motions and base bending moments are not sensitive to response delay due to VEF M3 and VWV M3 faults. VSL$^-$ and VSC faults are dominant in yaw and tower base torsional moments.

Figure 20 presents the effects of VSL and VCS faults on the power spectral density (PSD) of the platform roll, pitch, and yaw responses for LC3. The sample duration is 1 hour under faults in stationary condition. The response at the natural frequency in roll motion increases. VSL$^-$ and VCS faults slightly influenced platform pitch motion due to the small blade angle difference. The loss of aerodynamic thrust causes reduced amplitudes and changed frequencies in platform pitch and yaw in VSL$^+$.

The asymmetric force acting on the rotor triggers large aerodynamic excitation of the tower and the spar-type platform. The VSL$^-$ fault has a large effect on the yaw motions compared with the other fault cases in stationary responses. The yaw response is greatly increased, and roll and pitch resonant responses are relatively decreased under the VSL fault when the valve position is negative. In addition, the fault-induced frequency of 1.288 rad/s due to VCS and VSL$^-$ faults corresponds to the 1P frequency of the wind turbine at rated speed.[37]

5 | CONCLUDING REMARKS

This paper deals with numerical modeling and response analysis of the hydraulic pitch actuator in a floating spar-type wind turbine in valve fault conditions. The pitch-regulated NREL 5-MW wind turbine model mounted on the OC3-Hywind floater with three catenary mooring cables has been used in these simulations. Fully coupled time-domain simulations were conducted for the dynamic response analysis using SR with a baseline controller under various environmental conditions with correlated wind and waves. The baseline controller maintained a constant generator torque above the rated wind speed. The hydraulic pitch system was modeled by a pressure supply pump, directional control valve, hydraulic cylinder, and fluid reservoir. The valve spool position is controlled by a PI controller, where a voltage signal is determined from the piston position error that regulates the flows to the two-cylinder sides.

Up to 25% of the hydraulic system's failures are caused by oil contamination with poor filtration. In this paper, two mechanical and two electrical faults have been modeled to check the effect of faults. They include excessive friction (VEF), slit lock (VSL) on spool, wrong voltage applied (VWV), and circuit shortage (VCS) in the directional control valves. This results in sludge buildup on the surface of the spool and bore, which increases the possibility of excessive friction (VEF) or slit lock (VSL). Also, additional current through the solenoid changes its coil impedance and can lead to damages, resulting in the wrong voltage being applied (VWV) and circuit shortage (VCS).

VEF and VWV had minor effects on the floating wind turbine responses compared with the other faults. The faults VCS and VSL lead to an increased aerodynamic thrust due to the difference of the blade pitch angle between fault-free and faulty blade. Serious rotor imbalance occurs while the wind turbine is operating. As a consequence of the rotor imbalance, the platform's yaw and tower torsional moments increase. The VSL$^-$ fault is the most severe fault case regarding platform yaw motion and tower base bending moment. The fault-induced frequency incurring from VSL$^-$ fault is the 1P frequency of the wind turbine. If faults continue, the damage in the wind turbine structure will be amplified. In summary,

the difference of the blade pitch angle causes rotor imbalance, which affects the yaw motion and tower base torsional bending moment. The pitch angle difference also influences the aerodynamic thrust, platform pitch motion, and tower base fore-aft bending moment.

In order to validate the models of fault effects in the wind turbines, field measurements of the blade pitch actuator under faults are needed. In addition, faults affect the wind turbine performance and structural responses of wind turbines. Hence, it is important to detect, diagnose, and mitigate faults at the early stage before they propagate to failure of components.

ACKNOWLEDGEMENTS

This work was supported by the MIT-NTNU-Statoil Wind Turbine Program (project no. 40136503) funded by Equinor (formerly Statoil). The authors gratefully acknowledge the support of Equinor and the Research Council of Norway(Norges Forskningsråd) through the Centre for Ships and Offshore Structures (CeSOS) and Centre for Autonomous Marine Operations and Systems (AMOS) at NTNU for the present study.

ORCID

Seongpil Cho https://orcid.org/0000-0002-6613-4592
Erin E. Bachynski https://orcid.org/0000-0002-1471-8254
Amir R. Nejad https://orcid.org/0000-0003-0391-8696

REFERENCES

1. Ribrant J, Bertling L. Survey of failures in wind power systems with focus on Swedish wind power plants during 1997-2005. In Power Engineering Society General Meeting, 24–28 Jun 2007. IEEE, Energy Conversion. *IEEE Transactions: Stockholm Denmark*. 2007;22:1-8.
2. Gayo J B, Reliability-focused research on optimizing wind energy system design, operation and maintenance: tools, proof of concepts, guidelines & methodologies for a new generation, Final Publishable Summary of Results of Project ReliaWind, 2011.
3. Carroll J, McDonald A, McMillan D. Failure rate, repair time and unscheduled O&M cost analysis of offshore wind turbines. *Wind Energy*. 2016;19:1107-1119. https://doi.org/10.1002/we.1887
4. Tavner P. *Offshore Wind Turbines: Reliability*. London, UK: Availability and Maintenance, The Institution of Engineering and Technology (IET); 2012.
5. Dinwoodie I, McMillan D, Revie M, Lazakis I, Dalgic Y. Development of a combined operational and strategic decision support model for offshore wind. *Energy Procedia*. 2013;35:157-166.
6. Hau E. 2013. Wind Turbines: Fundamentals, Technologies, Application, Economics. Springer Science & Business Media.
7. Wind Nordzee, Operations report 2009, Technical Report OWEZ_R_000_20101112, Nordzee Wind, 2010.
8. Jiang Z, Karimirad M, Moan T. Dynamic response analysis of wind turbines under blade pitch system fault, grid loss, and shutdown events. *Wind Energy*. 2014;17:1385-1409. https://doi.org/10.1002/we.1639
9. Chaaban R, Ginsberg D, Fritzen CP. Structural load analysis of floating wind turbines under blade pitch system faults. *Wind Turbine Control and Monitoring*. 2014;301-334. Springer
10. Bachynski EE, Etemaddar M, Kvittem MI, Luan C, Moan T. Dynamic analysis of floating wind turbines during pitch actuator fault, grid loss, and shutdown. *Energy Procedia*. 2013;35:210-222.
11. Etemaddar M, Blanke M, Gao Z, Moan T. Response analysis and comparison of a spar-type floating offshore wind turbine and an onshore wind turbine under blade pitch controller faults. *Wind Energy*. 2016;19:35-50. https://doi.org/10.1002/we.1819
12. Chiang MH. *A novel pitch control system for a wind turbine driven by a variable-speed pump-controlled hydraulic servo system Mechatronics*. 2011;21:753-761.
13. Lu B, Li Y, Wu X and Yang Z 2009 A review of recent advances in wind turbine condition monitoring and fault diagnosis Proceedings of the 2005 IEEE International Conference on Robotics and Automation ICRA 2005 pp 2290-2295
14. Pros and cons of hydraulic pitch systems, https://www.fsenergy.com/technology/hydraulic-vs-electric-pitch/. Fritz Schur Energy.
15. Hansen MH, Kallesøe BS. *Servo-elastic dynamics of a hydraulic actuator pitching a blade with large deflections*. Journal of Physics: Conference Series; 2007 (Vol. 75, No. 1, p. 012077).
16. Frøyd L, Dahlahug OG. Effect of pitch and safety system design on dimensioning loads for offshore wind turbines during grid fault. *Energy Procedia*. 2012 Jan 1;24:36-43.
17. Rakoto L, Schorsch J, Kinnaert M. Modelling hydraulic pitch actuator for wind turbine simulation under healthy and faulty conditions. *IFAC-PapersOnLine*. 2015 Jan 1;48(21):577-582.
18. Jonkman J, Butterfield S, Musial W, Scott G. Definition of a 5-MW reference wind turbine for offshore system development. *Technical Report NREL/TP-500-38060 USA*. 2009.
19. Jonkman J. *Definition of the floating system for phase IV of OC3* Technical Report NREL/TP-500-47535 *USA*, 2010
20. SINTEF Ocean. Simo 4.15.0 user guide; 2018.
21. SINTEF Ocean. Riflex 4.15.0 user guide; 2018.
22. Larsen TJ, Hanson TD. A method to avoid negative damped low-frequency tower vibration for a floating, pitch controlled wind turbine. *Journal of Physics: Conference Series*. 2007;75:012073.

23. DSTI - Dynamic Sealing Technologies, Inc., How do rotary unions work in wind turbines? *Youtube Video*]. Retrieved from. https://www.youtube.com/watch?v=QvisCF0jWs0
24. Lyons William, Wind Turbine Tour [Youtube Video]. Retrieved from https://www.youtube.com/watch?v=8wK1qmRv_l8
25. Karpenko M, Sepehri N. Fault-tolerant control of a servohydraulic positioning system with crossport leakage. *IEEE Transactions on Control Systems Technology*. 2005 Jan;13(1):155-161.
26. Directional control valves, pilot-operated, with electrical position feedback and integrated electronics (OBS): RE29093, Rexroth, 2016.
27. Merritt HE. Hydraulic Control Systems. *John Wiley & Sons*. 1967.
28. Albers P. Motion Control in Offshore and Dredging. *Springer*. 2010.
29. Šulc B, Jan JA. Non linear modelling and control of hydraulic actuators. *Acta Polytechnica*. 2002;3(3): 41–47.
30. Hydraulic cylinders: 380 bar series-production range. *Liebherr*.
31. Dutton K, Thompson S. *Barraclough B*. Prentice Hall: The Art of Control Engineering; 1997.
32. Cho S, Gao Z, Moan T. Model-based fault detection, fault isolation and fault-tolerant control of a blade pitch system in floating wind turbines. *Renewable Energy*. 2017;120:306-321.
33. Watton J. *Modelling*. Monitoring and Diagnostic Techniques for Fluid Power Systems: Springer; 2007.
34. Jonkman J and Kilcher L. *TurbSim user's guide* Technical Report NREL *USA*, 2012
35. IEC 61400-1: Wind turbines—part 1: design requirements. *International Electrotechnical Commission*. 2005.
36. Hasselmann K, Barnett TP, Bouws E, et al. Measurements of wind-wave growth and swell decay during the Joint North Sea Wave Project (JONSWAP). *Ergänzungsheft*. 1973;8-12.
37. Jonkman JM, Jonkman BJ. Fast modularization framework for wind turbine simulation: full-system linearization. *Journal of Physics: Conference Series*. 2016; 753, 082010.
38. IEC 61400-3: Wind turbines – Part 3 Design requirements for offshore wind turbines. International Electrotechnical Commission. 2005.

How to cite this article: Cho S, Bachynski EE, Nejad AR, Gao Z, Moan T. Numerical modeling of the hydraulic blade pitch actuator in a spar-type floating wind turbine considering fault conditions and their effects on global dynamic responses. *Wind Energy*. 2019;1–21. https://doi.org/10.1002/we.2438

A4. Paper 4

Fault detection and diagnosis of a blade pitch system of a spar-type floating wind turbine based on a hybrid approach with Kalman filter and artificial neural network

Seongpil Cho, Minjoo Choi, Zhen Gao and Torgeir Moan

Submitted to Wind Energy

This paper is awaiting publication and is not included in NTNU Open

Previous PhD theses published at the Department of Marine Technology
(earlier: Faculty of Marine Technology)
NORWEGIAN UNIVERSITY OF SCIENCE AND TECHNOLOGY

Report No.	Author	Title
	Kavlie, Dag	Optimization of Plane Elastic Grillages, 1967
	Hansen, Hans R.	Man-Machine Communication and Data-Storage Methods in Ship Structural Design, 1971
	Gisvold, Kaare M.	A Method for non-linear mixed -integer programming and its Application to Design Problems, 1971
	Lund, Sverre	Tanker Frame Optimalization by means of SUMT-Transformation and Behaviour Models, 1971
	Vinje, Tor	On Vibration of Spherical Shells Interacting with Fluid, 1972
	Lorentz, Jan D.	Tank Arrangement for Crude Oil Carriers in Accordance with the new Anti-Pollution Regulations, 1975
	Carlsen, Carl A.	Computer-Aided Design of Tanker Structures, 1975
	Larsen, Carl M.	Static and Dynamic Analysis of Offshore Pipelines during Installation, 1976
UR-79-01	Brigt Hatlestad, MK	The finite element method used in a fatigue evaluation of fixed offshore platforms. (Dr.Ing. Thesis)
UR-79-02	Erik Pettersen, MK	Analysis and design of cellular structures. (Dr.Ing. Thesis)
UR-79-03	Sverre Valsgård, MK	Finite difference and finite element methods applied to nonlinear analysis of plated structures. (Dr.Ing. Thesis)
UR-79-04	Nils T. Nordsve, MK	Finite element collapse analysis of structural members considering imperfections and stresses due to fabrication. (Dr.Ing. Thesis)
UR-79-05	Ivar J. Fylling, MK	Analysis of towline forces in ocean towing systems. (Dr.Ing. Thesis)
UR-80-06	Nils Sandsmark, MM	Analysis of Stationary and Transient Heat Conduction by the Use of the Finite Element Method. (Dr.Ing. Thesis)
UR-80-09	Sverre Haver, MK	Analysis of uncertainties related to the stochastic modeling of ocean waves. (Dr.Ing. Thesis)
UR-81-15	Odland, Jonas	On the Strength of welded Ring stiffened cylindrical Shells primarily subjected to axial Compression
UR-82-17	Engesvik, Knut	Analysis of Uncertainties in the fatigue Capacity of Welded Joints

UR-82-18	Rye, Henrik	Ocean wave groups
UR-83-30	Eide, Oddvar Inge	On Cumulative Fatigue Damage in Steel Welded Joints
UR-83-33	Mo, Olav	Stochastic Time Domain Analysis of Slender Offshore Structures
UR-83-34	Amdahl, Jørgen	Energy absorption in Ship-platform impacts
UR-84-37	Mørch, Morten	Motions and mooring forces of semi submersibles as determined by full-scale measurements and theoretical analysis
UR-84-38	Soares, C. Guedes	Probabilistic models for load effects in ship structures
UR-84-39	Aarsnes, Jan V.	Current forces on ships
UR-84-40	Czujko, Jerzy	Collapse Analysis of Plates subjected to Biaxial Compression and Lateral Load
UR-85-46	Alf G. Engseth, MK	Finite element collapse analysis of tubular steel offshore structures. (Dr.Ing. Thesis)
UR-86-47	Dengody Sheshappa, MP	A Computer Design Model for Optimizing Fishing Vessel Designs Based on Techno-Economic Analysis. (Dr.Ing. Thesis)
UR-86-48	Vidar Aanesland, MH	A Theoretical and Numerical Study of Ship Wave Resistance. (Dr.Ing. Thesis)
UR-86-49	Heinz-Joachim Wessel, MK	Fracture Mechanics Analysis of Crack Growth in Plate Girders. (Dr.Ing. Thesis)
UR-86-50	Jon Taby, MK	Ultimate and Post-ultimate Strength of Dented Tubular Members. (Dr.Ing. Thesis)
UR-86-51	Walter Lian, MH	A Numerical Study of Two-Dimensional Separated Flow Past Bluff Bodies at Moderate KC-Numbers. (Dr.Ing. Thesis)
UR-86-52	Bjørn Sortland, MH	Force Measurements in Oscillating Flow on Ship Sections and Circular Cylinders in a U-Tube Water Tank. (Dr.Ing. Thesis)
UR-86-53	Kurt Strand, MM	A System Dynamic Approach to One-dimensional Fluid Flow. (Dr.Ing. Thesis)
UR-86-54	Arne Edvin Løken, MH	Three Dimensional Second Order Hydrodynamic Effects on Ocean Structures in Waves. (Dr.Ing. Thesis)
UR-86-55	Sigurd Falch, MH	A Numerical Study of Slamming of Two-Dimensional Bodies. (Dr.Ing. Thesis)
UR-87-56	Arne Braathen, MH	Application of a Vortex Tracking Method to the Prediction of Roll Damping of a Two-Dimension Floating Body. (Dr.Ing. Thesis)
UR-87-57	Bernt Leira, MK	Gaussian Vector Processes for Reliability Analysis involving Wave-Induced Load Effects. (Dr.Ing. Thesis)

UR-87-58	Magnus Småvik, MM	Thermal Load and Process Characteristics in a Two-Stroke Diesel Engine with Thermal Barriers (in Norwegian). (Dr.Ing. Thesis)
MTA-88-59	Bernt Arild Bremdal, MP	An Investigation of Marine Installation Processes – A Knowledge - Based Planning Approach. (Dr.Ing. Thesis)
MTA-88-60	Xu Jun, MK	Non-linear Dynamic Analysis of Space-framed Offshore Structures. (Dr.Ing. Thesis)
MTA-89-61	Gang Miao, MH	Hydrodynamic Forces and Dynamic Responses of Circular Cylinders in Wave Zones. (Dr.Ing. Thesis)
MTA-89-62	Martin Greenhow, MH	Linear and Non-Linear Studies of Waves and Floating Bodies. Part I and Part II. (Dr.Techn. Thesis)
MTA-89-63	Chang Li, MH	Force Coefficients of Spheres and Cubes in Oscillatory Flow with and without Current. (Dr.Ing. Thesis
MTA-89-64	Hu Ying, MP	A Study of Marketing and Design in Development of Marine Transport Systems. (Dr.Ing. Thesis)
MTA-89-65	Arild Jæger, MH	Seakeeping, Dynamic Stability and Performance of a Wedge Shaped Planing Hull. (Dr.Ing. Thesis)
MTA-89-66	Chan Siu Hung, MM	The dynamic characteristics of tilting-pad bearings
MTA-89-67	Kim Wikstrøm, MP	Analysis av projekteringen for ett offshore projekt. (Licenciat-avhandling)
MTA-89-68	Jiao Guoyang, MK	Reliability Analysis of Crack Growth under Random Loading, considering Model Updating. (Dr.Ing. Thesis)
MTA-89-69	Arnt Olufsen, MK	Uncertainty and Reliability Analysis of Fixed Offshore Structures. (Dr.Ing. Thesis)
MTA-89-70	Wu Yu-Lin, MR	System Reliability Analyses of Offshore Structures using improved Truss and Beam Models. (Dr.Ing. Thesis)
MTA-90-71	Jan Roger Hoff, MH	Three-dimensional Green function of a vessel with forward speed in waves. (Dr.Ing. Thesis)
MTA-90-72	Rong Zhao, MH	Slow-Drift Motions of a Moored Two-Dimensional Body in Irregular Waves. (Dr.Ing. Thesis)
MTA-90-73	Atle Minsaas, MP	Economical Risk Analysis. (Dr.Ing. Thesis)
MTA-90-74	Knut-Aril Farnes, MK	Long-term Statistics of Response in Non-linear Marine Structures. (Dr.Ing. Thesis)
MTA-90-75	Torbjørn Sotberg, MK	Application of Reliability Methods for Safety Assessment of Submarine Pipelines. (Dr.Ing. Thesis)
MTA-90-76	Zeuthen, Steffen, MP	SEAMAID. A computational model of the design process in a constraint-based logic programming environment. An example from the offshore domain. (Dr.Ing. Thesis)

MTA-91-77	Haagensen, Sven, MM	Fuel Dependant Cyclic Variability in a Spark Ignition Engine - An Optical Approach. (Dr.Ing. Thesis)
MTA-91-78	Løland, Geir, MH	Current forces on and flow through fish farms. (Dr.Ing. Thesis)
MTA-91-79	Hoen, Christopher, MK	System Identification of Structures Excited by Stochastic Load Processes. (Dr.Ing. Thesis)
MTA-91-80	Haugen, Stein, MK	Probabilistic Evaluation of Frequency of Collision between Ships and Offshore Platforms. (Dr.Ing. Thesis)
MTA-91-81	Sødahl, Nils, MK	Methods for Design and Analysis of Flexible Risers. (Dr.Ing. Thesis)
MTA-91-82	Ormberg, Harald, MK	Non-linear Response Analysis of Floating Fish Farm Systems. (Dr.Ing. Thesis)
MTA-91-83	Marley, Mark J., MK	Time Variant Reliability under Fatigue Degradation. (Dr.Ing. Thesis)
MTA-91-84	Krokstad, Jørgen R., MH	Second-order Loads in Multidirectional Seas. (Dr.Ing. Thesis)
MTA-91-85	Molteberg, Gunnar A., MM	The Application of System Identification Techniques to Performance Monitoring of Four Stroke Turbocharged Diesel Engines. (Dr.Ing. Thesis)
MTA-92-86	Mørch, Hans Jørgen Bjelke, MH	Aspects of Hydrofoil Design: with Emphasis on Hydrofoil Interaction in Calm Water. (Dr.Ing. Thesis)
MTA-92-87	Chan Siu Hung, MM	Nonlinear Analysis of Rotordynamic Instabilities in Highspeed Turbomachinery. (Dr.Ing. Thesis)
MTA-92-88	Bessason, Bjarni, MK	Assessment of Earthquake Loading and Response of Seismically Isolated Bridges. (Dr.Ing. Thesis)
MTA-92-89	Langli, Geir, MP	Improving Operational Safety through exploitation of Design Knowledge - an investigation of offshore platform safety. (Dr.Ing. Thesis)
MTA-92-90	Sævik, Svein, MK	On Stresses and Fatigue in Flexible Pipes. (Dr.Ing. Thesis)
MTA-92-91	Ask, Tor Ø., MM	Ignition and Flame Growth in Lean Gas-Air Mixtures. An Experimental Study with a Schlieren System. (Dr.Ing. Thesis)
MTA-86-92	Hessen, Gunnar, MK	Fracture Mechanics Analysis of Stiffened Tubular Members. (Dr.Ing. Thesis)
MTA-93-93	Steinebach, Christian, MM	Knowledge Based Systems for Diagnosis of Rotating Machinery. (Dr.Ing. Thesis)
MTA-93-94	Dalane, Jan Inge, MK	System Reliability in Design and Maintenance of Fixed Offshore Structures. (Dr.Ing. Thesis)
MTA-93-95	Steen, Sverre, MH	Cobblestone Effect on SES. (Dr.Ing. Thesis)
MTA-93-96	Karunakaran, Daniel, MK	Nonlinear Dynamic Response and Reliability Analysis of Drag-dominated Offshore Platforms. (Dr.Ing. Thesis)

MTA-93-97	Hagen, Arnulf, MP	The Framework of a Design Process Language. (Dr.Ing. Thesis)
MTA-93-98	Nordrik, Rune, MM	Investigation of Spark Ignition and Autoignition in Methane and Air Using Computational Fluid Dynamics and Chemical Reaction Kinetics. A Numerical Study of Ignition Processes in Internal Combustion Engines. (Dr.Ing. Thesis)
MTA-94-99	Passano, Elizabeth, MK	Efficient Analysis of Nonlinear Slender Marine Structures. (Dr.Ing. Thesis)
MTA-94-100	Kvålsvold, Jan, MH	Hydroelastic Modelling of Wetdeck Slamming on Multihull Vessels. (Dr.Ing. Thesis)
MTA-94-102	Bech, Sidsel M., MK	Experimental and Numerical Determination of Stiffness and Strength of GRP/PVC Sandwich Structures. (Dr.Ing. Thesis)
MTA-95-103	Paulsen, Hallvard, MM	A Study of Transient Jet and Spray using a Schlieren Method and Digital Image Processing. (Dr.Ing. Thesis)
MTA-95-104	Hovde, Geir Olav, MK	Fatigue and Overload Reliability of Offshore Structural Systems, Considering the Effect of Inspection and Repair. (Dr.Ing. Thesis)
MTA-95-105	Wang, Xiaozhi, MK	Reliability Analysis of Production Ships with Emphasis on Load Combination and Ultimate Strength. (Dr.Ing. Thesis)
MTA-95-106	Ulstein, Tore, MH	Nonlinear Effects of a Flexible Stern Seal Bag on Cobblestone Oscillations of an SES. (Dr.Ing. Thesis)
MTA-95-107	Solaas, Frøydis, MH	Analytical and Numerical Studies of Sloshing in Tanks. (Dr.Ing. Thesis)
MTA-95-108	Hellan, Øyvind, MK	Nonlinear Pushover and Cyclic Analyses in Ultimate Limit State Design and Reassessment of Tubular Steel Offshore Structures. (Dr.Ing. Thesis)
MTA-95-109	Hermundstad, Ole A., MK	Theoretical and Experimental Hydroelastic Analysis of High Speed Vessels. (Dr.Ing. Thesis)
MTA-96-110	Bratland, Anne K., MH	Wave-Current Interaction Effects on Large-Volume Bodies in Water of Finite Depth. (Dr.Ing. Thesis)
MTA-96-111	Herfjord, Kjell, MH	A Study of Two-dimensional Separated Flow by a Combination of the Finite Element Method and Navier-Stokes Equations. (Dr.Ing. Thesis)
MTA-96-112	Æsøy, Vilmar, MM	Hot Surface Assisted Compression Ignition in a Direct Injection Natural Gas Engine. (Dr.Ing. Thesis)
MTA-96-113	Eknes, Monika L., MK	Escalation Scenarios Initiated by Gas Explosions on Offshore Installations. (Dr.Ing. Thesis)
MTA-96-114	Erikstad, Stein O., MP	A Decision Support Model for Preliminary Ship Design. (Dr.Ing. Thesis)
MTA-96-115	Pedersen, Egil, MH	A Nautical Study of Towed Marine Seismic Streamer Cable Configurations. (Dr.Ing. Thesis)

MTA-97-116	Moksnes, Paul O., MM	Modelling Two-Phase Thermo-Fluid Systems Using Bond Graphs. (Dr.Ing. Thesis)
MTA-97-117	Halse, Karl H., MK	On Vortex Shedding and Prediction of Vortex-Induced Vibrations of Circular Cylinders. (Dr.Ing. Thesis)
MTA-97-118	Igland, Ragnar T., MK	Reliability Analysis of Pipelines during Laying, considering Ultimate Strength under Combined Loads. (Dr.Ing. Thesis)
MTA-97-119	Pedersen, Hans-P., MP	Levendefiskteknologi for fiskefartøy. (Dr.Ing. Thesis)
MTA-98-120	Vikestad, Kyrre, MK	Multi-Frequency Response of a Cylinder Subjected to Vortex Shedding and Support Motions. (Dr.Ing. Thesis)
MTA-98-121	Azadi, Mohammad R. E., MK	Analysis of Static and Dynamic Pile-Soil-Jacket Behaviour. (Dr.Ing. Thesis)
MTA-98-122	Ulltang, Terje, MP	A Communication Model for Product Information. (Dr.Ing. Thesis)
MTA-98-123	Torbergsen, Erik, MM	Impeller/Diffuser Interaction Forces in Centrifugal Pumps. (Dr.Ing. Thesis)
MTA-98-124	Hansen, Edmond, MH	A Discrete Element Model to Study Marginal Ice Zone Dynamics and the Behaviour of Vessels Moored in Broken Ice. (Dr.Ing. Thesis)
MTA-98-125	Videiro, Paulo M., MK	Reliability Based Design of Marine Structures. (Dr.Ing. Thesis)
MTA-99-126	Mainçon, Philippe, MK	Fatigue Reliability of Long Welds Application to Titanium Risers. (Dr.Ing. Thesis)
MTA-99-127	Haugen, Elin M., MH	Hydroelastic Analysis of Slamming on Stiffened Plates with Application to Catamaran Wetdecks. (Dr.Ing. Thesis)
MTA-99-128	Langhelle, Nina K., MK	Experimental Validation and Calibration of Nonlinear Finite Element Models for Use in Design of Aluminium Structures Exposed to Fire. (Dr.Ing. Thesis)
MTA-99-129	Berstad, Are J., MK	Calculation of Fatigue Damage in Ship Structures. (Dr.Ing. Thesis)
MTA-99-130	Andersen, Trond M., MM	Short Term Maintenance Planning. (Dr.Ing. Thesis)
MTA-99-131	Tveiten, Bård Wathne, MK	Fatigue Assessment of Welded Aluminium Ship Details. (Dr.Ing. Thesis)
MTA-99-132	Søreide, Fredrik, MP	Applications of underwater technology in deep water archaeology. Principles and practice. (Dr.Ing. Thesis)
MTA-99-133	Tønnessen, Rune, MH	A Finite Element Method Applied to Unsteady Viscous Flow Around 2D Blunt Bodies With Sharp Corners. (Dr.Ing. Thesis)
MTA-99-134	Elvekrok, Dag R., MP	Engineering Integration in Field Development Projects in the Norwegian Oil and Gas Industry. The Supplier Management of Norne. (Dr.Ing. Thesis)

MTA-99-135	Fagerholt, Kjetil, MP	Optimeringsbaserte Metoder for Ruteplanlegging innen skipsfart. (Dr.Ing. Thesis)
MTA-99-136	Bysveen, Marie, MM	Visualization in Two Directions on a Dynamic Combustion Rig for Studies of Fuel Quality. (Dr.Ing. Thesis)
MTA-2000-137	Storteig, Eskild, MM	Dynamic characteristics and leakage performance of liquid annular seals in centrifugal pumps. (Dr.Ing. Thesis)
MTA-2000-138	Sagli, Gro, MK	Model uncertainty and simplified estimates of long term extremes of hull girder loads in ships. (Dr.Ing. Thesis)
MTA-2000-139	Tronstad, Harald, MK	Nonlinear analysis and design of cable net structures like fishing gear based on the finite element method. (Dr.Ing. Thesis)
MTA-2000-140	Kroneberg, André, MP	Innovation in shipping by using scenarios. (Dr.Ing. Thesis)
MTA-2000-141	Haslum, Herbjørn Alf, MH	Simplified methods applied to nonlinear motion of spar platforms. (Dr.Ing. Thesis)
MTA-2001-142	Samdal, Ole Johan, MM	Modelling of Degradation Mechanisms and Stressor Interaction on Static Mechanical Equipment Residual Lifetime. (Dr.Ing. Thesis)
MTA-2001-143	Baarholm, Rolf Jarle, MH	Theoretical and experimental studies of wave impact underneath decks of offshore platforms. (Dr.Ing. Thesis)
MTA-2001-144	Wang, Lihua, MK	Probabilistic Analysis of Nonlinear Wave-induced Loads on Ships. (Dr.Ing. Thesis)
MTA-2001-145	Kristensen, Odd H. Holt, MK	Ultimate Capacity of Aluminium Plates under Multiple Loads, Considering HAZ Properties. (Dr.Ing. Thesis)
MTA-2001-146	Greco, Marilena, MH	A Two-Dimensional Study of Green-Water Loading. (Dr.Ing. Thesis)
MTA-2001-147	Heggelund, Svein E., MK	Calculation of Global Design Loads and Load Effects in Large High Speed Catamarans. (Dr.Ing. Thesis)
MTA-2001-148	Babalola, Olusegun T., MK	Fatigue Strength of Titanium Risers – Defect Sensitivity. (Dr.Ing. Thesis)
MTA-2001-149	Mohammed, Abuu K., MK	Nonlinear Shell Finite Elements for Ultimate Strength and Collapse Analysis of Ship Structures. (Dr.Ing. Thesis)
MTA-2002-150	Holmedal, Lars E., MH	Wave-current interactions in the vicinity of the sea bed. (Dr.Ing. Thesis)
MTA-2002-151	Rognebakke, Olav F., MH	Sloshing in rectangular tanks and interaction with ship motions. (Dr.Ing. Thesis)
MTA-2002-152	Lader, Pål Furset, MH	Geometry and Kinematics of Breaking Waves. (Dr.Ing. Thesis)
MTA-2002-153	Yang, Qinzheng, MH	Wash and wave resistance of ships in finite water depth. (Dr.Ing. Thesis)
MTA-2002-154	Melhus, Øyvin, MM	Utilization of VOC in Diesel Engines. Ignition and combustion of VOC released by crude oil tankers. (Dr.Ing. Thesis)

MTA-2002-155	Ronæss, Marit, MH	Wave Induced Motions of Two Ships Advancing on Parallel Course. (Dr.Ing. Thesis)
MTA-2002-156	Økland, Ole D., MK	Numerical and experimental investigation of whipping in twin hull vessels exposed to severe wet deck slamming. (Dr.Ing. Thesis)
MTA-2002-157	Ge, Chunhua, MK	Global Hydroelastic Response of Catamarans due to Wet Deck Slamming. (Dr.Ing. Thesis)
MTA-2002-158	Byklum, Eirik, MK	Nonlinear Shell Finite Elements for Ultimate Strength and Collapse Analysis of Ship Structures. (Dr.Ing. Thesis)
IMT-2003-1	Chen, Haibo, MK	Probabilistic Evaluation of FPSO-Tanker Collision in Tandem Offloading Operation. (Dr.Ing. Thesis)
IMT-2003-2	Skaugset, Kjetil Bjørn, MK	On the Suppression of Vortex Induced Vibrations of Circular Cylinders by Radial Water Jets. (Dr.Ing. Thesis)
IMT-2003-3	Chezhian, Muthu	Three-Dimensional Analysis of Slamming. (Dr.Ing. Thesis)
IMT-2003-4	Buhaug, Øyvind	Deposit Formation on Cylinder Liner Surfaces in Medium Speed Engines. (Dr.Ing. Thesis)
IMT-2003-5	Tregde, Vidar	Aspects of Ship Design: Optimization of Aft Hull with Inverse Geometry Design. (Dr.Ing. Thesis)
IMT-2003-6	Wist, Hanne Therese	Statistical Properties of Successive Ocean Wave Parameters. (Dr.Ing. Thesis)
IMT-2004-7	Ransau, Samuel	Numerical Methods for Flows with Evolving Interfaces. (Dr.Ing. Thesis)
IMT-2004-8	Soma, Torkel	Blue-Chip or Sub-Standard. A data interrogation approach of identity safety characteristics of shipping organization. (Dr.Ing. Thesis)
IMT-2004-9	Ersdal, Svein	An experimental study of hydrodynamic forces on cylinders and cables in near axial flow. (Dr.Ing. Thesis)
IMT-2005-10	Brodtkorb, Per Andreas	The Probability of Occurrence of Dangerous Wave Situations at Sea. (Dr.Ing. Thesis)
IMT-2005-11	Yttervik, Rune	Ocean current variability in relation to offshore engineering. (Dr.Ing. Thesis)
IMT-2005-12	Fredheim, Arne	Current Forces on Net-Structures. (Dr.Ing. Thesis)
IMT-2005-13	Heggernes, Kjetil	Flow around marine structures. (Dr.Ing. Thesis
IMT-2005-14	Fouques, Sebastien	Lagrangian Modelling of Ocean Surface Waves and Synthetic Aperture Radar Wave Measurements. (Dr.Ing. Thesis)
IMT-2006-15	Holm, Håvard	Numerical calculation of viscous free surface flow around marine structures. (Dr.Ing. Thesis)

IMT-2006-16	Bjørheim, Lars G.	Failure Assessment of Long Through Thickness Fatigue Cracks in Ship Hulls. (Dr.Ing. Thesis)
IMT-2006-17	Hansson, Lisbeth	Safety Management for Prevention of Occupational Accidents. (Dr.Ing. Thesis)
IMT-2006-18	Zhu, Xinying	Application of the CIP Method to Strongly Nonlinear Wave-Body Interaction Problems. (Dr.Ing. Thesis)
IMT-2006-19	Reite, Karl Johan	Modelling and Control of Trawl Systems. (Dr.Ing. Thesis)
IMT-2006-20	Smogeli, Øyvind Notland	Control of Marine Propellers. From Normal to Extreme Conditions. (Dr.Ing. Thesis)
IMT-2007-21	Storhaug, Gaute	Experimental Investigation of Wave Induced Vibrations and Their Effect on the Fatigue Loading of Ships. (Dr.Ing. Thesis)
IMT-2007-22	Sun, Hui	A Boundary Element Method Applied to Strongly Nonlinear Wave-Body Interaction Problems. (PhD Thesis, CeSOS)
IMT-2007-23	Rustad, Anne Marthine	Modelling and Control of Top Tensioned Risers. (PhD Thesis, CeSOS)
IMT-2007-24	Johansen, Vegar	Modelling flexible slender system for real-time simulations and control applications
IMT-2007-25	Wroldsen, Anders Sunde	Modelling and control of tensegrity structures. (PhD Thesis, CeSOS)
IMT-2007-26	Aronsen, Kristoffer Høye	An experimental investigation of in-line and combined inline and cross flow vortex induced vibrations. (Dr. avhandling, IMT)
IMT-2007-27	Gao, Zhen	Stochastic Response Analysis of Mooring Systems with Emphasis on Frequency-domain Analysis of Fatigue due to Wide-band Response Processes (PhD Thesis, CeSOS)
IMT-2007-28	Thorstensen, Tom Anders	Lifetime Profit Modelling of Ageing Systems Utilizing Information about Technical Condition. (Dr.ing. thesis, IMT)
IMT-2008-29	Refsnes, Jon Erling Gorset	Nonlinear Model-Based Control of Slender Body AUVs (PhD Thesis, IMT)
IMT-2008-30	Berntsen, Per Ivar B.	Structural Reliability Based Position Mooring. (PhD-Thesis, IMT)
IMT-2008-31	Ye, Naiquan	Fatigue Assessment of Aluminium Welded Box-stiffener Joints in Ships (Dr.ing. thesis, IMT)
IMT-2008-32	Radan, Damir	Integrated Control of Marine Electrical Power Systems. (PhD-Thesis, IMT)
IMT-2008-33	Thomassen, Paul	Methods for Dynamic Response Analysis and Fatigue Life Estimation of Floating Fish Cages. (Dr.ing. thesis, IMT)
IMT-2008-34	Pákozdi, Csaba	A Smoothed Particle Hydrodynamics Study of Two-dimensional Nonlinear Sloshing in Rectangular Tanks. (Dr.ing.thesis, IMT/ CeSOS)

IMT-2007-35	Grytøyr, Guttorm	A Higher-Order Boundary Element Method and Applications to Marine Hydrodynamics. (Dr.ing.thesis, IMT)
IMT-2008-36	Drummen, Ingo	Experimental and Numerical Investigation of Nonlinear Wave-Induced Load Effects in Containerships considering Hydroelasticity. (PhD thesis, CeSOS)
IMT-2008-37	Skejic, Renato	Maneuvering and Seakeeping of a Singel Ship and of Two Ships in Interaction. (PhD-Thesis, CeSOS)
IMT-2008-38	Harlem, Alf	An Age-Based Replacement Model for Repairable Systems with Attention to High-Speed Marine Diesel Engines. (PhD-Thesis, IMT)
IMT-2008-39	Alsos, Hagbart S.	Ship Grounding. Analysis of Ductile Fracture, Bottom Damage and Hull Girder Response. (PhD-thesis, IMT)
IMT-2008-40	Graczyk, Mateusz	Experimental Investigation of Sloshing Loading and Load Effects in Membrane LNG Tanks Subjected to Random Excitation. (PhD-thesis, CeSOS)
IMT-2008-41	Taghipour, Reza	Efficient Prediction of Dynamic Response for Flexible amd Multi-body Marine Structures. (PhD-thesis, CeSOS)
IMT-2008-42	Ruth, Eivind	Propulsion control and thrust allocation on marine vessels. (PhD thesis, CeSOS)
IMT-2008-43	Nystad, Bent Helge	Technical Condition Indexes and Remaining Useful Life of Aggregated Systems. PhD thesis, IMT
IMT-2008-44	Soni, Prashant Kumar	Hydrodynamic Coefficients for Vortex Induced Vibrations of Flexible Beams, PhD thesis, CeSOS
IMT-2009-45	Amlashi, Hadi K.K.	Ultimate Strength and Reliability-based Design of Ship Hulls with Emphasis on Combined Global and Local Loads. PhD Thesis, IMT
IMT-2009-46	Pedersen, Tom Arne	Bond Graph Modelling of Marine Power Systems. PhD Thesis, IMT
IMT-2009-47	Kristiansen, Trygve	Two-Dimensional Numerical and Experimental Studies of Piston-Mode Resonance. PhD-Thesis, CeSOS
IMT-2009-48	Ong, Muk Chen	Applications of a Standard High Reynolds Number Model and a Stochastic Scour Prediction Model for Marine Structures. PhD-thesis, IMT
IMT-2009-49	Hong, Lin	Simplified Analysis and Design of Ships subjected to Collision and Grounding. PhD-thesis, IMT
IMT-2009-50	Koushan, Kamran	Vortex Induced Vibrations of Free Span Pipelines, PhD thesis, IMT
IMT-2009-51	Korsvik, Jarl Eirik	Heuristic Methods for Ship Routing and Scheduling. PhD-thesis, IMT

IMT-2009-52	Lee, Jihoon	Experimental Investigation and Numerical in Analyzing the Ocean Current Displacement of Longlines. Ph.d.-Thesis, IMT.
IMT-2009-53	Vestbøstad, Tone Gran	A Numerical Study of Wave-in-Deck Impact usin a Two-Dimensional Constrained Interpolation Profile Method, Ph.d.thesis, CeSOS.
IMT-2009-54	Bruun, Kristine	Bond Graph Modelling of Fuel Cells for Marine Power Plants. Ph.d.-thesis, IMT
IMT-2009-55	Holstad, Anders	Numerical Investigation of Turbulence in a Sekwed Three-Dimensional Channel Flow, Ph.d.-thesis, IMT.
IMT-2009-56	Ayala-Uraga, Efren	Reliability-Based Assessment of Deteriorating Ship-shaped Offshore Structures, Ph.d.-thesis, IMT
IMT-2009-57	Kong, Xiangjun	A Numerical Study of a Damaged Ship in Beam Sea Waves. Ph.d.-thesis, IMT/CeSOS.
IMT-2010-58	Kristiansen, David	Wave Induced Effects on Floaters of Aquaculture Plants, Ph.d.-thesis, CeSOS.
IMT-2010-59	Ludvigsen, Martin	An ROV-Toolbox for Optical and Acoustic Scientific Seabed Investigation. Ph.d.-thesis IMT.
IMT-2010-60	Hals, Jørgen	Modelling and Phase Control of Wave-Energy Converters. Ph.d.thesis, CeSOS.
IMT-2010- 61	Shu, Zhi	Uncertainty Assessment of Wave Loads and Ultimate Strength of Tankers and Bulk Carriers in a Reliability Framework. Ph.d. Thesis, IMT/ CeSOS
IMT-2010-62	Shao, Yanlin	Numerical Potential-Flow Studies on Weakly-Nonlinear Wave-Body Interactions with/without Small Forward Speed, Ph.d.thesis,CeSOS.
IMT-2010-63	Califano, Andrea	Dynamic Loads on Marine Propellers due to Intermittent Ventilation. Ph.d.thesis, IMT.
IMT-2010-64	El Khoury, George	Numerical Simulations of Massively Separated Turbulent Flows, Ph.d.-thesis, IMT
IMT-2010-65	Seim, Knut Sponheim	Mixing Process in Dense Overflows with Emphasis on the Faroe Bank Channel Overflow. Ph.d.thesis, IMT
IMT-2010-66	Jia, Huirong	Structural Analysis of Intect and Damaged Ships in a Collission Risk Analysis Perspective. Ph.d.thesis CeSoS.
IMT-2010-67	Jiao, Linlin	Wave-Induced Effects on a Pontoon-type Very Large Floating Structures (VLFS). Ph.D.-thesis, CeSOS.
IMT-2010-68	Abrahamsen, Bjørn Christian	Sloshing Induced Tank Roof with Entrapped Air Pocket. Ph.d.thesis, CeSOS.
IMT-2011-69	Karimirad, Madjid	Stochastic Dynamic Response Analysis of Spar-Type Wind Turbines with Catenary or Taut Mooring Systems. Ph.d.-thesis, CeSOS.
IMT–2011-70	Erlend Meland	Condition Monitoring of Safety Critical Valves. Ph.d.-thesis, IMT.

IMT – 2011-71	Yang, Limin	Stochastic Dynamic System Analysis of Wave Energy Converter with Hydraulic Power Take-Off, with Particular Reference to Wear Damage Analysis, Ph.d. Thesis, CeSOS.
IMT – 2011-72	Visscher, Jan	Application of Particla Image Velocimetry on Turbulent Marine Flows, Ph.d.Thesis, IMT.
IMT – 2011-73	Su, Biao	Numerical Predictions of Global and Local Ice Loads on Ships. Ph.d.Thesis, CeSOS.
IMT – 2011-74	Liu, Zhenhui	Analytical and Numerical Analysis of Iceberg Collision with Ship Structures. Ph.d.Thesis, IMT.
IMT – 2011-75	Aarsæther, Karl Gunnar	Modeling and Analysis of Ship Traffic by Observation and Numerical Simulation. Ph.d.Thesis, IMT.
IMT – 2011-76	Wu, Jie	Hydrodynamic Force Identification from Stochastic Vortex Induced Vibration Experiments with Slender Beams. Ph.d.Thesis, IMT.
IMT – 2011-77	Amini, Hamid	Azimuth Propulsors in Off-design Conditions. Ph.d.Thesis, IMT.
IMT – 2011-78	Nguyen, Tan-Hoi	Toward a System of Real-Time Prediction and Monitoring of Bottom Damage Conditions During Ship Grounding. Ph.d.thesis, IMT.
IMT- 2011-79	Tavakoli, Mohammad T.	Assessment of Oil Spill in Ship Collision and Grounding, Ph.d.thesis, IMT.
IMT- 2011-80	Guo, Bingjie	Numerical and Experimental Investigation of Added Resistance in Waves. Ph.d.Thesis, IMT.
IMT- 2011-81	Chen, Qiaofeng	Ultimate Strength of Aluminium Panels, considering HAZ Effects, IMT
IMT- 2012-82	Kota, Ravikiran S.	Wave Loads on Decks of Offshore Structures in Random Seas, CeSOS.
IMT- 2012-83	Sten, Ronny	Dynamic Simulation of Deep Water Drilling Risers with Heave Compensating System, IMT.
IMT- 2012-84	Berle, Øyvind	Risk and resilience in global maritime supply chains, IMT.
IMT- 2012-85	Fang, Shaoji	Fault Tolerant Position Mooring Control Based on Structural Reliability, CeSOS.
IMT- 2012-86	You, Jikun	Numerical studies on wave forces and moored ship motions in intermediate and shallow water, CeSOS.
IMT- 2012-87	Xiang ,Xu	Maneuvering of two interacting ships in waves, CeSOS
IMT- 2012-88	Dong, Wenbin	Time-domain fatigue response and reliability analysis of offshore wind turbines with emphasis on welded tubular joints and gear components, CeSOS

IMT-2012-89	Zhu, Suji	Investigation of Wave-Induced Nonlinear Load Effects in Open Ships considering Hull Girder Vibrations in Bending and Torsion, CeSOS
IMT-2012-90	Zhou, Li	Numerical and Experimental Investigation of Station-keeping in Level Ice, CeSOS
IMT-2012-91	Ushakov, Sergey	Particulate matter emission characteristics from diesel enignes operating on conventional and alternative marine fuels, IMT
IMT-1-2013	Yin, Decao	Experimental and Numerical Analysis of Combined In-line and Cross-flow Vortex Induced Vibrations, CeSOS
IMT-2-2013	Kurniawan, Adi	Modelling and geometry optimisation of wave energy converters, CeSOS
IMT-3-2013	Al Ryati, Nabil	Technical condition indexes doe auxiliary marine diesel engines, IMT
IMT-4-2013	Firoozkoohi, Reza	Experimental, numerical and analytical investigation of the effect of screens on sloshing, CeSOS
IMT-5-2013	Ommani, Babak	Potential-Flow Predictions of a Semi-Displacement Vessel Including Applications to Calm Water Broaching, CeSOS
IMT-6-2013	Xing, Yihan	Modelling and analysis of the gearbox in a floating spar-type wind turbine, CeSOS
IMT-7-2013	Balland, Océane	Optimization models for reducing air emissions from ships, IMT
IMT-8-2013	Yang, Dan	Transitional wake flow behind an inclined flat plate----- Computation and analysis, IMT
IMT-9-2013	Abdillah, Suyuthi	Prediction of Extreme Loads and Fatigue Damage for a Ship Hull due to Ice Action, IMT
IMT-10-2013	Ramìrez, Pedro Agustìn Pèrez	Ageing management and life extension of technical systems- Concepts and methods applied to oil and gas facilities, IMT
IMT-11-2013	Chuang, Zhenju	Experimental and Numerical Investigation of Speed Loss due to Seakeeping and Maneuvering. IMT
IMT-12-2013	Etemaddar, Mahmoud	Load and Response Analysis of Wind Turbines under Atmospheric Icing and Controller System Faults with Emphasis on Spar Type Floating Wind Turbines, IMT
IMT-13-2013	Lindstad, Haakon	Strategies and measures for reducing maritime CO2 emissons, IMT
IMT-14-2013	Haris, Sabril	Damage interaction analysis of ship collisions, IMT
IMT-15-2013	Shainee, Mohamed	Conceptual Design, Numerical and Experimental Investigation of a SPM Cage Concept for Offshore Mariculture, IMT

IMT-16-2013	Gansel, Lars	Flow past porous cylinders and effects of biofouling and fish behavior on the flow in and around Atlantic salmon net cages, IMT
IMT-17-2013	Gaspar, Henrique	Handling Aspects of Complexity in Conceptual Ship Design, IMT
IMT-18-2013	Thys, Maxime	Theoretical and Experimental Investigation of a Free Running Fishing Vessel at Small Frequency of Encounter, CeSOS
IMT-19-2013	Aglen, Ida	VIV in Free Spanning Pipelines, CeSOS
IMT-1-2014	Song, An	Theoretical and experimental studies of wave diffraction and radiation loads on a horizontally submerged perforated plate, CeSOS
IMT-2-2014	Rogne, Øyvind Ygre	Numerical and Experimental Investigation of a Hinged 5-body Wave Energy Converter, CeSOS
IMT-3-2014	Dai, Lijuan	Safe and efficient operation and maintenance of offshore wind farms ,IMT
IMT-4-2014	Bachynski, Erin Elizabeth	Design and Dynamic Analysis of Tension Leg Platform Wind Turbines, CeSOS
IMT-5-2014	Wang, Jingbo	Water Entry of Freefall Wedged – Wedge motions and Cavity Dynamics, CeSOS
IMT-6-2014	Kim, Ekaterina	Experimental and numerical studies related to the coupled behavior of ice mass and steel structures during accidental collisions, IMT
IMT-7-2014	Tan, Xiang	Numerical investigation of ship's continuous- mode icebreaking in leverl ice, CeSOS
IMT-8-2014	Muliawan, Made Jaya	Design and Analysis of Combined Floating Wave and Wind Power Facilities, with Emphasis on Extreme Load Effects of the Mooring System, CeSOS
IMT-9-2014	Jiang, Zhiyu	Long-term response analysis of wind turbines with an emphasis on fault and shutdown conditions, IMT
IMT-10-2014	Dukan, Fredrik	ROV Motion Control Systems, IMT
IMT-11-2014	Grimsmo, Nils I.	Dynamic simulations of hydraulic cylinder for heave compensation of deep water drilling risers, IMT
IMT-12-2014	Kvittem, Marit I.	Modelling and response analysis for fatigue design of a semisubmersible wind turbine, CeSOS
IMT-13-2014	Akhtar, Juned	The Effects of Human Fatigue on Risk at Sea, IMT
IMT-14-2014	Syahroni, Nur	Fatigue Assessment of Welded Joints Taking into Account Effects of Residual Stress, IMT

IMT-1-2015	Bøckmann, Eirik	Wave Propulsion of ships, IMT
IMT-2-2015	Wang, Kai	Modelling and dynamic analysis of a semi-submersible floating vertical axis wind turbine, CeSOS
IMT-3-2015	Fredriksen, Arnt Gunvald	A numerical and experimental study of a two-dimensional body with moonpool in waves and current, CeSOS
IMT-4-2015	Jose Patricio Gallardo Canabes	Numerical studies of viscous flow around bluff bodies, IMT
IMT-5-2015	Vegard Longva	Formulation and application of finite element techniques for slender marine structures subjected to contact interactions, IMT
IMT-6-2015	Jacobus De Vaal	Aerodynamic modelling of floating wind turbines, CeSOS
IMT-7-2015	Fachri Nasution	Fatigue Performance of Copper Power Conductors, IMT
IMT-8-2015	Oleh I Karpa	Development of bivariate extreme value distributions for applications in marine technology,CeSOS
IMT-9-2015	Daniel de Almeida Fernandes	An output feedback motion control system for ROVs, AMOS
IMT-10-2015	Bo Zhao	Particle Filter for Fault Diagnosis: Application to Dynamic Positioning Vessel and Underwater Robotics, CeSOS
IMT-11-2015	Wenting Zhu	Impact of emission allocation in maritime transportation, IMT
IMT-12-2015	Amir Rasekhi Nejad	Dynamic Analysis and Design of Gearboxes in Offshore Wind Turbines in a Structural Reliability Perspective, CeSOS
IMT-13-2015	Arturo Jesùs Ortega Malca	Dynamic Response of Flexibles Risers due to Unsteady Slug Flow, CeSOS
IMT-14-2015	Dagfinn Husjord	Guidance and decision-support system for safe navigation of ships operating in close proximity, IMT
IMT-15-2015	Anirban Bhattacharyya	Ducted Propellers: Behaviour in Waves and Scale Effects, IMT
IMT-16-2015	Qin Zhang	Image Processing for Ice Parameter Identification in Ice Management, IMT
IMT-1-2016	Vincentius Rumawas	Human Factors in Ship Design and Operation: An Experiential Learning, IMT
IMT-2-2016	Martin Storheim	Structural response in ship-platform and ship-ice collisions, IMT
IMT-3-2016	Mia Abrahamsen Prsic	Numerical Simulations of the Flow around single and Tandem Circular Cylinders Close to a Plane Wall, IMT

IMT-4-2016	Tufan Arslan	Large-eddy simulations of cross-flow around ship sections, IMT
IMT-5-2016	Pierre Yves-Henry	Parametrisation of aquatic vegetation in hydraulic and coastal research,IMT
IMT-6-2016	Lin Li	Dynamic Analysis of the Instalation of Monopiles for Offshore Wind Turbines, CeSOS
IMT-7-2016	Øivind Kåre Kjerstad	Dynamic Positioning of Marine Vessels in Ice, IMT
IMT-8-2016	Xiaopeng Wu	Numerical Analysis of Anchor Handling and Fish Trawling Operations in a Safety Perspective, CeSOS
IMT-9-2016	Zhengshun Cheng	Integrated Dynamic Analysis of Floating Vertical Axis Wind Turbines, CeSOS
IMT-10-2016	Ling Wan	Experimental and Numerical Study of a Combined Offshore Wind and Wave Energy Converter Concept
IMT-11-2016	Wei Chai	Stochastic dynamic analysis and reliability evaluation of the roll motion for ships in random seas, CeSOS
IMT-12-2016	Øyvind Selnes Patricksson	Decision support for conceptual ship design with focus on a changing life cycle and future uncertainty, IMT
IMT-13-2016	Mats Jørgen Thorsen	Time domain analysis of vortex-induced vibrations, IMT
IMT-14-2016	Edgar McGuinness	Safety in the Norwegian Fishing Fleet – Analysis and measures for improvement, IMT
IMT-15-2016	Sepideh Jafarzadeh	Energy effiency and emission abatement in the fishing fleet, IMT
IMT-16-2016	Wilson Ivan Guachamin Acero	Assessment of marine operations for offshore wind turbine installation with emphasis on response-based operational limits, IMT
IMT-17-2016	Mauro Candeloro	Tools and Methods for Autonomous Operations on Seabed and Water Coumn using Underwater Vehicles, IMT
IMT-18-2016	Valentin Chabaud	Real-Time Hybrid Model Testing of Floating Wind Tubines, IMT
IMT-1-2017	Mohammad Saud Afzal	Three-dimensional streaming in a sea bed boundary layer
IMT-2-2017	Peng Li	A Theoretical and Experimental Study of Wave-induced Hydroelastic Response of a Circular Floating Collar
IMT-3-2017	Martin Bergström	A simulation-based design method for arctic maritime transport systems
IMT-4-2017	Bhushan Taskar	The effect of waves on marine propellers and propulsion

IMT-5-2017	Mohsen Bardestani	A two-dimensional numerical and experimental study of a floater with net and sinker tube in waves and current
IMT-6-2017	Fatemeh Hoseini Dadmarzi	Direct Numerical Simualtion of turbulent wakes behind different plate configurations
IMT-7-2017	Michel R. Miyazaki	Modeling and control of hybrid marine power plants
IMT-8-2017	Giri Rajasekhar Gunnu	Safety and effiency enhancement of anchor handling operations with particular emphasis on the stability of anchor handling vessels
IMT-9-2017	Kevin Koosup Yum	Transient Performance and Emissions of a Turbocharged Diesel Engine for Marine Power Plants
IMT-10-2017	Zhaolong Yu	Hydrodynamic and structural aspects of ship collisions
IMT-11-2017	Martin Hassel	Risk Analysis and Modelling of Allisions between Passing Vessels and Offshore Installations
IMT-12-2017	Astrid H. Brodtkorb	Hybrid Control of Marine Vessels – Dynamic Positioning in Varying Conditions
IMT-13-2017	Kjersti Bruserud	Simultaneous stochastic model of waves and current for prediction of structural design loads
IMT-14-2017	Finn-Idar Grøtta Giske	Long-Term Extreme Response Analysis of Marine Structures Using Inverse Reliability Methods
IMT-15-2017	Stian Skjong	Modeling and Simulation of Maritime Systems and Operations for Virtual Prototyping using co-Simulations
IMT-1-2018	Yingguang Chu	Virtual Prototyping for Marine Crane Design and Operations
IMT-2-2018	Sergey Gavrilin	Validation of ship manoeuvring simulation models
IMT-3-2018	Jeevith Hegde	Tools and methods to manage risk in autonomous subsea inspection,maintenance and repair operations
IMT-4-2018	Ida M. Strand	Sea Loads on Closed Flexible Fish Cages
IMT-5-2018	Erlend Kvinge Jørgensen	Navigation and Control of Underwater Robotic Vehicles
IMT-6-2018	Bård Stovner	Aided Intertial Navigation of Underwater Vehicles
IMT-7-2018	Erlend Liavåg Grotle	Thermodynamic Response Enhanced by Sloshing in Marine LNG Fuel Tanks
IMT-8-2018	Børge Rokseth	Safety and Verification of Advanced Maritime Vessels

IMT-9-2018	Jan Vidar Ulveseter	Advances in Semi-Empirical Time Domain Modelling of Vortex-Induced Vibrations
IMT-10-2018	Chenyu Luan	Design and analysis for a steel braceless semi-submersible hull for supporting a 5-MW horizontal axis wind turbine
IMT-11-2018	Carl Fredrik Rehn	Ship Design under Uncertainty
IMT-12-2018	Øyvind Ødegård	Towards Autonomous Operations and Systems in Marine Archaeology
IMT-13-2018	Stein Melvær Nornes	Guidance and Control of Marine Robotics for Ocean Mapping and Monitoring
IMT-14-2018	Petter Norgren	Autonomous Underwater Vehicles in Arctic Marine Operations: Arctic marine research and ice monitoring
IMT-15-2018	Minjoo Choi	Modular Adaptable Ship Design for Handling Uncertainty in the Future Operating Context
MT-16-2018	Ole Alexander Eidsvik	Dynamics of Remotely Operated Underwater Vehicle Systems
IMT-17-2018	Mahdi Ghane	Fault Diagnosis of Floating Wind Turbine Drivetrain-Methodologies and Applications
IMT-18-2018	Christoph Alexander Thieme	Risk Analysis and Modelling of Autonomous Marine Systems
IMT-19-2018	Yugao Shen	Operational limits for floating-collar fish farms in waves and current, without and with well-boat presence
IMT-20-2018	Tianjiao Dai	Investigations of Shear Interaction and Stresses in Flexible Pipes and Umbilicals
IMT-21-2018	Sigurd Solheim Pettersen	Resilience by Latent Capabilities in Marine Systems
IMT-22-2018	Thomas Sauder	Fidelity of Cyber-physical Empirical Methods. Application to the Active Truncation of Slender Marine Structures
IMT-23-2018	Jan-Tore Horn	Statistical and Modelling Uncertainties in the Design of Offshore Wind Turbines
IMT-24-2018	Anna Swider	Data Mining Methods for the Analysis of Power Systems of Vessels
IMT-1-2019	Zhao He	Hydrodynamic study of a moored fish farming cage with fish influence
IMT-2-2019	Isar Ghamari	Numerical and Experimental Study on the Ship Parametric Roll Resonance and the Effect of Anti-Roll Tank
IMT-3-2019	Håkon Strandenes	Turbulent Flow Simulations at Higher Reynolds Numbers

IMT-4-2019	Siri Mariane Holen	Safety in Norwegian Fish Farming – Concepts and Methods for Improvement
IMT-5-2019	Ping Fu	Reliability Analysis of Wake-Induced Riser Collision
IMT-6-2019	Vladimir Krivopolianskii	Experimental Investigation of Injection and Combustion Processes in Marine Gas Engines using Constant Volume Rig
IMT-7-2019	Anna Maria Kozlowska	Hydrodynamic Loads on Marine Propellers Subject to Ventilation and out of Water Condition.
IMT-8-2019	Hans-Martin Heyn	Motion Sensing on Vessels Operating in Sea Ice: A Local Ice Monitoring System for Transit and Stationkeeping Operations under the Influence of Sea Ice
IMT-9-2019|	Stefan Vilsen	Method for Real-Time Hybrid Model Testing of Ocean Structures – Case on Slender Marine Systems
IMT-10-2019	Finn-Christian W. Hanssen	Non-Linear Wave-Body Interaction in Severe Waves
IMT-11-2019	Trygve Olav Fossum	Adaptive Sampling for Marine Robotics
IMT-12-2019	Jørgen Bremnes Nielsen	Modeling and Simulation for Design Evaluation
IMT-13-2019	Yuna Zhao	Numerical modelling and dyncamic analysis of offshore wind turbine blade installation
IMT-14-2019	Daniela Myland	Experimental and Theoretical Investigations on the Ship Resistance in Level Ice
IMT-15-2019	Zhengru Ren	Advanced control algorithms to support automated offshore wind turbine installation
IMT-16-2019	Drazen Polic	Ice-propeller impact analysis using an inverse propulsion machinery simulation approach
IMT-17-2019	Endre Sandvik	Sea passage scenario simulation for ship system performance evaluation
IMT-18-2019	Loup Suja-Thauvin	Response of Monopile Wind Turbines to Higher Order Wave Loads
IMT-19-20119	Emil Smilden	Structural control of offshore wind turbines – Increasing the role of control design in offshore wind farm development
IMT-20-2019	Aleksandar-Sasa Milakovic	On equivalent ice thickness and machine learning in ship ice transit simulations
IMT-1-2020	Amrit Shankar Verma	Modelling, Analysis and Response-based Operability Assessment of Offshore Wind Turbine Blade Installation with Emphasis on Impact Damages
IMT-2-2020	Bent Oddvar Arnesen Haugaløkken	Autonomous Technology for Inspection, Maintenance and Repair Operations in the Norwegian Aquaculture
IMT-3-2020	Seongpil Cho	Model-based fault detection and diagnosis of a blade pitch system in floating wind turbines

ISBN 978-82-326-4438-4 (printed version)
ISBN 978-82-326-4439-1 (electronic version)
ISSN 1503-8181

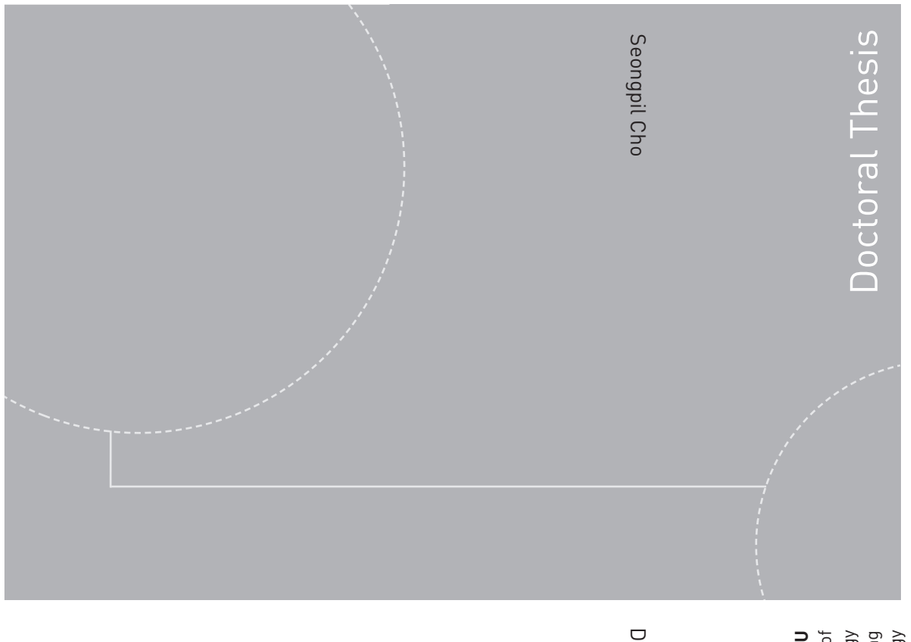

Doctoral theses at NTNU, 2020:40

Seongpil Cho

Model-based Fault Detection and Diagnosis of a Blade Pitch System in Floating Wind Turbines

NTNU
Norwegian University of
Science and Technology
Faculty of Engineering
Department of MarineTechnology

NTNU
Norwegian University of
Science and Technology

Doctoral theses at NTNU, 2020:40

NTNU

NTNU
Norwegian University of
Science and Technology